DEPENDENCE OF THE ELECTRICAL PROPERTIES OF IGNEOUS

ROCKS IN THE TASHKENT SEISMIC ZONE ON MOISTURE

CONTENT, PRESSURE AND TEMPERATURE[1]

M. Kh. Bakiyev, A. T. Bondarenko and Melis Kh. Bakiyev

Institute of Seismology, Uzbek Academy of Sciences, Tashkent,
O. Yu. Schmidt Institute of the Physics of the Earth, USSR Academy of Sciences, Moscow and
Central Institute of Geology of Nonferrous and Precious Metals, Moscow
(Presented by Academician M. A. Sadovskiy, January 3, 1975)

The empirical data on the variation of the elastic, mechanical, and electrical properties of rocks and minerals with pressure P, temperature t, and moist content W are of great interest in connection with the problem of prediction of earthquakes [1-5]. It has been noted by Sadovskiy, Barsukov, and other investigators that the resistivity of country rocks changes fairly sharply before earthquakes [6, 7]. Recently, Barsukov and Sorokin, working in the seismically-active Garm region, obtained electrometric data which may prove useful for short-term earthquake prediction [8]. The data on the variation of electrical conductivity σ of rocks in a seismically-active region with moisture content, pressure, and temperature would be useful in the interdisciplinary geophysical investigations in Central Asia, undertaken in the search for rock properties predictive of impending earthquakes. Until now no experimental data on the relation $\sigma = f(W, P, t)$ were available for rocks of the Tashkent region [9]. Our investigation was made on samples saturated with distilled water and 3 g/liter NaCl solution at a pressure of 1 atm and room temperature, and at pressures to 12 kilobars at temperatures of 200 to 1100° C by the method described by Parkhomenko and Bondarenko [10].

The following rocks were investigated: andesite, trachyandesite, hornblende andesite, dacite porphyry, diorite porphyry, diabase, granodiorite, rhyolite, dolomite, and limestone.

The nature of the relation $\sigma = f(W)$, and absolute values of σ in the moist igneous rocks of the region are governed mainly by the extent to which the rocks have been altered by secondary metasomatism. The range of variation of σ in

rocks saturated with a 3 g/liter NaCl solution is shown in Fig. 1. We see that the conductivity of rocks increases sharply as their moisture content increases to 1 percent. Analysis of the relationship $\log \sigma = f(W)$ shows that a steep increase of σ is characteristic of rocks containing secondary iron and alkali metal minerals (Fig. 1a). The high conductivity of these rocks is due to the presence of alkalis and iron in the pore solutions. Their concentration increases with the hydrolysis of the easily soluble secondary minerals in the process of saturation with water. Fresh andesites have values of σ lying in the cross-hatched field b. The values for hornblende andesite and andesite porphyry, containing chlorite, saussurite, epidote, and sericitized plagioclase lie in field c.

The range of conductivity for andesite, trachyandesite, and andesitic dacite at pressures from 0.2 to 12.3 kb and temperatures up to 600° C is shown in Fig. 2. As can be seen, $\sigma = f(P)$ varies little but there is tenfold increase in the value of σ per each 100° C.

The narrower limits of variation of $\sigma = f(P)$ in the interval t = 400 to 500° C outlines a transitional region in which extrinsic conductivity changes to intrinsic conductivity. The isobars, used to determine the activation energy E_0 of electrical conduction and the values of σ_0 are shown in Fig. 3. At a pressure of 1 atm the values of these properties in the temperature ranges 200 to 550, 550 to 800, and 800 to 1100° C are E_0 = 0.5 to 0.7, 0.66 to 0.84, and 1.8 to 2.4 eV, and σ_0 = -3.5 to -4.5, -2.8 to -3.5, and 0.8 to 4.8 ohm^{-1}·cm^{-1}, respectively (the isobars at P = 1 atm are not shown in Fig. 3). At 12.3 kb in the temperature range of 200 to 450° C, the mean value of E_0 is 0.73 eV and at t > 450° C, E_0 = 1.78 eV.

Our experiments show that the volcanic rocks of the Tashkent region exhibit fairly high resistivity when fully saturated with aqueous NaCl (Fig. 1). At pressures of 0.2 to 12.3 kb in the 200 to 600° C temperature range, they exhibit

)F IGNEOUS

ΛOISTURE

RE[1]

v

nt,
:ces, Moscow and
Moscow
(5)

;/liter NaCl solution
,ee that the conductivity
ly as their moisture
rcent.   Analysis of the
, shows that a steep
ristic of rocks contain-
'kali metal minerals
luctivity of these rocks
alkalis and iron in the
ncentration increases
 easily soluble second-
ss of saturation with
have values of σ lying
i b.   The values for
ndesite porphyry, con-
te, epidote, and seri-
field c.
rity for andesite, tra-
c dacite at pressures
emperatures up to
2. As can be seen,
t there is tenfold in-
er each 100° C.
f variation of σ = f(P)
500° C outlines a
ch extrinsic conductivity
ctivity. The isobars,
vation energy E_0 of
the values of σ_0 are
ssure of 1 atm the
 in the temperature
800, and 800 to 1100° C
ó to 0.84, and 1.8 to
 -4.5, -2.8 to -3.5,
$^{-1}$, respectively (the
not shown in Fig. 3).
ture range of 200 to
E_0 is 0.73 eV and at
v.

that the volcanic rocks
übit fairly high resis-
! with aqueous NaCl
f 0.2 to 12.3 kb in the
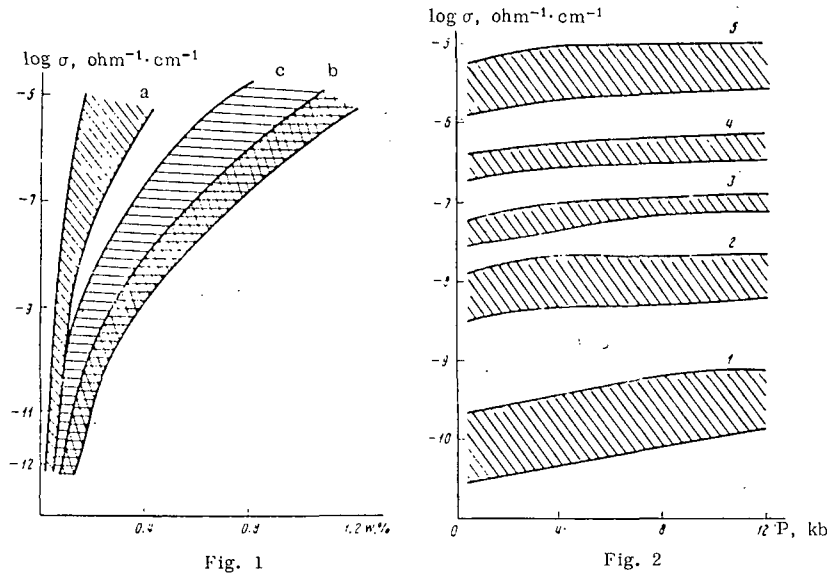range, they exhibit

Fig. 1

Fig. 2

Fig. 1.   Relation σ = f(W); concentration of NaCl solution = 3 g/liter; explanation in the text.

Fig. 2.   Dependence of the range of σ = f(P) of rocks on temperature (°C): 1 – 200°, 2 – 300°, 3 – 400°, 4 – 500°, 5 – 600°.
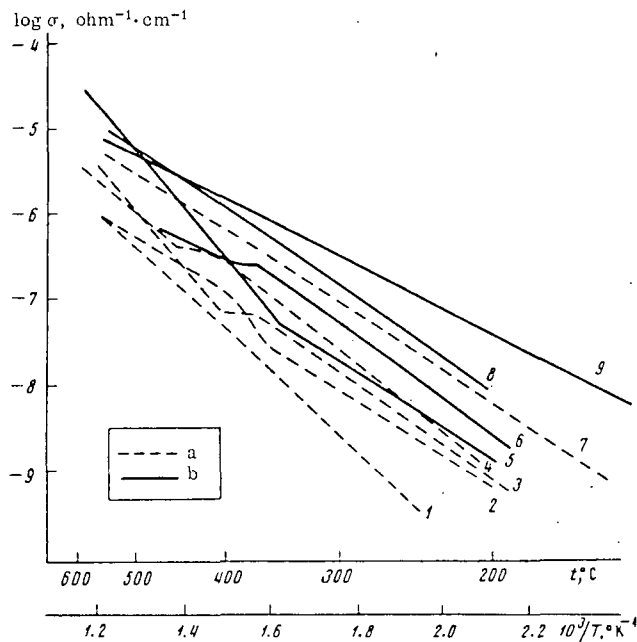

Fig. 3.   Relationship σ = f(t) at various pressures: a – 0.5 kb, b – 12 kb.   1 – alunite rock (sp. 699), 2 – hornblende andesite (sp. 302), 3 – diorite porphyry (hornblende andesite porphyry, sp. 84), 4 – granodiorite (sp. 2551), 5 – sp. 302, 6 – sp. 84, 7 – dacite porphyry (sp. 60), 8 – sp. 2551, 9 – sp. 60.

lower σ than rocks of similar composition from the Caucasus and in the Baikal region [10].
We believe that the high-resistivity [11] rocks of the Tashkent zone are a better medium for accumulation of electric charges upon increase in stress. This additional electric charge is probably promoted by intensive sericitization of the rocks, which, according to Rozanov and Timchenko [12] reduces their mechanical strength, makes them brittle, and susceptible to increased fracturing.

It follows from the analysis of experimental data [9, 10, 13, 15-17] that in those seismic zones of the crust in which compressional stresses predominate at depth, resistivity of the rocks must decrease sharply because extrusion of solutions from closed pores and fractures into open "main" channels, formed during plastic deformation of rocks.

Large changes in conductivity of metamorphic rocks observed during dehydration under various thermodynamic conditions [3, 4] suggest that electrometry is a promising method for prediction of deeper earthquakes [12]. It should be noted that dehydration and other physicochemical processes occurring under stress promote the concentration of the more mobile elements, alkalies and iron, and this tends to decrease the electrical resistance of the rocks [1, 12]. This is important, given the new data that indicate an increase of porosity and microfracturing of rocks during plastic deformation under nonhydrostatic stress [14, 15].

We conclude that, together with seismographic studies, tectonics of the crust and investigations of mechanical and chemical processes in it, recording of variation in electrical resistance of rocks in seismic regions should contribute to the solution of the problem of prediction of earthquakes. We believe that further investigations of resistivity of rock samples of different kinds under complex stresses would be useful for interpretation of data obtained on natural outcrops.

Received November 11, 1974

REFERENCES

1. Ulomov, V. I. Dinamika zemnoy kory Sredney Azii i prognoz zemletryaseniy (Dynamics of the Earth's Crust in Soviet Central Asia and Prediction of Earthquakes), Tashkent, 1974.

2. Tashkentskoye zemletryaseniye 26 aprelya 1966 g (The Tashkent Earthquake of April 26, 1966), Tashkent, 1971.

3. Bondarenko, A. T. Doklady Akad. Nauk SSSR, 208, No. 5, 1973.

4. Bondarenko, A. T. Doklady Akad. Nauk SSSR, 209, No. 1, 1973.

5. Volarovich, M. P., E. I. Bayuk et al. Fiziko-mekhanicheskiye svoystva gornykh porod i mineralov pri vysokikh temperaturakh i davleniyakh (Physical and Mechanical Properties of Rocks and Minerals under High Pressures and Temperatures), Nauka Press, 1973.

6. Sadovskiy, M. A. Vestn. Akad. nauk SSSR, No. 11, 1971.

7. Barsukov, O. M. Fizika Zemli, No. 7, 1968.

8. Barsukov, O. M. Ibid., No. 10, 1973.

9. Bondarenko, A. T., M. Kh. Bakiyev and Melis Kh. Bakiyev. In: Fizicheskiye svoystva gornykh porod pri vysokikh davleniyakh i temperaturakh (Physical Properties of Rocks at High Pressures and Temperatures), Nauka Press, Tbilisi, 1974.

10. Parkhomenko, E. I. and A. T. Bondarenko. Elektroprovodnost' gornykh porod pri vysokikh davleniyakh i temperaturakh (Electrical Conductivity of Rocks at High Pressures and Temperatures), Nauka Press, 1972.

11. Vorob'yev, A. A., E. K. Zavadovskaya and A. V. Kuz'mina. Zapasennaya energiya v shchelochnogaloidnykh soyedineniyakh (Energy Accumulated in alkali Halide Compounds), Tomsk, 1969.

12. Rozanov, Yu. A. and I. P. Timchenko. Geol. rudn. mestorozhd., No. 3, 1965.

13. Mutaliyev, N. Uzb. geol. zhurn., No. 1, 1971.

14. Luchitskiy, I. V. et al. In: Fizicheskiye svoystva gornykh porod pri vysokikh davleniyakh i temperaturakh (Physical Properties of Rocks at High Pressures and Temperatures), Tbilisi, 1974.

15. Marmorshteyn, L. M., F. Z. Rafayevich and A. A. Khalafov, Ibid.

16. Dobrynin, V. M. Fizicheskiye svoystva neftegazovykh kollektorov v glubokikh skvazhinakh (Physical Properties of Oil and Gas Reservoirs in Deep Wells), 1965.

17. Parkhomenko, E. I., E. B. Stefankevich and I. M. Vysokova. Fizika Zemli, No. 5, 1972.

Electric and Caliper Logs as Lithologic Indicators in Volcanic Rocks, Nevada Test Site

R. P. SNYDER

U.S. Geological Survey, Federal Center, Denver, Colorado

ABSTRACT

Electric logs are being used on Pahute Mesa at the Nevada Test Site for preliminary identification of volcanic rock units penetrated by drill holes. Induced and produced water in the drill holes have essentially the same resistivity, so the spontaneous potential curve is negated; and the resistivity curves measure, in effect, the pore space of the rock Degree of welding or amount and kind of alteration affect the pore space and, therefore, the resistivity. In general, resistivities are lowest in the bedded tuffs and increase proportional to welding in ash-flow tuffs, and are greatest in rhyolitic lava flows.

Caliper logs can be used to locate lithologic zones which will tend to slough or cave. These zones are the poorly indurated ash-fall tuffs, vitric and highly fractured ash-flow tuffs and rhyolites. Zeolitized ash-flow and ash-fall tuffs and unfractured rhyolites are competent.

INTRODUCTION

The U.S. Geological Survey, at the request of the Atomic Energy Commission, is evaluating volcanic rocks as test media at the Nevada Test Site. Of prime importance is lithologic identification of rock units penetrated by drill holes on Pahute Mesa.

Although numerous down-hole geophysical logs are used by various agencies participating in the Atomic Energy Commission program, in this paper only electric and caliper logs are considered as aids in interpreting volcanic lithology in the subsurface.

117

ELECTRIC LOGS

The quantitative interpretation of electric logs in these volcanic rocks is significantly different from the approaches suggested in the interpretation charts of the geophysical logging companies. The volcanic rocks at the depth of interest (below 2000 ft) are generally water saturated, and hydraulic tests indicate no large differences in produced-water resistivities in drill holes of the Pahute Mesa area. The SP (self-potential) log obtained in conjunction with the electric log exhibits little or no character and is of no use as an aid in lithologic interpretation. This absence of character is attributed to the lack of contrast in activity between drilling fluid and formation water which exists because water from nearby drill holes or from the hole being drilled is used as the drilling fluid. Drilling mud is seldom used because of its harmful effect in regard to hydraulic tests.

The electrical resistivity of the Pahute Mesa volcanic rocks is a function of the nature and amount of fluid in the interconnected pore space. As the rock matrix may be considered an insulator, lithology is inferred indirectly on the basis of resistivity. The resistivity of the Pahute Mesa volcanic rocks may be considered as related chiefly to two factors. The first is processes of emplacement by which porosities (amount of water present) are affected. For example, the ash-fall tuffs generally exhibit greater porosity than the flow rocks; consequently a lower resistivity may be expected in the ash-fall tuffs. Also, in the flow rocks, as welding increases, pore space
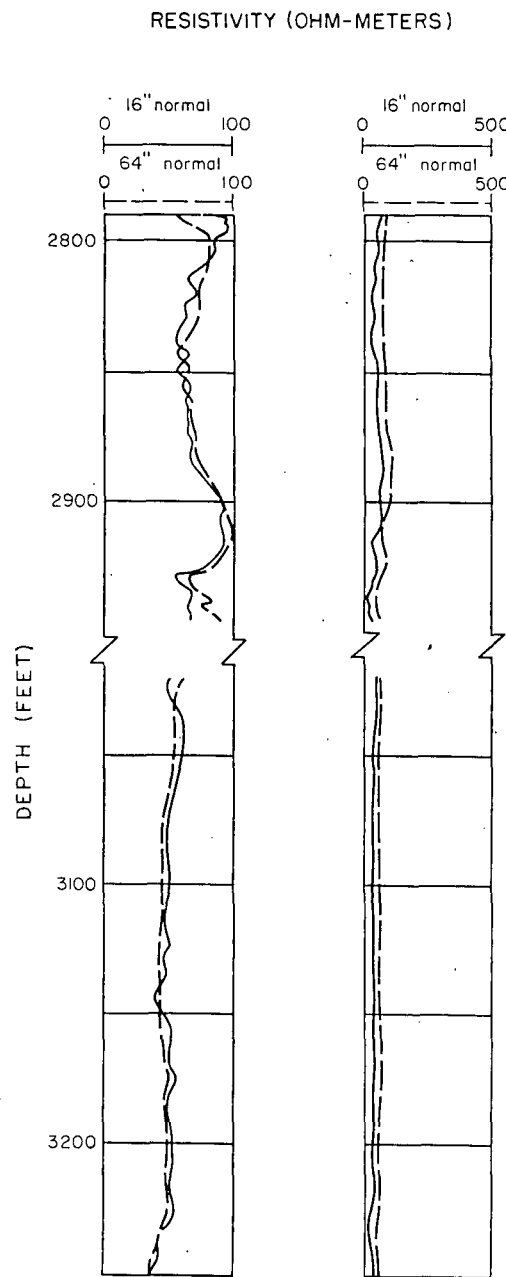
decreases, resulting in hig[...] processes, mainly alterati[...] water ion contents incre[...] resistivity. The lowering [...] volcanic rocks on Pahute saturated formations of [...] are equivalent to, and de[...] and the amount of inter[...] tions, however, measured pore water resistivity bec[...] Consequently, in zones [...] lower measured resistiviti[...]

Bedded ash-fall tuffs [...] than 100 ohm-meters. Fi[...] tions (Paintbrush Tuff) [...] additional detail.

Ash-flow tuffs have zo[...] matic representation of th[...] section of a simple coolin[...] dered at the top, bottom[...] zones. The lower partia[...] thinner than the upper c[...] increases progressively u[...] tion, through the partia[...] welded zone.

The electric log of a [...]

RESISTIVITY (OHM-METERS)

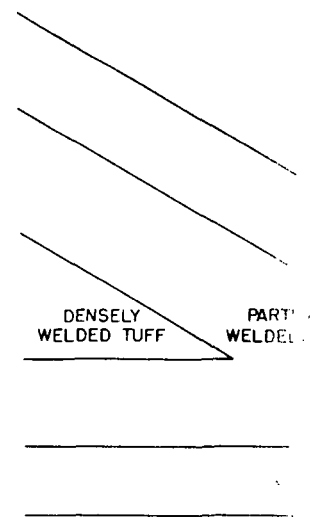Figure 1. Typical electric log resistivities in bedded ash-fall tuff.

Figure 2. Modified cro[...] ash-flow tuff (*after* Smith, 1[...]

decreases, resulting in higher resistivities. The second factor is environmental processes, mainly alteration such as zeolitization and argillization where pore-water ion contents increase with increasing alteration, causing a decrease in resistivity. The lowering of resistivity, due to alteration, is common in all the volcanic rocks on Pahute Mesa. Other things being equal, in unaltered water-saturated formations of equivalent porosity, measured formation resistivities are equivalent to, and dependent upon, the resistivity of the produced water and the amount of interconnected porosity of the rock. In unaltered formations, however, measured produced water resistivity generally exceeds actual pore water resistivity because the bound ions have remained in the rock pores. Consequently, in zones of equivalent porosity, altered intervals tend to have lower measured resistivities.

Bedded ash-fall tuffs beneath Pahute Mesa have resistivities generally less than 100 ohm-meters. Figure 1 shows the electric log of two bedded tuff sections (Paintbrush Tuff) in drill hole UE2Od. The more sensitive scale gives additional detail.

Ash-flow tuffs have zones exhibiting various degrees of welding. A diagrammatic representation of the ideal ash-flow is shown in Figure 2. The type cross section of a simple cooling unit has a densely welded zone in the center, bordered at the top, bottom, and distal edges by partially welded and nonwelded zones. The lower partially welded and nonwelded zones are usually much thinner than the upper counterparts or they may be missing entirely. Porosity increases progressively upward and downward from the densely welded portion, through the partially welded zone, and into the nonwelded to slightly welded zone.

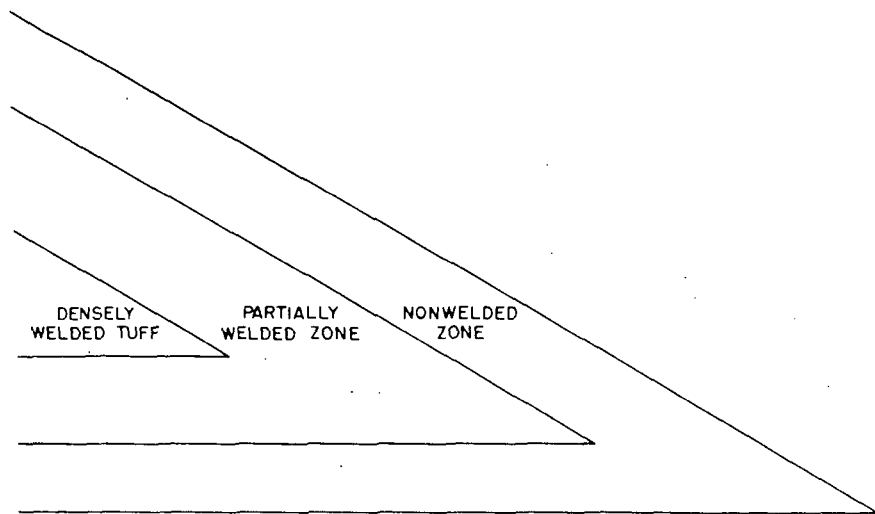The electric log of a section of an ash-flow tuff (Tiva Canyon Member,

DENSELY WELDED TUFF   PARTIALLY WELDED ZONE   NONWELDED ZONE

Figure 2. Modified cross section showing zonal variations of a simple cooling unit, ash-flow tuff (*after* Smith, 1960).

Paintbrush Tuff) is shown in Figure 3. The resistivities decrease upward and downward from a central zone of dense welding, through a moderately welded surrounding zone, and into the encasing nonwelded to slightly welded zone at the top and bottom of the flow. The nonwelded section is thinnest at the bottom of the flow. In the nonwelded to slightly welded zone, resistivities are generally less than 100 ohm-meters, overlapping with those of ash-fall tuffs, but tending to be closer to 100 ohm-meters. Moderately welded ash-flows range in resistivity from about 100 to 200 ohm-meters; densely welded ash-flows, from 200 to more than 1000 ohm-meters in very dense vitric sections. The boundary between slightly welded and moderately welded tuff or between moderately welded and densely welded tuff cannot be picked accurately on a resistivity log because of generally gradational contacts, but by the use of drill cuttings or core it can be picked within 10 ft. At a depth of 2775 ft, as shown in Figure 3, the apparent resistivity dropped suddenly from about 90 ohm-meters (using the 64-inch normal curve) to about 30 ohm-meters. This rapid change in apparent resistivity indicates a change in rock type, in this case from an ash-flow to an ash-fall tuff. This type of resistivity change differs from the above-mentioned change in an ash-flow tuff where the resistivity changes gradually through layers having varying degrees of welding. Thus, contacts between rocks having different apparent resistivities can be picked within 2 to 5 ft, whereas contacts between rocks having gradational resistivity boundaries are picked by use of drill cuttings and so accuracy in picking contacts is dependent upon the speed with which the cuttings are brought to the surface.

The rhyolitic rocks underlying Pahute Mesa have apparent resistivities ranging from 100 to more than 1000 ohm-meters. Figure 4 illustrates typical resistivities through a rhyolite section (unnamed rhyolite of Dead Horse volcanic center). The 64-inch normal curve indicates a reading of about 2000 ohm-meters for both rhyolites. The abrupt shifts in the log at about the 3560- and 3935-ft levels indicate lithologic changes. There is a scale
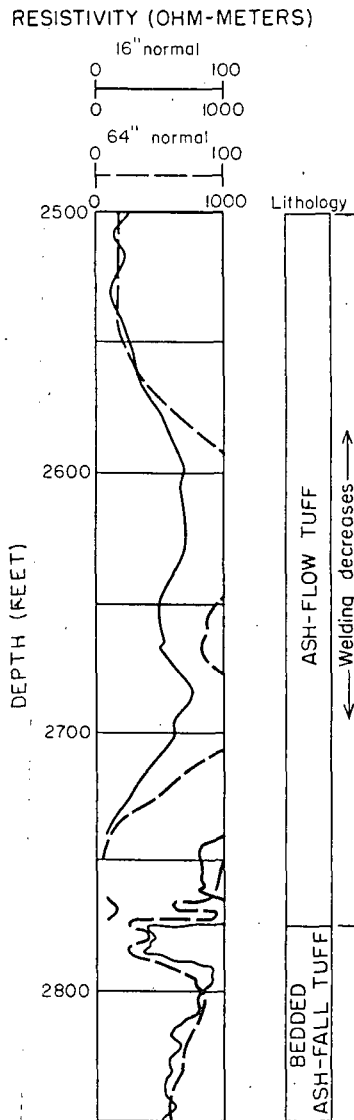

Figure 3. Effect of welding on the resistivity of ash-flow tuff.
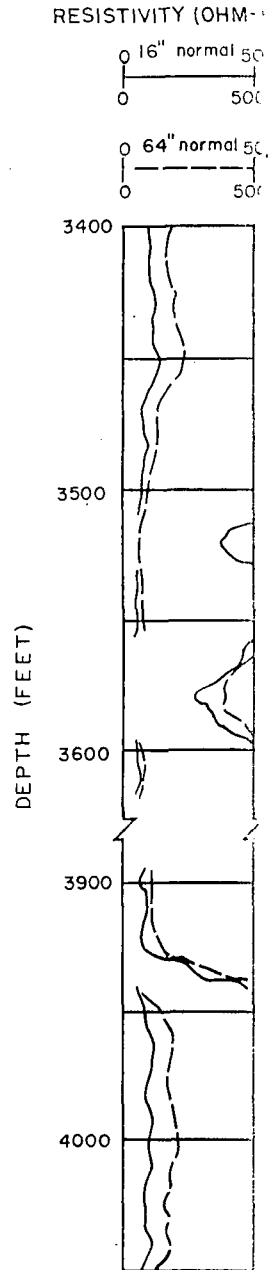
Figure 4. Electric log in rhyolitic flow rocks ar. tuff.

RESISTIVITY (OHM-METERS)

0 16" normal 500

0 5000

0 64" normal 500

0 5000

Lithology

RESISTIVITY (OHM-METERS)

0 16" normal 500

0 5000

0 64" normal 500

0 5000

Lithology

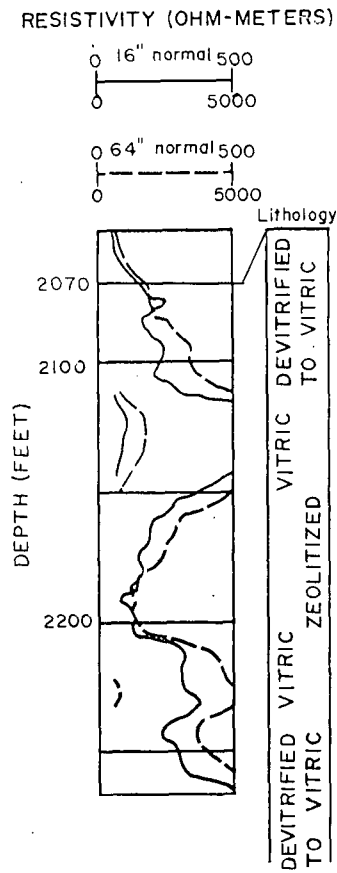Figure 5. Electric log resistivities in a rhyolitic lava flow illustrating resistivity changes caused by alteration.

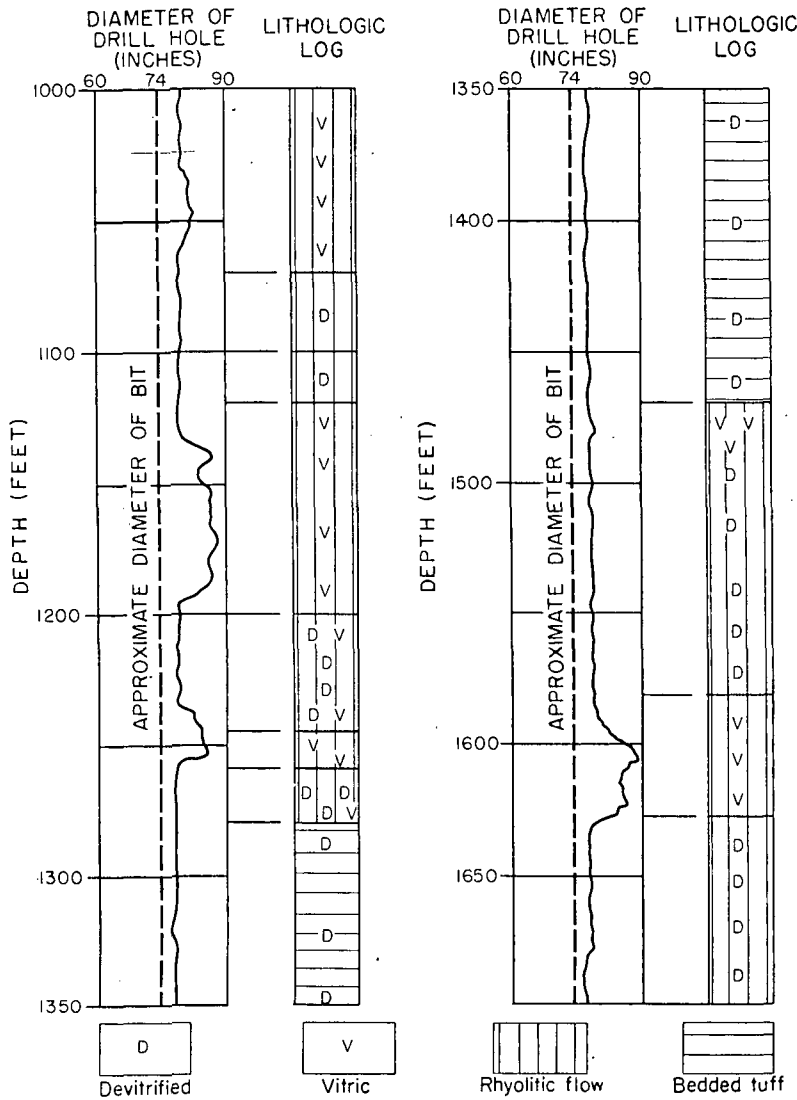Figure 4. Electric log obtained in rhyolitic flow rocks and welded tuff.

Figure 6. Caliper and abridged lithologic log of U20g drill hole shows most vitric zones more susceptible to caving than devitrified zones.

Figure 7. Caliper log sho
dency of bore hole to slou₍
fall tuffs, and to stand in r₍

or decrease gradually be₍
    The illustrations indic.
should be emphasized ₍
available cuttings and co₍

    Caliper logs, in additio .
lithologic indicators, part

change between the upper and lower portions of the log; above the break the log is on the 5000-ohm-meter scale, and below the break the log is on the 500-ohm-meter scale.

The more vitric a rock, the higher its resistivity because the unaltered rock has very little porosity. As alteration changes the rock from vitric to zeolitized (or argillized) the resistivity becomes lower. Figure 5 illustrates the varying resistivities through a section of alternating vitric (fresh) and zeolitized (altered) rhyolite (rhyolite of Area 20). Resistivities generally increase

Electric logs can be us. ·
the field geologist in th₍
holes. Various volcanic r₍
by the electric log. Varia₍
in these ranges. As por

or decrease gradually because of gradual increases or decreases in alteration.

The illustrations indicate a sizeable overlap in resistivity values, and it should be emphasized that interpretation requires careful examination of available cuttings and cores.

CALIPER LOGS

Caliper logs, in addition to being hydrologic and drilling aids, are useful as lithologic indicators, particularly in some of the large-diameter (4 to 6 ft) drill holes. Until recently, none of the standard geophysical logging tools had been successfully adapted for use in these holes. Now a decentralized resistivity tool has been successfully used in at least two large-diameter holes.

A section of rhyolite and bedded tuff penetrated by a large-diameter drill hole is shown in Figure 6. Above the water table vitric rocks tend to cave more readily than devitrified or zeolitized rocks. Includ'd in the vitric rock classification are vitrophyres of both ash-flow tuffs and rhyolites as well as vitric, bedded, ash-fall tuffs. As a rock becomes devitrified, cementation generally increases, so in most altered rocks there is little or no caving (Fig. 7). In general, the denser rocks, ash-flow tuffs, and rhyolites contain more fractures than do the less dense ash-fall tuffs, and if these fractures are close enough together some caving may result.
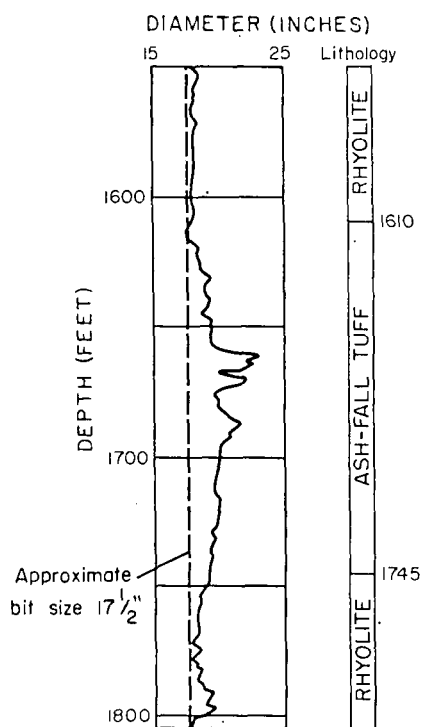
Figure 7. Caliper log showing tendency of bore hole to slough in ashfall tuffs, and to stand in rhyolite.

CONCLUSIONS

Electric logs can be used, with care, to indicate lithology and thereby assist the field geologist in the identification of volcanic rocks penetrated by drill holes. Various volcanic rocks have ranges of apparent resistivities as recorded by the electric log. Variation in porosity seems to be the major factor involved in these ranges. As porosity decreases, apparent resistivity increases; thus

bedded ash-fall tuffs have the lowest apparent resistivities, ash-flow tuff apparent resistivities increase as welding increases, and rhyolitic lava flows with very little porosity have high apparent resistivities.

As alteration (devitrification, zeolitization, and argillization) increases, apparent resistivities decrease in any of the volcanic rocks.

Caliper logs often discriminate between different lithologies. Soft, vitric ash-fall tuffs and vitric flow rocks tend to cave as do highly fractured flow rocks. Well-indurated, altered, ash-fall tuffs and slightly fractured devitrified flow rocks tend not to cave. The geologist must have drill cuttings and core before he finally decides as to the lithology, but electric logs and caliper logs can augment rock identification which may be based on sketchy cutting returns.

REFERENCES CITED

Smith, R. L., 1960, Zones and zonal variations in welded ash flows: U.S. Geol. Survey Prof. Paper 354-F, p. 149-159.

Applications
in Volcani

U.S. Geological

Electric logs are the
tacts in volcanic rocks
electric log, of several
between an ash-flow tuff
are most useful in the qua
ship exists between sonic
Acoustic logs using full-
Young's modulus values
possible to determine ma
rock types by using only a

For several years the
interpretation of geophysi
Test Site. We have utiliz
have served as consultan
in borehole investigations
ging programs in these in
four major categories.
(1) Lithologic identifi
logs as lithologic indicato
log interpretation.
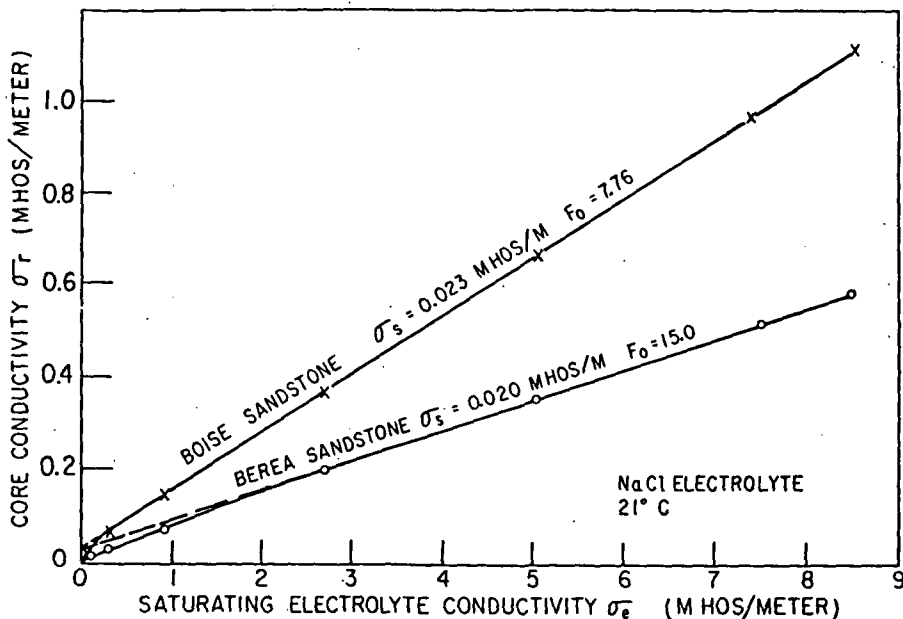
FIG. 7. Core conductivity versus saturating electrolyte conductivity.

tortuosity coefficient t as shown by equation (B18):

$$\theta = \cos^{-1}(1/t).\qquad (B18)$$

The proof of equation (B18) is interesting, as it depends on the equivalence (Wyllie, 1954; Pirson, 1958) of surface porosity and volume porosity.

Surface porosity ϕ_s is defined as the ratio of the cross-sectional area of the pore space voids to the total cross-sectional area of the rock specimen. Hence, in Figure 8 (cf. Figure 9), the surface porosity describes the ratio of the elliptical cross-sectional area[2] $\pi R_e R_p$ of the equivalent electrolyte path to the cross-sectional area of the core $\pi R_r{}^2$, i.e.,

$$\phi_s = \frac{R_p R_e}{R_r{}^2}.\qquad (B19)$$

The volume porosity ϕ_v describes the ratio

[2] Perpendicular to the core axis.

FIG. 8. Idealistic partial longitudinal section of a rock core (cf. Figure 9). R_e = true radius of circular equivalent electrolyte path area; R_p = major axis of elliptical area of electrolyte path perpendicular to mean current flow; R_r = radius of rock core.

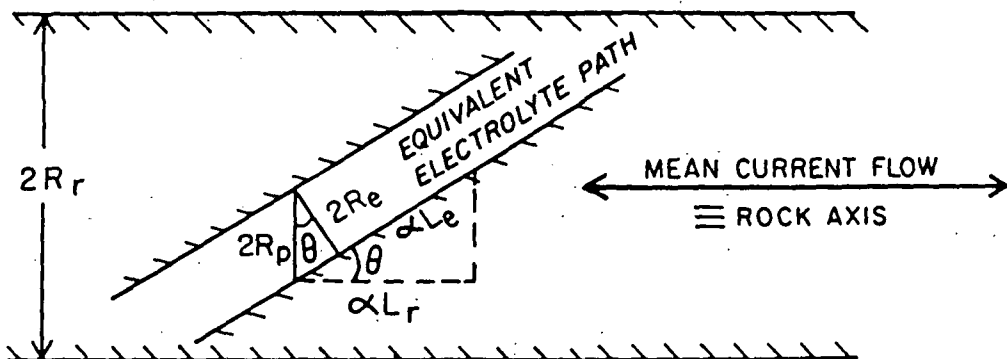of the total volume of the pore paths to that of the rock, i.e.,

$$\phi_e = \frac{\pi R_e^2 L_e}{\pi R_r^2 L_r}. \qquad (B20)$$

The right hand sides of equations (B19) and (B20) can be equated to obtain the identity

$$R_e/R_p = L_r/L_e. \qquad (B21)$$

Since, by definition, $\theta = \cos^{-1}(R_e/R_p)$ and $t = L_e/L_r$, it follows that equation (B18) is valid.

Thus, we see that the equating of surface porosity to volume porosity necessitates that the divergence angle θ be an alternative representation of the tortuosity coefficient t. This concept is indicated in Figure 8, where we have made

$$\cos\theta = \frac{2R_e}{2R_p} = \frac{\alpha L_r}{\alpha L_e} \equiv \frac{L_r}{L_e} = 1/t. \qquad (B22)$$

Figure 8 can also be used to illustrate the relation between porosity and the diminution coefficient. From equation (B10), we see that the latter may be represented as

$$d = \frac{\pi R_e^2}{\pi R_r^2} = \frac{R_e^2}{R_r^2}. \qquad (B23)$$

Compare this with the surface porosity as given by equation (B19). We see that the porosity ϕ will always be larger than the diminution coefficient d except for the one case where the angle of divergence is zero; in this case R_e and R_p will be identical as will be ϕ and d.

The foregoing has demonstrated that the pore geometry of a porous rock can be described in terms of t, d and θ. Figure 9, for example, represents an actual rock core specimen described by Fraser and Ward (1963). In this figure, the accordian-like pore structure is defined by t, d and θ, and is equivalent electrically to the actual pore structure.

4. Relations between Porosity and Formation Factor

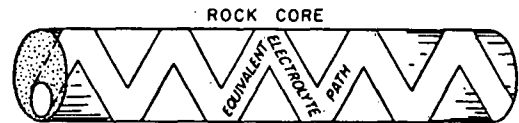The formation factors of rocks, as defined by equation (B11), are observed to increase as

FIG. 9. Graphical representation of electrical pore space geometry of Bandera sandstone; $t=2.28$, $d=0.074$, $\theta=64°$.

the porosities decrease. This is logical since a less porous (saturated) rock contains less conducting electrolyte than a more porous rock. However, the formation factors of a suite of rocks are not related uniquely to their corresponding porosities. In fact, two rocks of identical porosity can have formation factors which vary by 30 percent or more. This is due to the many pore configurations possible for a given pore volume.

In spite of this inherent complication, it has been found that the formation factors of a suite of rocks can be crudely related to their corresponding porosities according to the following equation:

$$F = \phi^{-m}. \qquad (B24)$$

This is known as Archie's Law and seems to be a reasonable approximation for many rocks. The cementation factor is called "m." The greater the cementation, the larger the value of m between the practical limits $1.3 < m < 2.3$.

Usually we find the following:

For slightly consolidated sandstones $F = \phi^{-1.4}$
For consolidated sandstones $F = \phi^{-1.7}$
For limestones and dolomites $F = \phi^{-2.0}$

A more general relation is the Winsauer equation

$$F = c\phi^{-k}. \qquad (B25)$$

F and ϕ may be obtained in the laboratory on cores. The Archie and Winsauer equations have found more utility in petroleum engineering than in mineral exploration. However, they do demonstrate the importance of porosity in determining resistivity for any rock.

Since ϕ is pressure dependent, then both F and ρ_r are pressure dependent. Thus, ρ_r can be expected to increase with depth below the
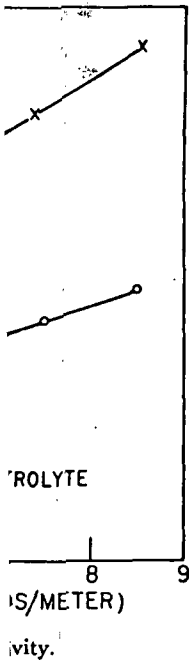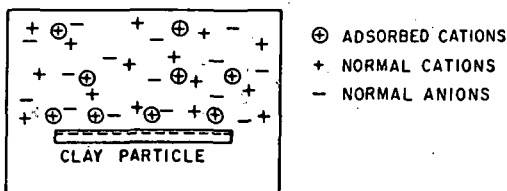
FIG. 10. Diagrammatic representation of ions adsorbed on clay particle.

surface until a horizon is reached where the rock minerals become semiconductive by virtue of a high temperature (in the order of 1,100°C). This would appear to occur at a depth of about 70–80 km (Cantwell, 1960).

5. The Effect of Clay on Rock Resistivity

At this juncture we will consider only the classical petroleum engineering approach to sedimentary rocks containing clay particles (i.e., "dirty sands"). Later the concept will be broadened. A clay or shale particle acts as a separate conducting path additional to the solution path. At the low frequencies of alternating current employed in petroleum well logging, it is customary to consider the impedance of the clay as being purely resistive. This resistance is usually substantially lower than the mineral grain resistance. The origin of this abnormally high clay mineral conductivity lies in the double layer of adsorbed cations as shown in Figure 10. The cations are required to balance the charge due to substitution within the crystal lattice, and to broken bonds (Grim, 1953). The finite size of the cations prevents the formation of a single layer. Rather, a "double layer" is formed; it consists of a "fixed layer" immediately adjacent to the clay surface and a "diffuse layer" which drops off in density exponentially with distance from the fixed layer. The diffuse layer, in contrast to the fixed layer, is free to move under the influence of an applied electric field. The cations of the diffuse layer add to the normal ion concentration and thus increase the density of charge carriers. The net result is an increased "surface conductivity." Although clay minerals exhibit this property to a high degree because of their large ion exchange capacity, all minerals exhibit it to a minor extent. All rocks con-

taining clay minerals possess an abnormally high conductivity on this account.

The effect of disseminated clay or shale on rock resistivities becomes increasingly important as the conductance through the pores diminishes. Increased alteration, such as chloritization, kaolinitization, serpentization, gives rise to increased surface conductivity. This is particularly evident in sheared serpentinite and other ultrabasic rocks, but is rarely evident in granitoid rocks which, when sheared, suffer mylonitization, i.e., production of minimum surface area per unit volume of mineral grains.

The conductivity of clay minerals is dependent on both solution composition and normality (Berg, 1952; Wyllie, 1955). However, above a certain normality characteristic of the rock specimen, the conductivity of the clay minerals apparently becomes constant; this value represents the maximum conductivity of the clay minerals. If we could measure directly this actual maximum clay mineral conductivity, the value could be designated σ_{so}. However, in rocks, we can only measure the apparent maximum value σ_s.

Returning to Figure 7, we see that there is a linear relation between rock conductivity and saturating electrolyte conductivity, for large values of electrolyte salinity, although not for low salinities. This plot implies that the projected straight line intercept on the ordinate represents the observed or apparent maximum conductivity of the conductive solids σ_s since, at this point, the rock is saturated with pure nonconducting water. The equation which fits the straight line portions of the curves of Figure 7 is as follows:

$$\sigma_r = \frac{\sigma_e}{F_o} + \sigma_s \qquad (B26)$$

where σ_r, σ_e and σ_s represent the observed conductivities of the rock, electrolyte, and *conductive solids as distributed in the core*, respectively; and F_o (the inverse of the slope) is termed the true formation factor of the rock.

Equation (B26) states that the actual conductivity of the rock is equal to the theo-

ss an abnormally
count.
d clay or shale on
creasingly impor-
hrough the pores
eration, such as
on, serpentiniza-
l surface conduc-
vident in sheared
basic rocks, but is
ocks which, when
ion, i.e., produc-
rea per unit vol-

r minerals is de-
composition and
llie, 1955). How-
ality characteris-
e conductivity of
ly becomes con-
s the maximum
erals. If we could
l maximum clay
value could be
n rocks, we can
maximum value

) see that there is
ck conductivity
conductivity, for
alinity, although
plot implies that
intercept on the
rved or apparent
the conductive
the rock is satu-
ting water. The
ght line portions
follows:

(B26)

nt the observed
electrolyte, and
ted in the core,
erse of the slope)
n factor of the

hat the actual
qual to the theo-

---

retical rock conductivity assuming only ionic conduction *plus* the conductivity of the conductive solids. This means that, empirically, the conductive solids are in parallel with the electrolyte paths for clay-containing sandstones.

It is important to realize that the σ_s from Figure 7 does not give a true conductivity σ_{s0} for the conductive solids. This is because a maze of interconnected tortuous paths composed of a complex series-parallel arrangement of electrolytic and solid conducting components *cannot* permit the true conductivity of the conductive solids σ_{s0} to be determined by any method of interpretation of monofrequency electrical data. Rather, this value of σ_s is simply the *excess* conductivity of the rock system with respect to the saturating electrolyte. Empirically, this excess conductivity acts in parallel with the normal rock ionic conductivity and becomes increasingly significant at low electrolyte conductivities.

6. Frequency-Dependence of Conductivity: Induced Polarization

To this point in our discussion it has been tacitly assumed that resistivity—or its inverse, conductivity—is independent of the frequency of the applied electric field. In many sedimentary rocks this is true, but in most igneous and metamorphic rocks and in sedimentary rocks containing clay or metallic minerals it is not true. The causes of this frequency dependence or dispersion include normal dielectric effect, electrokinetic response of air bubbles in the rock pores, electrode polarization, and membrane polarization (Mayper, 1959). The normal dielectric effect is usually not appreciable. The electrokinetic effect may be minimized in the laboratory by vacuum saturation of rock specimens (Keevil, 1961), while in the field it is an unknown but probably unimportant contributor because of the increased solubility of air in water as hydrostatic head is increased with depth. Hence only two phenomena shall be described herein: electrode polarization and membrane polarization (Madden and Marshall, 1958; Madden and Marshall,
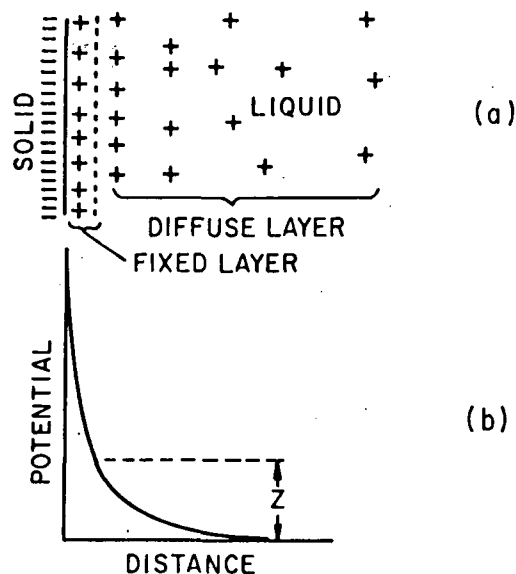
Fig. 11. (a) Hypothetical anomalous ion distribution near a solid-liquid interface; (b) Corresponding potential distribution.

1959a, b, Marshall and Madden, 1959; Keevil, 1961; Keevil and Ward, 1962).

(a) Electrode polarization

Whenever there is a change in the mode of current conduction, e.g. from ionic to metallic, energy is required to cause the current to flow across the interface. This energy barrier can be considered to constitute an electrical impedance. To visualize it, let us digress and consider the ionic double layer which exists at any interface between a solid and a liquid.

The surfaces of most solids possess a very small net attraction for either cations or anions, as we mentioned earlier for clay minerals. Let us now study this in more detail. Immediately adjacent to the outermost solid layer is adsorbed a layer of essentially fixed ions, one or a few molecular layers in thickness (Figure 11(a)). These are not truly exchangeable and, hence, constitute the "fixed layer," although they can often be removed upon application of a strong physical force.

Adjacent to the fixed layer of adsorbed ions there is a group of relatively mobile ions, either of the same or opposite charge, known as the diffuse layer. The *anomalous* number

of ions in this zone decreases exponentially from the fixed layer outward to the normal ion concentration of the liquid. (The normal balanced distribution of anions and cations has been deleted from Figure 11(a) for clarity.) The particular distribution of ions shown is only one of several possible distributions, but it is the most common. The electrical potential across the double layer has been plotted also; the potential drop across the diffuse layer is known as the Zeta potential (Z).

While the fixed layer is relatively stable, the diffuse layer thickness is a function of temperature, ion concentration in the "normal" electrolyte, valency of the ions, and the dielectric constant of the medium. Most of the anomalous charge is contained within a plane distance d from the surface, where (Grahame, 1947)

$$d = [K_e kT/8\pi ne^2v^2]^{1/2} \qquad (B27)$$

n = normal ion concentration of the electrolyte
v = valence of the normal ions
e = elementary charge
K_e = the dielectric constant of the medium
k = Boltzman's constant
T = temperature

The thickness is, therefore, governed by the balance between the attraction of unlike charges at the solid surface and the thermal redistribution of ions. Obviously, increasing n, the salinity, or v, the valence, *decreases* the double layer thickness.

Returning now to polarization at electrodes, it may be stated that there are two paths by which current may be carried across an interface between an electrolyte and a metal (Figure 12). These are called the faradaic and nonfaradaic paths. Current passage in the faradaic path is the result of an electrochemical reaction such as the oxidation or reduction of some ion, and involves diffusion of the ions toward or away from the interface. The charge is carried physically across the interface by conversion of atom to ion or vice versa. In the latter (nonfaradaic) case, charged particles do not cross the interface; rather, current is carried by the charging and

discharging of the double layer. (Recall that the diffuse layer is mobile and may be "thinned" out momentarily by the application of an electric field.) The double layer then behaves as a condenser in series with the resistance of the solution. The nonfaradaic component, thus, may be represented by a simple capacitance insofar as the variation of its impedance with frequency is concerned. However, the nonfaradaic path may become frequency-independent at very high frequencies, when the inertia of the ions inhibits their sympathetic oscillation with frequency.

In the faradaic path, the ion diffusion impedance is not representable in so simple a fashion and, in fact, may not be adequately represented by any combination of fixed capacitors and resistors. It is customarily referred to as the Warburg impedance W and its magnitude varies inversely with the square root of the electrical frequency.

The interfacial impedances of many metal-electrolyte interfaces may be described roughly as follows. Above 1,000 cps, the major part of the electric current is carried across the interface by means of the nonfaradaic path; hence, the interfacial impedance varies with frequency as approximately f^{-1}. As the frequency is lowered, more and more current is carried via the faradaic path, and so the low frequency impedance varies with frequency in the range $f^{-1/2}$ to f^0 depending on the magnitude of the impedance ratio W/R.

Note that the impedance of the circuit of Figure 12 is infinite at zero frequency because the Warburg impedance is expressed
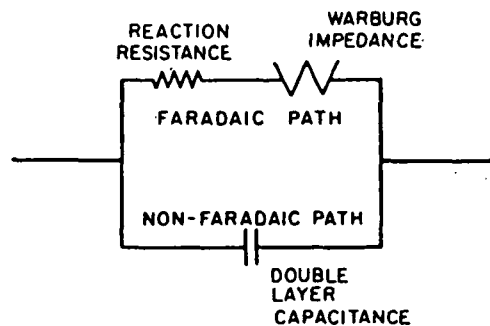

FIG. 12. Circuit analog of interfacial impedance.

ouble layer. (Recall that
s ,mobile and may be
entarily by the applica-
field.) The double layer
ndenser in series with the
lution. The nonfaradaic
ay be represented by a
nsofar as the variation of
frequency is concerned.
adaic path may become
nt at very high fre-
nertia of the ions inhibits
cillation with frequency.
path, the ion diffusion
resentable in so simple a
may not be adequately
combination of fixed
tors. It is customarily
rburg impedance W and
es inversely with the
ctrical frequency.
impedances of many
rfaces may be described
Above 1,000 cps, the
ctric current is carried
by means of the non-
, the interfacial imped-
ency as approximately
, is lowered, more and
d via the faradaic path,
ency impedance varies
range $f^{-1/2}$ to f^0 depend-
of the impedance ratio

dance of the circuit of
e at zero frequency
impedance is expressed

WARBURG
IMPEDANCE

C PATH

DAIC PATH
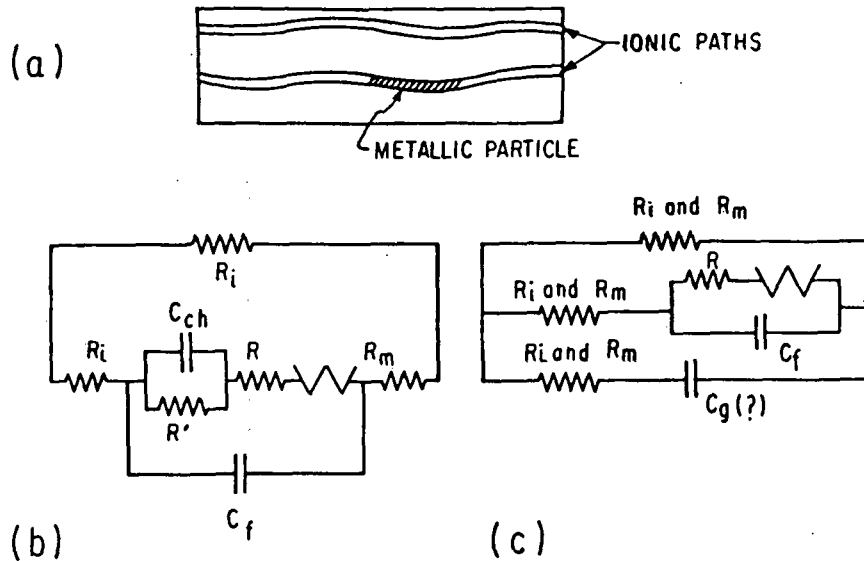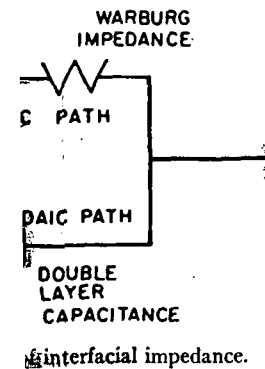
DOUBLE
LAYER
CAPACITANCE

interfacial impedance.

FIG. 13. Simplified representation of mineralized rock (a), and the corresponding equivalent circuit (b); (c) equivalent circuit representative of all mineralized rocks, massive to disseminated.

as $k(1+i)/\sqrt{f}$, where k is a constant, and the capacitive reactance, of course, as $i/2\pi fC$. It is important not to confuse zero frequency with direct current in this circuit, since its resistance to dc is not infinite, but is finite and indeterminate. The ambiguity lies in the derivation (Grahame, 1952) of the Warburg impedance, wherein it is assumed that the reaction products at the interface have no effect on the diffusion impedance and so can be omitted from the derivation. The derivation assumes that it is impossible to carry on such a reaction indefinitely in the same direction because the products of the reaction will accumulate and stop the reaction. Therefore, the interfacial impedance is not defined for direct current by the circuit of Figure 12.

All of the above discussion applies to a pure electrode in a pure electrolyte. The concepts, however, are important in understanding the processes occurring when current is passed through a rock. Any rock sample is "dirty" from the viewpoint of the physical chemist since the electrodes (metallic mineral grains) and electrolytes (pore solutions) are anything but pure. Nevertheless we perhaps are justified in employing equivalent circuits based on pure systems

since a phenomenological explanation for rock behavior results. With this caution, one might suggest the equivalence of the elementary rock system of Figure 13(a) with the equivalent circuit of Figure 13(b), where

W = Warburg impedance
  = $k(1+i)/\sqrt{f}$; k is a constant
C_F = double layer capacitance
C_{CH} = chemical capacitance
R = reaction resistance
R' = a resistance representing second and higher order reactions
R_i = resistance of ionic path
R_m = resistance of metallic vein path or particle

In noting these circuit elements, it must be appreciated that one chemical reaction at the interface may lead to a chain of subsequent reactions involving electrons, ions, and molecules of all reaction products present. At each point of the reaction chain, the accumulation of the reaction product represents a capacitance C_{CH} to the electrode. The escape of the product is achieved either by diffusion, represented by a Warburg impedance W, or by a reaction represented by a resistor R. The product of this reaction in turn follows a

and transition than the
ng the impurity levels.
n in a solid occurs as a
ons moving through the
result of defects in it. The
ion is a missing atom or
chottky defect). The dif-
ancy through the lattice
rt of charge.

process, two energies are
half that required to pro-
ositely charged lattice de-
ht of the potential barrier
nt sites occupied by the
xcitation energy E of the
of these two energies. The
en by the equation

$$= \sigma_0^{-E/kT} \qquad \text{(B76)}$$

ortional to the number of
Frenkel defect may also
nic conductivity; its dif-
same law. Frenkel and
re illustrated in Figure 27.
has estimated E and σ_0,
h of the three conduction
was able to indicate the
e of importance of each
es. Hughes' data is given

mechanism above 1,100°C.
nic because, when an iron
in contact with the mag-
te, iron diffuses into the
ie magnesium.
of the above knowledge to

ad Frenkel defects; ion in box is
efect, ion in box is displaced in
ittel, 1953).

Table 2

Type of Semiconduction	σ_0	E	Range of Importance
Extrinsic	10^{-4} mho/cm	1 ev	600°C.
Intrinsic	10^{-1} mho/cm	3.3 ev	600 to 1,100°C.
Ionic	10^5 mho/cm	3.0 ev	1,100°C.

the explanation of the distribution of electrical conductivity in the mantle is clear only in a general way. The conductivity for mantle rock can be computed from laboratory values of σ_0 and E, *assuming* the temperature distribution is known. The limits of the temperature distribution are estimated in one of two ways: (a) by assuming that the material is everywhere at its melting point except in the outer 700 kms for a maximum, and (b) by assuming that the temperature gradient is adiabatic for a minimum. The gross assumptions involved leave our knowledge of the mantle temperature and conductivity on rather precarious grounds, although there is general agreement in the literature (Runcorn 1956, Lubimova 1958, Jacobs 1956, Verhoogen 1956, Uffen 1952, Lahiri and Price 1939, Tozer 1959, Noritomi 1961). The best estimates of electrical conductivity of the Mantle are derived from studies of geomagnetic fluctuations and the magnetotelluric method (Eckhardt, Larner, and Madden 1963; Srivastava, Douglass, and Ward 1963).

13. Conduction in the Earth's Core

We can reasonably expect the high-temperature conductivity of a metal to be a function of Θ_D and temperature T. Kittel (1953) gives the conductivity of a metal in the form

$$\sigma = \frac{e^2 M k \Theta_D^2}{2p^3 \overline{Q}_s T} \qquad \text{for } T \gg \Theta_D \qquad \text{(B77)}$$

where

$e =$ charge on electron
$M =$ mass of the lattice oscillators
$k =$ Boltzmann constant
$\Theta =$ Debye temperature of lattice $\equiv \hbar\omega/k$
$p = \hbar k =$ electronic momentum

$\overline{Q}_s =$ mean scattering cross section for an isolated ion
$\hbar = h/2\pi$ where $h =$ Planck's constant
$\omega =$ frequency of lattice oscillators

In deriving this formula, the wave function for the electron was taken in a form which neglected modulation by the lattice. Increased pressure will, therefore, modify the wave function so, presumably, we may write, as did Elsasser (1950)

$$\sigma = \frac{C\Theta_D^2}{T} \qquad \text{(B78)}$$

where C lumps the constants and also assumes a dependency on pressure to account for modulation of the electronic wave function. The Debye temperature is found experimentally, and theoretically, to be proportional to the velocity of sound.

Runcorn (1956) modified Elsasser's estimate on the above formula to yield a value of $\sigma \approx 3 \times 10^4$ mhos/cm for the core of earth.

The choice of the high temperature metal theory for prediction of the electrical conductivity of the core is based on the assumption that the core consists of iron or an iron-nickel mixture.

14. Acknowledgments

References Cited

Archie, G. E., 1942, The electrical resistivity log as an aid in determining some reservoir characteristics: A.I.M.E., Trans., v. 146, p. 54–61.

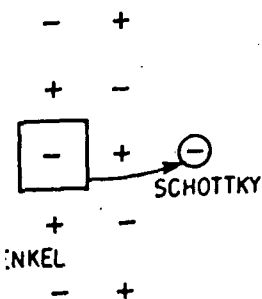Berg, J. W., Jr., 1952, Conductivity study of aqueous kaolin NaCl mixtures: Producers Monthly, v. 16, no. 3, p. 36–41.

Cantwell, T., 1960, Detection and analysis of low frequency magnetotelluric signals: Ph.D. Thesis, Mass. Inst. of Tech.

Collett, L. S., 1959, Laboratory investigations of overvoltage, *in* Overvoltage research and geophysical applications, J. R. Wait, editor: Pergamon Press.

Dakhnov, V. N., 1959, Geophysical well logging; translated from the Russian by G. V. Keller: Colorado School of Mines, Quarterly, v. 57, no. 2, 1962, p. 374.

Eckhardt, D., Larner, K., and Madden, T., 1963, Long period magnetic fluctuations and mantle electrical conductivity estimates: J. Geophys. Res. v. 68, p. 6279.

Elsasser, W. M., 1950, The earth's interior and geomagnetism: Rev. Mod. Phys., v. 22, p. 1.

Evjen, H. M., 1948, Theory and practice of low-frequency electromagnetic exploration: Geophysics, v. 13, no. 4, p. 584.

Fraser, D. C., Keevil, N. B., Jr., and Ward, S. H., 1964, Conductivity spectra of rocks from the Craigmont ore environment: Geophysics, v. 29, no. 5, p. 832–847.

Fraser, D. C., and Ward, S. H., 1963, Electrical pore space geometry of porous media: Univ. of Calif., Inst. of Eng. Res., Rpt. No. MT-63-1, 48 p.

Grahame, D. C., 1947, The electrical double layer and the theory of electrocapillarity: Chem. Rev., v. 41, p. 441–501.

—— 1952, Mathematical theory of the faradaic admittance: Jour. Electrochem. Soc., v. 99, p. 370c–385c.

Crim, R. E., 1953, Clay mineralogy: New York, McGraw-Hill Book Co., Inc.

Hallof, P. G., 1961, Variable frequency induced polarization data compared with drilling results at four properties: Northern Miner, Nov. 30.

Hughes, H., 1955, The pressure effect on the electrical conductivity of peridot: Jour. Geophys. Res., v. 60, p. 187.

Jacobs, J. A., 1956, The earth's interior: Handbuch der Physik, Geophysik I, Springer Verlag, p. 364–400.

Keevil, N. B., Jr., 1961, A laboratory investigation of induced polarization: M.S. Thesis, University of California, Berkeley.

Keevil, N. B., Jr., and Ward, S. H., 1962, Electrolyte activity: its effect on induced polarization: Geophysics, v. 27, no. 5, p. 677–690.

Keller, G. V., 1959, Analysis of some electrical transient measurements on igneous, sedimentary, and metamorphic rocks; Overvoltage research and geophysical applications: New York, Pergamon Press.

Keller, G. V., and Licastro, P. H., 1959, Dielectric constant and electrical resistivity of natural-state cores: U. S. Geol. Surv. Bull. 1052-H.

Kittel, C., 1953, Introduction to solid state physics: New York, John Wiley and Sons, Inc.

Kumar, A., 1962, Induced polarization in sedimentary rocks: M.S. Thesis in Engineering, Univ. of Calif., Berkeley.

Lahiri, B. N., and Price, A. T., 1939, Electromagnetic induction in nonuniform conductors and the determination of the conductivity of the earth from terrestrial magnetic variations: Phil. Trans., Roy. Soc. Lond., Ser. A, v. 237, p. 509.

Lubimova, H. A., 1958, Thermal history of the earth with consideration of the variable thermal conductivity of its mantle: Geophys. Jour., v. 1, p. 115–134.

Madden, T. R., and Marshall, D., 1958, A laboratory investigation of induced polarization: M.I.T. report to A.E.C., RME 3156.

—— 1959a, Electrode and membrane polarization: M.I.T. report to A.E.C., RME 3157.

—— 1959b, Induced polarization, a study of its causes and magnitudes in geologic materials: Final M.I.T. report to A.E.C.

Marshall, D. J., and Madden, T. R., 1959, Induced polarization, a study of its causes: Geophysics, v. 24, no. 4, p. 790–816.

Mayper, V., 1959, The normal effect, *in* Overvoltage research and geophysical applications, J. R. Wait, editor: Pergamon Press, p. 125–158.

Noritomi, K., 1961, Electrical conductivity of rock and the determination of the electrical conductivity of the earth's interior: J. Min. College, Akita Univ. 1, p. 27–59.

Panofsky, W. K. H., and Phillips, Melba, 1962, Classical electricity and magnetism, 2nd Edition: Addison-Wesley Publishing Co., Inc.

Patnode, H. W., and Wyllie, M. R., 1950, The presence of conductive solids in reservoir rocks as a factor in electric log interpretation: A.I.M.E., Trans., v. 189, p. 47–52.

Pirson, S. J., 1958, Oil reservoir engineering: New York, McGraw-Hill Book Company, Inc.

Runcorn, S. K., 1956, The magnetism of the earth's body: Handbuch der Physik, Geophysik I, Springer Verlag, p. 498–532.

Srivastava, S. P., Douglass, J. L., and Ward, S. H., 1963, The application of the magnetotelluric and telluric methods in central Alberta: Geophysics, v. 28, no. 3, p. 426–446.

Tozer, D. C., 1959, Electrical properties of the earth's interior, *in* Physics and chem. of the

:astro, P. H., 1959, Dielec-
lectrical resistivity of nat-
S. Geol. Surv. Bull. 1052-

troduction to solid state
John Wiley and Sons, Inc.
luced polarization in sedi-
S. Thesis in Engineering,
:eley.
rice, A. T., 1939, Electro-
in nonuniform conductors
ion of the conductivity of
:strial magnetic variations:
oc. Lond., Ser. A, v. 237, p.

;8, Thermal history of the
tion of the variable thermal
iantle: Geophys. Jour., v. 1,

iarshall, D., 1958, A labora-
of induced polarization:
:.C., RME 3156.
de and membrane polariza-
o A.E.C., RME 3157.
i polarization, a study of its
ides in geologic materials:
to A.E.C.
Madden, T. R., 1959, In-
a study of its causes: Geo-
p. 790–816.
: normal effect, in Overvolt-
physical applications, J. R.
ion Press, p. 125–158.
Electrical conductivity of
mination of the electrical
: earth's interior: J. Min.
1, p. 27–59.
and Phillips, Melba, 1962,
and magnetism, 2nd Edi-
:ey Publishing Co., Inc.
Wyllie, M. R., 1950, The
.ve solids in reservoir rocks
ectric log interpretation:
189, p. 47–52.
reservoir engineering: New
Book Company, Inc.
i, The magnetism of the
dbuch der Physik, Geo-
erlag, p. 498–532.
iuglass, J. L., and Ward,
iplication of the magneto-
aethods in central Alberta:
i. 3, p. 426–446.
:lectrical properties of the
Physics and chem. of the

earth, v. 3: McGraw-Hill Book Company, Inc.;
p. 414–436,

Uffen, R. J., 1952, A method of estimating the melting point gradient in the earth's mantle: Trans., Amer. Geophys. Union, v. 33, p. 893.

Vacquier, V., Holmes, C. R., Kintzinger, P. R., and Lavergne, M., 1957, Prospecting for groundwater by induced electrical polarization: Geophysics, v. 22, p. 660–687.

Van Vlack, L. H., 1959, Elements of materials science: Reading, Addison-Wesley Publishing Company.

Verhoogen, J., 1956, Temperatures within the earth, in Physics and chem. of the earth, v. 1: New York, McGraw-Hill Book Company, p. 17–43.

Wait, J. R., 1959, The variable-frequency method, in Overvoltage research and geophysical applications, J. R. Wait, editor: New York, Pergamon Press.

Wyllie, M. R., 1955, Role of clay in well-log interpretation, in Clays and clay technology: State of Calif., Dept. of Nat. Res., Bull. 169, p. 282–305.

———— 1954, The fundamentals of electric log interpretation: New York, Academic Press.

References for General Reading

Ananyan, A. A., 1958, Dependence of electrical conductivity on moisture content: Izvestiya, Geophysics Series, no. 4, p. 878–881.

Bleil, D. F., 1953, Induced polarization: a method of geophysical prospecting: Geophysics, v. 18, no. 3, p. 636–661.

Coster, H. P., 1946, The electrical conductivity of rocks at high temperatures: Monthly Notices of Roy. Astron. Soc. Geoph. Supp., 5, p. 193.

Henkel, J. H., 1958, Some theoretical considerations of induced polarization: Geophysics, v. 23, no. 2, p. 299–304.

Henkel, J. H., and Collins, T. C., 1961, Induced polarization in electrolyte saturated earth plugs: Geophysics, v. 22, p. 205–210.

Henkel, J. H., and Van Nostrand, R. G., 1957, Experiments in induced polarization: A.I.M.E., Trans., v. 9, p. 355–359.

Keller, G. V., 1960, Pulse-transient behavior of brine-saturated sandstones: U. S. Geol. Surv., Bull. 1083-D, p. 111–129.

Mandel, P., Jr., Berg, J. W., Jr., and Cook, K. L.,

1957, Resistivity studies of metalliferous synthetic cores: Geophysics, v. 22, no. 2, p. 398–411.

McEuen, R. B., Berg, J. W., Jr., and Cook, K. L., 1959, Electrical properties of synthetic metalliferous ore: Geophysics, v. 29, no. 3, p. 510–530.

Nosske, G., 1959, Eine neue leichte Feldansruestung fuer die induzierte Polarisation mit Gleichstromimpulsen: Zeitschrift fuer angewandte Geologie, Heft 11, p. 528–533.

Parkhomenko, E. I., and Bondarenko, A. T., 1960, Effect of unilateral pressure upon electrical resistance of rock: Izvestiya, Geophysics Series, no. 2, p. 214–219.

Perkins, F. M., Jr., Osoba, J. S., and Ribe, K. H., 1956, Resistivity of sandstones as related to the geometry of their interstitial water: Geophysics, v. 21, no. 4, p. 1071–1084.

Piskunov, L. I., 1958, On a quantitative relation between the dielectric constant and the electrical resistivity of rocks: Izvestiya Geophysics Series, no. 9, p. 658–659.

Rokitansky, I. I., 1959, The nature of induced polarization of ion-conducting soils: Izvestiya, Geophysics Series, no. 7, p. 752–756.

Runcorn, S. K., 1955, The electrical conductivity of the earth's mantle: A.G.U., Trans., v. 36, p. 191.

Schufle, J. A., 1959, Cation exchange and induced electrical polarization: Geophysics, v. 24, p. 164–166.

Sumi, F., 1961, The induced polarization method in ore investigation: Geoph. Prosp., v. 19, no. 3, p. 459–477.

Volarovich, M. P., and Bondarenko, A. T., 1960, A study of electrical resistance in samples of rocks at all-round pressure up to 100 kg/cm²: Izvestiya, Geophysics Series, no. 7, p. 631–635.

Winsauer, W. O., Shearin, H. M., Jr., Masson, P. H. and Williams, M., 1952, Resistivity of brine-saturated sands in relation to pore geometry: A.A.P.G., Bull., v. 36, no. 2, p. 253–277.

Winsauer, W. O., and McCardell, W. M., 1953, Ionic double-layer conductivity in reservoir rock: A.I.M.E., Trans., v. 198, p. 129–134.

Zharkov, V. N., On the electrical conductivity and temperature of the earth's mantle: Izvestiya, Geophysics Series, no. 4, p. 260–266.

Zwikker, C., 1954, Physical properties of solid materials: Interscience Publ., 300 p.

Electrical Conductivities in Oil-Bearing Shaly Sands

M. H. WAXMAN
MEMBER AIME

L. J. M. SMITS

SHELL DEVELOPMENT CO,
HOUSTON, TEX.
KONINKLIJKE/SHELL EXPLORATIE EN
    PRODUKTIE LABORATORIUM
RIJSWIJK, THE NETHERLANDS

ABSTRACT

A simple physical model was used to develop an equation that relates the electrical conductivity of a water-saturated shaly sand to the water conductivity and the cation-exchange capacity per unit pore volume of the rock. This equation fits both the experimental data of Hill and Milburn and data obtained recently on selected shaly sands with a wide range of cation-exchange capacities.

This model was extended to cases where both oil and water are present in the shaly sand. This results in an additional expression, relating the resistivity ratio to water saturation, water conductivity and cation-exchange capacity per unit pore volume. The effect of shale content on the resistivity index-water saturation function is demonstrated by several numerical examples.

INTRODUCTION

A principal aim of well logging is to provide quantitative information concerning porosity and oil saturation of the permeable formations penetrated by the borehole.

For clean sands, the relationships between measured physical quantities and porosity or saturation are well known. However, the presence of clay minerals greatly complicates log interpretation, particularly the electrical resistivity and SP logs, and considerably affects evaluation of hydrocarbon-bearing formations. The conductance and electrochemical behavior of shaly sands and their relation to log interpretation have been studied by many workers. Wyllie[1] and Lynch[2] reviewed this work in some detail.

Virtually all laboratory measurements of electrical resistivity and electrochemical potential of shaly sands published to date are the work of Hill and Milburn.[3] Their measurements were made on about 300 cores covering a large variety of sedimentary rocks, and a wide range of equilibrating NaCl solution concentrations. Hill and Milburn described their conductivity data by an empirical equation in which the shaly sand conductivity C_o was expressed as a function of the solution conductivity C_w and two parameters b and F_{01}. The quantity b was shown to be a measure of the effective clay content of the rock, being approximately proportional to the cation-exchange capacity of the rock divided by its pore volume. The latter ratio is designated as Q_v in this paper and has the dimensions meq/ml or equiv/liter. Q_v is identical with the term representing the concentration of fixed charges in the Meyer-Sievers[4] and Teorell[5] theory of permselective membrane behavior. F_{01} is a formation resistivity factor referred to a hypothetical equilibrating solution resistivity of 0.01 ohm m at 25C,* where clay effects presumably are minimized. F_{01} was correlated to porosity by an Archie-type equation.[6] The Hill-Milburn equation describes their data with a standard deviation of approximately 1 percent and a maximum deviation of ±10 percent.

Shaly sands behave as permselective cation-exchange membranes, their electrochemical efficiencies increasing with increasing clay content. The electrochemical potential data of Hill and Milburn were expressed graphically, and demonstrate that the membrane efficiency (or cation transport number) of these sands is a function only of the b value (i.e., Q_v) and the respective salt concentrations of the two solutions forming the liquid junction in the sand. The diffusion potentials are not dependent on F_{01} or any parameter relating to the porosity or pore geometry of the rock.

The Hill-Milburn resistivity equation correctly predicts a decreasing sand conductivity C_o with decreasing solution conductivity C_w. However, at some low value of C_w, the calculated C_o-C_w function goes through a minimum; with further decrease in C_w, the predicted sand conductivity increases sharply. As pointed out by Hill and Milburn, an increasing value of C_o with decreasing C_w is physically meaningless. Since this occurs below the range of practical values of C_w, the usefulness of the empirical equation is not affected when

---

*This value is four times less than the resistivity of a saturated NaCl solution at 25C.

applied to water-saturated sands. However, as will be discussed later, the equation cannot be extended to oil-bearing shaly sands since the minimum in the C_o-C_w curve then is shifted to higher C_w values.

In this paper an equation for shaly sands is developed which relates the resistivity ratio to water saturation, water conductivity and an independently determined shaliness parameter, using a simple physical model and modern concepts of the nature of the electrical charge of clay minerals.

THE MODEL

The essential features of the shaly sand conductivity plots (C_o vs C_w) are shown in Fig. 1. In the range of dilute equilibrating electrolyte solutions (from 0, to about 0.1 to 0.5 m_{NaCl}), the sand conductivity increases sharply with increasing solution concentration at a greater rate than can be accounted for by the increase in C_w. With further increase in equilibrating solution conductivity, the sand conductivity increases linearly.

The model consists of two resistance elements in parallel, one component consisting of the free electrolyte contained in the pore volume of the rock C_{el} and another resulting from the conductance contribution of the exchange cations associated with the clay C_c. We can write

$$C_{rock} = C_c + C_{el} \quad \cdots \cdots \quad (1)$$

and

$$C_o = xC_e + yC_w \quad \cdots \cdots \quad (2)$$

where C_o, C_e and C_w are the specific conductances of core, clay exchange cations and equilibrating salt solution, respectively; and x and y are appropriate geometric constants. We assume that the electrolyte solution in the porous system has the same electrical conductivity as that for the equilibrating solution, i.e., Donnan effects are neglected.
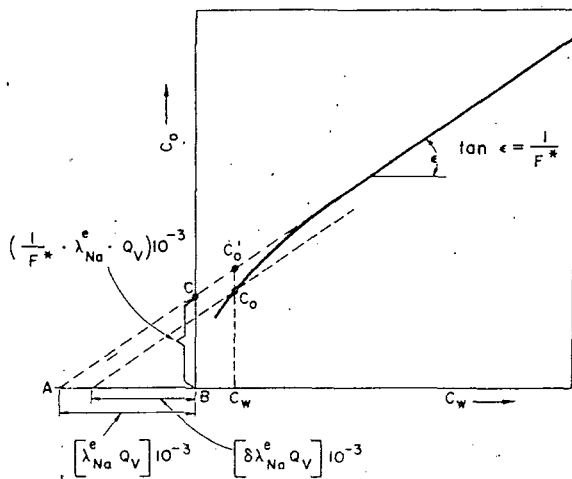
The sharp increase in conductance with increasing concentration of electrolyte in the dilute range is attributed to an increasing exchange-cation mobility. Conductance due to exchange cations can proceed by cation migration in the electric field from one fixed exchange site on the clay particles to another, from assemblages of clay platelets to exchange sites on other assemblages and through the free electrolyte. An increase in clay content and available exchange sites with little or no free electrolyte present should decrease the energy required for electrical conduction and, consequently, result in an increase in exchange-cation mobility. Further, if increasing concentrations of salt solutions were introduced in the pores, there should be another and energetically easier path through the solution, again accompanied by a significant increase in exchange-cation mobility. At some relatively high concentration of equilibrating electrolyte solution, further increase in concentration should make little difference in exchange-ion mobility, i.e., this mobility should then reach a constant and maximum value. At higher electrolyte concentrations, the sand conductivity will increase linearly with increase in solution conductivity.

Various self-diffusion and activation energy measurements of ionic diffusion in three-dimensional matrices having fixed charge sites support these assumptions. Richman and Thomas[7] reported values of the self-diffusion coefficients for Na+ ion in cylindrical rods of a synthetic ion-exchange resin. The concentration of counter ions Q_v in this material varied from 1.5 to 1.7 equiv/liter. These authors observed that the diffusion coefficient D increased by a factor of about 4.8 as the equilibrating electrolyte solution was varied from deionized water to 0.03 N NaCl, and then remained constant as the concentration was increased further. Activation energies for self-diffusion of the Na+ ion decreased from about 10.3 to about 2.2 kcal mole^{-1} as the external salt concentration was increased from 0.01 to 0.07 N.

Similar measurements were made in bentonite-water plugs by Lai and Mortland.[8] Their data show a decrease in the activation energy for self-diffusion of the Na+ ion with increasing clay concentrations in salt-free bentonite plugs. Lai and Mortland also reported measurements of the self-diffusion of Na+ ion in bentonite plugs (0.5 gm clay/2 ml system) equilibrated with varying concentrations of NaCl solution. The diffusion coefficient increased from about 2.3 to 4.8 × 10^{-6} sq cm sec^{-1} when the solution concentration in equilibrium with the plug was increased from 0.01 to 1 N NaCl.

Recently, Gast[9] reported measurements of the self-diffusion coefficients of sodium and chloride ions in a 3.75 percent Na-bentonite gel containing increasing amounts of NaCl. The self-diffusion coefficient for sodium ion increased from about 2.3 × 10^{-6} to 8 × 10^{-6} sq cm sec^{-1} with increase in NaCl concentration from 0 to about 0.06 N; no significant change in D was observed for the chloride ion. Calculated self-diffusion coefficients obtained from conductivity data on the same systems,

FIG. 1 — CORE CONDUCTIVITY (C_o) AS A FUNCTION OF EQUILIBRATING SOLUTION CONDUCTIVITY (C_w).

the use of a two-component model as in Eq. 1 and the Nernst-Einstein equation were in excellent agreement with the observed coefficients.

We assume next that the electric current transported by the counterions associated with the clay travels along the same tortuous path as the current attributed to the ions in the pore water. Thus, the geometric parameters x and y of Eq. 2 are assumed to be equal. By analogy with the idea of formation resistivity factor for clean sands,

$$x = y = \frac{1}{F^*} , \quad \cdots \cdots \cdots \quad (3)$$

where F^* is the shaly sand formation resistivity factor. We can then write

$$C_o = \frac{1}{F^*} (C_e + C_w) \quad \cdots \cdots \cdots \quad (4)$$

For clean sands, $C_e = 0$, and F^* reduces to F, the usual formation factor defined as C_w/C_o. This assumption is justified since the cation transport numbers are independent of any parameter relating to rock porosity or pore geometry, as indicated by the electrochemical data of Hill and Milburn.[3] Various expressions for the cation transport number (and hence, electrochemical potentials) can be derived from conductivity equations based on a parallel conductance model, depending on the number of resistor elements considered.[10,11] Under these conditions, the resulting cation transport numbers would not be independent of geometric "cell constant" parameters such as x, y and F^* unless these parameters are equal.

For the straight-line portion of the conductivity curve where a constant and maximum exchange-cation mobility has been assumed, we write

$$C_e = \frac{\mathcal{F}\mu_{Na}^e}{1000} Q_v = \frac{\lambda_{Na}^e}{1000} Q_v , \quad \cdots \cdots \quad (5)$$

where C_e = specific conductance of the clay counter ions, mho cm^{-1}

$\mathcal{F}$ = faraday

μ_{Na}^e = maximum sodium exchange ion mobility, sq cm volt^{-1} sec^{-1}

Q_v = concentration of sodium exchange cations associated with the clay, equiv/liter

λ_{Na}^e = maximum equivalent ionic conductance of the sodium exchange ions, sq cm equiv^{-1} ohm^{-1}

Since C_e is a constant over this range of C_w values, the slope of the straight-line portion of the conductivity curve is equal to the reciprocal of the formation factor $1/F^*$ (Fig. 1); the intercept $\overline{BC}$, obtained by extrapolating the straight-line portion of the conductivity plot to the C_o axis, is equal to C_e/F^*; and the line segment $\overline{AB}$ is equal to C_e or $(\lambda_{Na}^e Q_v)/1,000$.

Required tests of the model are (1) demonstration of a proportionality between segments $\overline{AB}$ obtained

from C_o-C_w plots, and Q_v values determined independently by analytical methods for a variety of shaly sands, and (2) correlation of F^*'s obtained from slopes of C_o-C_w plots to porosity and pore geometry of the rocks.

C_e is expressed as a volume conductivity in Eq. 5. This model cannot differentiate between a volume and a surface conductance mechanism for the clay counterions, since either consideration results in the volume concentration term Q_v in Eq. 5. Considering the exchange ion contributions as a surface conductance, we obtain

$$C_s = \mathcal{F}\mu_{Na}^e Q_s , \quad \cdots \cdots \cdots \quad (6)$$

where C_s is the specific surface conductance of the clay (ohm^{-1}) and Q_s is the number of equivalents of exchange cation per unit of surface area. Further,

$$C_e = SgC_s = Q_s Sg\mathcal{F}\mu_{Na}^e , \quad \cdots \cdots \quad (7)$$

where S is the specific surface area of the clay (sq cm/gm clay) and g is the weight of clay per unit of rock pore volume (gm clay/cu cm). Comparing Eqs. 5 and 7,

$$Q_s Sg = Q_v /1,000 . \quad \cdots \cdots \cdots \quad (8)$$

Clearly the volume concentration term Q_v and the associated volume conductivity are simpler to measure and use than the parameters of Eqs. 7 and 8 which are required to describe the surface conductivity mechanism, i.e., surface concentration of fixed charge sites, specific surface area of the clay, etc.

Returning to the curved portion of the conductivity curve in the low C_w region, we assume an exponential rise of the counterion mobility up to its constant and maximum mobility at higher solution conductivities. This assumption is based on conductivity data for synthetic ion-exchange resin plugs, e.g., the work of Sauer et al.[12] It may be tested by comparison with shaly sand conductivity data, and by extrapolation to $C_w = 0$ for comparison with literature data for clay conductivities.

The general equation for water-saturated shaly sands then becomes

$$C_o = \frac{1}{F^*} (BQ_v + C_w) , \quad \cdots \cdots \quad (9)$$

with

$$B = [1 - a \exp (-C_w /\gamma)]0.001\lambda_{Na}^e . (10)$$

C_o and C_w have the units mho cm^{-1}. B is introduced to represent the equivalent conductance of the counterions as a function of solution conductivity C_w with units in mho sq cm/meq. The value of γ is determined by the rate of increase of the counterion mobility from that at zero water conductivity up to its constant value at the higher water conductivities.

The parameter a is determined by the mobility of the exchange cations at $C_w = 0$,

$$a = 1 - \frac{(\lambda_{Na}^e)'}{\lambda_{Na}^e}, \quad \ldots \ldots \ldots (11)$$

where $(\lambda_{Na}^e)'$ is the equivalent ionic conductance of the exchange cations at $C_w = 0$.

COMPARISON WITH EARLIER WORK

Similar assumptions as to the equivalence of the cell factors for surface and bulk solution conductivity were made by Cremers and Laudelout[13-15] in their work on clay mineral suspensions and gels. Their data indicate that isoconductivity points exist for different clay mineral gel-salt systems. By extrapolating the straight-line portions of the C_o vs C_w plots for a series of gels consisting of varying percentages of the identical clay species, a common isoconductivity point is found. Cremers and Laudelout observed that the conductivity at an isoconductivity point is independent of gel porosity. By comparison, they found that their form of the F-ϕ function is in formal agreement with that derived from theories by Burger[16] and Fricke,[17] relating electrical conductance of stationary particles in dilute suspensions to particle shape factors and porosity. The Cremers-Laudelout F-ϕ relation clearly is not applicable to shaly sands; moreover, the accuracy of the Cremers-Laudelout data does not permit calculation of reliable values of exchange-cation mobilities for clay plugs equilibrated at any salt concentration.[18]

The proposed mechanism differs from that suggested by Wyllie and his co-workers.[1,10,12] They represented the conduction process by an equivalent resistor model containing three resistance components in parallel instead of two as suggested here. Two resistor elements are common to both models; the third consists of conductive solid and electrolyte solution elements in series. Contributions from this component can account for the sharp increase in the conductivity curves at low C_w values, rather than an increase in exchange-ion mobility. The Wyllie model requires four geometric parameters, three of which are independent. These can be obtained by appropriate manipulation of the conductivity equation under various limiting conditions.

Some comparison should be made with the work of de Witte.[19] He concluded from empirical considerations that the conductivity behavior of water-bearing shaly sands could adequately be represented by the equation

$$C_o = A_D + B_D C_w, \quad \ldots \ldots \ldots \ldots (12)$$

where A_D and B_D are constants. Eq. 12 is similar to that originally proposed by Patnode and Wyllie[20] and neglects the curved portion of the conductivity plots at low C_w's. However, de Witte defined a "maximum formation factor", the limiting value of

apparent formation factor as $R_w \to 0$, namely $F_m = 1/B_D$. F_m is identical to F^* of this paper. de Witte also recognized a shaliness factor A_D/B_D which was "an absolute rock parameter... independent of R_w". In this paper, A_D/B_D is equal to the maximum specific conductance of the exchange cations of the clay $(\lambda_{Na} Q_v)/1,000$.

EXPERIMENTAL PROCEDURES AND DATA

Conductivity data for about 315 shaly sand cores have been published by Hill and Milburn.[3] These data include independent cation-exchange capacity and Q_v determinations on 36 samples. Additional unpublished measurements including Q_v and conductivity data on some 54 cores, together with conductivity data on 167 other samples, were made available to us by H. J. Hill. The conductivity data generally include three to four experimental points in the straight-line portion of the curve ($C_w > 0.05$ mho cm^{-1}) and one to two points in the curved region, but these usually were obtained at equilibrating solution conductivities greater than 7 m mho cm^{-1} (solution resistivities less than about 1.4 ohm m). Group 1 refers to all the above samples.

While a large variety of rock types is represented in Group 1, the distribution of Q_v values is weighted heavily in the range $0 \leq Q_v \leq 1$ equiv/liter; this group contains about 94 percent of the total number of samples. Another set of shaly sands (Group 2) was selected on the basis of a wider distribution of Q_v values; with these samples, conductivity measurements at low equilibrating solution conductivities (down to about 2.1 m mho cm^{-1}) were emphasized. Conductivity data for Group 2 cores are probably the most accurate and complete with respect to range of Q_v and C_w values examined.

GROUP 1

Independent Q_v determinations, together with C_o-C_w measurements, were described for a selected set of sands by Hill and Milburn.[3] Petrophysical and conductivity data for this set are presented in Table 1. Similar measurements were carried out on 54 additional cores. A description of these samples is given in Table 2; petrophysical characteristics and conductivity data are summarized in Table 3. Table 4 gives general characteristics and petrophysical data for the remaining samples used in the conductivity studies.

Experimental procedures employed in these conductivity measurements were described by Hill and Milburn.[3]

Q_v Determinations

Cation-exchange capacities (CEC) as determined by Hill and Milburn (Table 1) were measured chromatographically using ammonium acetate solutions. Further CEC determinations (Table 3) were made using a procedure suggested by Mortland and Mellor.[21] This method requires repeated equilibration of the crushed rock sample with concentrated $BaCl_2$ solution and washing to remove excess barium ions, followed by conductometric

$\dfrac{\overline{r}}{m}$ ±
Vitte
hich
at of
mum
s of

A
ores
iese
city
onal
and
with
iade
iata
ints
0.05
ved
at
in 7
out
les.
ited
ited
this
aber
p.2)
n of
vity
luc-
ere
res
vith

ith
ted
cal
in
on
les
ics
3.
ro-
in

se
ill

ed
ed
te
3)
id
ed
th
re
ic

At.

titration with standard $MgSO_4$ solution. Results are equivalent to the ammonium acetate method.

Core porosities were calculated from the following measurements made prior to the CEC determinations: (1) bulk volumes measured by mercury displacement and (2) grain volumes determined by buoyancy weighings under brine.

GROUP 2

Shaly Sand Samples

Shaly sand samples were selected which varied widely both in CEC and in manner of clay distribution. The range of Q_v values extended from 0 to 1.5 meq/ml. Cores where $0.3 < Q_v < 1.5$ originated from a lower Tertiary horizon and contained fairly pure montmorillonite as the clay fraction, mainly

TABLE 1 — PETROPHYSICAL AND CONDUCTIVITY DATA, SHALY SANDS (HILL AND MILBURN[3])

Suite	Sample Number	Porosity (%)	Air Permeability (md)	Q_v Exp. (equiv./liter)	F*	C_o (Conductivity Units, m mho cm^{-1})					
1						9.50	20.2	53.2	87.7	147.0	217.4 —C_w
Clean Sandstone, Miocene, Weeks Island	25	20.3	18.9	0.076	16.0	0.650	1.31	3.39	5.62	9.43	13.6
	31	21.8	12.8	0.081	18.2	0.620	1.23	3.11	5.07	8.40	12.0
	34	21.9	55.9	0.060	17.4	0.660	1.35	3.43	5.66	9.49	12.3
	38	23.2	1475.	0.018	9.90	0.990	2.06	5.37	9.14	15.0	22.0
2						9.40	21.9	52.6	87.7	222.0	—C_w
Clean Sandstone, Cretaceous Paluxy Sand, Quitman, Texas and Mitchell Creek, Texas	16	11.8	17.5	0.008	53.0	0.180	0.410	1.02	1.72	4.19	
	21	13.9	0.5	0.247	31.5	0.480	0.960	1.94	3.06	7.29	
	25	15.7	0.2	0.225	29.9	0.500	0.990	2.02	3.19	7.66	
	39	21.2	343.	0.033	13.5	0.750	1.75	4.24	7.13	16.6	
	48	22.4	480.	0.088	14.7	0.790	1.82	4.21	7.07	15.3	
4, Group 1						7.25	12.0	53.2	87.9	147.0	219.3 —C_w
Shaly Sandstone, Eocene, Lower Wilcox Sand, Sheridan, Texas	5	9.5	0.2	0.578	66.6	0.230	0.340	1.02	1.54	2.42	3.42
	44	16.5	0.9	0.232	32.8	0.330	0.500	1.80	2.88	4.67	6.79
	47	17.5	16.6	0.215	27.7	0.360	0.530	2.05	3.34	5.53	7.97
	51	18.6	12.6	0.073	20.6	0.390	0.630	2.62	4.32	7.24	10.6
	52	18.7	48.0	0.239	20.6	0.470	0.730	2.77	4.48	7.32	10.8
4, Group 2	19	20.3	0.1	0.293	33.0	0.340	-	1.80	2.92	4.61	6.79
5, Group 1						6.60	45.9	90.9	128.	208.	—C_w
Shaly Sandstone, Oligocene, Frio Sand, Seeligson, Texas	28	20.1	46.0	0.327	24.6	0.400	2.22	3.99	5.48	8.68	
	36	23.1	313.	0.075	16.7	0.480	2.96	5.48	7.68	12.6	
						6.30	90.1	218.			—C_w
5, Group 2	4	16.2	3.5	0.347	47.2	0.260	2.14	4.76			
	13	23.1	117.	0.225	19.4	0.510	5.03	11.5			
	17	23.9	91.0	0.249	18.6	0.550	5.36	12.0			
	18	24.1	1000.	0.171	15.0	0.530	6.21	14.6			
	23	24.5	156.	0.195	15.9	0.540	6.01	13.9			
	24	24.5	907.	0.146	13.2	0.600	7.21	16.6			
	27	24.8	988.	0.138	13.4	0.690	7.21	16.5			
6						15.0	20.8	47.6	92.5	148.	213. —C_w
Very Shaly Sandstone, Cretaceous, Taylor Sand, Big Foot, Texas	16	23.9	1.5	0.699	17.1	-	2.50	3.50	-	9.81	13.5
	22	25.6	1.6	0.887	19.9	-	2.70	3.94	-	9.03	12.3
	27	26.8	1.0	0.767	17.6	1.94	2.57	-	6.48	9.75	13.3
	33	27.4	6.1	0.798	15.0	2.02	2.70	-	7.41	11.2	15.3
	38	28.2	3.6	0.750	15.8	2.02	2.67	-	7.12	10.7	14.7
	42	28.4	6.6	0.617	14.0	2.00	2.67	-	7.65	11.7	16.2
	43	28.6	6.4	0.645	15.0	2.02	2.67	-	7.35	11.0	15.3
	45	29.3	5.6	0.605	13.8	2.05	2.77	-	7.85	11.9	16.5
	47	30.8	5.4	0.502	12.7	2.17	2.93	-	8.49	12.8	17.9
8						10.0	23.0	92.0	21.6		—C_w
Limestone, Cretaceous, Pettit Limestone, Chapel Hill, Texas	64	26.5	494.	0.148	11.6	0.930	2.12	8.39	18.8		
9						6.00	24.0	58.0	148.	214.	—C_w
Limestone, Jurassic, Smackover Limestone, Magnolia, Arkansas	21	17.5	1.3	0.045	29.8	0.210	0.820	1.94	5.00	7.20	

TABLE 3 — PETROPHYSICAL AND CONDUCTIVITY DATA, SHALY SANDS

Suite	Sample Number	Porosity (%)	Air Permeability (md)	Brine[†] Permeability (md)	C_v Exp. (equiv./liter)	F*	C_o (Conductivity Units, m mho cm^{-1})			
							21.3	37.3	81.9	226. −C_v
1 Clean Sandstone	1	21.7	-	48.1	0.093	17.6	1.33	2.26	4.91	13.1
	2	16.6	0.38	0.04	0.302	36.3	0.840	1.30	2.61	6.55
	3	24.4	-	166.	0.083	13.7	1.72	2.96	6.31	16.9
	4	20.2	.-	290.	0.036	16.6	1.33	2.41	5.16	13.8
	5	24.2	-	119.	0.051	12.9	1.76	2.99	6.66	17.8
	6	21.2	28.	19.6	0.104	16.8	1.42	2.45	5.16	13.7
	7	20.5	34.	21.5	0.097	17.7	1.38	2.36	4.97	13.1
	8	20.8	51.	36.2	0.069	17.6	1.38	2.44	5.16	13.2
	9	20.4	59.	40.1	0.076	17.2	1.32	2.33	5.00	13.4
	10	24.5	-	220.	0.049	12.6	1.73	3.11	6.66	18.2
	11	14.5	0.19	-	0.454	49.7	0.740	1.11	2.05	4.92
2 Shaly Sandstone	1	20.2	80.	56.3	0.085	19.4	1.24	2.16	4.53	11.9
	2	21.1	141.	70.	0.102	18.2	1.32	2.32	4.97	12.7
	3	25.8	-	440.	0.050	11.4	1.93	3.42	7.45	20.2
	4	19.3	67.	40.	0.112	24.7	0.960	1.65	3.52	9.34
	5	20.7	226.	158.	0.062	18.7	1.28	2.23	4.77	12.4
	6	20.0	146.	83.	0.067	20.8	1.16	2.03	4.31	11.2
	7	18.9	95.	132.	0.065	22.1	1.15	2.05	4.25	10.6
	8	18.2	48.	33.	0.123	28.2	0.950	1.66	3.35	8.34
	9	16.1	12.	6.9	0.158	33.0	0.770	1.30	2.70	7.05
	10	14.9	3.3	1.1	0.298	36.3	0.791	1.29	2.57	6.51
	11	15.9	1.3	0.16	0.254	37.1	0.840	1.31	2.55	6.43
	12	11.6	0.3	0.05	0.281	74.3	0.391	0.670	1.27	3.20
	13	18.6	59.	31.	0.100	25.1	0.932	1.64	3.42	9.19
	14	17.4	5.9	2.1	0.206	31.2	0.850	1.46	2.93	7.52
	15	16.3	3.7	16.2	0.185	35.8	0.840	1.44	2.89	6.70
3 Shaly Sandstone	1	5.4	0.08	0.011	0.433	232.	0.130	0.230	0.410	1.04
	2	26.1	-	94.	0.191	16.0	1.69	2.83	5.77	14.7
	3	25.9	436.	191.	0.135	14.4	1.73	2.89	6.03	16.0
	4	23.9	69.	48.9	0.453	17.0	2.03	3.16	6.16	14.3
	5	24.8	704.	226.	0.200	14.6	1.90	3.14	6.26	16.2
	6	25.7	-	210.	0.175	14.5	1.73	2.92	6.03	16.0
4 Very Shaly Sandstone	1	15.0	-	0.[‡]	2.494	89.4	1.58	1.80	2.28	3.91
	2	11.9	0.35	0.[‡]	2.057	119.0	0.860	1.05	1.42	2.62
	3	8.7	0.09	0.06	1.578	168.0	0.420	0.570	0.830	1.67
	4	25.5	-	0.[‡]	1.436	29.8	2.50	3.06	4.66	9.45
	5	25.3	.-	0.001	1.440	33.0	2.63	3.22	4.66	8.93
	6	12.2	0.83	0.[‡]	1.669	117.9	0.780	0.950	1.32	2.55
	7	27.2	-	0.006	1.332	25.3	2.73	3.45	5.29	11.0
	8	29.0	-	0.15	0.689	18.3	2.34	3.30	5.77	13.4
	9	26.7	-	0.04	1.074	22.0	2.36	3.22	5.36	11.8
	10	26.2	-	0.02	1.228	24.9	2.39	3.06	5.03	10.7
	11	28.4	-	0.29	0.857	17.5	2.56	3.62	6.26	14.4
	12	27.7	-	0.04	1.085	21.1	2.50	3.30	5.65	12.3
	13	25.3	-	0.001	1.530	32.0	2.45	3.01	4.45	5.93
	14	23.2	-	0.001	1.541	31.1	2.53	3.14	4.63	9.22
	15	29.8	-	0.44	0.776	16.8	2.66	3.81	6.61	15.1
	16	12.8	0.38	0.0004	1.587	97.5	0.820	1.04	1.50	2.97
	17	27.5	4.4	0.09	0.898	20.1	2.36	3.30	5.58	12.7
	18	31.4	-	0.33	0.639	14.9	2.34	3.69	7.07	16.4
	19	29.0	5.8	0.24	0.922	17.8	2.80	3.36	6.07	14.2
	20	32.2	-	0.19	0.860	18.8	2.50	3.33	5.98	13.5
	21	30.2	-	0.04	0.887	20.4	2.47	3.33	5.69	12.7
	22	29.0	-	0.01	1.066	22.6	2.47	3.33	5.36	11.7
	23	27.2	-	0.002	1.316	24.6	2.73	3.45	5.29	11.2

[†] Brine containing 12 g NaCl per liter.

[‡] At 300 psi differential pressure.

TABLE 2 — DESCRIPTION OF SAMPLES INVESTIGATED

Suite	Type of Formation	Description	Age and Locality
1	Clean sandstone	Clean, medium to fine grained (340 to 80μ), friable quartz sand; major cementing material present: calcite and quartz	Miocene, Weeks Island, La.
2	Shaly sandstone	Micaceous, shaly, fine grained to silty (140 to 65μ), hard quartz sand; cementing material: chiefly quartz	Eocene, lower Wilcox sand, Sheridan, Tex.
3	Shaly sandstone	Highly calcareous, shaly, medium to fine grained (255 to 110μ) arkosic sandstone; cementing material: chiefly calcite	Oligocene, Frio sand, Seeligson, Tex.
4	Very shaly sandstone	Very shaly, very fine grained to silty (105 to 59μ), consolidated quartz sand	Cretaceous, Taylor sand, Big Foot, Tex.

TABLE 5 — COMPOSITION OF CLAY FRACTION (<2μ) OF SHALY SANDS

Core	Kaolinite (percent)	Illite (percent)	Chlorite (percent)	Montmorillonite (percent)
1	100	tr	—	—
2	90	7.5	2.5	—
3	90	7.5	2.5	—
4	100	tr	—	—
5	100	—	tr	—
6	90	7.5	2.5	—
7	100	—	—	—
8	100	—	—	—
9	90	7.5	2.5	—
10	65	35	—	—
11	65	35	—	—
12	100	—	—	—
13	100	—	—	—
14	100	—	—	—
15	100	—	—	—
16	100	—	—	—
17	100	—	—	—
18	20	40	—	20
19	20	40	—	20
20	20	40	—	20
21	12	8	—	80
22	12	8	—	80
23	8	8	—	84
24	12	8	—	80
25	—	—	—	100
26	tr	tr	—	100
27	—	tr	—	100

surrounding the grains and interstitial. The cores in which $0 < Q_v < 0.5$ came from an Eocene and an Albian horizon and contained mainly kaolinite and illite. In these cores, the clay occurs around the grains, but mainly in thin laminae. The compositions of the clay fractions (<2 μ) of the samples are given in Table 5.

Cylindrical cores 2.54 cm in diameter and 2 to 4 cm long were cut with their axes parallel to the bedding planes. After extraction with chloroform and ether, they were encased in epoxide resin. The cores then were equilibrated with a deaerated, saturated NaCl solution, and stored in this solution for several months before the experiments were started.

Apparatus

Electrical conductivities were measured with an accuracy of 0.1 percent using an impedance bridge. The cell was similar to that described by Hill and Milburn;[3] contact between the platinized platinum electrodes and the cores was achieved through the equilibrating electrolyte solution in the end compartments of the cell. The measuring frequency was 1,592 cycles/second. Tests indicated that measured conductivities were independent of frequency, at least from 50 to 20,000 cycles/second. Measurements were conducted at a constant temperature of 25 ± 0.05C.

TABLE 4 — DESCRIPTION AND PETROPHYSICAL CHARACTERISTICS OF ROCKS INVESTIGATED

Age, Locality	Number of Samples	Conductivity Points per Sample	Range of Equilibrating NaCl Solutions (Normality)	Porosity Range (percent)	Permeability Range (md)	Range of F* Values	Range of Q_v (equiv/liter)
Upper Cretaceous, Nacatosh Field, Bellevue, La.	51	4	0.11 -2.5	7-14	<0.1-680	6-56	0.04-0.30
Pliocene, Ventura Field, Calif.	39	5	0.06 -3.06	4-16	0.13- 19	22-120	0.1 -0.45
Cretaceous, Viking Formation, Alta., Canada	34	4	0.12 -4.79	14-30	0.6 -664	8-28	0.03-0.36
Permian, Spraberry Formation, Midland, Tex.	27	4	0.048-1.86	5-15	<0.1- 1.5	10-146	0.02-0.15
Mississippian, Sanders Formation, Monroe County, Miss.	4	5	0.01 -3.25	8-12	—	30-75	0.02-0.05
Eocene, Gohlke Field, Victoria, Tex.	3	5	0.01 -3.25	16-20	—	19-21	0.03-0.05
Miocene, Weeks Island Field, La.	2	5	0.01 -3.25	20-25	—	15-22	0.01-0.02
Cretaceous, Big Foot Formation, Tex.	4	5	0.01 -3.25	3-20	—	10-11	0.2 -0.4
Pliocene, Ventura Field, Calif.	3	5	0.01 -3.25	4-16	—	31-41	0.2 -0.3

The contribution of the electrode compartments was determined by measuring the conductivity of cells with the cores replaced by perspex rings having an internal diameter equal to the nominal diameter of the cores (2.54 cm) and varying in length from 1 to 5 cm. The "cell constant" of the electrode compartments was obtained by extrapolating the conductance data to zero length. The influence of small variations in core diameter on this cell constant was determined by measuring conductivities with perspex rings 3 cm long, but varying in internal diameter from 2.0 to 2.8 cm.

Cores with higher clay content (Q_v greater than 0.2 meq/ml) were in danger of falling apart upon flushing with NaCl solutions of a concentration lower than 0.072 molal. To prevent their disintegration, these cores were fitted at each end with a plate of highly permeable, fired Bentheim sandstone. These plates were 2.54 cm in diameter and a few millimeters thick and were cut from a long bar previously mounted in epoxide. They were glued to the cores at the resin rim at each axial end of the cores. Before mounting, the electrical cell constant of the plates was determined so that appropriate corrections could be made for the electrical conductivity determinations.

NaCl Solutions

The salt used was Analar reagent NaCl, fused overnight at 500C and stored until use in a dessiccator in which $CaCl_2$ was the drying agent. Salt solutions were made up by weight.

The concentrations of the salt solutions in use frequently were verified by conductivity measurements at 25C. The accuracy of these electrical concentration determinations is somewhat better than 0.1 percent, except for concentrations higher than 4 molal. At these higher concentrations, the change of conductivity with concentration becomes increasingly smaller and accurate results cannot be expected. For solutions with concentrations greater than 4 molal, checks were made gravimetrically by evaporation of a known weight of solution.

Cation-Exchange Capacity Measurements

The determinations of CEC per unit pore volume of the shaly sand cores were made on pieces of rock adjacent to the places from where the cores had been removed because the method used was destructive. The cores were selected for the investigation from homogeneous portions of rock. Some duplicate determinations of exchange capacities were made at different adjacent pieces of rock, and the measure of agreement can be seen in Table 6. These cores have become valuable as a result of having undergone many electrochemical measurements;[11] in order that they be available for further work, some accuracy in the exchange capacities has been sacrificed. We do not believe, however, that this is a serious disadvantage since no systematic errors are introduced. The Q_v values cited in the second sample set of Table 6 were used in further calculations since they were taken closer to the

TABLE 6 — MEASUREMENTS OF Q_v FOR ADJACENT SAMPLES OF ROCK

	Q_v (meq/cu cm)	
Core	First Sample	Second Sample
21	0.30	0.29
22	0.70	0.72
23	0.78	1.04
24	0.58	0.81
25	1.37	1.27
26	1.62	1.47
27	1.20	1.48

cores of interest.

Measuring Procedure

As shaly sands may fall apart when kept in contact with brine of very low salinity, the investigation was started at high NaCl concentrations. At each concentration the cores were equilibrated by repeated flushing and storing in a desiccator filled with the appropriate salt solution. We considered the cores to be at equilibrium with the salt solution when, upon further flushing, the conductivity measurements scattered within the measuring accuracy of about 0.1 percent.

At high salt concentrations, equilibrium is reached very slowly. Equilibrating times of 2 to 3 months frequently were required. Nevertheless, in all cores except those from extremely clean sands, the first two or three conductivity points at descending NaCl concentration were found to be irreproducible. When the measurements were repeated after the cores had been flushed and "equilibrated" again with brines of higher salinity, much higher conductivities were recorded. The shalier the sand, the more pronounced was this effect.

To investigate the phenomenon, a few cores with varying clay content were selected. A typical example is shown in Fig. 2. Here the conductivity of a moderately shaly core is given as a function of saturating brine conductivity for a sequence of
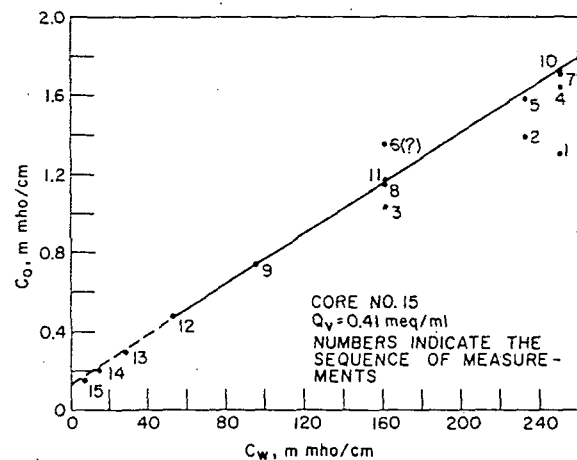

FIG. 2 — ELECTRICAL CONDUCTIVITY (C_o) OF A SHALY CORE AS A FUNCTION OF THE CONDUCTIVITY OF THE EQUILIBRATING BRINE (C_w).

observations obtained under equilibrating conditions as previously described. It is seen that reproducible data were obtained only from Point 7 on.

The reproducible data are considered now as equilibrium data. The clay of this particular core occurs mainly in laminae. Effects demonstrated in Fig. 2 are less pronounced when the clay is more homogeneously distributed, and also when the cores are first saturated with an NaCl solution of a concentration lower than about 1 molal. This behavior of the conductivity of shaly sands may be caused primarily by the almost complete dehydration of the clay due to the Soxhlet extraction procedure and the heating during encasing in epoxide resin. It is presumed from the above observations that rehydration of the clay, and therefore reactivation of the clay counterions, is an extremely slow process as far as saturated solutions are concerned because of their lower water activity. Grim[22] reported that completely dehydrated montmorillonite is extremely difficult to re-equilibrate with water.

Results of the equilibrium conductivity measurements made at 25C on the shaly sands equilibrated with NaCl solutions at 10 different concentrations varying from saturated solutions of 6.144 to 0.018 molal, are given in Table 7. Origin of the samples, their porosities and Q_v values also are in Table 7. Some representative plots of core conductivity C_o vs electrolyte solution conductivity C_w are presented in Fig. 3 for cores with different values of Q_v.

DISCUSSION OF DATA

Values of F^* and $\lambda_{Na}^e Q_v/1,000$ were calculated from the slopes and intercepts ($\overline{AB}$, Fig. 1), respectively, of the straight-line portions of the conductivity plots. Extrapolations were made with Eq. 9 and the method of least mean squares. These calculated values of $\lambda_{Na}^e Q_v/1,000$ were plotted against the independently determined values of Q_v for the 90 cores of Group 1 (Fig. 4). The data were fitted by a straight line passing through the origin and a method of reduced regression where both variables are considered subject to error. The
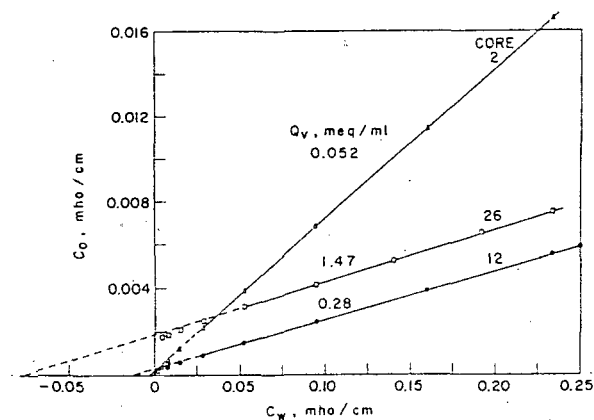
correlation coefficient for the resulting relation

$$[(10^{-3})\lambda_{Na}^e Q_v]_{\underset{plot}{cond.}} = 0.0383[Q_v]_{anal.},$$

. . . . (13)

was 0.981, with B_{max} or λ_{Na}^e equal to 38.3 sq cm equiv^{-1} ohm^{-1}. Confidence limits of 10 and 90 percent (80 percent of the expected values lie between these limits) for λ_{Na}^e were 36.9 and 39.6 sq cm equiv^{-1} ohm^{-1}.

The method of least mean squares was used to calculate F^* and intercept $\overline{AB}$ values from the conductivity data obtained with Group 2 cores. Values of λ_{Na}^e were calculated from the adjacent Q_v determinations for each of the individual samples (Table 8). The average value of λ_{Na}^e for this set was 46.3 sq cm equiv^{-1} ohm^{-1}, and the standard deviation was 15.8 sq cm equiv^{-1} ohm^{-1}. The value of λ_{Na}^e obtained from cores in Group 1 lies within the above standard deviation.

F^* values were plotted vs the Hill-Milburn F_{01} values for the total of 535 cores of Group 1, and it is apparent that the two parameters are equivalent. The data were fitted by a straight line through the origin, and the slope was determined to be 1.031 by reduced regression methods; the 10 and 90 percent confidence limits of the slope were 1.023 and 1.039, respectively. The correlation coefficient for this relation was essentially unity.

The various relations between F_{01} and porosity found for some four different formations by Hill and Milburn[3] also must hold between F^* and porosity as well. Similar correlations are shown for Group 2 sands (Fig. 5). For the Eocene sand, $m = 1.74$; for the lower Tertiary sand, $m = 2.43$. In both sets, a few cores obviously do not belong to the same group with similar pore geometries. We have no detailed explanation for these deviations.

We conclude that the formation resistivity factor F^*, defined as the reciprocal of the slope of a plot of C_o vs C_w, is related to porosity according to Archie's[6] first empirical equation

$$F^* = \varphi^{-2} \quad . . . . (14)$$

Similarly, other forms of Eq. 14, as suggested by

FIG. 3—ELECTRICAL CONDUCTIVITY (C_o) OF THREE SHALY CORES VS EQUILIBRATING BRINE CONDUCTIVITY (C_w).
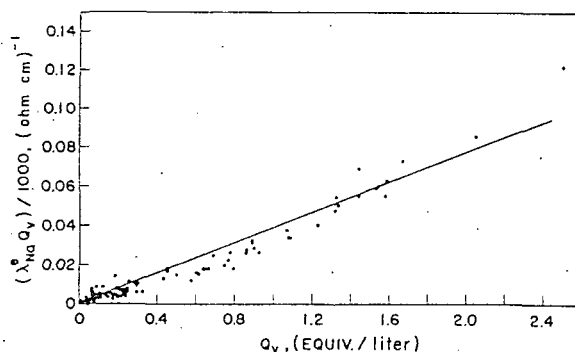
FIG. 4 — PLOT OF $[\lambda_{Na}^e Q_v]$ OBTAINED FROM CONDUCTIVITY CURVES VS Q_v DETERMINED BY DIRECT MEASUREMENT FOR GROUP 1 CORES.

TABLE 7 — CONDUCTIVITY OF CORES C_o AT NaCl SOLUTION CONDUCTIVITY C_w, (m mho/cm)

Core No.	Geological Age	Depth	Porosity (%)	Q_v	250.5	233.5	192.2	160.0	139.8	94.5	52.49	28.22	14.92	7.802	4.049	2.085	←C_w
1	Eocene	12859 ft	23.9	0.017	-	19.1	-	13.2	-	7.85	4.43	2.44	1.282	0.680	0.3625	0.1929	C_o
2	Eocene	12486 ft	21.2	0.052	-	16.6	-	11.41	-	6.84	3.87	2.14	1.169	0.6435	0.3609	0.2049	
3	Eocene	12665 ft	23.1	0.052	-	-	-	14.35	-	8.59	4.86	2.68	1.451	0.7877	0.4345	0.2408	
4	Eocene	12552 ft	8.0	0.26	-	-	-	-	-	2.01	1.14	0.643	0.3674	0.206	0.1198	0.0700	
5	Eocene	12737 ft	15.4	0.20	-	-	-	11.01	-	6.61	3.80	2.16	1.219	0.7105	0.4296	0.2677	
6	Eocene	12687 ft	21.5	0.095	13.6	12.7	-	8.75	-	5.27	3.03	1.712	0.971	0.568	0.330	0.2073	
7	Eocene	12692 ft	17.1	0.053	-	8.84	-	6.14	-	3.73	2.14	1.212	0.7005	0.4135	0.2524	0.1599	
8	Eocene	12692 ft	17.1	0.053	-	9.22	-	6.41	-	3.89	2.23	1.258	0.7154	0.414	0.2473	0.1515	
9	Eocene	12883 ft	19.9	0.085	-	13.1	-	9.03	-	5.44	3.14	1.79	1.025	0.602	0.3698	0.2342	
10	Eocene	12697 ft	12.5	0.253	1.62	-	-	1.06	-	0.671	0.402	0.239	0.1459	0.0924	0.0598	0.0391	
11	Eocene	12697 ft	12.5	0.253	-	-	-	0.967	-	0.592	0.350	0.211	0.1265	0.0798	0.0490	0.0323	
12	Eocene	12884 ft	11.0	0.28	5.89	5.53	-	3.85	-	2.404	1.46	0.895	0.5737	0.3616	0.2461	0.1993	
13	Eocene	12884 ft	11.0	0.28	-	-	-	3.80	-	2.39	1.48	0.926	0.6022	0.4155	0.2888	0.2246	
14	Eocene	12884 ft	11.0	0.28	-	7.52	-	5.29	-	3.32	2.00	1.233	0.7965	0.5455	0.3800	0.2940	
15	Eocene	12698 ft	9.2	0.41	1.73	-	-	1.16	-	0.755	0.479	0.311	0.2052	0.1416	0.0948	0.0687	
16	Eocene	12955 ft	10.3	0.67	-	-	-	3.01	-	1.956	1.30	0.895	0.6576	0.505	0.3788	0.3225	
17	Eocene	12720 ft	14.0	0.33	-	-	-	4.19	-	2.72	1.82	1.25	0.9227	0.6824	0.553	0.4730	
18	Albian	1523.5 m	25.9	0.59	-	13.9	-	9.86	-	6.39	4.11	2.734	1.924	1.353	1.070	0.9409	
19	Albian	1521.5 m	25.9	0.59	-	14.7	-	10.44	-	6.61	4.13	2.626	1.746	1.238	0.8949	0.7140	
20	Albian	1521.5 m	25.9	0.59	20.1	18.8	-	13.2	-	8.28	5.09	3.171	2.062	1.405	1.016	0.7641	
21	Lower Tertiary	1045.5 m	23.8	0.29	-	-	13.62	-	9.98	6.96	4.17	2.55	1.571	0.957	0.7039	0.5585	
22	Lower Tertiary	1044.3 m	22.5	0.72	-	7.58	6.43	-	4.95	3.69	2.52	1.79	1.351	1.092	0.9523	0.8956	
23	Lower Tertiary	981.6 m	24.2	1.04	-	10.36	8.83	-	6.88	5.21	3.63	2.61	1.960	1.576	1.356	1.2720	
24	Lower Tertiary	1040.4 m	21.6	0.81	-	6.36	5.46	-	4.28	3.27	2.34	1.77	1.380	1.102	0.9952	0.9707	
25	Lower Tertiary	1021.1 m	18.7	1.27	-	5.46	4.72	-	3.76	2.97	2.24	1.77	1.481	-	-	-	
26	Lower Tertiary	981.9 m	22.9	1.47	-	7.50	6.49	-	5.21	4.13	3.14	2.48	2.046	1.826	1.597	1.503	
27	Lower Tertiary	983.4 m	20.9	1.48	-	7.04	6.10	-	4.90	3.88	2.97	2.41	2.039	-	-	-	

TABLE 8 — FRACTION (δ) OF MAXIMUM EQUIVALENT CONDUCTANCE (λ_{Na}^e) AS A FUNCTION OF WATER CONDUCTIVITY

Core No.	Q_v (meq/cm^3)	$(\lambda_{Na}^e Q_v)/1000$ (mho/cm)	$\lambda_{Na}^e/1000$ (mho cm^2/meq)	The Value of δ for C_w in mho/cm =					
				0.05249	0.02822	0.01492	0.007802	0.004049	0.002085
1	0.017	0.00232	(0.136)	0.929	0.803	(0.383)	(0.254)	(0.182)	(0.127)
2	0.052	0.00264	0.0507	0.979	0.848	0.647	0.513	0.412	0.315
3	0.052	0.00268	0.0515	0.959	0.793	0.573	0.417	0.327	0.239
4	0.26	0.00287	0.0110	0.961	1.032	1.00	0.758	0.614	0.456
5	0.20	0.00412	0.0206	1.014	0.969	0.787	0.676	0.571	0.462
6	0.095	0.00415	0.0437	1.027	0.922	0.789	0.683	0.514	0.436
7	0.053	0.00589	(0.111)	0.921	0.780	0.685	0.574	0.472	0.381
8	0.053	0.00584	(0.110)	0.910	0.750	0.620	0.503	0.402	0.316
9	0.085	0.00443	0.0521	1.039	0.978	0.838	0.707	0.604	0.491
10	0.253	0.01376	0.0544	0.952	0.786	0.648	0.530	0.416	0.313
11	0.253	0.00857	0.0339	0.993	1.00	0.830	0.711	0.525	0.413
12	0.28	0.01243	0.0444	1.016	0.941	0.857	0.670	0.557	0.545
13	0.28	0.01617	0.0578	0.996	0.909	0.804	0.708	0.578	0.515
14	0.28	0.01384	0.0494	0.957	0.888	0.813	0.733	0.610	0.548
15	0.41	0.02433	0.0593	0.968	0.868	0.726	0.604	0.452	0.363
16	0.67	0.02898	0.0433	1.006	0.964	0.911	0.826	0.681	0.627
17	0.33	0.02947	0.0893	1.014	0.963	0.913	0.784	0.712	0.656
18	0.59	0.02354	0.0399	1.003	0.952	0.881	0.732	0.671	0.712
19	0.59	0.01853	0.0314	0.985	0.904	0.809	0.723	0.609	0.800
20	0.59	0.01463	0.0248	1.005	0.953	0.840	0.733	0.640	0.673
21	0.29	0.00872	0.0301	1.056	1.085	0.954	0.729	0.734	0.790
22	0.72	0.0374	0.0519	1.005	0.956	0.892	0.836	0.802	0.777
23	1.04	0.0454	0.0437	0.996	0.925	0.833	0.762	0.715	-
24	0.81	0.0526	0.0649	1.002	0.975	0.896	0.793	0.774	0.778
25	1.27	0.0724	0.0570	1.010	0.981	0.941	-	-	-
26	1.47	0.0771	0.0524	1.008	0.969	0.907	0.844	0.806	0.781
27	1.48	0.0783	0.0529	1.012	1.004	0.964	-	-	-
Average →			0.0463	0.990	0.916	0.821	0.690	0.592	0.524
Std. dev. →			0.0158	0.034	0.082	0.111	0.110	0.130	0.159

Values between parentheses considered not reliable because of extreme deviation from the rest of the assembly, probably due to Q_v determination. They were not used in calculating the average.

For $C_w > 0.060$ mho/cm, $\delta = 1$.

Winsauer *et al.*,[23] can be used to relate $F*$ to porosity.

The two major tests of the proposed conductivity model, as discussed previously, are met.

Conductivity data obtained for Group 2 cores are quite detailed in the curved portion of the C_o-C_w plots ($2.085 < C_w < 52.49$ m mho cm^{-1}) and permit calculation of the increase in counterion mobility with increasing equilibrating electrolyte concentrations within this concentration range. The increase in μ_{Na}^e has been represented by a simple empirical relation (Eq. 10) for B as a function of C_w and two constants a and γ.

$$\delta = [1 - a \exp (-C_w/\gamma)] \quad \ldots \ldots (15)$$

$$B = \delta\lambda_{Na}^e/1000 \quad \ldots \ldots \ldots (16)$$

The equivalent conductance of the clay counterions is denoted by B, with $\lambda_{Na}^e/1,000$ representing B at its maximum value ($\delta = 1$) in the straight-line portions of the C_o-C_w curves.

Values of δ, at each value of C_w and for each core, were calculated from the ratio of the measured C_o values to the hypothetical values (C_o') of C_o, calculated from the straight-line extrapolation at the same C_w (Fig. 1). Since the same formation factor $F*$ applies throughout the entire electrolyte concentration range,

$$r = \frac{C_o}{C_o'} = \frac{C_w + (\delta\lambda_{Na}^e Q_v)/1000}{C_w + (\lambda_{Na}^e Q_v)/1000} , \quad . \ (17)$$

thus,

$$\delta = (r - 1) \frac{(1000)C_w}{\lambda_{Na}^e Q_v} + r \quad \ldots \ldots (18)$$
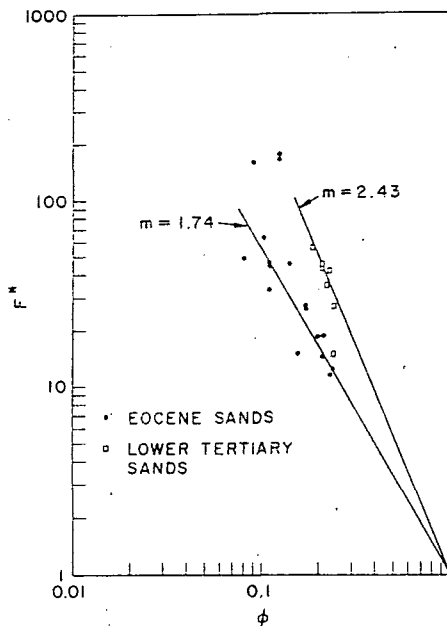
Values of δ, together with their average values and standard deviations, are given as a function of C_w in Table 8.

Values of B as a function of C_w were calculated according to Eq. 16 using average values of δ and λ_{Na}^e (Fig. 6). The empirical equation representing B as a function of C_w at 25C is found to be

$$B = [1 - 0.6 \exp (-C_w/0.013)]0.046$$
$$\text{mho cm}^2 \text{ meq}^{-1} , \quad \ldots \ldots \ldots (19)$$

and, as shown in Fig. 6, provides a reasonable fit for these data. Eqs. 9, 10 and 19 describe available shaly sand data about as well as does the Hill-Milburn equation.

Extrapolation to $C_w = 0$ using Eq. 19 results in a calculated value for the equivalent conductance of the sodium exchange ion $(\lambda_{Na}^e)'$ of 18.4 sq cm equiv^{-1} ohm^{-1}. This is substantially equal to the value of equivalent conductance of sodium exchange ions of about 18 sq cm equiv^{-1} ohm^{-1} which can be deduced from conductivity measurements of sodium montmorillonite-distilled water gels at 25.0C reported by Van Olphen and Waxman.[24] While this agreement is quite comforting, some caution should be observed since the calculated value of $(\lambda_{Na}^e)'$ is obtained by extrapolating an empirical relation beyond observed data.

The assumption in the model of an exponential increase of counterion mobility with increase in solution conductivity is justified by comparison with shaly sand conductivity data and by the apparent agreement of extrapolated conductivity at $C_w = 0$ with clay gel conductivities.

A further general criterion for the model follows from the thermodynamic relation between electrical transport numbers calculated for conditions of nonzero electric current flux and zero concentration gradient, and diffusion potentials measured under conditions of nonzero concentration gradient and zero electric current flux. It should be possible to
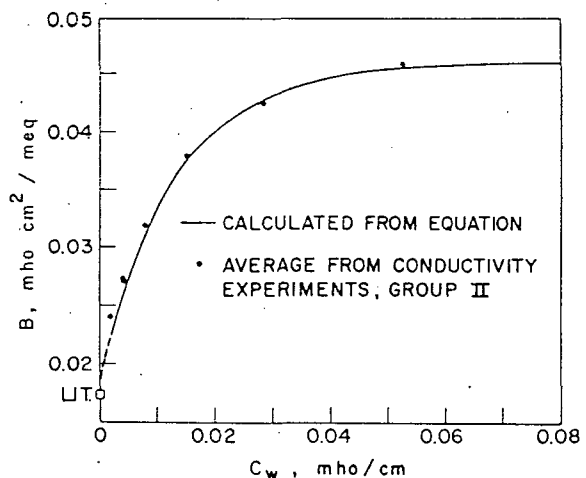

FIG. 5 — SHALY SANDS FORMATION RESISTIVITY FACTOR ($F*$) VS POROSITY (ϕ).

FIG. 6 — EQUIVALENT CONDUCTIVITY (B) OF THE COUNTERIONS ASSOCIATED WITH CLAY AS A FUNCTION OF EQUILIBRATING ELECTROLYTE CONDUCTIVITY (C_w).

obtain expressions for the cation and anion transport numbers from the conductance model. These expressions then can be introduced into the equation for the diffusion potential generated by a liquid junction in the shaly sand. This is discussed by Smits[11] who compared experimental diffusion potentials in shaly sands with calculated potentials based on theory, including parameters developed from the conductance model. Excellent agreement was obtained between both sets of potentials.

CONDUCTIVITY EQUATION FOR OIL-BEARING SHALY SANDS

The conductivity equation for water-bearing shaly sands is extended to describe the conductivity of shaly sands containing both oil and brine.

When water saturation S_w is less than unity, the exchange ions associated with the clay become more concentrated in the remaining pore water. This concentration Q_v' is related to Q_v and S_w according to

$$Q_v' = Q_v / S_w \qquad \ldots \ldots \ldots \ldots \qquad (20)$$

where Q_v' is the effective concentration of exchange ions at $S_o > 0$. We assume that the mobility of the exchange ions is unaffected by the partial replacement of water. Then the conductivity of the counterions is given by BQ_v/S_w (mho cm^{-1}). This assumption was based initially on field evidence which indicates that the SP deflection opposite oil-bearing rocks is reduced when compared with the SP response opposite water-bearing sections of the same reservoir. Reduction of the total electrical potential is attributed to an increase in permselective membrane efficiency of the oil-bearing sands relative to the efficiency of the same sands at $S_w = 1$. The diffusion potential across these sands comprises one of the components of the total SP response. This increase in the membrane efficiency of the sands is associated with an increased effective clay content which must be due to a decrease in the volume of pore space filled with water. A similar suggestion was made earlier by Hill and Milburn[3] and later by de Witte.[19] The equivalent Hill-Milburn assumption is

$$b' = b/S_w , \qquad \ldots \ldots \ldots \ldots \ldots \qquad (21)$$

recalling that the b parameter is approximately proportional to Q_v.

LABORATORY EVIDENCE FOR Q_v' ASSUMPTION

Laboratory data obtained by McLaughlin[25] support the assumption stated in Eq. 20. These data consist of diffusion potential measurements using shaly sands at conditions of water saturation equal to and less than unity. The respective membrane efficiencies are interpreted from the measured emf's using Fig. 13 of Ref. 3, and are expressed in terms of the b and b' parameters.

A group of plugs were cut from cores taken from a formation in the Gohlke field, Texas. Diffusion potentials in the samples were measured using two NaCl solutions having concentrations equal to the original mud filtrate and formation water, respectively. These potentials were measured both at $S_w = 1$ and at residual oil conditions.

As indicated above, values of b' were determined at S_{or} from the emf measurements. Similarly, b values were determined for these sands at $S_w = 1$. A plot of b vs $b'S_w$ is given in Fig. 7. Considering the experimental problems inherent in the determination of S_w, comparison of b values with values of $b'S_w$ shows remarkably good agreement.

The assumption of Eq. 20 rules out the use of the Hill-Milburn equation to describe the conductance behavior of oil-bearing shaly sands. With decrease in S_w and the accompanying increase in Q_v' or b', the minima in the calculated conductivity curves are shifted to quite high values of C_w, well within the range of practical field values. Thus, depending on the original values of b and the particular values of S_w, substantial portions of the conductivity curves will indicate increasing sand conductivities with decreasing C_w's (at constant S_o values) and will be physically meaningless.

We further assume that the conductivity of an oil-bearing shaly sand can be described by an equation analogous to Eq. 9 for water-saturated sands,

$$C_t = \frac{1}{G*} (C_w + BQ_v / S_w) \ldots \ldots \ldots (22)$$

Here C_t is the specific conductance of a partially water-saturated sand and $G*$ is a geometric factor, being a function of porosity, water saturation and pore geometry, but independent of clay content (Q_v). $G*$ is expected to increase with decreasing S_w since the water-filled pore space is decreasing, apart from complications due to distribution of the two phases in the pore network of the rock.

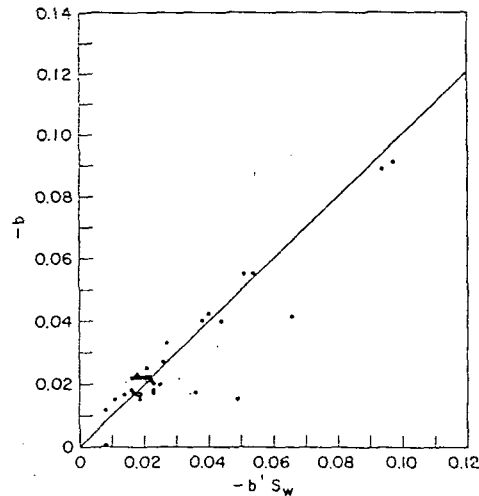For clay-free or "clean" sandstones, $F*$ and $G*$ reduce to

FIG. 7 — EFFECT OF OIL SATURATION ON DIFFUSION POTENTIALS OF SHALY SANDS.

$$F = C_w / C_o = R_o / R_w , \quad \cdots \cdots \cdots (23)$$

and

$$G = C_w / C_t = R_t / R_w \quad \cdots \cdots \cdots (24)$$

The resistivity ratio I is defined as

$$I = R_t / R_o = C_o / C_t = G/F , \quad \cdots \cdot (25)$$

and according to Archie's second empirical relation,[6]

$$I = S_w^{-n} \quad (= G/F) \quad \cdots \cdots \cdots (26)$$

The value of n may differ from the value of m in Eq. 14.

By analogy, we define

$$G*/F* = S_w^{-n*} , \quad \cdots \cdots \cdots \cdots (27)$$

where $n*$ is the exponent for a hypothetical rock having the same pore geometry as the shaly sand, but whose clay content is inactive, i.e., $n*$ is independent of Q_v. For the limiting cases $Q_v = 0$ or $C_w \to \infty$, Eq. 27 reduces to Eq. 26.

Combining Eqs. 9, 22, 25 and 27, we obtain for the resistivity ratio

$$I = S_w^{-n*} \left[\frac{C_w + BQ_v}{C_w + BQ_v / S_w} \right] \quad \cdots \cdots (28)$$

Eq. 28 can be expressed in terms of water resistivity

$$I = S_w^{-n*} \left[\frac{1 + R_w BQ_v}{1 + R_w BQ_v / S_w} \right] , \quad \cdots \cdots (29)$$

where the units of water resistivity R_w and the term BQ_v are ohm m and (ohm m)$^{-1}$, respectively. For Q_v expressed as meq/ml or equiv/liter, the numerical value of B in Eq. 28 is

$$B = [1 - 0.6 \exp(-0.77/R_w)]4.6 \cdot$$
$$\cdots \cdots \cdots \cdots \cdots \cdots \cdots (30)$$

Figs. 8 through 11 demonstrate the effects of
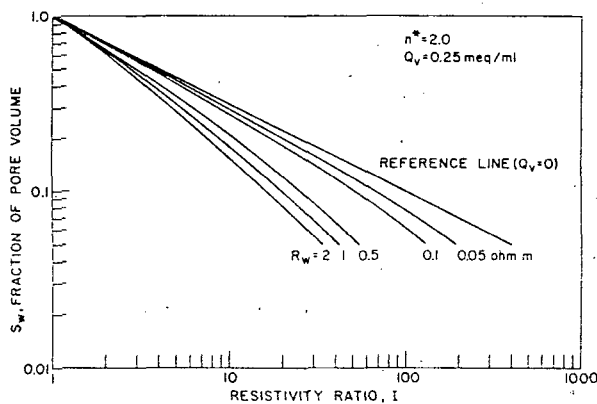
FIG. 8 — WATER SATURATION AS A FUNCTION OF RESISTIVITY INDEX, WITH VARIABLE WATER RESISTIVITY.

variation of clay content, water salinity and pore geometry on the I-S_w relationship, as predicted by Eq. 29. We observed that even small amounts of clay have a marked effect on the resistivity ratio. Significant departures from the simple I-S_w relation (Eq. 26) are noted with increasing water resistivity at constant Q_v; further, $\log S_w$ is nonlinear with respect to $\log I$.

As a final example, an illustration of the influence of clay in a reservoir sand on electric log interpretation is given. We assume a resistivity ratio of $I = 4$ obtained from log readings, and estimate the
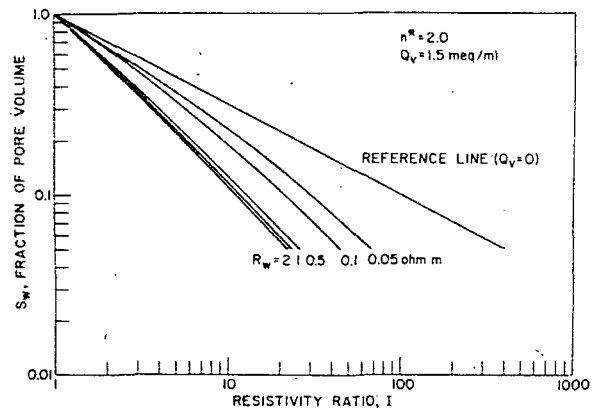
FIG. 9 — WATER SATURATION AS A FUNCTION OF RESISTIVITY INDEX, WITH VARIABLE WATER RESISTIVITY.
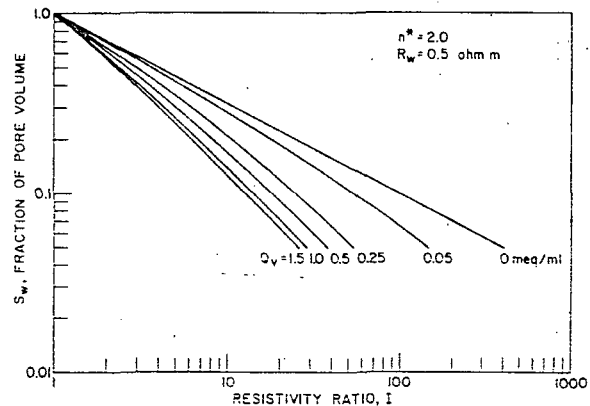
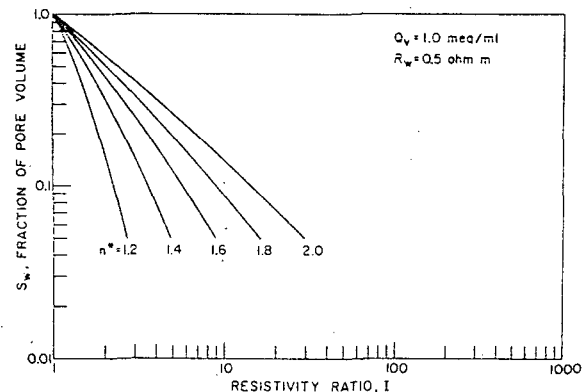FIG. 10 — WATER SATURATION AS A FUNCTION OF RESISTIVITY INDEX, WITH VARIABLE Q_v.

FIG. 11 — WATER SATURATION AS A FUNCTION OF RESISTIVITY INDEX, WITH VARIABLE $n*$.

value of n^* to be 2. For a clean sand, these values lead to an oil saturation $S_o = 0.50$ by the Archie relation (Eq. 26). The influence of various degrees of shaliness associated with different water resistivities for this example is shown in Fig. 12. Oil-in-place estimates are increased considerably from 33 to 47 percent with increasing values of Q_v above the clean sand estimate in certain fresh water zones.

CONCLUSIONS

An equation has been developed, based on a physical model, that relates the electrical conductivity of a water-saturated shaly sand to the water conductivity and the clay content of the sand. Clay contents are expressed by the cation-exchange capacities per unit pore volume of the rocks which can be determined by independent analyses. Various criteria established to test the model are satisfied by shaly sand conductivity data. These data further permit determination of sand conductivities and clay counterion mobilities down to very low equilibrating electrolyte solution conductivities.

The model is extended to describe the conductivity of oil-bearing shaly sands. An expression is developed which relates the resistivity ratio to water saturation, water resistivity and CEC per unit pore volume of rock. This equation generally predicts higher oil-in-place estimates than are obtained from the usual clean sand relations.

NOMENCLATURE

a = dimensionless constant, Eqs. 10 and 11

A_D = constant in de Witte's equation[19] (Eq. 12 in this paper)

B_D = constant in de Witte's equation[19] (Eq. 12 in this paper)

b = Hill-Milburn parameter[3] related to effective clay content of shaly sand at $S_w = 1$

b' = Hill-Milburn parameter[3] related to effective clay content in oil-bearing shaly sand

B = equivalent conductance of clay exchange
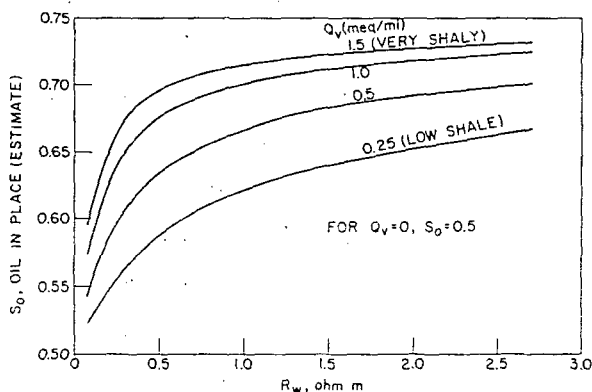
cations (sodium) as a function of C_w at 25C (Eq. 10), mho sq cm meq^{-1}

C_c = conductance contribution of clay exchange cations to shaly sand conductivity, ohm^{-1} or mho

C_e = specific conductance of clay exchange cations, mho cm^{-1}

C_{e1} = conductance contribution of bulk electrolyte solution to conductivity of shaly sand, ohm^{-1} or mho

C_o = specific conductance of sand, 100 percent saturated with aqueous salt solution, mho cm^{-1}

C_o' = hypothetical specific conductance of shaly sand at low values of C_w defined in Eq. 17, mho cm^{-1}

C_s = specific surface conductance of clay, ohm^{-1} or mho

C_t = specific conductance of a partially water-saturated sand, mho cm^{-1}

C_w = specific conductance of aqueous electrolyte solution, mho cm^{-1}

D = self-diffusion coefficient, sq cm sec^{-1}

F_{01} = Hill-Milburn formation resistivity factor[3] for shaly sands

F = formation resistivity factor for clean sand

F^* = formation resistivity factor for shaly sand (this paper)

$\mathcal{F}$ = faraday

g = weight of clay per unit of rock pore volume, gm clay/cu cm

G = formation resistivity factor for partially water-saturated clean sand, Eq. 24

G^* = formation resistivity factor for partially water-saturated shaly sand

I = resistivity index, Eq. 25

m = porosity exponent or lithology factor, Eq. 14

m_{NaCl} = molal concentration of NaCl solution, mol NaCl/1,000 gm water

N = aqueous electrolyte solution concentration, Normality, moles solute/liter solution

n = Archie saturation exponent for clean sands, Eq. 26

n^* = saturation exponent for shaly sand

Q_s = surface concentration of clay exchange cations, equiv cm^{-2}

Q_v = volume concentration of clay exchange cations, meq ml^{-1} or equiv liter^{-1}

Q_v' = volume concentration of clay exchange cations in oil-bearing shaly sand (Eq. 20), meq ml^{-1} or equiv liter^{-1}

r = ratio of measured to hypothetical shaly sand conductivities at identical C_w's, Eq. 17

R_o = resistivity of sand 100 percent saturated with aqueous salt solution, ohm m

FIG. 12 — OIL-IN-PLACE ESTIMATES AS A FUNCTION OF CLAY CONTENT OF SAND AND FORMATION WATER RESISTIVITY (ASSUMED CONDITIONS, $I = 4$, $n^* = 2$).

R_t = resistivity of a partially water-saturated sand, ohm m

R_w = resistivity of equilibrating aqueous salt solution, ohm m

S = specific surface area of clay, sq cm/gm clay

S_o = fractional oil saturation

S_{or} = residual oil saturation

S_w = fractional water saturation

x = geometric cell constant for shaly sand, Eq. 2

y = geometric cell constant for shaly sand, Eq. 2

γ = constant defined by Eq. 10, mho cm^{-1}

δ = ratio of equivalent conductance of clay exchange cations to the maximum value of this equivalent conductance at higher salt concentrations, Eqs. 15 and 16

λ_{Na}^e = maximum equivalent ionic conductance of sodium exchange cations associated with clay (25C), sq cm equiv^{-1} ohm^{-1}

$(\lambda_{Na}^e)'$ = equivalent ionic conductance of sodium exchange cations associated with clay (25C) at $C_w = 0$, sq cm equiv^{-1} ohm^{-1}

μ_{Na}^e = maximum sodium exchange ion mobility (25C), sq cm volt^{-1} sec^{-1}

ϕ = porosity

ACKNOWLEDGMENTS

REFERENCES

1. Wyllie, M. R. J.: "Log Interpretation in Sandstone Reservoirs", *Geophysics* (Aug., 1960) Vol. 25, 748.

2. Lynch, E. J.: *Formation Evaluation*, Harper and Row, New York (1962) 212.

3. Hill, H. J. and Milburn, J. D.: "Effect of Clay and Water Salinity on Electrochemical Behavior of Reservoir Rocks", *Trans.*, AIME (1956) Vol. 207, 65-72.

4. Meyer, K. H. and Sievers, J. F.: "La Perméabilité des Membranes, I. Théorie de la Perméabilité Ionique", *Helv. Chem. Acta* (1936) Vol. 19, 649.

5. Teorell, T.: "An Attempt to Formulate a Quantitative Theory of Membrane Permeability", *Proc.*, Soc. Exptl. Biol. Med. (1935) Vol. 33, 282.

6. Archie, G. E.: "The Electrical Resistivity Log as an Aid in Determining Some Reservoir Characteristics", *Trans.*, AIME (1942) Vol. 146, 54-67.

7. Richman, D. and Thomas, H. C.: "Self-Diffusion of Sodium Ion in a Cation Exchange Resin", *J. Phys. Chem.* (1956) Vol. 60, 237.

8. Lai, T. M. and Mortland, M. M.: "Self-Diffusion of Exchangeable Ions in Bentonite", *Proc.*, Ninth Natl. Conf., Clays and Clay Minerals, Pergamon Press, Ltd., The Macmillan Co., New York (1960) 229.

9. Gast, R. G.: "Applicability of Models to Predict Rates of Cation Movement in Clays", *Proc.*, Soil Sci. Soc. of America (1966) Vol. 30, 48.

10. McKelvey, J. G., Jr., Southwick, P. F., Spiegler, K. S. and Wyllie, M. R. J.: "The Application of a Three-Element Model to the S.P. and Resistivity Phenomena Evinced by Dirty Sands", *Geophysics* (1955) Vol. 20, 913.

11. Smits, L. J. M.: "SP Log Interpretation in Shaly Sands", *Soc. Pet. Eng. J.* (June, 1968) 123-136.

12. Sauer, M. C., Jr., Southwick, P. F., Spiegler, K. S. and Wyllie, M. R. J.: "Electrical Conductance of Porous Plugs. Ion Exchange Resin-Solution Systems", *Ind. and Eng. Chem.* (1955) Vol. 47, 2187.

13. Cremers, A. and Laudelout, H.: "On the Isoconductivity Value of Clay Gels", *Soil Science* (1965) Vol. 100, 298.

14. Cremers, A. and Laudelout, H.: "Conductivité Electrique des Gel Argileux et Anisometrie de leurs Eléments", *J. Chim. Phys.* (1965) Vol. 62, 1155.

15. Cremers, A. and Laudelout, H.: "Surface Mobilities of Cations in Clays", *Proc.*, Soil Sci. Soc. of America (1966) Vol. 30, 570.

16. Burger, H. C.: "Das Leitvermögen verdünnter mischkristallfreien Legierungen", *Physik. Z.* (1919) Vol. 20, 73.

17. Fricke, H.: "A Mathematical Treatment of the Electric Conductivity and Capacity of Disperse Systems", *Phys. Rev.* (1924) Vol. 24, 575.

18. Cremers, A. and Laudelot, H.: Personal communication (May, 1967).

19. de Witte, A. J.: "Saturation and Porosity from Electric Logs. Part I", *Oil and Gas J.* (March 4, 1957) 89.

20. Patnode, H. W. and Wyllie, M. R. J.: "The Presence of Conductive Solids in Reservoir Rocks as a Factor in Electric Log Interpretation", *Trans.*, AIME (1950) Vol. 189, 47-52.

21. Mortland, M. M. and Mellor, J. L.: "Conductometric Titration of Soils for Cation Exchange Capacity", *Proc.*, Soil Sci. Soc. of America (1954) Vol. 18, 363.

22. Grim, R. E.: *Clay Mineralogy*, McGraw-Hill Book Co., New York (1953).

23. Winsauer, W. O., Shearin, A. M., Jr., Masson, P. H. and Williams, M.: "Resistivity of Brine-Saturated Sands in Relation to Pore Geometry", *Bull.*, AAPG (1952) Vol. 36, No. 2, 253.

24. Van Olphen, H. and Waxman, M. H.: "Surface Conductance of Sodium Bentonite in Water", *Proc.*, Fifth Natl. Conf., Clays and Clay Minerals, NAS-NRC (1958) Pub. 566, 61.

25. McLaughlin, W. A.: Personal communication.

★★★

Results of Test Drilling at Newberry Volcano, Oregon

—and some implications for geothermal prospects in the Cascades

by
Edward A. Sammel
U.S. Geological Survey
Menlo Park, California

Abstract

Test drilling by the Geothermal Research Program of the U.S. Geological Survey (USGS) in the Newberry caldera, a large Quaternary volcano located immediately east of the Cascade Range in west-central Oregon, has demonstrated that high-temperature (265°C) geothermal fluid exists in permeable rocks at a depth of 930 meters. Heat flow beneath the caldera floor may be about 1500 milliwatts per square meter, but much of the heat is dissipated by ground-water flow at shallow depths, thereby effectively masking the geothermal anomaly.

During a flow test in the drill hole, initial well-head pressure was 57 bars, and the initial mass flow rate was approximately 1.5 kilograms per second. Most of the fluid discharged consisted of steam and carbon dioxide. The liquid discharged appeared to be predominantly condensed steam.

Geophysical studies in the Cascade Range have previously encouraged the belief that the geothermal potential in the area is high. The results at Newberry appear to confirm this belief and provide incentives for additional exploration over a large area of Washington, Oregon, and California.

Introduction

Newberry Volcano in west central Oregon has been a source of interest to geothermal investigators during at least the past decade. The young rhyolitic deposits and active fumaroles in the caldera of this large volcano, as well as the hundreds of cinder cones, fissure vents, and pumice rings on the flanks of the mountain have intrigued geologists for many years and have been the focus of numerous recent investigations. Studies by Peterson and Groh (1969); MacLeod, Walker, and McKee (1975); and MacLeod and others (1981), in particular, suggest the possible significance of the area as a source of geothermal energy. Estimates by Brook and others (1978), based largely on the presence of fumaroles and analogies to other Quaternary volcanoes, have indicated that temperatures in a geothermal reservoir at Newberry might be as high as 250°C. During the past summer (1981), test drilling by the U.S. Geological Survey (USGS) demonstrated the presence of even hotter geothermal fluids at moderate depths beneath the caldera floor.

Newberry Volcano, centered about 40 kilometers (km) south of Bend, Oregon (Figure 1), is among the largest Quaternary volcanoes in the conterminous United States. Its caldera has an area of nearly 45 square kilometers (km²) and the volcano and its lava flows cover an area greater than 1200 km². Paulina Peak, the highest remnant of the former mountain, stands at an altitude of 2434 m on the rim of the present caldera. The altitude of the caldera floor is 1932 m, which is about 610 m higher than the adjacent La Pine and Fort Rock valleys. Two lakes, Paulina and East, occupy much of the caldera floor and contribute to the scenic beauty of the area. The caldera is a reserved recreational area within the Deschutes National Forest and is part of the Newberry Caldera KGRA.

The flow rocks and explosive ejecta that form the volcano range in composition from basaltic to rhyolitic and were extruded over a long period in Pleistocene and Holocene time. In most respects, Newberry is similar to the Medicine Lake volcano in northern California. Like Medicine Lake, it lies a significant distance east of the main Cascade Range.
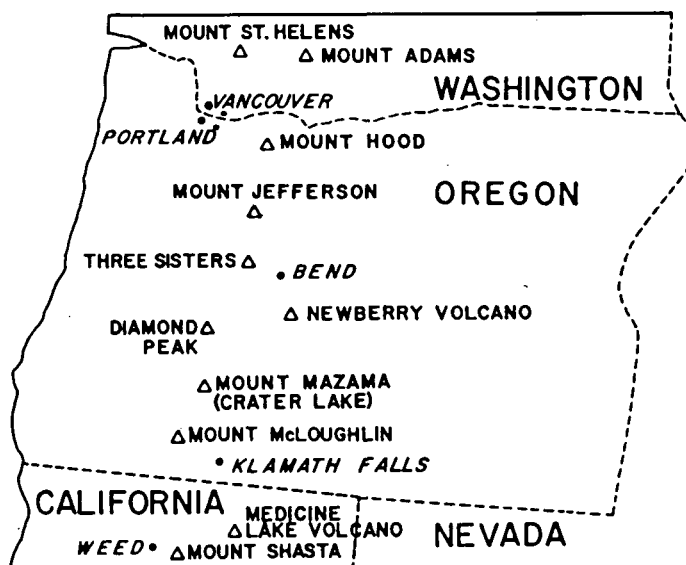

Figure 1. Map showing locations of some major volcanoes in the High Cascades Range of Washington, Oregon, and California.

Although Newberry is usually grouped with volcanoes of the Cascade Range, it is not clear how its origin and history are related to the subduction zone and crustal plate collisions that have apparently been causal factors in the construction of the High Cascades. Newberry's position as the western outpost of a trend of progressively younger silicic volcanism that can be traced through central Oregon (MacLeod, Walker, and McKee, 1975) may complicate the picture but it is probably safe to assume, for the present, that volcanism at Newberry is related to the same tectonic forces that produced the Cascade volcanoes.

The most recent volcanism at Newberry occurred about 1400 years ago when rhyolitic pumice was erupted and a large mass of obsidian flowed from a vent in the caldera. Current activity is limited to a few thermal springs (probably drowned fumaroles) which occur on the margins of Paulina and East Lakes and in a small pond, "Lost Lake," adjacent to the large obsidian flow. Temperatures of these springs are generally low, but may range to at least 62°C depending on the lake levels and lake-water temperatures. Despite the fact that 1400 years have elapsed since the last eruption, "considering the long time over which eruptions took place on Newberry, the volcano should be considered dormant but capable of future eruptions. . . . " (MacLeod and others, 1981, p. 91).

Test Drilling

In 1977 the Geothermal Research Program of the USGS drilled a small-diameter wireline core hole (Newberry 1) on the flank of the volcano about 4 km northeast of East Lake at an altitude of about 1900 m. In the core hole, pumice from the eruption of Mount Mazama (about 6700 years old) was encountered at a depth of 1 m, and the drill then penetrated cinders, breccia, tuffaceous sediments, pumice, ash-flow tuffs, ash-fall deposits, and basaltic to andesitic flow rocks to a total depth of 386 m. The lava flows range in thickness from 0.3 m to 70 m and comprise only about 44 percent of the section.
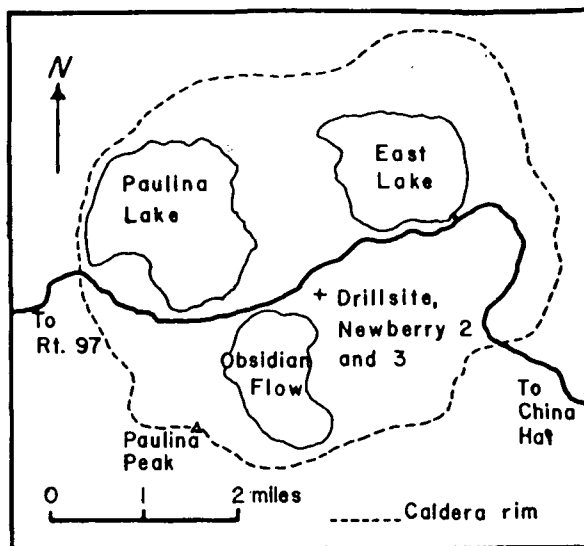

Figure 2. Map of Newberry caldera, showing the site of test holes Newberry 2 and 3.

Only small amounts of formation fluid were encountered by the drill hole, and mud circulation could not be maintained during most of the drilling. Caving was a common occurrence; as a result, the drill pipe was ultimately stuck in the hole and most of it abandoned. The hole was completed by setting 1½-inch pipe to 210 m, the final available depth, for the purpose of obtaining heat-flow measurements. The temperature profile (Figure 3) shows several zones in which ground-water flow probably affects the temperatures, notably at 154 m where the top of a black vesicular basalt flow was encountered. The maximum temperature of 9°C occurred in this zone. Because of the obvious convective disturbance, no heat-flow values have been calculated for this site.

A second test hole (Newberry 2) was spudded by the USGS in 1978, this time on the floor of the caldera, 400 m east of the big obsidian flow, at an altitude of 1935 m (Figure 2). The siting of the hole was based primarily on environmental and access criteria, although it was considered important to drill in the east half of the caldera where the more recent silicic volcanism had occurred. Rocks in the first 310 m, drilled by the mud-rotary
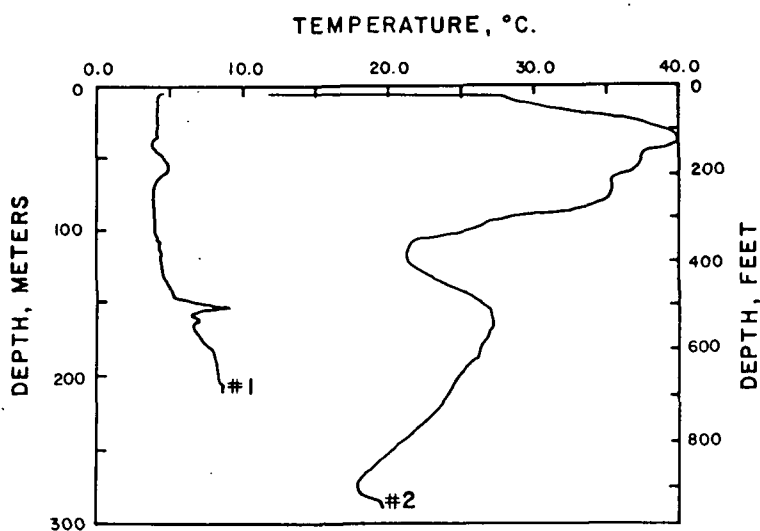

Figure 3. Temperature profiles in test holes Newberry 1 and Newberry 2. The profiles were obtained in November, 1978, one year after completion of Newberry 1 and one month after drilling to 313 m in Newberry 2.

method in order to allow for future reduction in diameter, consisted largely of pumice, cinders, ash, volcanic sediments, and thin flow rocks, similar to those in the flank hole. A notable addition was a 56-m-thick *obsidian flow* encountered at 42 m. The interval from 102 m to 335 m was subsequently cored in an offset hole, Newberry 3, with core recovery ranging between 40 percent in the interval 102 m to 186 m, and 87 percent from 186 m to 335 m.

Test-hole 2 was deepened by wireline coring during the summers of 1979 and 1981 as funds became available, and reached its final depth of 932 m on September 18, 1981. A highly generalized lithologic log of the hole, based on field observations of the core (Figure 5), reveals that a possibly deep lake once existed beneath the drill site (core interval 322 to 381 m), that the volcanic sediments and pyroclastic deposits which predominate in the upper 610 m give way to increasingly thick flow rocks in the lowest 320 m, and that there is an overall upward increase in the silica content of the rocks.

Permeabilities in the massive flow rocks are probably low, but breccia zones, volcanic sediments, and fractured, vesicular interflow zones may have much higher permeabilities. Loss of drilling fluids (up to 90 or 95 percent) occurred during most of the drilling in the upper 610 m of the hole, but little or no formation water entered the hole in this section. Hydrostatic pressures in the drill hole would always have exceeded possible pressures in the formations drilled, however, and the lack of formation-fluid returns does not indicate the absence of ground water in the rocks. Below 610 m, there was no increased loss of drilling fluid, and the overall permeability of the massive flow rocks in the lowest one-third of the hole is probably extremely low.

Thermal Gradients and Heat Flow

A temperature profile obtained in the upper 313 m of Newberry 2 in November 1978 (Figure 3) differs only in minor details from one obtained two and one-half years later in the same depth interval (Figure 4). During the
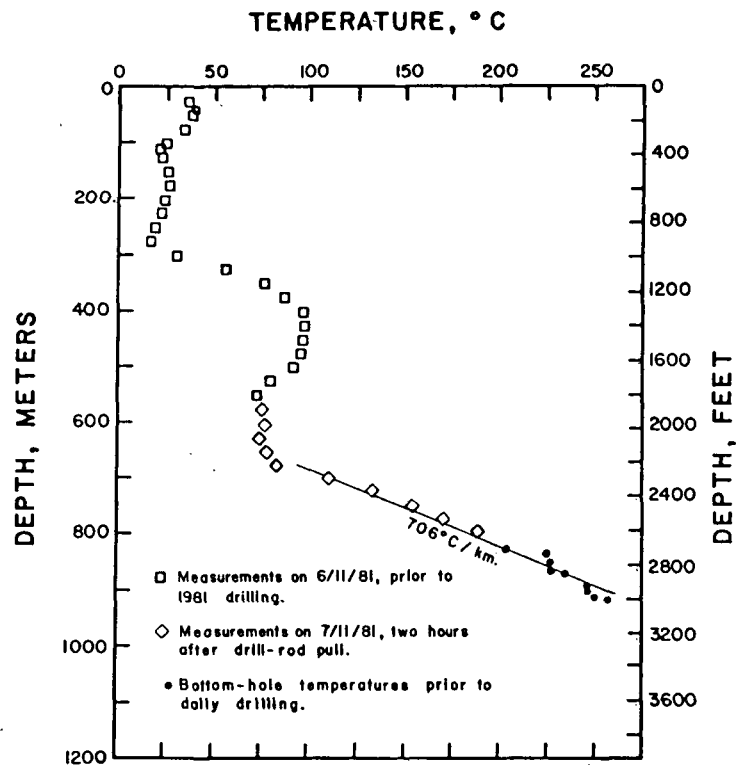
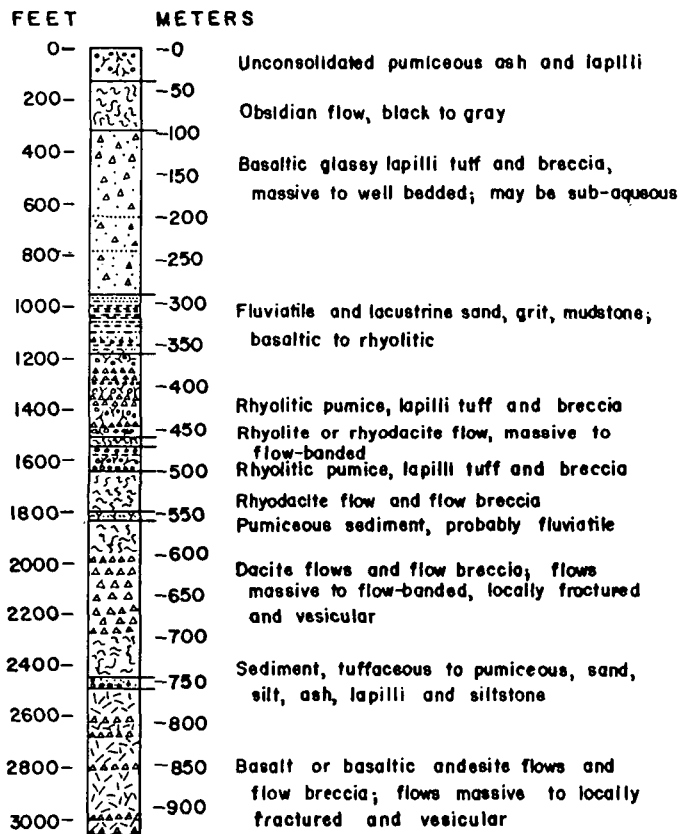**Figure 4.** *Composite temperature profile of Newberry 2.*

Figure 5. *Preliminary generalized lithologic log of Newberry 2. Descriptions of the upper 305 m of core were made from core in the adjacent hole, Newberry 3. rock names are based solely on visual examinations and have not been confirmed by chemical analyses.*

intervening time the hole had been deepened to 631 m. The warm bulges in the upper 640 m of the profile remained at virtually constant temperatures through-out the drilling period.

Most of the rocks in the vicinity of the temperature anomalies appear to have high permeabil-ities and probably low thermal conductivities, and the tempera-ture profiles are probably not conductive phenomena. The probable cause of the anomalous temperatures is warm water that rises in faults or fracture zones and moves laterally in permeable zones within the crater-fill material and flow rocks. The maximum temperature in the hottest of these convective zones, near the 425 m depth, was 100°C. Between the thermal bulges are zones, as at 120, 275, 550, and 625 m, where cooler water may carry off some of the geothermal heat and redistribute it within the caldera. Nearly all these convective anomalies in the temperature profile can be correlated with core samples that appear to have higher than normal, although still low, permeabilities. The converse is not true, however, and many zones of apparently permeable rock do not show significant temperature anomalies.

Estimates of heat flow in crustal rocks are calculated from two measurable quantities, the conductive thermal gradient and the thermal conductivity of the rock. The temperature profile in the depth interval 675 to 930 m for Newberry 2 (Figure 4) provides a reasonably firm basis for an estimate of the thermal gradient. Although at least three slightly differing segments of the profile can be defined when the data are examined in detail, for the present purpose an average gradient

through the entire interval is probably justified. The gradient calculated for this interval is 706°C per kilometer.

The second parameter, thermal conductivity, can be estimated, pending the results of laboratory tests on the core. A value of 5 mcal cm-^{1}s-^{1}°K-^{1} may be a reasonable estimate of the average conductivity of the zone, comprising as it does about 65 percent massive, unaltered basaltic andesite and andesitic flow rocks, the remainder being largely hydrothermally altered flow rocks. Using the calculated average thermal gradient and the estimated thermal conductivity, conductive heat flow through the lower part of the caldera rocks penetrated at the drill site is calculated to be about 35 Heat Flow Units (μcal cm-^{2}s-^{1}) or about 1500 milliwatts per square meter (mW m-^{2}). This preliminary estimate will be revised when conductivity measurements on the core have been made and evaluated. The significance of the estimate is uncertain because the origin and configuration of the temperature profile below the bottom of the drill hole are not known and because it can only be assumed at this time that the upper end of the conductive gradient is established by the convective effects of ground-water flow.

Preliminary Flow-Test Results

On September 29 and 30, 1981, a 20-hour flow test was made in Newberry 2. The producing zone was a 2-m section of altered, vesicular basaltic andesite penetrated at a depth of 930 m. Heavy mud (up to 10.8 lbs/gal) had been pumped into this zone in order to control gas emissions and high well-head pressures that were encountered at this depth 10

days previously. The drill pipe was stuck near the bottom of the 7.70-cm (3.032-inch) hole.

Flow was induced by swabbing drilling mud from inside the 6.07-cm (2.39-inch) NX wireline drill pipe to a depth of 427 m. The fluid pressure in the formation was not measured, but can be estimated from the weight of the fluid column in the drill hole as flow began. The estimated formation pressure is 62 bars (890 pounds per square inch), which is significantly higher than the pressure of saturated steam at the measured bottom-hole tempera-ture of 265°C (52 bars-730 psi). The excess pressure is believed to be due to the partial pressures of gases in the formation. At the well head, initial pressure ahead of a 1-inch choke was 57 bars (800 psi).

Flow was allowed to continue for 20 hours while samples of fluid and gas were collected at a separator. Preliminary estimates of flow rates indicate that the initial mass flow rate from the reservoir was approximately 1.5 kilograms per second (kg/s; 12,000 lbs/hr). At the end of 20 hours, pressure at the well head had declined to 9 bars (120 psi) and the mass flow rate was approximately 0.7 kg/s (5400 lbs/hr).

Preliminary estimates of the constituents of the gas phase suggest that steam was predomi-nant and that the noncondensable gas consisted largely of CO_2 with minor amounts of H_2S and methane. Concentrations of chloride in the liquid phase were extremely low, suggesting that the liquid was almost entirely composed of condensed steam. Chemical and isotopic analyses of the liquid and gas, to be completed during the next few months, will elucidate the composition of the formation fluids, enable more precise mass flow calculations to be made, and perhaps afford clues concerning characteristics of the geothermal reservoir.

Conclusions

It is premature to offer extensive interpretations of the drilling results or to speculate on many of their implications. The following comments can probably be made with some assurance, however.

In the setting of a recently active caldera, the high conductive thermal gradient, averaging 706°C/km through a depth interval of one-fourth kilometer, and the high temperature, 265°C at 930 meters, strongly imply the presence of a shallow crustal heat source. The distribution of post-Mazama (<6700-year-old) rhyolitic deposits over much of the eastern two-thirds of the caldera (MacLeod and others, 1981) suggests that the heat source could be a cooling, but possibly still molten, magma body. The probable smallest depth to such a body is less than 2 kilometers on the basis of an extrapolated thermal gradient and the assumption that thermal conductivity in rocks beneath the caldera does not increase with depth. The actual depth could be significantly greater than 2 kilometers and is probably indeterminate on the basis of available evidence.

Data from geophysical investigations at Newberry are in part conflicting and are at best inconclusive. Stanley (1981) found no evidence for a large magma chamber beneath Newberry in his magneto-telluric (MT) data. M. Iyer (oral commun., 1981) similarly finds no evidence in teleseismic studies made several years ago for a body of molten rock. The limit of resolution for the teleseismic data is perhaps 3 km, however. Iyer's data do show a large velocity contrast in the area, with higher velocities localized beneath the caldera. Williams and Finn (1981), on the basis of a reinterpretation of gravity data from Newberry, find a gravity high that suggests the presence of a large intrusive body, perhaps 3 km thick, at a shallow depth and extending well beyond the margins of the caldera. The teleseismic data may tend to confirm the gravity interpretation, and the MT data do not rule out the presence of a largely solidified intrusive body. Any further conclusions at this time regarding the nature and size of the heat source would be highly speculative.

The production of fluids from a zone less than 2 m thick at Newberry encourages the belief that a deeper hole might encounter additional permeable rocks that would afford larger sustained flows and perhaps even higher temperatures. The nature and origin of the geothermal fluid remain matters for speculation, however. Possible origins are: (1) the fluid encountered by the drill hole is hot reservoir water that flashed in the formation near the borehole; (2) the fluid is saturated steam at or near a boiling liquid surface; (3) the fluid is dry steam, residual from a previously saturated hot rock and/or derived from small quantities of recharge; (4) if the fluid encountered is hot water, it could be discharged upward from a deeper and presumably hotter reservoir. Although some of these possibilities seem more likely than others, a choice of the most likely must be deferred until all analyses have been completed.

Several facts having implications for geothermal prospects in the Cascade region may be noted.

First, the underlying high-temperature anomaly and the associated conductive thermal gradient at Newberry are masked by the flow of cooler water only a short distance above. Such masking is probably common in the Cascades.

Second, preliminary analysis of the core and the temperature data from Newberry 2 suggest that small flows of ground water in permeable sections of volcanic rocks are capable of intercepting large heat flows and redistributing the heat over larger areas. The resulting convective transport of heat is likely to be predominantly lateral. An uncompleted hydrologic study by the author and colleagues suggests that at Newberry little of the precipitation percolates deep beneath the crater. The same lack of connected vertical permeability that results in sealing out the meteoric water also prevents the surface discharge of most geothermal fluids.

Third, at Newberry a mass of hot and perhaps partly molten rock either underlies the caldera at shallow depths or heats geothermal fluids at greater depths in the crust. These findings

support the hypothesis of Smith and Shaw (1975) that areas of young silicic volcanism are the best targets for exploration for igneous-related geothermal systems. It is in such areas that shallow crustal magma reservoirs or cooling plutons are most likely to exist. Geologic and geophysical investigations suggest that other hidden geothermal systems may be present in the Cascade Range.

The results of the Newberry drilling, even though incomplete and, at present, ambiguous, should encourage those engaged in geothermal exploration in the Cascades and perhaps stimulate additional efforts. Whether or not new exploration occurs at Newberry Volcano, the most important outcome of the present study may be to point the way to undiscovered resources in the entire Cascade region.

References

Brook, C.A., and others, 1978, Hydrothermal convection systems with reservoir temperatures $\geq 90°C$, in Muffler, L.J.P., ed., Assessment of Geothermal Resources of the United States—1978: U.S. Geological Survey Circular 790, p. 18-85.

MacLeod, N.S., Sherrod, D.R. Chitwood, L.A., and McKee, E.H., 1981, Newberry volcano, Oregon, in Johnston, D.A., and Julie Donnelly-Nolan, eds., Guides to some Volcanic Terranes in Washington, Idaho, Oregon, and Northern California: U.S. Geological Survey Circular 838, p. 85-91.

MacLeod, N.S., Walker, G.W., and McKee, E.H., 1975, Geothermal significance of eastward increase in age of Upper Cenozoic rhyolitic domes in southeast Oregon: Second U.N. Symposium on the Development and Use of Geothermal Resources, Proceedings, v. 1, p. 465-474.

Peterson, N.V., and Groh, E.A., 1969, The ages of some Holocene volcanic eruptions in the Newberry volcano area, Oregon: The Ore Bin, v. 31, p. 73-87.

Smith, R.L., and Shaw, H.R., 1975, Igneous-related geothermal systems, in White, D.E., and Williams, D.L., eds., Assessment of geothermal resources of the United States—1975: U.S. Geological Survey Circular 726, p. 58-83.

Stanley, W.D., 1981, Magnetotelluric survey of the Cascade volcanoes region, Pacific Northwest: 51st Annual International Meeting, Society of Exploration Geophysicists, Los Angeles, CA, Geothermal Special Session 3, Oct. 13, 1981, Technical Program Abstracts and Biographies, G3.7.

Williams, D.L., and Finn, Carol, 1981, Gravity anomalies in subvolcanic intrusions in the Cascade Range and elsewhere: 51st Annual International Meeting, Society of Exploration Geophysicists, Los Angeles, CA, Geothermal Special Session 3, Oct. 13, 1981, Technical Program Abstracts and Biographies, G3.5.

Use of multiple regression for petrophysical characterization of granites as a function of alteration

Project 690038

F.P. Agterberg, T.J. Katsube[1], and S.N. Lew.
Economic Geology and Mineralogy Division

Abstract

Micropores of crystalline rocks potentially contribute to retarding the migration of radionuclides. In this paper the relation between porosity and formation factor (bulk rock resistivity over pore water resistivity) is statistically analyzed by multiple regression using dummy variables. The results show that a linear relationship exists between porosity and the reciprocal of the formation factor. It is also shown that pocket porosity first increases and later decreases with increasing degree of alteration. The tortuosity initially remains constant but becomes larger when the granites considered reach their highest degree of alteration. The average formation factor increases with the progress of alteration. These trends indicate the effect that alteration has on the pore structure.

Résumé

Les micropores des roches cristallines pourraient contribuer à retarder la migration des radionucléides. Dans le présent rapport, la relation entre la porosité et le facteur de formation (résistivité de la roche sur résistivité de l'eau interstitielle) est analysée statistiquement par régression multiple sur des variables simulées. Les résultats indiquent qu'il existe une relation linéaire entre la porosité et la réciproque du facteur de formation. Ils démontrent également que la porosité des poches commence par s'accroître pour ensuite diminuer avec l'augmentation du degré d'altération. Constante au début, la tortuosité augmente lorsque les granites considérés atteignent leur maximum d'altération. Le facteur de formation moyen s'accroît à mesure que progresse l'altération. Ces rapports donnent une idée des effets de l'altération sur la structure poreuse de la roche.

[1] Resource Geophysics and Geochemistry Division

Introduction

A study of the pore structure of crystalline rocks is being carried out under the Canadian Nuclear Fuel Waste Management Program. This is due to the potential for micropores to contribute to retarding the migration of radionuclides (Agterberg et al., 1984; Katsube and Kamineni, 1983). Porosity and formation factor (bulk electrical resistivity of the rock over pore fluid electrical resistivity) are important parameters used to characterize the pore structure. It is well known that the following empirical relationship exists between the formation factor (F) and porosity (ϕ) (Schlumberger, 1972),

$$F = a \phi^{-n} \qquad (1)$$

The symbols a and n are coefficients that vary according to rock type. Equation (1) is known as the Archie formula (Archie, 1942). Various physical models have been proposed to explain this relationship, but none of them are totally satisfactory. Katsube et al. (1985) indicated that if the existence of pocket pores is considered in the tortuosity model commonly used to describe pore structure in crystalline rocks (Wadden and Katsube, 1982; Katsube and Kamineni, 1983; Walsh and Brace, 1984), as shown in Figure 53.1a, then the following relationship should exist between the effective porosity (ϕ_E) and formation factor,

$$\phi_E = \phi_P + \tau^2 (1/F) \qquad (2)$$

where

ϕ_P = pocket porosity
τ = tortuosity

The effective porosity is the sum of the porosity of all interconnected pores. Isolated pores are excluded. The tortuosity is a parameter indicating how tortuous a pore is, and is larger than unity. If it is assumed that τ is constant, then equation (2) indicates that a linear relationship should exist between ϕ_E and 1/F (Fig. 53.1b).
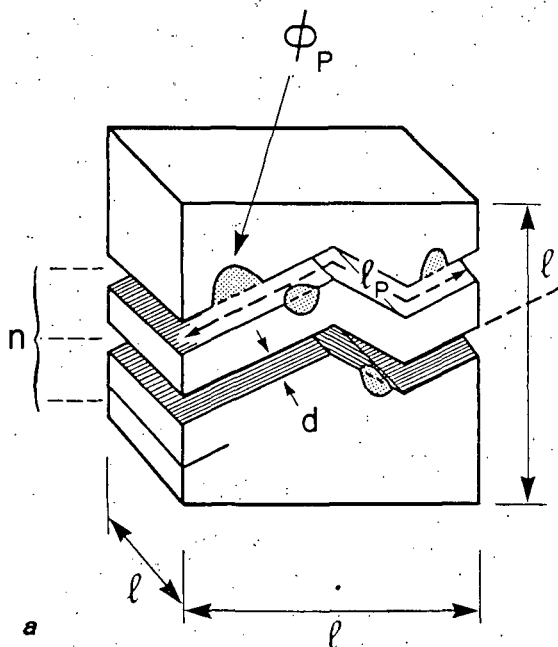
The effective porosity and formation factor have been determined for 152 granitoid core samples. Katsube et al. (1985) showed that when ϕ_E is plotted against 1/F as in Figure 53.2, there is a general trend suggesting that τ is constant. This suggestion, however, could not be confirmed previously due to the scatter of the data. One of the main reasons for the scatter appears to be the difference in the degree of alteration. It was also proposed that τ and ϕ_P are constant within a group of rocks with similar degrees of alteration, but vary when the degree of alteration varies. However, this also could not be confirmed because of the scatter of the data. Consequently, the multiple regression analysis method was applied to determine, (1) whether τ can be considered constant and a linear relationship exists between ϕ_E and 1/F, and (2) whether τ and ϕ_P vary with the degree of alteration. This paper discusses the results of this multiple regression analysis.
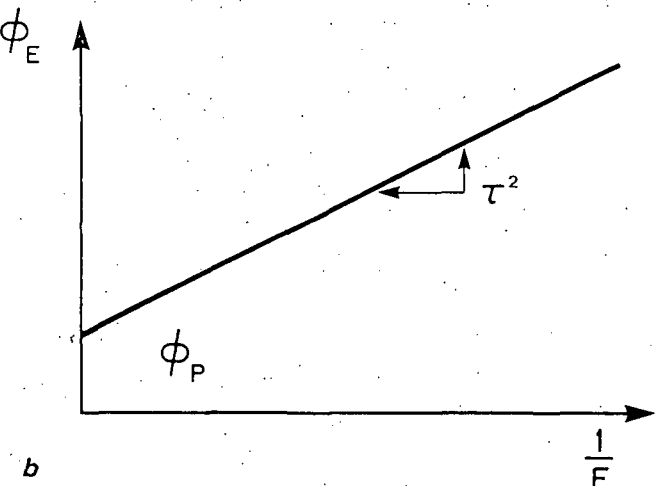
Description of data

The effective porosity is determined by measuring the difference in mass between vacuum-saturated and oven-dried rock samples. The formation factor is determined by taking the ratio of the bulk electrical resistivity of the rock sample to the electrical resistivity of the pore water for five different concentrations of pore water. The samples are 4.5 cm in diameter, and 1.0 cm in thickness. Details of the measuring and sampling methods are described in Katsube (1981). A total of 152 granitoid samples have been collected from Whiteshell (WN), Underground Research Laboratory (URL) at Lac du Bonnet, and Atikokan (ATK) research sites. The rock samples are divided into four groups designated 1-4 on the basis of the degree of pink coloration: grey (1); pinkish-grey (2); greyish-pink (3); pink (4), (Katsube and Kamineni, 1983). Grey and pink indicate the lowest and highest degree of alteration, respectively. The porosity, formation factor and alteration data are listed in Table 53.1.

Theory of multiple regression with dummy variables

Consider a dependent variable y which is related to p independent variables x_i ($i=1,2,...,p$) as:

$$y = \beta_0 + \beta_1 x_1 + ... + \beta_p x_p \qquad (3)$$

where the β_k ($k=0,1,...,p$) are unknown parameters to be estimated.

Figure 53.1(a,b). *Theoretical relationship between effective porosity (ϕ_E) and formation factor (F). Parameters characterizing pore structure are: aperture (d), tortuosity ($\tau = \ell_P/\ell$), path density (n) and pocket porosity (ϕ_P) (after Katsube et al., in press).*
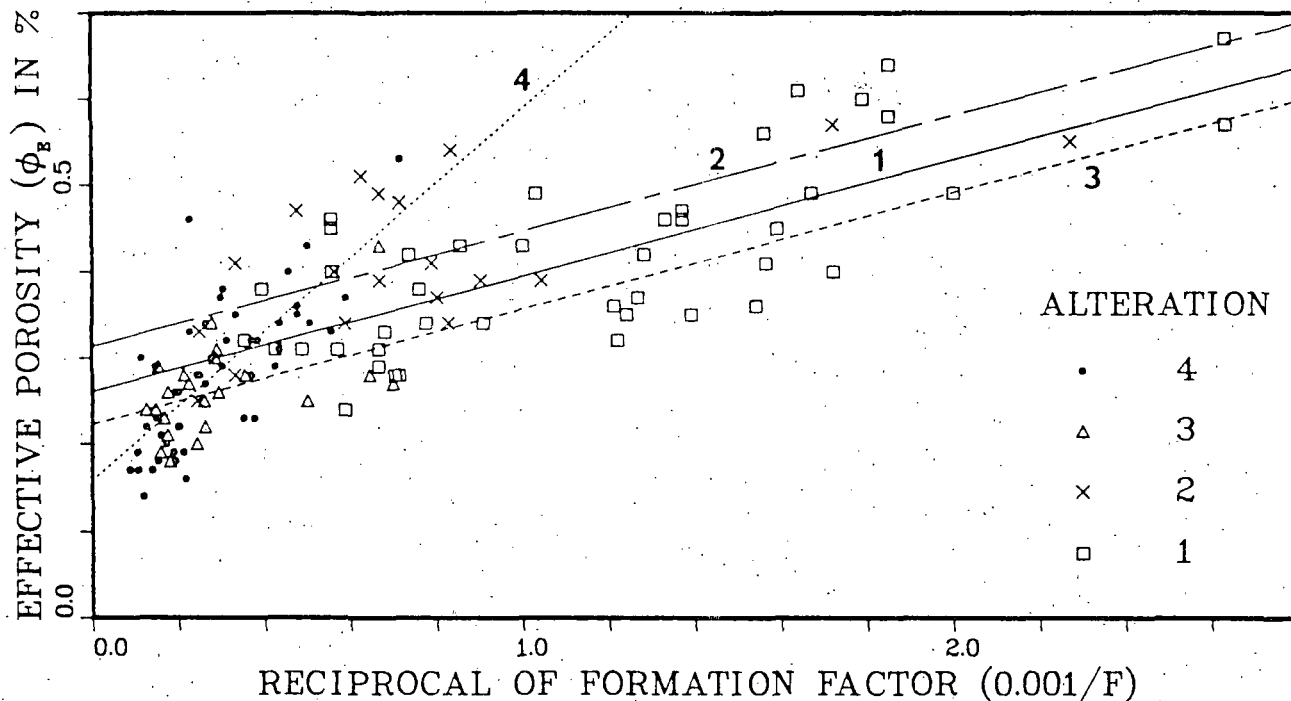
Figure 53.2. Actual data for measurements of effective porosity ($\emptyset_E$) plotted against reciprocal of formation factor (1/F). Final solution consisting of 4 straight lines for different degrees of alteration has been superimposed (also see Fig. 53.4).

Suppose that we have n observations with each observation consisting of (p+1) numbers:

$$y_j, x_{1j},..., x_{pj} \quad \text{for } j = 1,2,..., n \tag{4}$$

Based upon the n observations, we want to estimate the unknown (p+1) parameters β_k (k=0,1,2,...,p).

In multiple regression, y in (3) is assumed to be the expected or 'true' value of a random variable Y with

$$\begin{aligned} Y &= y + \varepsilon \\ &= \beta_0 + \beta_1 x_1 + ... + \beta_p x_p + \varepsilon \end{aligned} \tag{5}$$

where ε is called the residual. The latter is the same random variable as Y except that its expected value is equal to zero. For each observation j (=1,2,...,n) as in (4), y_j is considered to be an observed value of the random variable Y_j with the expected value:

$$\begin{aligned} E(Y_j) &= y_j \\ &= \beta_0 + \beta_1 x_{1j} + ... + \beta_p x_{pj} \end{aligned} \tag{6}$$

However, the corresponding residual ε_j of Y_j has the same expected value, zero for all j=1,2,...,n.

In addition, the Y_j (j=1,2,...,n) are, as usually assumed to be normally distributed with identical variance in order to apply the standard statistical significance tests to the estimated parameters and residuals. Under the linear model in (5), the (p+1) parameters β_k (k=0,1,...,p) are estimated by the method of least squares (LS method) which minimizes the sum of squares of the residuals.

The preceding theory can be found in statistical textbooks (e.g., Kendall, 1980). Computer programs to carry out the estimation of the coefficients and residuals are available in statistical packages such as SPSS, SAS, and BMDP. The method of dummy variables used in this paper is a variant of multiple regression analysis and can be applied

using these same computer programs. We have used SPSS for calculations and DISSPLA for plotting of diagrams. Reviews of use of dummy variables have previously been given in Gujarati (1970) and Agterberg (1974).

In the present application, effective porosity (y) is related to reciprocal of formation factor (x) for granitic rocks with four different types of alteration (cf. Table 53.1). In the analysis of the data, we multiply the porosity and reciprocal of the formation factor by 100 and 1000, respectively. These four groups will as before be denoted by the index j = 1, ..., 4.

For each alteration j (j=1,2,3,4), we assume a linear equation, as in (6),

$$E(Y_j) = y_j = \alpha_j + \beta_j x_j \tag{7}$$

From the observations, α_j and β_j (j=1,2,3,4) in the preceding four equations can be estimated by a_j and b_j by applying the LS method four times separately.

However, suppose that $\beta_\ell = \beta_m$ but $\alpha_\ell \neq \alpha_m$ in the preceding equation (7). By applying the regressions separately, one for j = ℓ and the other for j=m, the estimators b_ℓ and b_m for β_ℓ and β_m would not be equal. Hence, we would obtain two estimators b_ℓ and b_m for a single parameter $\beta_\ell = \beta_m$. The technique of dummy variables permits us to obtain only one estimator for $\beta_\ell = \beta_m$ and one for each of α_ℓ and α_m. In addition, the hypothesis $\beta_\ell = \beta_m$ can be evaluated by the application of significance tests.

Consider two sets of observations, one for the ℓ-th alteration and the other for the m-th alteration, i.e.

$$(y_{\ell i}, x_{\ell i}) \quad i=1,2,...,n_\ell \qquad \text{and}$$

$$(y_{mj}, x_{mj}) \quad j=1,2,...,n_m.$$

Table 53.1. Physical properties of crystalline rocks from research areas: URL (Underground Research Laboratory in Lac du Bonnet), WN (Whiteshell Nuclear Research Establishment) and ATK (Atikokan)

Sample (Borehole)-(Depth in m)	Alteration	ϕ_E	F	Sample (Borehole)-(Depth in m)	Alteration	ϕ_E	F
URL1-46.25	4	0.30	8.79	WN1-460.4	4	0.37	1.67
URL1-68.35	4	0.22	8.03	WN2-24.55	4	0.26	5.24
URL1-100.3	3	0.24	6.78	WN2-55.25	1	0.16	16.4
URL1-131.2	3	0.28	2.84	WN2-85.10	1	0.18	10.5
URL1-177.0	1	0.31	2.35	WN2-98.30	4	0.26	5.02
URL1-230.4	1	0.31	2.05	WN2-124.5	4	0.28	4.13
URL1-254.2	1	0.34	1.29	WN2-145.6	4	0.28	4.00
URL1-302.3	1	0.33	1.47	WN4-408.8	4	0.28	2.70
URL1-357.1	1	0.37	0.75	WN4-468.8	4	0.38	3.30
URL1-397.7	1	0.38	1.32	WN4-482.2	4	0.32	3.20
URL1-433.1	1	0.61	0.61	WN4-505.3	3	0.33	4.40
URL1-496.6	1	0.36	0.65	WN4-551.0	3	0.32	2.70
URL1-527.3	1	0.35	0.72	WN4-564.2	3	0.32	2.60
URL1-592.5	1	0.42	0.78	WN4-603.7	4	0.30	3.60
URL1-615.8	2	0.36	0.83	WN4-631.3	2	0.39	1.50
URL1-662.3	1	0.46	0.73	WN4-659.9	2	0.46	1.80
URL2-256.2	1	0.32	0.82	WN4-692.5	2	0.41	3.00
URL2-448.2	1	0.41	0.64	WN4-719.4	2	0.43	1.50
URL2-586.1	1	0.49	0.50	WN4-746.8	2	0.45	1.80
URL2-705.8	1	0.40	0.58	WN4-789.5	1	0.47	2.10
URL2-798.8	2	0.37	0.58	WN4-809.3	1	0.48	1.40
URL2-871.7	2	0.55	0.44	WN4-540.8	1	0.54	1.20
URL2-1001.3	1	0.67	0.38	WN4-863.5	1	0.49	1.50
URL2-1095.0	1	0.57	0.38	WN4-906.4	1	0.40	1.80
URL5-16.5	2	0.40	1.78	WN4-928.2	1	0.51	1.60
URL5-77.0	2	0.33	4.02	ATK1-13.3	4	0.27	3.80
URL5-108.2	4	0.53	1.40	ATK1-39.9	3	0.20	4.10
URL5-126.8	1	0.38	2.54	ATK1-79.2	3	0.21	5.70
URL5-156.9	2	0.41	1.27	ATK1-94.4	3	0.34	3.60
URL5-199.3	4	0.34	1.98	ATK1-111.3	3	0.19	3.56
URL5-246.8	4	0.37	3.36	ATK1-128.3	3	0.25	6.00
URL5-239.8	1	0.43	1.17	ATK1-163.1	3	0.26	3.40
URL5-333.9	1	0.42	1.36	ATK1-174.1	3	0.28	4.70
URL5-370.1	1	0.56	0.64	ATK1-237.9	3	0.22	3.80
URL5-451.1	1	0.60	0.56	ATK1-283.4	3	0.19	6.30
URL5-497.0	1	0.58	0.54	ATK1-320.9	2	0.34	1.70
URL7-132.0	3	0.25	3.82	ATK1-361.2	2	0.25	4.10
URL7-134.1	3	0.31	3.46	ATK1-400.3	3	0.26	5.70
URL7-135.4	3	0.30	3.48	ATK1-433.3	2	0.28	3.00
URL7-137.2	3	0.27	4.47	ATK1-475.3	1	0.32	2.60
URL7-138.4	3	0.18	5.53	ATK1-505.2	1	0.31	1.50
URL7-139.7	4	0.17	11.5	ATK1-539.9	1	0.45	1.01
URL7-140.6	4	0.16	4.61	ATK1-594.0	1	0.45	0.63
URL7-143.2	4	0.19	9.56	ATK1-630.2	1	0.49	0.60
URL7-144.0	4	0.23	6.77	ATK1-671.0	1	0.43	1.00
URL7-145.7	4	0.22	5.02	ATK1-715.0	3	0.24	8.00
URL7-147.5	4	0.19	5.30	ATK1-747.1	2	0.39	1.10
URL7-147.7	4	0.19	4.71	ATK1-788.1	1	0.47	0.73
URL7-148.1	4	0.18	6.55	ATK1-812.3	1	0.35	0.81
URL7-150.2	4	0.18	5.17	ATK1-849.2	1	0.24	1.70
URL7-155.3	4	0.21	6.29	ATK1-901.9	1	0.34	1.10
URL7-157.6	4	0.17	7.21	ATK1-923.8	3	0.29	6.50
URL7-138.2	4	0.14	8.41	ATK1-979.7	1	0.29	1.50
URL7-159.2	4	0.17	9.36	ATK1-1021.2	1	0.46	7.50
URL7-161.7	4	0.20	5.81	ATK1-1034.2	4	0.34	3.80
URL7-161.3	4	0.22	4.95	ATK1-1063.4	1	0.49	0.97
URL7-163.7	4	0.23	2.65	ATK1-1079.4	3	0.23	2.00
URL7-166.5	4	0.29	2.35	ATK1-1097.2	4	0.29	6.80
URL7-170.7	4	0.23	2.84	ATK1-1121.6	4	0.46	4.60
URL7-174.3	3	0.28	1.55	ATK1-1140.4	1	0.64	0.54
URL7-177.6	3	0.27	1.43	ATK5-106.4	1	0.29	2.45
URL7-181.0	2	0.39	0.96	ATK5-224.3	4	0.22	4.96
URL7-181.8	2	0.37	1.25	ATK5-337.4	1	0.27	2.33
URL7-184.7	2	0.34	1.21	ATK5-423.9	2	0.26	4.38
URL7-188.0	1	0.31	1.75	ATK5-534.1	1	0.40	1.66
URL7-192.9	4	0.28	1.40	ATK5-625.7	1	0.29	4.28
URL7-197.8	1	0.28	1.42	ATK5-708.6	1	0.35	0.90
WN1-138.4	4	0.35	3.01	ATK5-817.9	1	0.40	0.45
WN1-160.7	4	0.29	3.31	ATK5-867.6	1	0.34	0.90
WN1-223.7	3	0.43	1.95	ATK5-918.3	1	0.34	0.86
WN1-245.8	3	0.36	2.14	ATK5-951.2	1	0.29	1.53
WN1-294.3	4	0.40	2.17	ATK5-975.5	1	0.37	0.91
WN1-303.3	4	0.33	1.83	ATK5-1050.2	1	0.37	0.70
WN1-345.3	3	0.35	2.08	ATK5-1107.8	1	0.44	0.67
WN1-384.6	4	0.31	2.30	ATK5-1228.5	1	0.29	1.96
WN1-410.5	4	0.34	2.27				

By combining the two sets of observations and defining two new dummy variables, we obtain:

$$
\begin{array}{cccc}
y_{\ell 1} & 0 & x_{\ell 1} & 0 \\
\vdots & \vdots & \vdots & \vdots \\
y_{\ell n_\ell} & 0 & x_{\ell n_\ell} & 0 \\
y_{m1} & 1 & x_{m1} & x_{m1} \\
\vdots & \vdots & \vdots & \vdots \\
y_{mn_m} & 1 & x_{mn_m} & x_{mn_m}
\end{array} \tag{8}
$$

Instead of two sets of observations, n_ℓ observations for the ℓ-th alteration and n_m observations for the m-th alteration, with one dependent variable and one independent variable, we now have a single set of $(n_\ell+n_m)$ observations with one dependent variable and three independent variables.

Consider now the following model:

$$ Y_{\ell m} = \gamma_0 + \gamma_1 z_1 + \gamma_2 z_2 + \gamma_3 z_3 + \epsilon_{\ell m} \tag{9} $$

Using the data in (8) where the first column is considered as consisting of the expected values for $Y_{\ell m}$, and the second, third and fourth columns are representing z_1, z_2 and z_3, respectively, and using the LS method of multiple regression, LS estimators c_0, c_1, c_2 and c_3 are obtained for γ_0, γ_1, γ_2 and γ_3.

If c_3 is statistically significant (i.e., $\gamma_3 \neq 0$) according to the statistical significance test, the hypothesis $\beta_\ell = \beta_m$ should be rejected under the assumptions of the model. Otherwise, i.e. if γ_3 can be assumed to be zero, c_2 may be regarded as an estimator of $\beta_\ell = \beta_m$. However, a better estimator of γ_2 may be obtained by repeating the multiple regression after deleting z_3 as an independent variable. Similarly, we can test $\alpha_\ell = \alpha_m$ by examining c_1 following the same procedure as for c_3.

The model can be extended to incorporate more than two groups. A version in which all four groups are considered simultaneously will be introduced and used at the end of the next section.

Application of multiple regression with dummy variables

The four groups of Table 53.1 were compared pairwise according to the method explained in the previous section. The results are shown in Table 53.2. Each multiple regression run yielded 4 coefficients c_0 to c_3 which were evaluated for statistical significance according to an F-test as follows. Suppose that one of the coefficients and its corresponding independent variable x_{ij} are omitted. Then the squared multiple correlation coefficient R^2 which provides a measure of the total degree of fit provided by a multiple regression equation will be reduced. This difference is only statistically significant if it exceeds a critical value determined by the numbers of observations in the groups compared to one another. An F-value can be computed to evaluate this difference. If the contribution of the variable is not statistically significant, this F-value is equal to one on the average. Each estimated F-value can be transformed into a probability P that the contribution of the corresponding variable is not significant (Table 53.2).
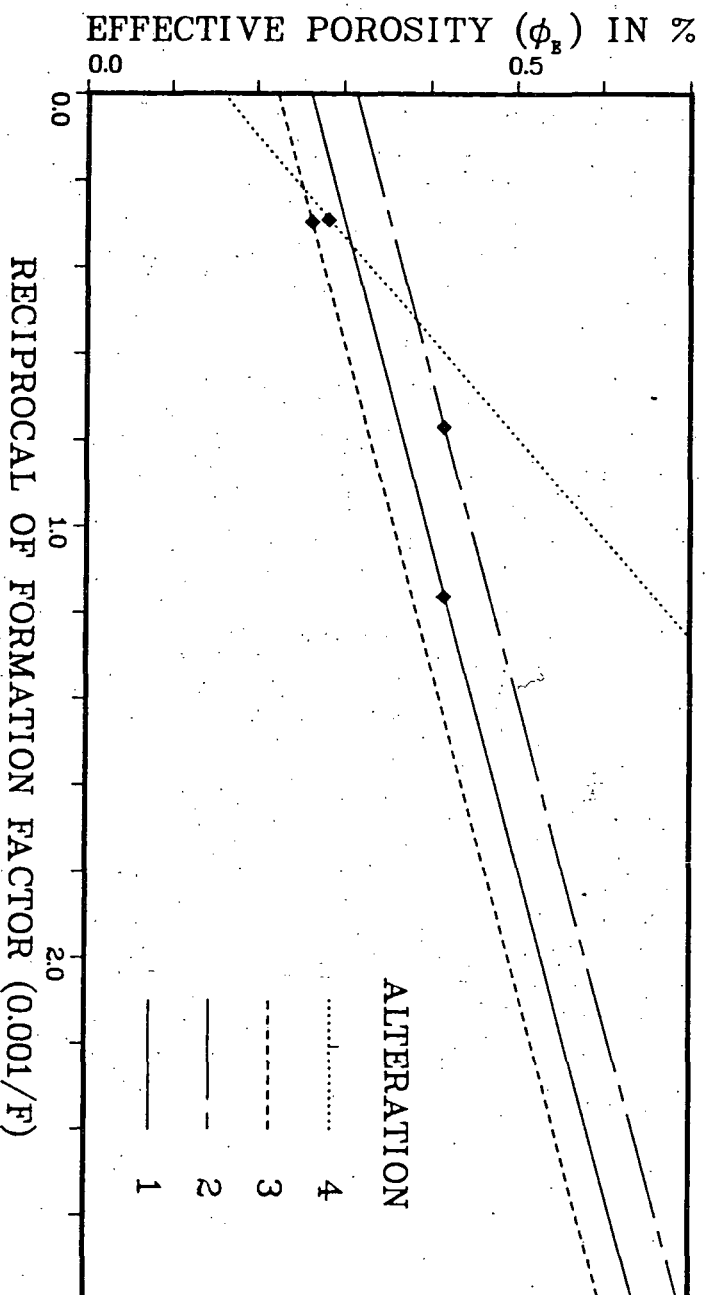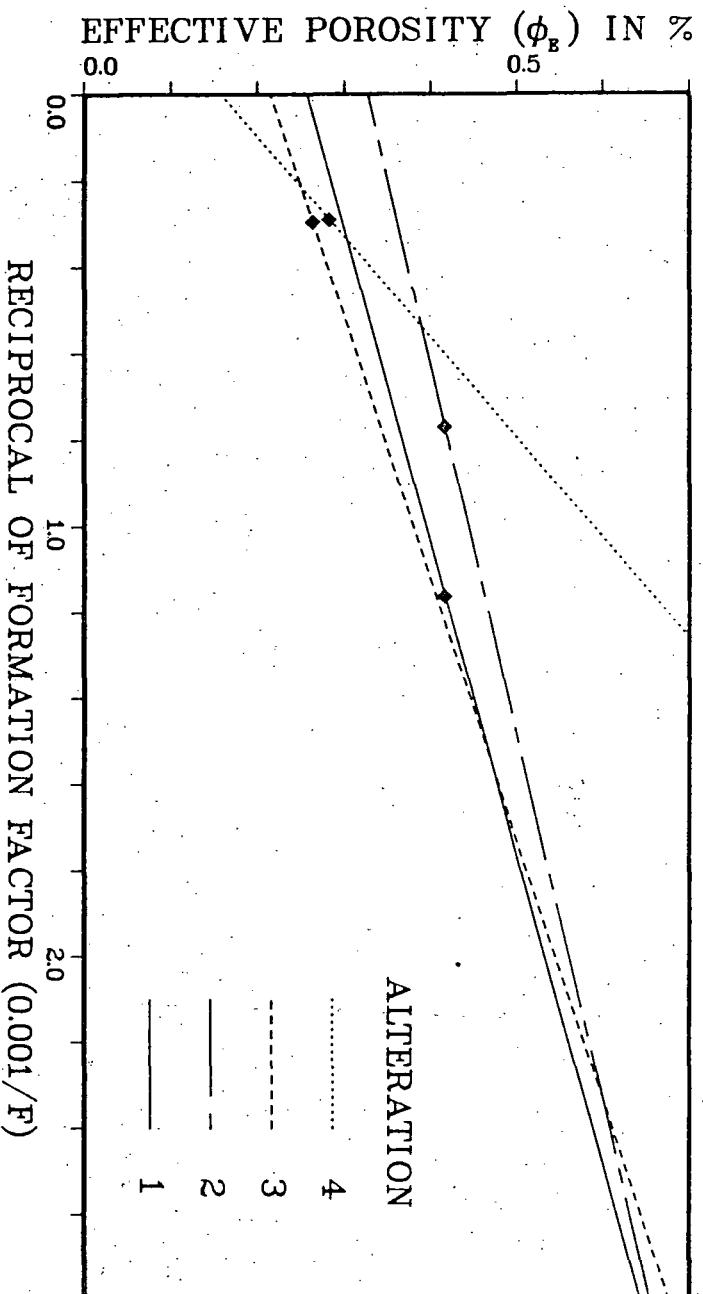
The values of R^2 and estimated standard deviations of residuals s_e are also shown in Table 53.2 for the six multiple regressions performed. The s_e-values suggest that the average deviation from the fitted regression lines decreases slightly with increasing degree of alteration. Inspection of the coefficients of Table 53.2 illustrates that c_0, c_2, $(c_0 + c_1)$ and $(c_2 + c_3)$ are almost equal to one another for all four groups in the six different pairs. This allows us to extract the following four linear relationships:

Group 1: $y_1 = 0.256 + 0.138x_1$
Group 2: $y_2 = 0.326 + 0.117x_2$
Group 3: $y_3 = 0.214 + 0.165x_3$
Group 4: $y_4 = 0.157 + 0.431x_4$

These lines are shown graphically in Figure 53.3. They also represent the best-fitting lines of least squares resulting from bivariate regressions. We have approximately $\epsilon_{ij} = \epsilon_i = \epsilon_j$ where ϵ_{ij} represents the residuals for y_{ij} in a pairwise comparison (i, j); ϵ_i is for y_i and ϵ_j for y_j in corresponding bivariate regressions. Inspection of Table 53.2 shows that the coefficients c_0 and c_2 are statistically significant in all six solutions. The F-values are less than one for c_3 in the pairwise comparisons (1, 2), (1, 3) and (2, 3). This indicates that the slopes of the lines, for groups 1 to 3 are probably equal to one another. $P_3 = 0.000$, 0.000 and 0.004 for the 3 pairwise comparisons involving Group 4.

Table 53.2. Pairwise comparison of groups of samples with different degrees of alteration (i,j) using model of equations (8) and (9) in the text. Each coefficient c (c_0-c_4) is followed by its F-ratio which was converted into the probability P that the coefficient is equal to zero. The multiple correlation coefficient squared (R^2) and estimated standard deviation of residuals (s_e) are also listed for each regression solution.

(i, j)	(1, 2)	(1,3)	(1, 4)	(2, 3)	(2, 4)	(3, 4)
c_0	0.256	0.256	0.256	0.326	0.326	0.214
F_0	107.739	132.543	132.113	157.373	147.540	82.804
P_0	0.000	0.000	0.000	0.000	0.000	0.000
c_1	0.070	-0.042	-0.099	-0.112	-0.169	-0.057
F_1	3.136	1.425	10.515	9.443	25.446	3.688
P_1	0.082	0.237	0.000	0.004	0.000	0.059
c_2	0.138	0.138	0.138	0.117	0.117	0.165
F_2	51.913	63.865	63.658	16.574	15.538	5.695
P_2	0.000	0.000	0.000	0.000	0.000	0.020
c_3	-0.022	0.026	0.293	0.048	0.314	0.266
F_3	0.304	0.103	19.414	0.355	21.094	9.143
P_3	0.584	0.750	0.000	0.555	0.000	0.004
R^2	0.523	0.712	0.704	0.704	0.670	0.514
s_e	0.071	0.064	0.065	0.060	0.062	0.055

EFFECTIVE POROSITY (ϕ_E) IN %

RECIPROCAL OF FORMATION FACTOR (0.001/F)

ALTERATION
······· 4
- - - - 3
— — 2
——— 1

Figure 53.3. *Effect of degree of alteration on the ϕ_E versus 1/F relationship. Four straight lines fitted by pairwise comparison of groups with different degrees of alteration. Group means (diamonds) are also shown.*

EFFECTIVE POROSITY (ϕ_E) IN %

RECIPROCAL OF FORMATION FACTOR (0.001/F)

ALTERATION
······· 4
- - - - 3
— — 2
——— 1

Figure 53.4. *Schematic diagram for the different degrees of alteration 1-4. Final solution obtained by multiple regression with 3 dummy variables (see Table 53.3). Group means (diamonds) are also shown.*

It may therefore be concluded that Group 4 has a different slope. The coefficient c_1 is not statistically significant for level of significance $\alpha = 0.05$ in three pairwise comparisons: (1, 2) with $P_1 = 0.082$, (1, 3) with $P_1 = 0.237$ and (3, 4) with $P_1 = 0.059$. It is noted that from the pairwise comparisons (1,2) and (1,3), it could be inferred that $c_1 = 0$ suggesting the same intercept for alterations 1, 2 and 3. However, the results in Table 53.2 also indicate that the difference in intercept between alterations 2 and 3 is statistically significant. This inconsistency arises from the fact that only two alterations are compared in each regression of Table 53.2. It suggests that more than two groups should be compared simultaneously as will be done later in this section. In the final solution (Fig. 53.2, 53.4), the intercept of alteration 1 is between those of 2 and 3.

It was initially decided to rerun the multiple regressions for pairs (i, i + 1) which have one or more P-values greater than 0.05 in Table 53.2. Dropping the variable with least effect in each of the runs (1, 2), (2, 3) and (3, 4) gave the following results:

Pair (1, 2): $y_1 = 0.262 + 0.133x_1$; $y_2 = 0.314 + 0.133x_2$
Pair (2, 3): $y_2 = 0.322 + 0.123x_2$; $y_3 = 0.227 + 0.123x_3$
Pair (3, 4): $y_3 = 0.178 + 0.256x_3$; $y_4 = 0.178 + 0.374x_4$

All coefficients are statistically significant ($P > \alpha = 0.05$) in these new runs. Although this presents an advantage with respect to the earlier result shown in Figure 53.3, the new result has nine, instead of eight coefficients because there are now two different solutions for y_2 and y_3. Because the resulting lines for Groups 2 and 3 are not approximately coinciding, it was decided to perform a single multiple regression with 3 dummy variables separating all four groups but forcing the slopes of Groups 1, 2 and 3 to be equal to one another. The model for this run is:

$$y = \gamma_0 + \gamma_1 d_1 + \gamma_2 d_2 + \gamma_3 d_3 + \gamma_4 x + \gamma_5 d_3 x + \varepsilon \quad (10)$$

where $y = y_j$, $x = x_j$ ($j = 1, ..., 4$); $d_1 = 0$ if $x = x_1$ (and 1 otherwise); $d_2 = 0$ is $x = x_1$ or x_2 (and 1 otherwise); and $d_3 = 0$ if $x = x_1$, x_2 or x_3 (and 1 if $x = x_4$).

The estimated coefficients for the new run are shown in Table 53.3. The R^2-value amounts to 0.703. The standard deviation of residuals amounts to $s_e = 0.062$. Assuming that this pooled value for s_e can be used for all four groups, the final solution becomes:

Group 1: $y_1 = 0.261 + 0.134x_1$
Group 2: $y_2 = 0.313 + 0.134x_2$
Group 3: $y_3 = 0.223 + 0.134x_3$
Group 4: $y_4 = 0.158 + 0.431x_4$

Table 53.3. Final multiple regression result using model of equation (10) in the text. F-ratios and corresponding probabilities P show that coefficients c probably differ from zero indicating that the effects of all variables used are statistically significant.

i	c_i	F_i	P_i
0	0.2611	183.8	0.000
1	-0.0656	7.1	0.009
2	-0.0899	18.6	0.000
3	0.0519	8.2	0.005
4	0.1341	86.0	0.000
5	0.2968	21.4	0.000

The F- and P-values in Table 53.2, show that the variables in this model all contribute significantly. The final result is shown graphically in Figures 53.2 and 53.4. In Figures 53.3 and 53.4, the average x- and y-values for the groups are also shown with

Group 1: $\bar{x}_1 = 1.163$; $\bar{y}_1 = 0.416$
Group 2: $\bar{x}_2 = 0.770$; $\bar{y}_2 = 0.416$
Group 3: $\bar{x}_3 = 0.296$; $\bar{y}_3 = 0.263$
Group 4: $\bar{x}_4 = 0.282$; $\bar{y}_4 = 0.291$

Discussion and conclusions

The multiple regression analysis consists of estimating 8 coefficients in 4 linear equations (one equation for each group of samples). The grouping is based on the degree of alteration 1-4. The results of the analysis indicate that while the intercept varies for different groups, the slope is identical for groups 1 to 3, but is larger for group 4. This confirms the assumption that ϕ_p (intercept) varies with alteration, but τ (square root of the slope) is independent of alteration until an alteration degree of 4 is reached. Since the values of ϕ_E and $1/F$ were multiplied by 10^2 and 10^3 for the analysis, the true values of the intercepts, slopes and averages for x and y are respectively 10^{-2}, 10, 10^{-3} times those shown in the solutions. Therefore, the values of τ for groups 1-3 is 1.16, and for group 4 is 2.08.

The value of ϕ_p increases as the degree of alteration progresses from 1 to 2, but then decreases with further progress of alteration. The mean of $1/F$ decreases as alteration progresses. These trends, as well as the trends observed for τ, are shown in Figure 53.4. Based on the model presented by Katsube et al. (1985), the changes in τ and ϕ_p in relation to alteration can be explained as follows. It is assumed the basic pore structure of an unaltered rock can be represented by alteration 1 in Figure 53.4. As the alteration progresses to degree 2, certain minerals along the connecting paths are leached, pocket pores form and the tortuosity remains constant. This explains the parallel shift of the lower line 1 to the upper line 2 in Figure 53.4. As alteration progresses to alteration 3, deposition takes place, the paths are narrowed (alteration 3) and some of the pocket pores are sealed off from the network of connecting pores. The tortuosity remains constant. When the paths are narrowed, the aperture decreases and the formation factor (F) will increase (equation 1). Thus, the average of $1/F$ shifts along the upper line towards the lower end of the abscissa, as shown in Figure 53.4. The sealing of the pocket pores results in the parallel shift of line 2 to the lower line 3 in Figure 53.4. As the alteration progresses to degree 4, the thickness of the deposition layer increases and finally some paths are sealed and more of the pocket pores are blocked off from the main connecting path. This results in an increase in tortuosity (τ) and a further decrease in pocket porosity (ϕ_p) as shown in the shift of data to a line with a larger gradient and a decrease in the intercept in Figure 53.4. This model is identical to that proposed by Katsube and Kamineni (1983).

The results of the multiple regression analysis provide a firm statistical basis which supports the physical model suggested by Katsube et al. (1985): τ and ϕ_p are constants that vary with the degree of alteration, and thus a linear relationship exists between ϕ_E and $1/F$. This physical model is very useful for characterizing the pore structure of rocks. This study shows that multiple regression analysis using dummy variables is very useful for analyzing the pore structure data. Previously it was shown that the statistical method for decomposition of mixtures of normal distributions was also an effective method for obtaining information on intermediate pores that were buried in data dominated by the effect of micro and nano pores (Agterberg et al., 1984). The use of statistical methods is becoming essential in the study of pore structure of crystalline rocks.

References

Agterberg, F.P.
1974: Geomathematics: Mathematical Background and Geo-Science Applications. Elsevier, Amsterdam. 596 p.

Agterberg, F.P., Katsube, T.J., and Lew, S.N.
1984: Statistical analysis of granite pore size distribution data, Lac du Bonnet batholith, eastern Manitoba; in Current Research, Part A, Geological Survey of Canada, Paper 84-1A, p. 29-38.

Archie, G.E.
1942: The electrical resistivity log as an aid in determining some reservoir characteristics; Trans. American Institute for Mining Engineers, 146: 54-67.

Gujarati, D.
1970: Use of dummy variables in testing for equality between sets of coefficients in linear regressions: A generalization; American Statistician, v. 24 (5), p. 18-21.

Katsube, T.J.
1981: Pore structure and pore parameters that control radionuclide transport in crystalline rocks; Proc. Tech. Prog. International Powder and Bulk Solids Handling and Processing, Rosemont, Ill., May 12-14, p. 394-409.

Katsube, T.J. and Kamineni, D.C.
1983: Effect of alteration on pore structure of crystalline rocks: core samples from Atikokan, Ontario. Canadian Mineralogist, v. 21, p. 637-644.

Katsube, T.J., Percival, J.B., and Hume, J.P.
1985: Characterization of the rock mass by pore structure parameters; Atomic Energy of Canada Limited, Technical Record TR-299.

Kendall, M.G.
1980: Multivariate Analysis (Second edition); Griffin, London, 210 p.

Schlumberger
1972: Log interpretation manual/principles, vol. I, Houston, Schlumberger Well Services, Inc.

Wadden, M.M. and Katsube, T.J.
1982: Radionuclide diffusion rates in crystalline rocks; Chemical Geology, v. 36, p. 191-214.

Walsh, J.B. and Brace, W.T.
1984: The effect of pressure on porosity and the transport properties of rock; Journal of Geophysical Research, v. 89, p. 9425-9431.

BOREHOLE GEOPHYSICAL INVESTIGATIONS
IN THE SOUTH TEXAS URANIUM DISTRICT

By JEFFREY J. DANIELS, JAMES H. SCOTT, PAUL D. BLACKMON,

and HARRY S. STARKEY, Denver, Colo.

Abstract.—Contrasts of electrical properties between uranium deposits and their host rocks in South Texas are subtle. In places where deposits are small or deep, conventional geophysical well-logging techniques and hole-to-hole measurements may be the only practical method to detect changes in rock properties associated with the occurrence of uranium ore deposits. Two separate ore-producing areas in South Texas were chosen for studying borehole geophysical techniques applied to uranium-exploration problems. Extensive measurements of physical properties were made on cores and taken from holes where electrical-resistivity, induced-polarization and gamam-ray logs were run. These analyses show that: (1) induced-polarization anomalies are caused by a change in pyrite content and clay-sized material content and (2) resistivity anomalies are associated with a change in clay-sized material content and cementation. In addition to conventional borehole techniques, hole-to-hole induced-polarization and resistivity tests were made in South Texas. These measurements were made by placing a current source down one hole and a receiver cable down an adjacent hole whose separation ranged from 30 to 300 m and hole depths varied from 80 to 270 m. These tests show that hole-to-hole measurements can be used to detect changes in physical properties, associated with uranium ore, that occur between boreholes. Hole-to-hole measurements provide a link between surface measurements and well logs and can minimize the amount of drilling needed to locate an ore deposit. Accordingly, borehole geophysics will become an increasingly important evaluation tool as mineral exploration goes deeper.

Uranium was first discovered in western Karnes County in the Coastal Plains of southeast Texas in 1954. Since then, extensive exploration has uncovered most of the shallow, high-grade (more than 0.20-percent U_3O_8) uranium ore in this district. Further exploration efforts will be concentrated on shallow, low-grade deposits (less than 0.02-percent U_3O_8) and on higher grade, deeper deposits.

Economical exploration for these low-grade deposits will require the development of new techniques that will minimize the amount of exploration drilling. Successful exploitation of the deposits, by efficient mining operations, will require economic techniques to establish the physical and chemical properties of the host rocks. Here, borehole geophysical techniques will be useful in delimiting ore and in providing an inexpensive means of determining physical and chemical rock properties.

Uranium minerals in South Texas have been found in bentonitic clay, silt, or tuffaceous sand in various stratigraphic positions ranging in age from Eocene to Pliocene (Eargle and Weeks, 1968). The uranium minerals occur in four different geologic units: the Goliad Sand of Pliocene age, the Oakville Sandstone of Miocene age, the Catahoula Tuff of Miocene age, and the Jackson Group of Eocene age (Eargle, and others, 1971). At the present time, most of the exploration activity is concentrated in the Oakville, Catahoula, and Jackson.

This study is primarily concerned with property 1 in the Oakville and property 2 in the Catahoula. (Exact locations of properties 1 and 2 are proprietary information.) A line of holes was drilled on property 1 in order to gather borehole geophysical data and cores from which data on mineralogic and physical rock properties were obtained. The borehole geophysical information at property 1 included induced-polarization, gamma-ray, and resistivity well logs. Hole-to-hole resistivity and IP (induced-polarization) measurements were also made in a line of drill holes on property 1. Borehole geophysical measurements on property 2, where the drill holes penetrate the Catahoula Tuff, include gamma-ray and neutron well logs and hole-to-hole resistivity and IP measurements.

GEOLOGY

A geologic cross section for a line across property 1 is shown in figure 1. The sand-clay beds dip to the east. The sands are unconsolidated and contain fine- to medium-sized grains. The lower sand contains the highest gamma-ray count and is the "ore sand" in this area. A sand is assumed to be an "ore sand" if its gamma-ray count is at least five times higher than the background gamma-ray count.

343

WEST

EAST

FIGURE 1.—Geologic cross section on property 1 through holes drilled in the Oakville Sandstone.

EXPLANATION

Clay   Sand   Sandy clay   Clayey sand   Calcium carbonate cement   4 Borehole number

Concentration changes of selected minerals
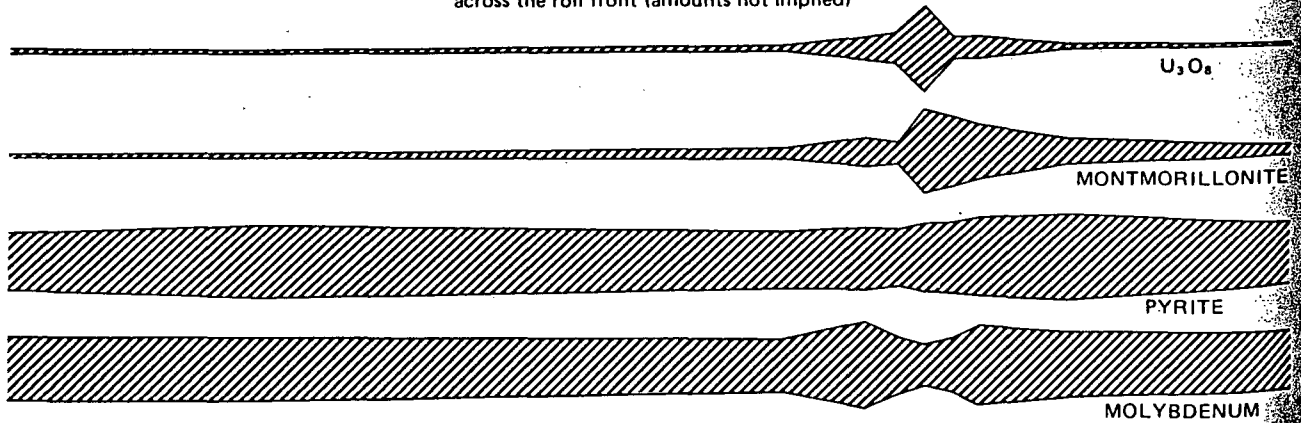across the roll front (amounts not implied)

U_3O_8

MONTMORILLONITE

PYRITE

MOLYBDENUM

etrographic analysis of cores from the "ore sand" icates that the dominant minerals are quartz, mont-illonite, and illite while the minor constituents are ite, pyrite, and jordisite. Marcasite, clinoptilolite, anatase are found only in trace amounts. A sum-y of the analysis of the sand-clay, pyrite, molyb-um, and uranium oxide (U_3O_8) for the ore sand in eholes 3 through 8 is given in table 1. References lay content in this paper refer to clay-sized parti-; (<2 micrometers) rather than clay mineral con-t. In general, there is an increase in pyrite content oss the ore zone, while the total clay content ains relatively unchanged across the ore zone. lybdenum content and the montmorillonite clay ction increase with an increase in U_3O_8.

LE 1.—*Sand, total clay, montmorillonite, pyrite, U_3O_8, and olybdenum content for samples in boreholes 3–8, property 1*

x, parts per million; ?, questionable; <, less than; and ___, no data]

te	Depth, in meters	Sand	Total clay	Montmorillonite	Pyrite	U_3O_8	Mo(ppm)
				Percent			
	75	9.2	63.2	25.0	1.65	0.037	46
	69	83.4	5.3	3.7	.5	.0014	4
	66	69.5	10.1	6.1	1.05	.0024	16
	49	44.5	34.6	6.9	?	.0003	<2
	72	86.9	3.38	2.3	.3	.002	2
	75	85.0	6.3	3.8	.6	.0017	12
	70	69.3	13.6	6.8	1.8	.0075	18
	66	19.3	55.0	17.0	1.35	<.0002	2
	77	4.4	62.4	12.5	.2	.13	36
	64	78.9	8.4	4.2	.5	<.0002	2
	78	8.1	62.7	31.4	.1	.007	100
	77	72.5	8.0	4.0	.65	.002	44
	73	85.4	3.9	1.4	1.15	.0011	2
	75	77.0	11.8	8.3	.40	.002	23
	72	81.0	5.3	3.2	2.0	.003	4
	70	79.0	6.2	3.1	.75	.046	36
	67	65.0	12.0	6.0	1.7	.0007	12
	76	85.0	4.6	2.8	1.5	.14	200
	69	79.0	7.7	4.6	1.4	.017	60
	73	84.0	5.6	2.8	1.0	.003	4
	65	28.0	50.0	15.0	2.0	<.0002	2
	79	83.5	4.3	1.7	1.0	.0070	100
	76	82.8	5.2	2.1	.25	.091	100
	73	84.3	5.4	2.2	1.7	.0065	120
	71	70.0	8.3	1.7	.3	.005	65
	69	20.0	8.3	4.2	.3	.0002	8
	78	80.6	6.8	3.4	—	.014	50
	69	42.7	20.2	8.1	1.45	.0003	10
	79	85.7	3.9	2.0	.40	.0075	46
	80	78.2	6.0	2.4	.40	.0032	42
	71	69.6	14.5	7.3	.65	.0065	26
	74	78.2	5.9	3.5	.85	.0065	80
	76	76.8	7.1	2.8	1.05	.046	240
	80	72.4	14.0	8.4	1.3	.0095	65
	70	38.5	24.4	14.6	1.2	.0003	4
	74	83.3	5.9	3.5	1.8	.0095	100
	72	80.0	9.1	6.3	2.15	.0034	18
	75	82.8	4.4	2.6	1.0	.029	70
	77	86.0	3.2	1.9	1.1	.021	50
	79	85.5	2.9	1.1	1.2	.0055	100
	80	83.9	3.6	2.2	.50	.0045	44
	81	79.3	4.2	2.1	1.4	.0038	36

A "roll-front" uranium deposit has been defined by abin (1970) as: ". . . a C-shaped interface between e altered and unaltered portions of a sandstone ong which uranium has been deposited. The inter-ce probably is caused by oxidizing agents moving wn dip through a carbonaceous and pyritic water turated sandstone (reducing environment)."

The general geologic characteristics of the roll front on property 1 are shown in figure 1. On the basis of the gamma-ray logs, the front can be divided into three geochemical zones: an "oxidized" zone, an "ore" zone, and a "reduced" zone. However, the mineral content and color of the lower sand indicates a reducing environment for the cross section. Fresh sand samples indicate the presence of H_2S gas. It is possible that an oxidized-reduced front existed at an earlier time, but the "oxidized" zone has been reduced by the introduction of H_2S gas.

A lithologic cross section for property 2 (fig. 2) shows a sand-shale sequence similar to that for property 1. There is no comprehensive mineral analysis available for property 2. However, gamma-ray and lithologic logs indicate the presence of a roll front as indicated in figure 2.

RESISTIVITY AND INDUCED-POLARIZATION CORE-SAMPLE MEASUREMENTS

Resistivity and IP measurements were made on core samples taken from various depths in the "ore sand" on property 1. The unconsolidated core samples were packed into a soft plastic tube for making the IP and resistivity measurements. Figure 3 shows the sample measuring system that was used. The input signal was generated from a constant-current source and the signal was received by a recorder-integrator.

The input signal was a square wave with an off-time of the same duration as the positive and negative on-time (± 5 mA). An analog integrator was used to provide a continuous record of the transient response of the sample. The integrator was started at time t_d and recorded a continuous record of the integrated transient signal as is shown in figure 3. The curves represent the transient signal, the integrated positive transient signal, and the integrated negative transient signal.

Table 2 shows the results of these measurements. The resistivity was calculated using the following equation:

$$\rho = K(V_p/I)$$

where ρ is the resistivity of the sample,

K   is the geometric factor,

V_p is the primary voltage, and

I   is the current put into the sample.

Induced polarization, IP, was calculated by dividing area A by area B shown in figure 3, where each is measured over an equal time interval.

Comparison of table 2 with table 1 shows that the relationship between electrical properties and mineral-
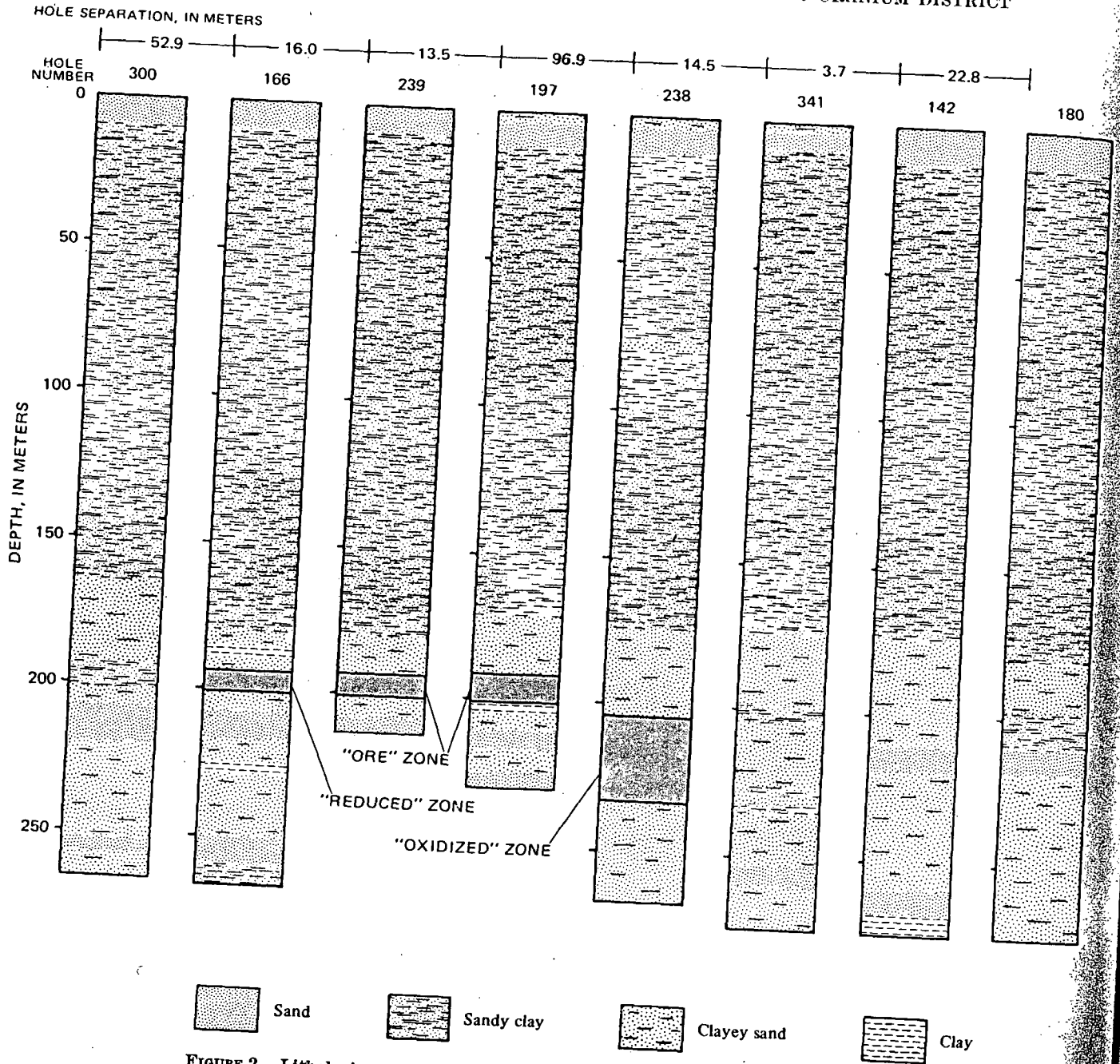
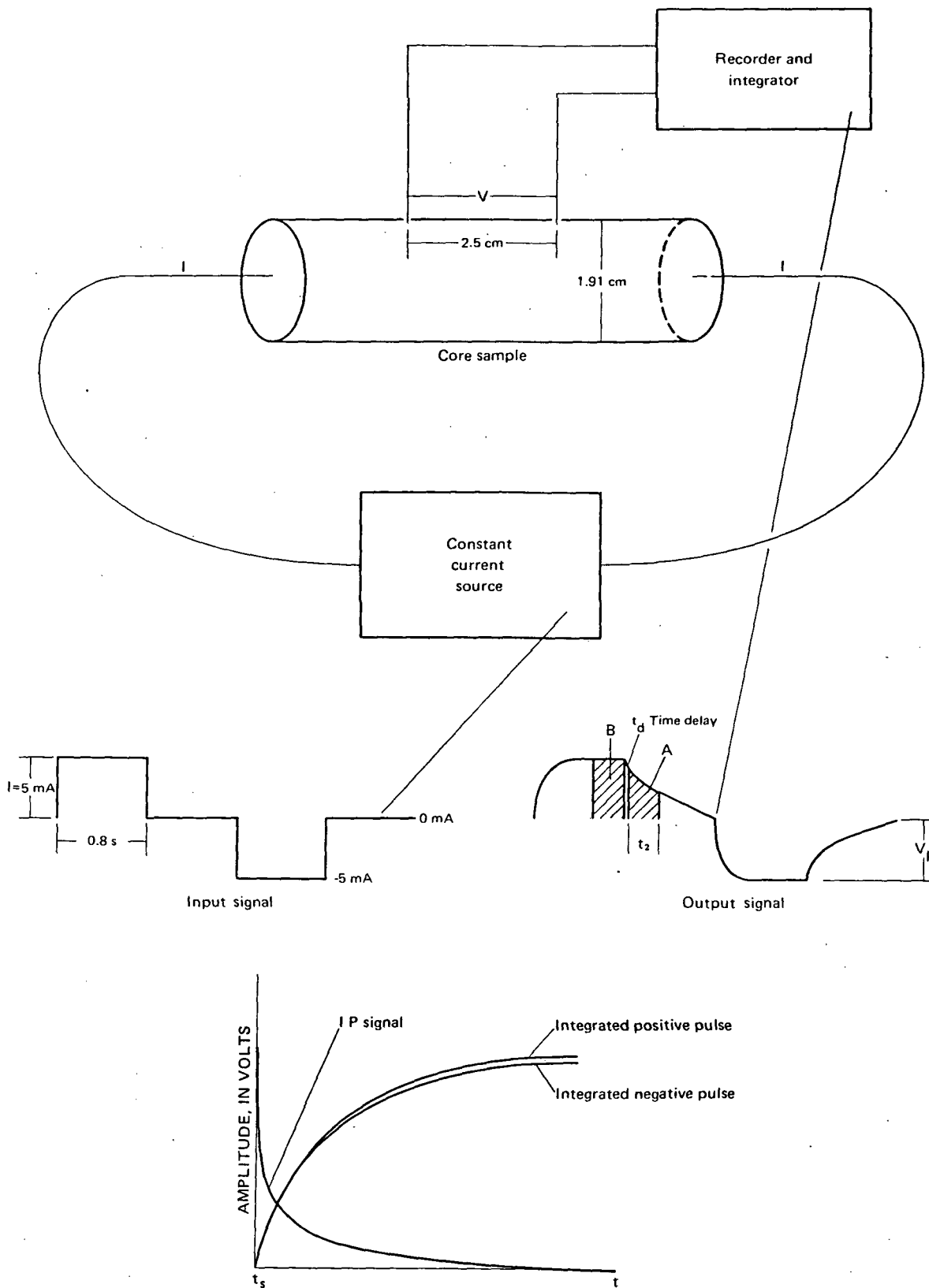FIGURE 2.—Lithologic cross section for property 2. Holes drilled in the Catahoula Tuff.

FIGURE 3.—IP (induced polarization) and resistivity laboratory measuring system. A and B are areas of equal time intervals (t_2) and (t_s-t) is the time interval over which the area was measured. Sample used here is 5–13.

TABLE 2.—*IP and resistivity laboratory measurements on core samples taken from the South Texas uranium district boreholes 3-8, property 1*

[ρ, resistivity; Ω·m, ohm meters; IP, induced polarization; mv/V, millivolts per volt]

Sample No.	Depth, in meters	ρ (Ω·m)	IP $\frac{mV}{V}$	Sample No.	Depth, in meters	ρ (Ω·m)	IP $\frac{mV}{V}$
3-29	75	3.17	2.4	6-19	79	13.4	1.8
19	69	11.69	3.4	15	76	10.8	1.6
15	66	11.0	3.0	10	73	11.5	4.4
24	72	12.9	5.4	4	69	6.21	1.5
5	49	7.06	1.4	7	71	11.7	1.0
9	63	3.44	1.8	18	78	11.7	0.79
28	75	13.06	2.3	7- 4	69	5.63	1.1
4-12	70	6.82	2.9	5	69	9.2	2.0
6	66	4.05	0.1	19	79	14.5	3.1
26	77	2.16	1.3	21	80	12.7	1.9
2	64	10.31	1.2	8	71	10.2	1.9
27	78	3.14	0.0	11	74	13.8	2.5
25	77	15.4	2.6	15	76	11.2	2.8
17	73	12.61	2.1	22	80	8.3	1.4
22	75	8.47	1.9	8- 6	70	5.4	0.9
5-13	72	11.28	5.0	11	74	11.9	2.9
5	67	8.66	2.5	9	72	13.5	2.4
10	70	11.2	3.0	13	75	13.3	2.0
22	76	10.1	4.4	15	77	13.5	1.7
8	69	11.0	2.9	19	79	13.1	2.2
15	73	12.1	2.9	22	80	13.4	1.1
23	77	3.36	0.09	24	81	13.1	1.5
2	65	4.8	0.2				

ogy is not simple. Resistivity is approximately inversely proportional to the clay content. In general, samples whose resistivity is less than 5 Ω·m (ohm meters) contain more than 50 percent clay, while samples with resistivities greater than 5 Ω·m contain less than 50 percent clay. Figure 4 is a plot of resistivity versus clay content and clearly shows the high correlation between them. From this relationship, a prediction formula for clay content can be derived from resistivity logs for property 1.

The relationship between IP effect and mineral content is more complicated than that between resistivity and mineral content. Clay and pyrite are the two constituents which have the largest effect on the IP. In general, samples containing a high pyrite content have a high IP response. However, this relationship is affected by the clay content. Sample 5-2 in tables 1 and 2 has a relatively high pyrite content, but its high clay content offsets the IP effect of the pyrite causing the total IP of the sample to be low. When the sand and clay content is constant, such as in samples 6-10 and 6-15, the IP effect is increased by an increase in the pyrite content. Figure 5 demonstrates the relation-
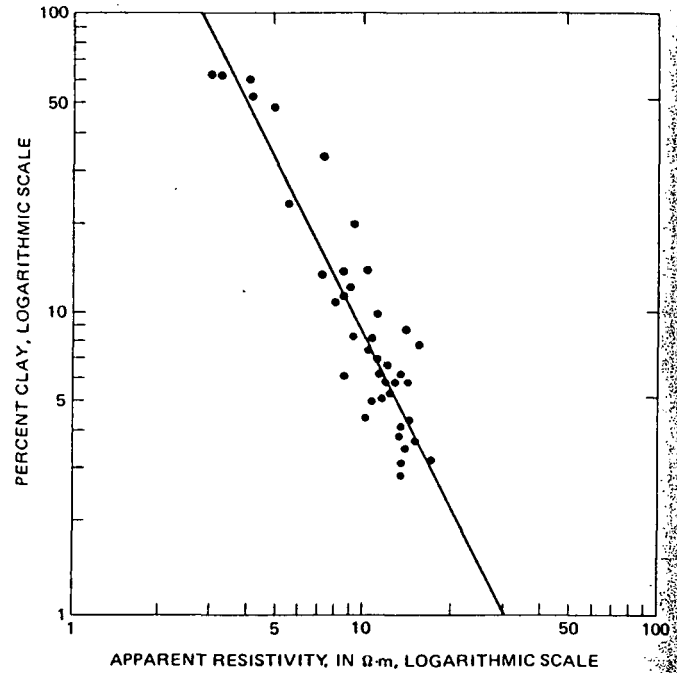
FIGURE 4.—The effect of clay-sized (<2 micrometers) particle content on resistivity for the sample values shown in tables 1 and 2.
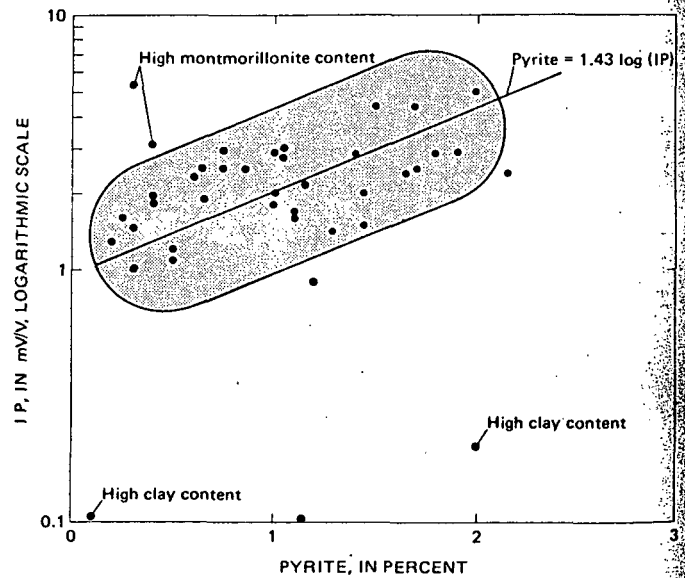

FIGURE 5.—Relationship between pyrite and IP (induced polarization) effect for the sample values (dots) shown in tables 1 and 2. Envelope represents area of low clay content.

ship between pyrite content and IP effect. The two points above the envelope drawn around the high concentration of points contain an abnormally high percentage of montmorillonite while the two points below the line contain a high percentage of kaolinite.

The relationship between clay content and IP effect

is not as clear as the relationship between pyrite and IP effect. Figure 6 shows the effect of clay on IP. There is a general decrease in IP effect as the clay content is increased for clay percentages greater than 10 percent. If the total clay content is less than 10 percent, clay does not appear to have a significant effect on IP. When total clay content is high (>50 percent, in this case), the IP effect is low, except where the montmorillonite content is high.
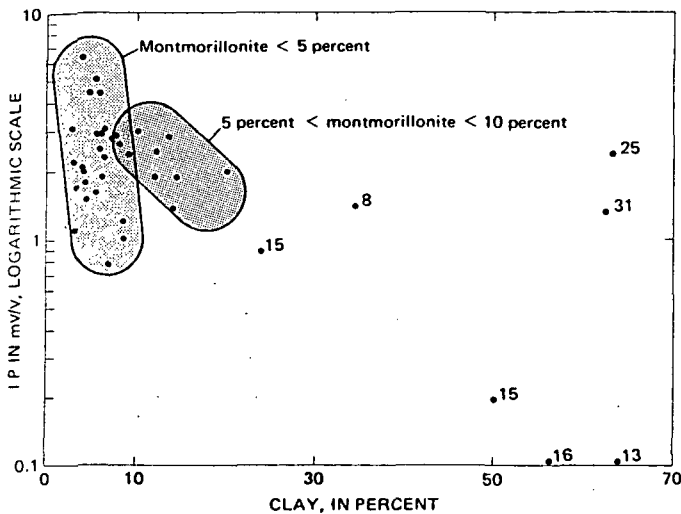

FIGURE 6.—Effect of clay-sized material on IP (induced polarization) response. The numbers on the scattered points give the percentage of montmorillonite in the clay.

GEOPHYSICAL WELL LOG RESULTS

Geophysical well-log information for property 1 and log data close to property 2 are shown in figures 7 and 8, respectively. The log suite for property 1 includes lithology, gamma-ray, resistivity, and induced-polarization logs, while for property 2, the suite consists of lithology, neutron, and gamma-ray logs.

The largest gamma-ray anomaly on property 1 occurs in the lower sand shown in figure 1. The anomaly increases from left to right as the "ore" content increases, and this is characteristic of a roll-front deposit. A low count is shown except for a single spike on the logs from drill holes 1 and 2, which are at a distance from the "ore" in the "oxidized" zone. As the "ore" zone is approached, from the "oxidized" side, the anomaly is first represented by two thin high-count zones at drill holes 3, 4, and 5, which broaden to form a single maximum over the "ore"-zone drill holes 6 and 7). The anomaly then decreases away from the "ore" on the "reduced" side of the roll-front drill holes (9 and 10). This anomaly pattern is similar to that shown by Rubin (1970) for Wyoming-type uranium roll-front deposits. This pattern, along with the geo-

logic information (table 1) supports the idea that the "ore" may have been originally deposited at a typical oxidized-reduced interface which was later reduced.

The resistivity and induced-polarization logs provide important rock-characteristic information about property 1. It has been shown in figure 4 that there is a correlation between the clay content and the resistivity response. This information shows that the clay content is approximately constant across the "ore" zone. The high resistivity anomaly just above the "ore" sand is caused by a calcite-cemented sand layer. The resistivity of the "ore" sand is not anomalous when compared with either the horizontal or vertical position of the "ore". However, an induced-polarization high-amplitude anomaly does occur in the "ore" sand. This anomaly corresponds to the high pyrite and montmorillonite content shown in figure 1.

Figure 8 shows the lithologic, gamma-ray, and neutron logs for property 2. The high gamma-ray count occurs in the lower clayey sand section. Individual roll fronts are difficult to distinguish, however, a deposit of the roll-front type is indicated in the gamma-ray logs with a peak between drill holes 239 and 197. The "oxidized" side of the roll front occurs at drill hole 238. The neutron logs register higher values in the less clayey zones. The high gamma-ray zones in drill holes 239 and 197 correspond to "low" shaly (or clayey) zones as indicated by the neutron logs.

The nature of the neutron logs makes it difficult to predict the actual amount of clay contained in these zones. The logs and information taken from property 1 indicate that a resistivity log would be useful in quantitatively establishing the amount of clay contained in the "ore" sand. The amount of clay could be a factor in determining whether or not a low-grade deposit, such as the deposit in figure 9, is economic as an in-situ solution-mining deposit. The suite of logs shown in figure 8 also fails to give any indication of the amount of calcite cementation in the sands or the pyrite-montmorillonite content as is shown by figure 7 in the resistivity and induced-polarization logs.

Figure 9 shows the ore-zone section of the logs for boreholes 6 through 8 on property 1. The pyrite and clay content is shown for the depths corresponding to the log depths. The correlation that was shown in figure 5 for pyrite and laboratory IP can also be seen for the pyrite content and IP logs shown in figure 9. The samples contain a high clay content in places where the high pyrite values do not correspond to high IP values. A point-for-point correlation cannot be expected since the pyrite sample covers approximately 3 cm² (square centimeters) of the borehole surface and does not penetrate outside the borehole,
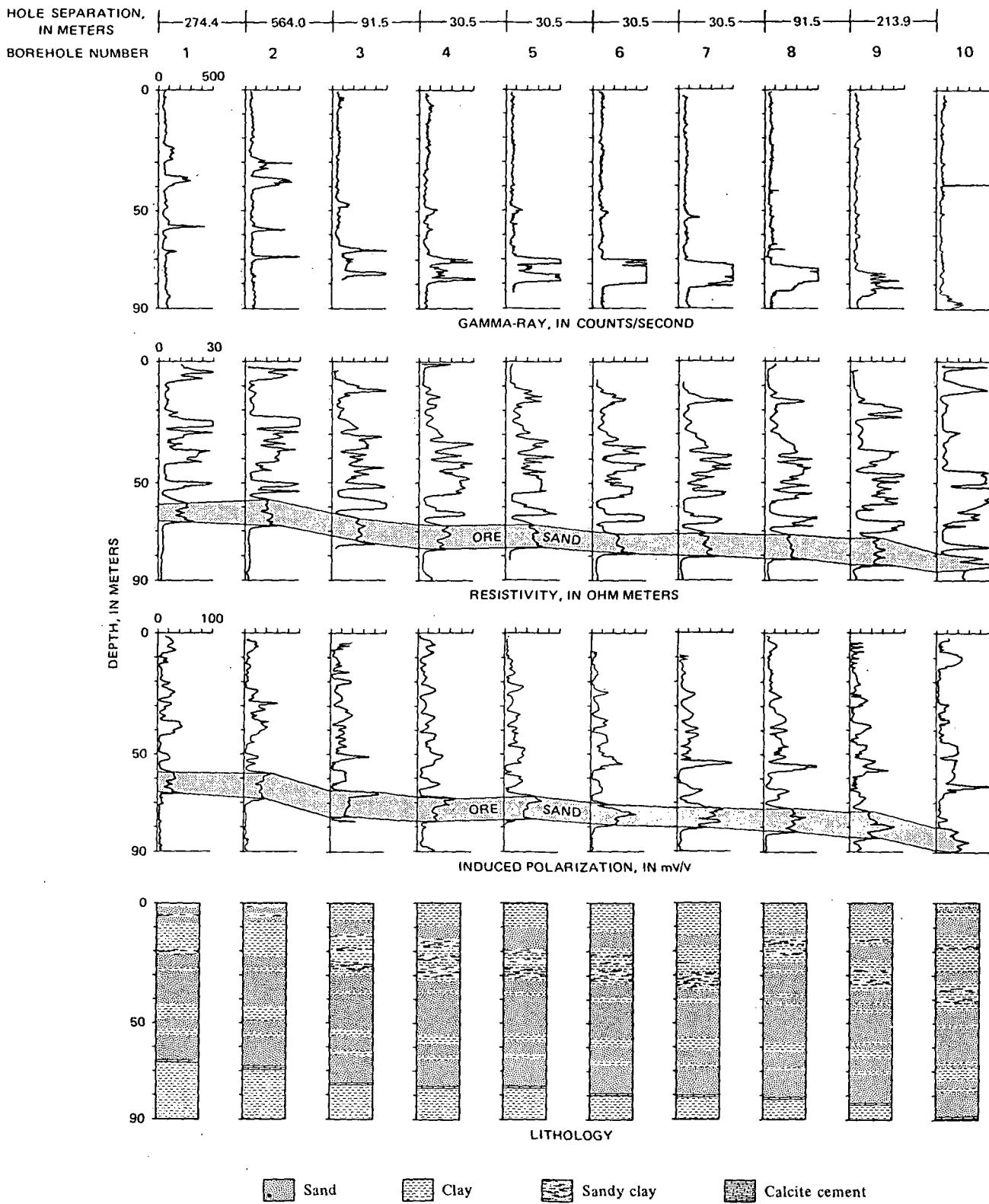
FIGURE 7.—Borehole data across a south Texas uranium roll-front deposit (property 1).

while the IP logging tool has an effective length of about 1 meter (m) and is affected by the borehole wall.

Laboratory resistivity and IP values given in table 2 are shown as dots on the resistivity and IP logs in figure 9. Laboratory resistivity values correspond closely to log values in spite of the difference in sampling between the two techniques. However, laboratory and log IP values correlate only in a very gross sense owing to the different charging and recording times for the two measurements. The IP logging tool, which operates at 10 Hz (hertz), records the ratio of a point voltage measured at 5-ms (milliseconds) delay on the transient decay to the primary voltage V_p, while the laboratory measurements, made at approximately 0.3 Hz, are integrated over a time interval on the decay curve. Anderson and Keller (1964) have also noted the lack of correspondence between laboratory and field induced-polarization measurements.

HOLE-TO-HOLE ELECTRICAL MEASUREMENTS

Hole-to-hole measurements are made by placing a current source down a borehole and a voltage measuring device down an adjacent borehole. By using this setup it is possible to eliminate much of the near-surface geologic noise inherent in conventional surface electrical measurements and to detect the small contrasts in electrical properties associated with roll-front uranium deposits.

Hole-to-hole resistivity and induced-polarization measurements were made on property 1 and property 2 using the measurement system shown in figure 10. The source transmitter was an induced-polarization transmitter that is capable of transmitting 20 amperes at 400 volts. The source electrode pair used for the examples in this paper was the surface-to-downhole electrode pair. The receiver was a time-domain IP receiver using signal sampling similar to that shown in figure 3.

Figure 11 shows hole-to-hole IP and resistivity measurements made on property 1. These measurements show an increase in the induced polarization across the roll-front ore zone (source at hole 3 and receiver at hole 8) in contrast to induced-polarization measurements off the roll front (source at hole 1 or hole 9 and receiver at hole 2 or hole 10, respectively). This increase corresponds to the increase shown in the well logs in figure 7.

The resistivity values can be explained by reference to the well logs in figure 7. A resistivity high occurs just above the "ore" sand in the calcite-cemented sand. The calcite-cemented sand is almost completely replaced by clay in drill hole 1. The presence of the calcite-cemented sand causes the resistivity high in the hole-to-hole measurements between holes 3 and 8 and holes 9 and 10 and the resistivity low in the measurements between holes 1 and 2. Recent experience indicates that a higher density of measurement points would probably help to clarify these relationships.

Figure 12 shows hole-to-hole induced-polarization and resistivity measurements made in "reduced" ground on property 2. The gamma-ray logs show a very small anomaly in drill hole 2 at a depth of about 150 m. The neutron log shows that this is a clayey sand. The hole-to-hole resistivity measurements between drill holes 1 and 2 show a resistivity high in the vicinity of the sand located at a depth of about 120 m in drill hole 2. In general, the resistivity hole-to-hole measurements show high values in the sands and low values in the clays.

The induced-polarization hole-to-hole measurements in figure 11 also show high values in the sands. However, the induced-polarization measurements in the lower sand are less erratic than the resistivity measurements and show essentially the same profile for each set of hole-to-hole measurements.

Figure 13 shows gamma-ray logs, neutron logs, and hole-to-hole measurements across an oxidized-reduced front on property 2. The gamma-ray logs have higher values than in figure 12, but they are not high enough to consider this a good ore deposit. The neutron logs do not exhibit much variation from the upper shale section to the lower sand section.

The hole-to-hole resistivity survey exhibits a resistivity low in the lower sand. This low is negative and is probably due to the effect of the geometry rather than a true resistivity low. The induced polarization shows a high value in the lower sand. The presence of an induced-polarization high across an oxidized-reduced roll front is similar to the correspondence of high induced-polarization values and the occurrence of the oxidized-reduced interface seen on property 1.

CONCLUSIONS

Studies of physical properties on property 1 indicate that:

1. There is a high degree of correlation between clay content and resistivity.
2. There is good correlation between pyrite content and induced-polarization response.
3. There is an inverse correlation between induced-polarization response and [total] clay content.
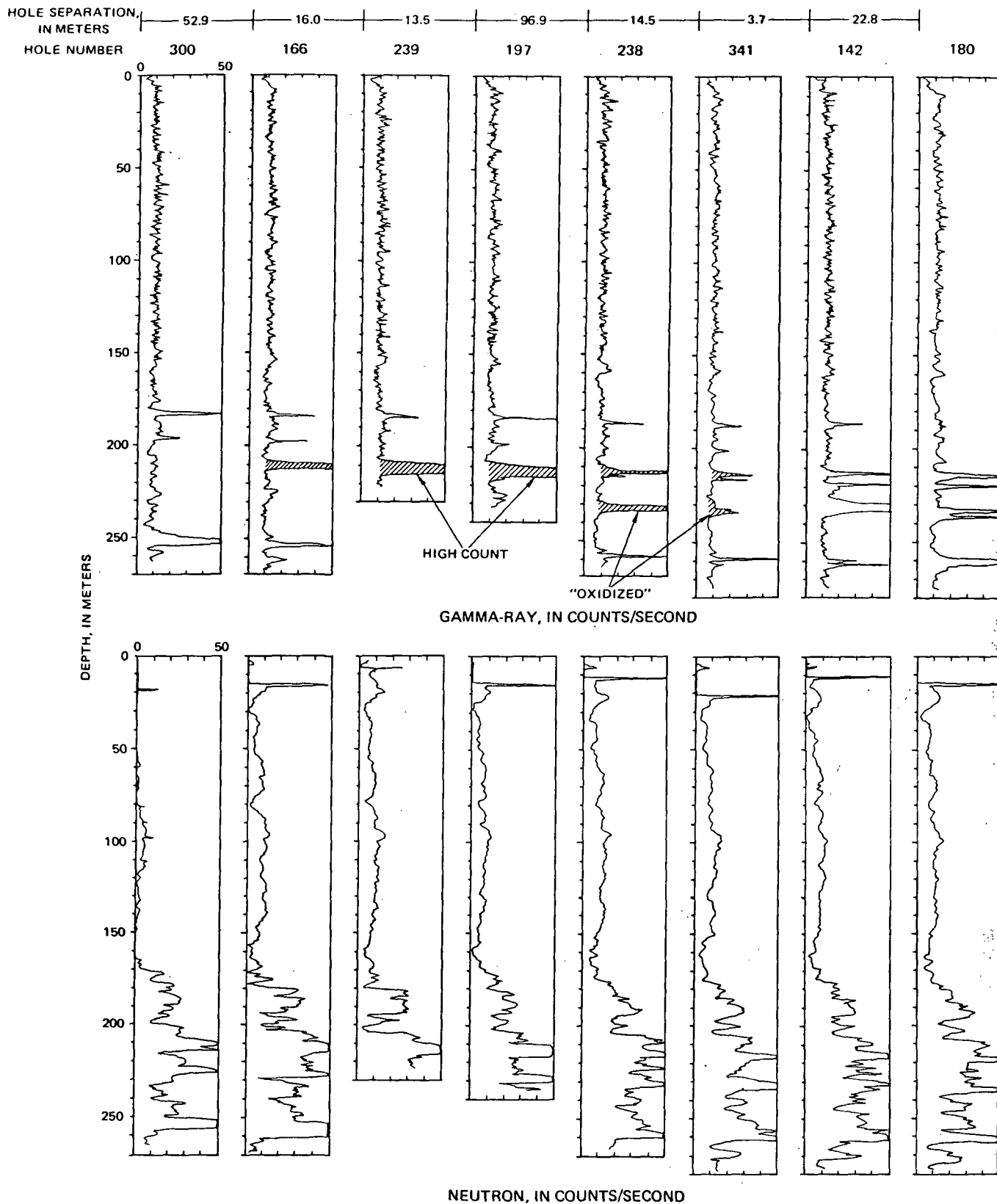
FIGURE 8.—Well log information for property 2.

| HOLE SEPARATION, IN METERS | 52.9 | 16.0 | 13.5 | 96.9 | 14.5 | 3.7 | 22.8 |
| HOLE NUMBER | 300 | 166 | 239 | 197 | 238 | 341 | 142 | 180 |

LITHOLOGY
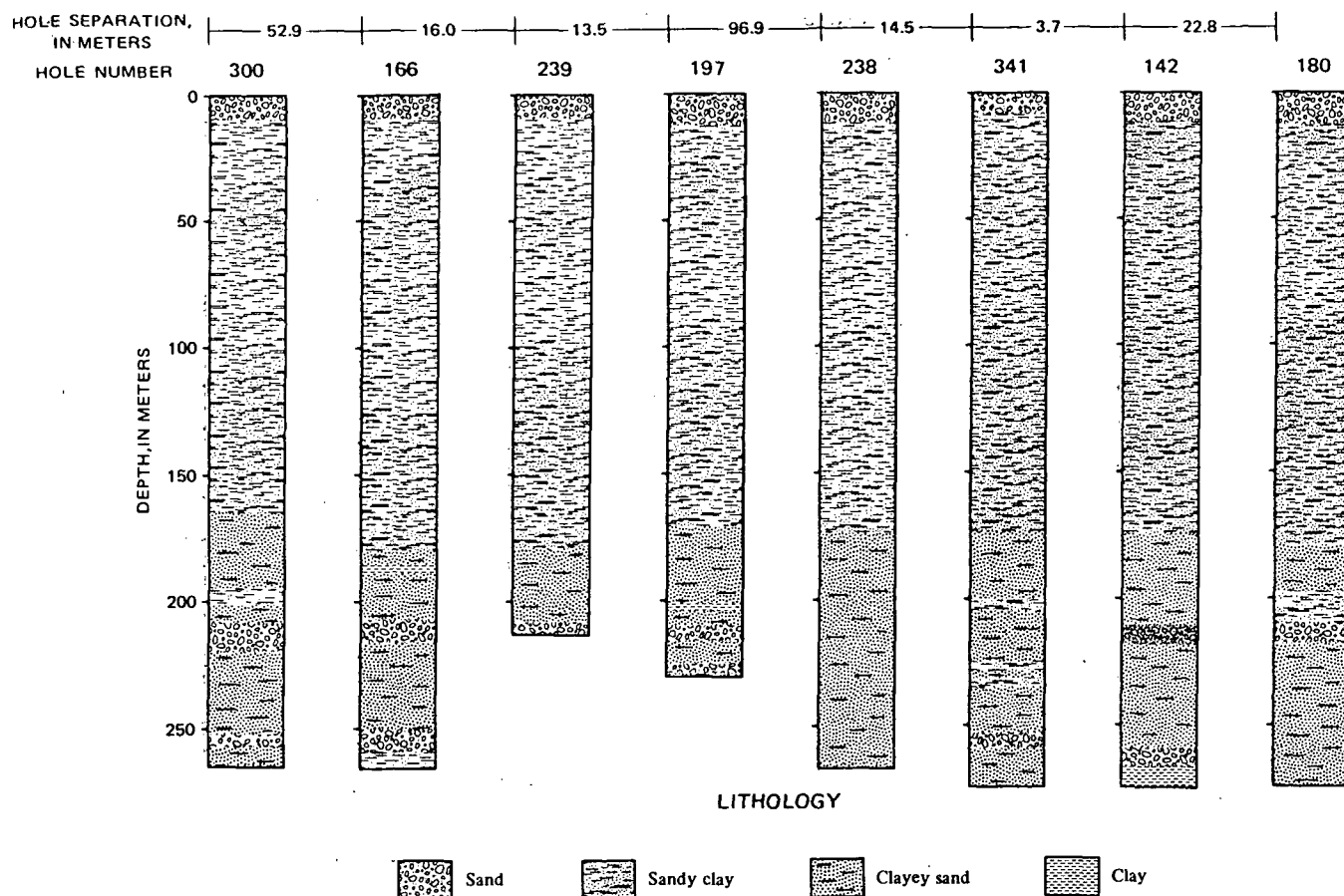
Sand   Sandy clay   Clayey sand   Clay

FIGURE 8.—Continued.

These relationships imply that it may be possible to use resistivity logs to predict clay content and to use this clay-content information to correct the induced-polarization logs so that they can be used to predict pyrite content. The estimation of pyrite could be important in establishing the historical movement of the roll front. The estimation of clay and pyrite content will be important guides in determining geological engineering parameters necessary for solution mining.

Hole-to-hole induced-polarization and resistivity measurements exhibit anomalies similar to the conventional induced-polarization and resistivity well logs. Hole-to-hole induced-polarization measurements can detect the anomaly associated with roll-front deposits at a considerable savings in drilling time and cost.

It must be cautioned that the conclusions drawn in this paper are derived from work on only two deposits in South Texas. More data is needed to confirm these results. In particular, the correlation between pyrite and induced-polarization response may be reflecting more general characteristics of the roll-front environment than just the pyrite content. These results do show that borehole measurements contain quantitative information which can aid the explorationist in evaluating the economics of marginal-grade uranium deposits.

REFERENCES CITED

Anderson, L. A., and Keller, G. V., 1964, A study in induced polarization: Geophysics, v. 29, no. 5, p. 848–864.

Eargle, D. H., Hinds, G. W., and Weeks, A. M. D., 1971, Uranium geology and mines, South Texas: Texas Univ., Bur. Econ. Geol., Guidebook no. 12, 59 p.

Eargle, D. H., and Weeks, A. M. D., 1968, Factors in the formation of uranium deposits, Coastal Plain of Texas: South Tex. Geol. Soc. Bull., v. 9, no. 3, 12 p.

Rubin, Bruce, 1970, Uranium roll front zonation in the southern Powder River basin, Wyoming: Wyo. Geol. Assoc. Earth Science Bull., v. 3, no. 4, p. 5–12.
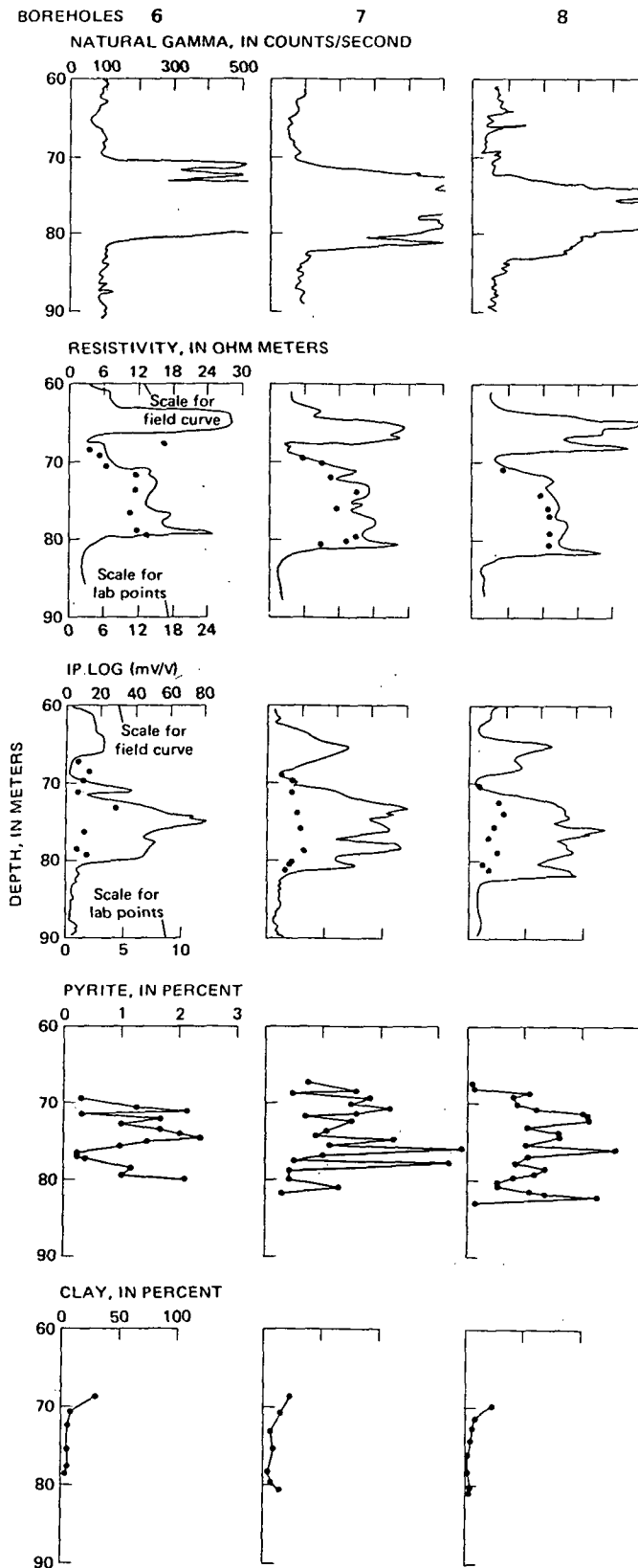
FIGURE 9.—Analysis of natural gamma count, resistivity, IP, and pyrite and clay content in the "ore" zone, for boreholes 6 through 8 on property 1.
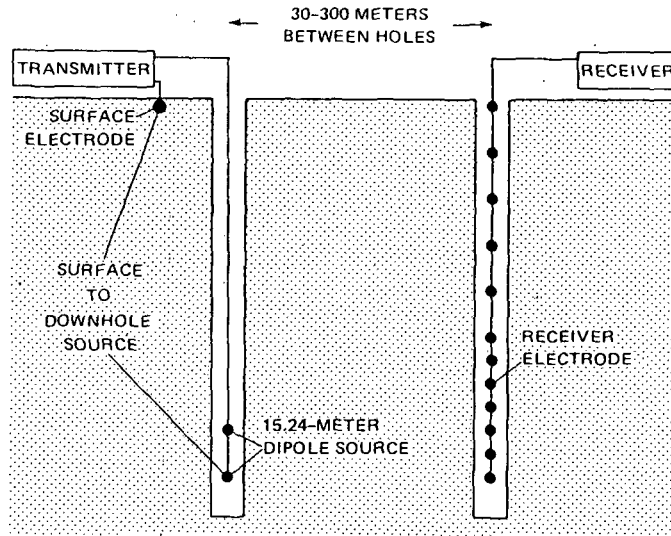
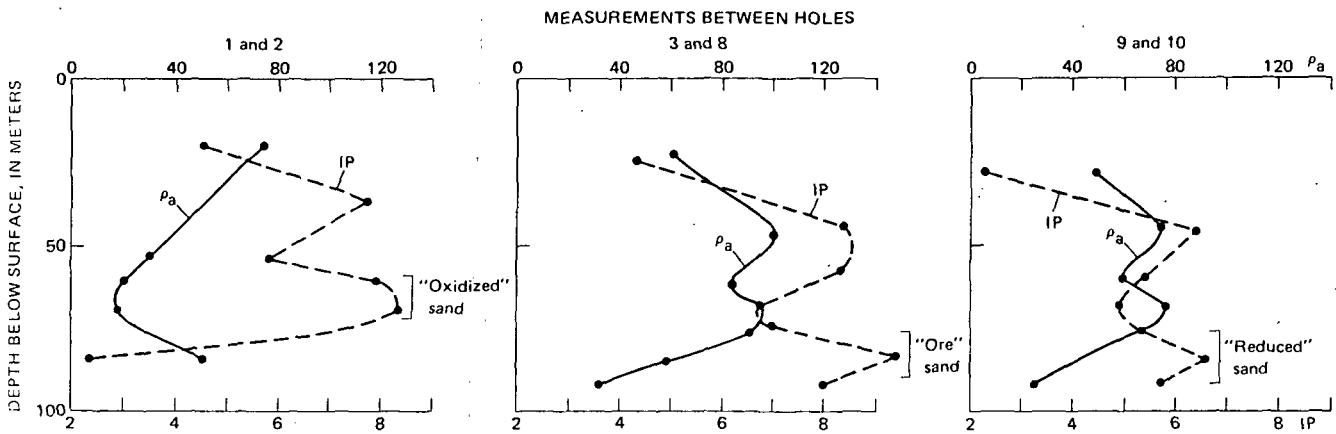FIGURE 10.—Source-receiver electrode configuration for hole-to-hole measurements.

FIGURE 11.—Hole-to-hole resistivity (ρ_a), in ohm meters, and induced polarization (IP) measurements, in millivolts per volt, on property 1. Source current, 10 amperes; receiver dipole length, 15.24 meters. There is a source electrode at the surface and one at a depth of 46 meters.
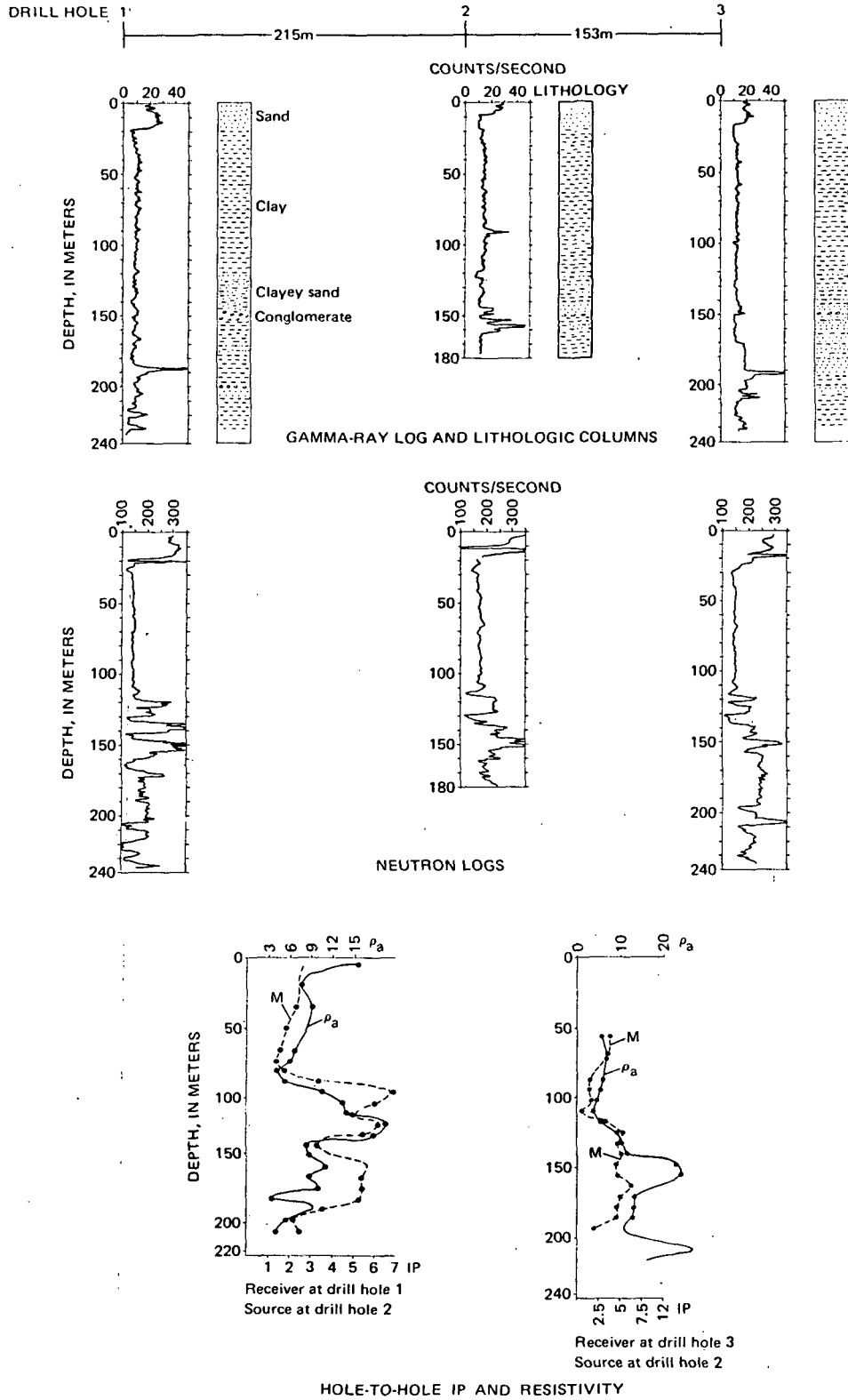
FIGURE 12.—Well logs and hole-to-hole measurements in a non-"ore" zone on property 2. Surface electrode to downhole electrode is 154.2 meters and current is 5 amperes on hole-to-hole IP (induced potential) and ρ_a (resistivity) logs. Apparent resistivity is measured in ohm meters, and IP is measured in millivolts per volt.
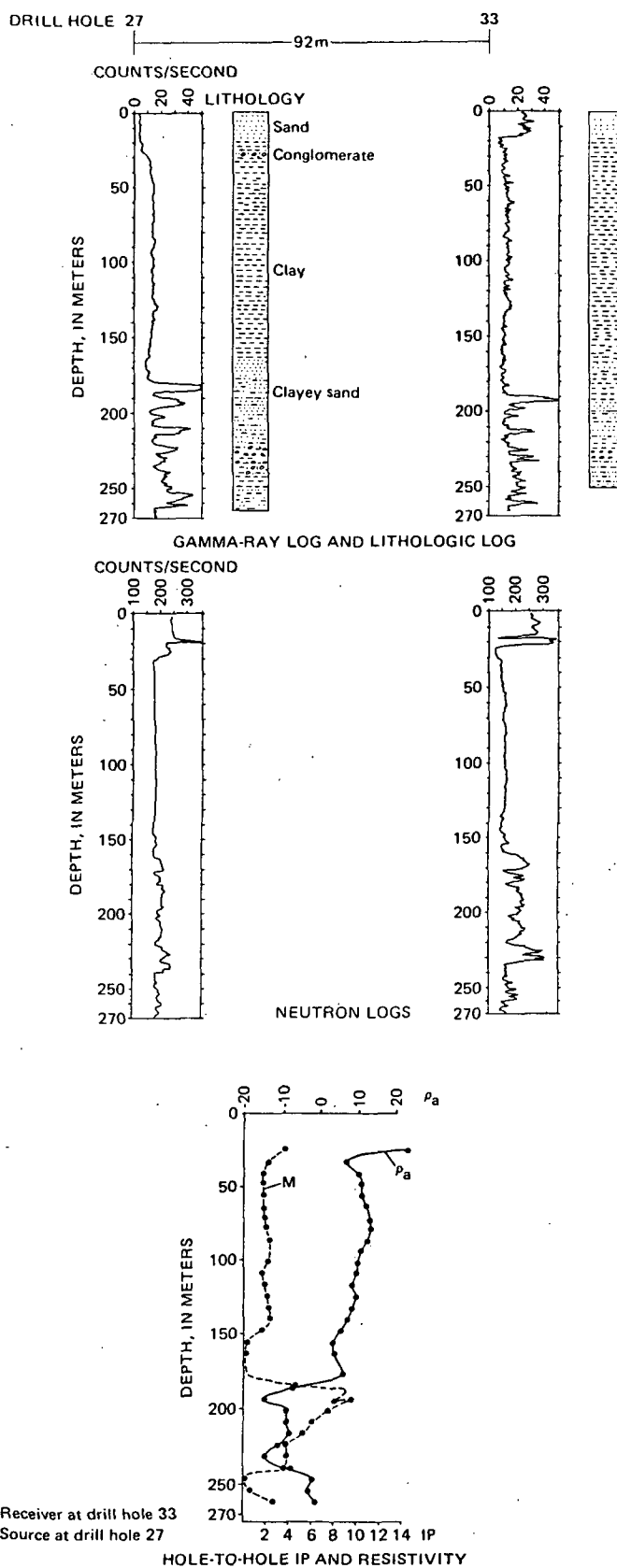
FIGURE 13.—Well logs and hole-to-hole measurements across a roll-front deposit on property 2. Surface electrode to down-hole electrode is 152.4 meters, and current is 5 amperes on hole-to-hole IP (induced polarization) and ρ_a (resistivity) log. Apparent resistivity is measured in ohm meters, and IP is measured in millivolts per volt. Receiver dipole separation is 15.24 meters.

INDUCED POLARIZATION, A STUDY OF ITS CAUSES*

DONALD J. MARSHALL† AND THEODORE R. MADDEN‡

ABSTRACT

The causes of induced electrical polarization include not only the polarization of metal-solution interfaces, but also effects associated with the coupling of different flows. Electro-osmotic, thermal electric, and ion diffusion effects are among such examples. A study of the physical properties of geologic materials indicates that only electrode interface and diffusion flow phenomena are important sources of induced polarization effects.

It was attempted to find characteristic differences between these two phenomena. Theoretical and experimental considerations show that the kinetic processes involved are quite similar in the two cases. This leads to difficulties in identifying the polarizing agent from electrical measurements, although the effects of well mineralized zones are easily recognized.

INTRODUCTION

During the past ten years an increasing interest has developed around the geophysical applications of electrical measurements that go under the popular name of induced polarization measurements.[1] The primary motivation has been the application of these measurements to the detection of sulphide mineralization. It is believed that the phenomenon taking place when electric current passes through a mineralized zone is essentially the same phenomenon that occurs at a polarized electrode (Bleil, 1953).

A polarized electrode is one that hinders the flow of electric current between the electrode and the solution in which it is immersed. Chemical or electro-chemical barriers exist which the current carriers must overcome in order to allow current flow to pass across the electrode-liquid interface. Forcing a net current flow to take place across this interface entails an added voltage drop above and beyond that needed to overcome the ohmic losses in the solution and in the electrode. This additional voltage is called the overvoltage.

The picture that is used to explain the induced polarization effects in mineralized rocks involves the ionic current flow in the rock polarizing the metal particles within the rock. When the inducing current is turned off, the overvoltages that were set up fall off with time. Since it also takes a finite time to build up these overvoltages, one finds that the impedance of these zones decreases with increasing frequency, so that the measurements can also be made in the frequency domain. Qualitatively then, these effects behave somewhat as the ordinary

[1] The term induced polarization is perhaps a poor one, because it has so many different connotations. It would be more descriptive if we used the expression, induced electrical interfacial polarization, but we shall not attempt to force such a tongue-twisting term on our fellow geophysicists. In any case the measurements involve the transient or frequency dependent electrical properties of the ground.

. PP. 790–816, 16 FIGS.

ˈ OF ˈITS CAUSES*

ˈE R. MADDEN‡

.ly the polarization of metal-solution
rent flows. Electro-osmotic, thermal
study of the physical properties of
ffusion flow phenomena are impor-

ˑ these two phenomena. Theoretical
involved are quite similar in the two
ˈgent from electrical measurements,
ized.ˑ

ˈst has developed around the
ts that go under the popular
primary motivation has been
ˈction of sulphide mineraliza-
ˈe when electric current passes
e phenomenon that occurs at

ˈw of electric current between
ˈmersed. Chemical or electro-
ˑ must overcome in order to
ˈquid interface. Forcing a net
ˈtails an added voltage drop
ˈmic losses in the solution and
ˈe overvoltage.

polarization effects in miner-
ˈock polarizing the metal par-
ˈs turned off, the overvoltages
ˈakes a finite time to build up
of these zones decreases with
ˈ also be made in the frequen-
ˈve somewhat as the ordinary

use it has so many different connota-
nduced electrical interfacial polariza-
ˈm on our fellow geophysicists. In any
ˈpendent electrical properties of the

dielectric property of the materials. These effects, however, occur at audio and sub-audio frequencies which are much too low for the ordinary displacement currents to be of any significance. Irrespective of the origin of the phenomenon, any time dependent or frequency dependent behavior of the electrical impedance of rock materials at these low frequencies is referred to as an induced polarization effect.

INDUCED POLARIZATION MEASUREMENTS AND PARAMETERS

Before going on to the more general study of the possible causes of these effects, it seems worthwhile at this point to review some of the measurement techniques and to correlate the widely different ways of describing the observed polarization effects that are in current use. Results of field measurements will also be presented to demonstrate the usefulness of these measurements in mining exploration.

Several different techniques are used to measure these effects, and several different parameters are used to describe the results of these measurements. When the measurements are made in the time domain, it is a common procedure to turn the current source on for a period, and then turn it off for a period before starting a new cycle with opposite polarity. The voltage remaining just at the beginning of the off-period, or at some fixed interval later, is often measured and compared with the on-period voltage. The polarization is evaluated in terms of mv/volt. Another practice consists of integrating the off-period voltage. The polarization effects are then evaluated in terms of mv-sec/volt.

When the measurements are made in the frequency domain it is the usual practice to compare the impedance at some alternating frequency with that of some very low frequency which is often referred to as the dc impedance. The effect is then evaluated as a certain percentage increase in the conductance at the ac frequency. Sometimes phase shift measurements are made. These phase shifts are usually very small, of the order of one degree or less.

The significance and the interrelation of these varied parameters can be better understood if the ideas used to describe the polarization of a mineralized zone are transcribed into an equivalent circuit (see Figure 1).

In Figure 1, R' stands for the impedance of the complete rock section. It is made up of unblocked ionic conduction paths, R, in parallel with other paths, Z, which are blocked by metallic or semi-conducting minerals. R_m stands for the resistance of the electronic conducting minerals, and R_e stands for the resistance of the electrolytes in the blocked pore paths. C is the electrode capacitance and R_{chem} represents the hindrance to the transfer of electrons between the metallic mineral and the solution.

Because time and frequency domain data are related to each other, when the phenomenon is linear, through the Fourier transform, we can expect to derive frequency information from the transient measurements or vice versa. There is not an exact one to one correspondence between a point in the frequency domain,

and a point in the time domain, but there is often an approximate one. The percentage frequency effect and the mv/volt parameters are found to be closely related (Madden and Marshall, 1958). If the percentage decrease in impedance is used instead of the percentage increase in conductivity, the relationship is given as percent effect at frequency $f_i \cong 0.1$ mv/volt value at $t_i = 1/2\pi f_i$.

The integrated decay voltage is a little different. It is not unlikely that $R_{chem} \gg R_m + R_e$, so that the dc impedance of $Z = Z(0)$ is approximately equal to R_{chem}. If we make this assumption, and if the integration is carried out long enough, we have that the mv-sec/volt value $= 1,000$ CR.

In all these parameters we have a large role played by R, the resistance of the unblocked paths. Small values of R can short circuit the polarizing effects,

$$\frac{R'(o) - R'(f)}{R'(o)\,R'(f)} = \frac{Z(o) - Z(f)}{Z(o)\,Z(f)} = \frac{1}{Z(f)} - \frac{1}{Z(o)}$$

$$\frac{R'(o) - R'(f)}{R'(o)\,R'(f)} \times 2\pi \times 10^5 = \text{"METAL FACTOR"}$$

R' IN OHM FEET

FOR $Z(o) \gg Z(f)$
$$M.F. \approx 1/Z(f)$$
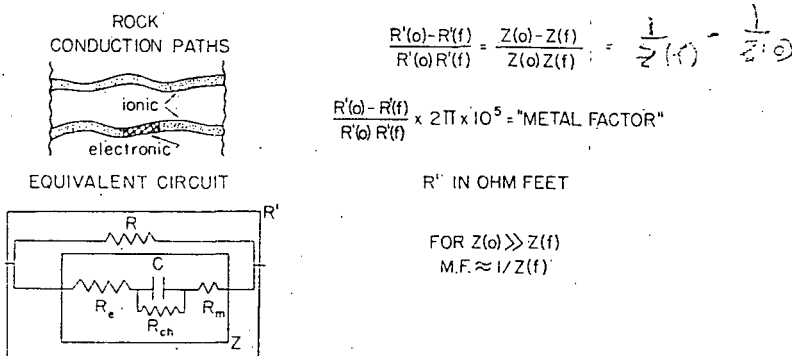
FIG. 1. Diagrammatic representation of section of conducting paths in rock, and the equivalent circuit.

resulting in very small parameter values, while a very tight rock may give large frequency effects without many metallic minerals being present. Since R is in parallel with Z it would seem advisable to look at the change in conductivity of R', for this is just the change in conductivity of Z. When the measurements are made in the frequency domain, this is simply done, and is equal to the frequency effect divided by the dc resistivity. To give reasonably sized values, this parameter is defined as $2\pi[R'(0) - R'(f)] \times 10^5/R'(0)R'(f)$ when using units of ohm-feet for the resistivity. It is called the "metal factor" because of its correlation with metallic mineral content. Using the assumptions previously mentioned concerning the parameters of Figure 1, the metal factor, m.f. $\cong 2\pi \times 10^5/Z(f)$, and is therefore proportional to the ac conductivity of those paths that are blocked off by metallic minerals. The more metal a rock contains, the more paths that will be blocked, and thus the higher the metal factor. As the metallic content continues to increase, the individual paths will have higher ac conductivities, and this two-fold effect starts to skyrocket upwards the values of the metal factor. This is helpful in increasing the signal-to-noise ratio between

an approximate one. The per-
:eters are found to be closely
entage decrease in impedance
iductivity, the relationship is
olt value at $t_i = 1/2\pi f_i$.

:rent. It is not unlikely that
:(0) is approximately equal to
itegration is carried out long
)00 CR.

layed by R, the resistance of
circuit the polarizing effects,

$$\frac{)}{f)} = \frac{Z(o)-Z(f)}{Z(o)Z(f)} = \frac{1}{Z(f)} - \frac{1}{Z'(o)}$$

$\times 10^5 =$ "METAL FACTOR"

N OHM FEET

$R Z(o) \gg Z(f)$
$F \approx 1/Z(f)$

:cting paths in rock, and the

:ry tight rock may give large
being present. Since R is in
he change in conductivity of
Z. When the measurements
:one, and is equal to the fre-
ve reasonably sized values,
$10^5/R'(0)R'(f)$ when using
e "metal factor" because of
ing the assumptions previ-
:re 1, the metal factor, m.f.
he ac conductivity of those
more metal a rock contains,
higher the metal factor. As
idual paths will have higher
:yrocket upwards the values
:ignal-to-noise ratio between

the effect of well mineralized zones, and the effect of only slightly mineralized
zones. This parameter does favor the rocks having conductive electrolytes in
the pores, and thus it is not quite so useful when dealing with sedimentary rocks.

Some typical metal factor values evaluated at 10 cps encountered in igneous
areas are shown in Table I.

Similar parameters can be evaluated from the transient measurements. The
only one that seems to be used is derived by dividing the mv-sec/volt value by
the resistivity. This parameter is essentially proportional to C, the interfacial
capacitance per unit cube, but is more often referred to as the effective zero fre-
quency dielectric constant. The frequency measurements could also be evaluated
in terms of an effective dielectric constant, but we specifically wish to avoid the

TABLE I
COMMON METAL FACTOR VALUES (10 cps)

Rock Type and Mineralization	Metal Factors
unmineralized granites	<1
unmineralized basic rocks	1–10
finely disseminated sulphides	10–100
disseminated sulphides (1–3%)	100–1,000
fracture filling sulphides (3–10%)	1,000–10,000
massive sulphides	>10,000

use of the term dielectric constant in describing these effects. First of all this so-
called effective dielectric constant is not constant, but varies widely as a func-
tion of frequency. Secondly, the huge values obtained at low frequencies seem to
imply a rather anomalous dielectric phenomenon, while actually the only really
anomalous phenomenon is associated with the resistive properties. The interfacial
capacitance C is quite large, being of the order of 30 $\mu f/cm^2$, but is not anomalous
since the interfacial layer is so thin. The anomalous feature of this layer is its
high resistance, despite the fact that it is very thin. If it were not for this high
resistance, the interfacial capacitance, which is no different from the capacitance
of a similar thickness of ordinary fluid, would play no role.

In the remainder of this paper the polarizing effects will be referred to the
frequency domain, and we shall speak of percentage frequency effects and metal
factors.

FIELD RESULTS

The increased resolving power of induced polarization measurements over
ordinary resistivity measurements in detecting sulphides is demonstrated by
some field examples shown in Figures 2–7. The data were taken using 100 ft.
dipoles for both the sender and receiver. The data are plotted with the abscissa
representing the separation between sender and receiver, and the ordinate repre-
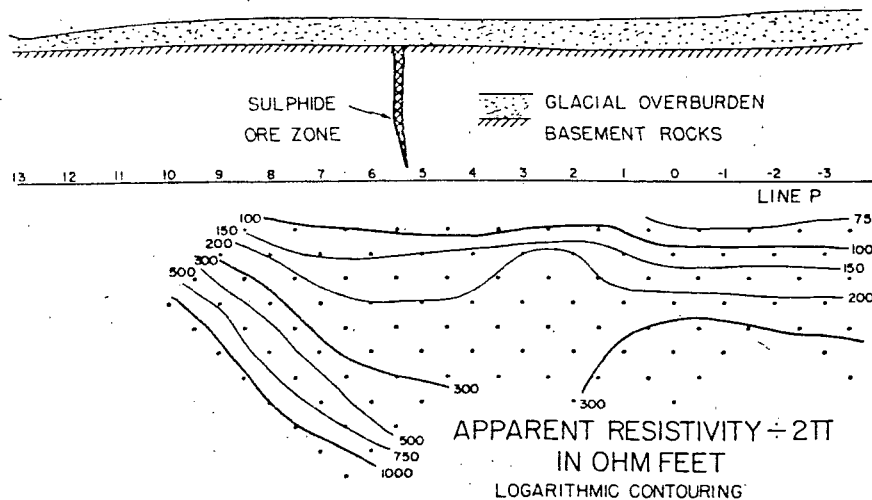
DONALD J. MARSHALL AND THEODORE R. MADDEN

FIG. 2. Resistivity measurements using colinear dipoles.

senting the center position of the spread. In this way a sort of cross-section of the measured apparent electrical parameters are presented. Of course it is not an exact mapping, but it bears certain similarities (Hallof, 1957). The actual measured values have not been shown, merely being represented by dots, but the contours of these values are drawn in. In all these examples there is a clear cut advantage to the induced polarization measurements.

The frequency spectrum of these induced polarization effects are spread out smoothly enough so that the impedance, even though varying with frequency, remains almost purely resistive at any one frequency. This allows one to use

FIG. 3. Frequency variations of apparent resistivity at 60 cps.

APPARENT METAL FACTOR MAP (f=60~)
LOGARITHMIC CONTOURING
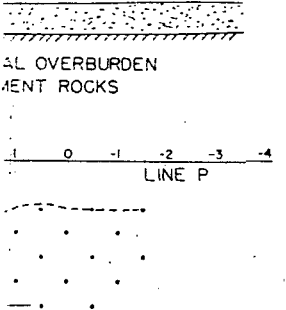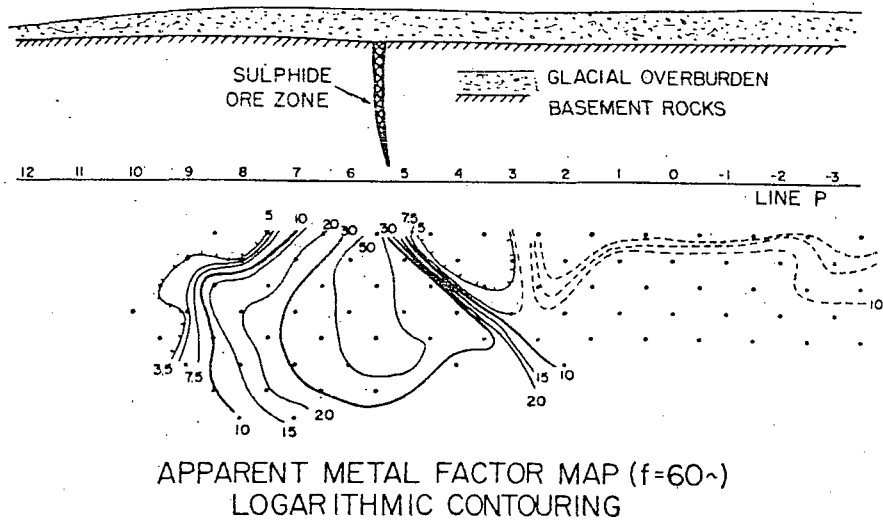
FIG. 4. Metal factor values computed from field measurements.

ordinary resistivity type curves to predict or interpret the apparent polarization effects of a given zone (Hallof, 1957).

COMPLICATIONS TO THE SIMPLE THEORY

The application of induced polarization measurements to the detection of sulphide mineralization is not as simple as it has been assumed in the previous discussion. One reason, of course, is that other semi-conducting minerals such as graphite, magnetite, and pyrolusite cause similar polarization effects. Polari-

APPARENT RESISTIVITY ÷ 2π
IN OHM FEET
LOGARITHMIC CONTOURING

FIG. 5. Resistivity measurements using colinear dipoles.

% FREQUENCY CHANGE OF ρ_a
LOGARITHMIC CONTOURING
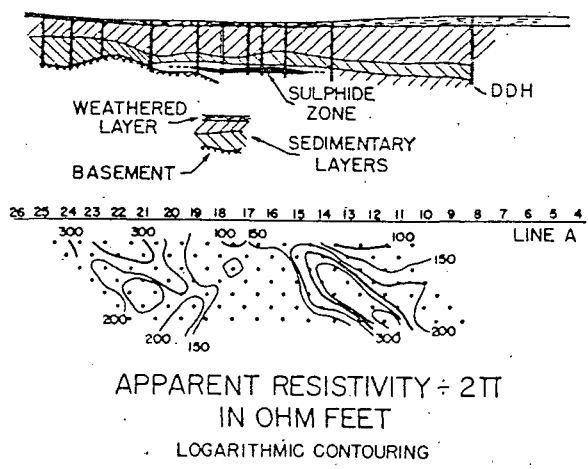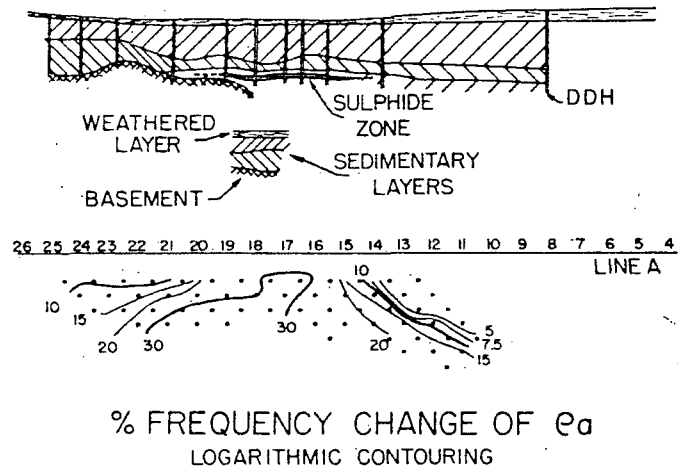
FIG. 6. Frequency variations of apparent resistivity at 60 cps.

zation can also occur, however, without the presence of any semi-conducting minerals: Schlumberger, in perhaps the first reference to induced polarization methods, stated that background polarization effects drowned out the effect of the sulphide minerals (Schlumberger, 1920). This view is somewhat exaggerated, but Vacquier in his work showed that clay minerals could lead to finite polarization effects (Vacquier et al., 1957). Other groups have also been observing these effects (Henkel and Van Nostrand, 1957; Brant, personal communication).

Because of the presence of these complicating factors, this present study was taken up. It was hoped that through an increased understanding of the causes of induced polarization in geologic materials, one could better interpret the electri-

APPARENT METAL FACTOR MAP ($f = 60 \sim$)
LOGARITHMIC CONTOURING
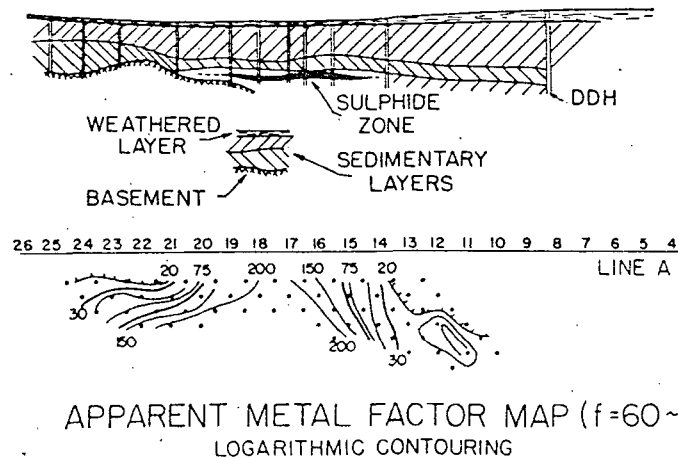
FIG. 7. Metal factor values computed from field measurements.

cal measurements. It seems appropriate then to attack this problem from a fresh point of view, starting with more general concepts rather than a specific model such as that given in Figure 1.

POLARIZATION AS ENERGY STORAGE

The observation that we have is that the polarizable materials are capable of maintaining, for a certain time, an electric current flow after an applied current field is turned off. Actually what is observed is a voltage gradient, and this does not guarantee that electric current is flowing, as will be apparent later, but some sort of flow will be taking place. This is a manifestation that energy is stored in the medium when current is passed through, and usually at least some of this energy is released by maintaining electric current flow after the driving field is turned off. The five ordinary forms of energy storage are, electric, magnetic, mechanical, thermal, and chemical. It is conceivable that any one or all of these are involved in the phenomenon. The picture presented in Figure 1 assumed that the energy was stored as electric energy in the capacitor C. This is the simplest and most direct form of setting up an electric polarization effect.

Another obvious form of energy storage is in the magnetic field. It is known that an electric current always sets up a magnetic field, and that when the current is turned off, the collapsing magnetic field returns its stored energy back into electrical energy. This effect can be very complicated when the geometry of the current flow is irregular, but for simple half-space geometries the solutions are well known (Sunde, 1949). When colinear spreads are used to make the field measurements, these electromagnetic effects behave qualitatively much like the polarization effects of mineralized zones. A two-fold increase of apparent conductivity takes place as the frequency is increased. The frequencies at which the effect is observed, however, are usually quite high, unless large separations in conductive areas are involved. For a separation of 2,000 ft in an area whose resistivity is 300 ohm-ft, no appreciable effect is observed until frequencies of 10 cps or higher are used. When the ground conductivities are not homogeneous, the electromagnetic effects can become quite different. This is especially true when horizontal variations of conductivity exist. Measurements have been made in the field where the apparent resistivity increased by more than three fold as the frequency was increased (Madden et al., 1957). These effects are again limited to the higher frequencies, however.

POLARIZATION THROUGH THE COUPLING OF FLOWS

The electromagnetic effects can be avoided, as has been mentioned, by using low enough frequencies, but anomalous polarization effects are still found when low frequencies are used. The possible effects of mechanical, thermal, and chemical energy storage must be investigated therefore. To store energy in these forms, a coupling must exist between the electric current flow and other flows such as heat and matter. The existence of such a coupling will then allow the stored

energy on its release to cause electric current flow again, and thus the phenomenon will be a form of induced electric polarization. A simple illustration of this idea is given in Figure 8. For instance, through electro-osmotic coupling, an electric current flow will cause a solvent flow through a capillary system. This flow may build up a hydrostatic pressure, either by building up a hydrostatic head against gravity, or perhaps through the blocking action of an impermeable bed. When the electric current is turned off, the hydrostatic pressure built up will drive the solvent back, and the solvent flow in turn will cause an electric current flow.
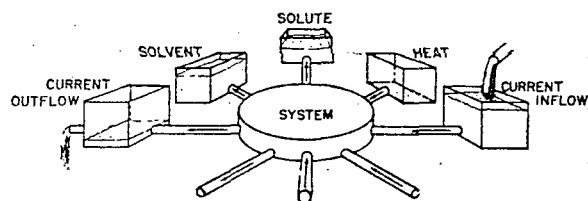
INDUCED POLARIZATION
THROUGH COUPLED FLOWS

Fig. 8. Pictorial representation of the coupling of flows and the development of counter forces in a system.

This flow almost immediately builds up an electric potential which opposes any further current flow, and which is observed as a polarization voltage.

In a similar way any heat flow induced by the current flow can store energy thermally if temperature differences are set up. The solute flow can cause concentration differences to build up, and this represents a chemical energy.

The study of such couplings and their interrelations is the main area of investigation of steady-state thermodynamics. According to the principles of steady-state thermodynamics, the equations describing a general electrolyte system with coupling are[2]

$$
\begin{matrix}
\text{flow cations} = \\
\text{flow anions} = \\
\text{flow solvent} = \\
\text{flow heat} =
\end{matrix}
\begin{bmatrix} J_p \\ J_n \\ J_s \\ J_q \end{bmatrix}
=
\begin{bmatrix}
L_{11} L_{12} L_{13} L_{14} \\
L_{21} L_{22} L_{23} L_{24} \\
L_{31} L_{32} L_{33} L_{34} \\
L_{41} L_{42} L_{43} L_{44}
\end{bmatrix}
\begin{bmatrix}
-\nabla\mu_p - FZ_p\nabla\phi \\
-\nabla\mu_n - FZ_n\nabla\phi \\
- \nabla P \\
- \nabla T/T
\end{bmatrix}
\tag{1}
$$

where

ϕ = electric potential; μ = chemical potential; P = pressure;
T = temperature; $L_{ij} = L_{ji}$; F = Faraday's constant; and Z = ion valence.

[2] This is not the form of these equations usually found, but we follow Eckart here in an attempt to avoid the presence of arbitrary potential terms that appear in the formulations given in Denbigh and DeGroot (Eckart 1940, Denbigh 1951, DeGroot 1952).

<div style="left column">

)w again, and thus the phenome-
ion. A simple illustration of this
electro-osmotic coupling, an elec-
:gh a capillary system. This flow
· building up a hydrostatic head
ig action of an impermeable bed.
)static pressure built up will drive
:ill cause an electric current flow.
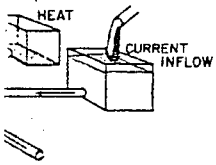
ATION
FLOWS

.vs and the development of counter

:tric potential which opposes any
ι polarization voltage.
.he current flow can store energy
. The solute flow can cause con-
:resents a chemical energy.
:lations is the main area of inves-
·ding to the principles of steady-
ig a general electrolyte system

$$\begin{bmatrix} \vdots \\ \vdots \\ \vdots \\ \vdots \end{bmatrix} \begin{bmatrix} -\nabla\mu_p - FZ_p\nabla\phi \\ -\nabla\mu_n - FZ_n\nabla\phi \\ -\nabla P \\ -\nabla T/T \end{bmatrix} \quad (1)$$

: $P =$ pressure;
istant; and $Z =$ ion valence.

but we follow Eckart here in an attempt
·ar in the formulations given in Denbigh

</div>

<div style="right column">

The column on the left represents the flow vectors, while the column on the right of (1) represents the generalized forces. The L_{ij} matrix consists of the terms relating to the properties of the media such as the conductance and permeability.

These relationships assume a linear behavior of the medium, and this is always observed for small-flow densities. Onsager's relationships, $L_{ij} = L_{ji}$, is based on extensions of thermodynamics to situations involving slight deviations from equilibrium. It also appears to be verified experimentally for small-flow densities. This relationship is of great help in organizing the experimental results.

From these relationships the possible magnitudes of electrical polarization can be deduced in terms of the coupling coefficients. Many of these coefficients are well known from other studies. For instance, the solvent-electric current flow coupling known as electro-osmosis or streaming potential has been studied by geophysicists because of the effects on self-potential logging (Wylie, 1955). The soil mechanics engineers also have made such studies because of the possible applications in soil consolidation (Casagrande, 1952).

The thermo-electric properties are not as well known, although at present a great effort is being made to develop efficient thermo-electric materials because of their possible use in energy conversion. The measure of this efficiency is exactly the same parameter that evaluates its induced polarization capabilities. These studies are concentrating on semi-conducting materials. It is quite apparent, from data to be shown later, that geologic materials do not have the required properties.

The coupling effects between solute flow and electric currents are also very well known, being an important part of the subject matter of electro-chemistry. These effects are familiar to geophysicists using self-potential measurements, for they are represented by the familiar diffusion potential phenomena.

ELECTRO-OSMOTIC COUPLING

To investigate the possible influence of electro-osmotic coupling on induced electrical polarization we can rewrite equation (1), assuming that all the induced forces except ∇P are zero, and ignoring any dependence of μ on pressure. We also combine J_p and J_n to give us the current flow I.

$$I = F(Z_pJ_p + Z_nJ_n) = -F^2[L_{11}Z_p^2 + L_{22}Z_n^2 + (L_{12} + L_{21})Z_pZ_n]\nabla\phi \\ - F(L_{13}Z_p + L_{23}Z_n)\nabla P \quad (2)$$

$$J_s = -F(L_{31}Z_p + L_{32}Z_n)\nabla\phi - L_{33}\nabla P. \quad (3)$$

In the ultimate steady-state a hydrostatic pressure will build up to prevent any further electro-osmotic solvent flow. The pressure gradient needed to prevent the solvent flow can be calculated from (3) by setting $J_s = 0$. When this pressure gradient is introduced into (2) we obtain, using Onsager's relationship $L_{ij} = L_{ji}$,

</div>

$$I(\text{steady-state}) = - \left\{ F^2[L_{11}Z_p{}^2 + L_{22}Z_n{}^2 + (L_{12} + L_{21})Z_pZ_n] \right.$$

$$\left. - \frac{F^2(L_{13}Z_p + L_{23}Z_n)^2}{L_{33}} \right\} \nabla\phi. \tag{4}$$

The term multiplying $-\nabla\phi$ is the effective conductivity in the steady-state, σdc. If high frequencies are used, no pressure gradient can build up, and from (2) we have that the high frequency conductivity is

$$\sigma_{ac} = F^2[L_{11}Z_p{}^2 + L_{22}Z_n{}^2 + (L_{12} + L_{21})Z_pZ_n]. \tag{5}$$

The maximum frequency effect is given by

$$\frac{\sigma_{ac}}{\sigma_{dc}} = \frac{1}{[1 - F^2(L_{13}Z_p + L_{23}Z_n)^2/\sigma_{ac}L_{33}]}. \tag{6}$$

The coefficients used are not the parameters in common usage. The streaming potential, which represents the potential induced by an applied pressure gradient, can be given in terms of these same coefficients, however.

$$\left(\frac{\nabla\phi}{\nabla P}\right)_{I=0} = \xi = - F(L_{13}Z_p + L_{23}Z_n)/\sigma_{ac}. \tag{7}$$

Thus it is possible to rewrite (6) as

$$\frac{\sigma_{ac}}{\sigma_{dc}} = 1 \bigg/ \left[1 - \frac{\xi^2\sigma_{ac}}{L_{33}}\right]. \tag{8}$$

The maximum polarization effect can, therefore, be determined in terms of the conductivity, the permeability, and the streaming potential, which are all easily measured parameters. In Table II are given some results of such measurements on geologic materials.

TABLE II

MEASURED ELECTRO-OSMOTIC COUPLING COEFFICIENTS
AND POSSIBLE POLARIZATION EFFECTS

Sample	Streaming Potential mv/atm.	Maximum % Frequency Effect	Investigator
quartz s.s.	8	.03	Kermabon
quartz s.s.	9	.0002	Kermabon
red s.s.	5.5	.02	Kermabon
shale	1	.05	Kermabon
limestone	2	.03	Kermabon
kaolinite (dispersed, Na)	30	2.0	Olsen
kaolinite (natural flocculated, Ca)	17	.02	Olsen
kaolinite (flocculated, .1 N NaCl)	0.7	.007	Olsen

$Z_n{}^2 + (L_{12} + L_{21})Z_pZ_n]$

$$\left.\begin{array}{c} {}^2 \\ {} \end{array}\right\} \nabla\phi. \tag{4}$$

onductivity in the steady-state,
radient can build up, and from
:y is

$_2 + L_{21})Z_pZ_n]. \tag{5}$

$$\overline{Z_n)^2/\sigma_{ac}L_{33}]} \tag{6}$$

in common usage. The stream-
iduced by an applied pressure
fficients, however.

$+ L_{23}Z_n)/\sigma_{ac}. \tag{7}$

$$\left[\begin{array}{c} \text{ie} \\ - \end{array}\right]. \tag{8}$$

ore, be determined in terms of
aming potential, which are all
i some results of such measure-

Coefficients FFECTS		
laximum % Frequency Effect	Investigator
.03	Kermabon
.0002	Kermabon
.02	Kermabon
.05	Kermabon
.03	Kermabon
2.0	Olsen
.02	Olsen
.007	Olsen

The values listed in the table indicate that the electro-osmotic effects are relatively unimportant in causing induced electrical polarization.

THERMO-ELECTRIC COUPLING

A very similar analysis can be carried out to investigate the possible influence of thermo-electric effects. The thermo-electric coupling is more complicated because of the role played by the chemical potentials, which depend both on the temperature and on the concentration of the solute. In general, unlike the electro-osmotic case, to evaluate the polarization contribution it would be necessary to measure both cross-coupling effects; the thermally induced potential gradients and the electrically induced thermal gradients.

If we ignore pressure effects

$$\nabla\mu_j = \frac{\partial\mu_i}{\partial T}\nabla T + \sum_j \frac{\partial\mu_i}{\partial C_j}\nabla C_j.$$

The time scale for heat flow at ordinary temperatures is much shorter than the time scale for diffusion flow, so that for certain time scales we can assume the concentrations remain unchanged. This allows us to set

$$\nabla\mu_i \cong -S_i\nabla T = -TS_i\frac{\Delta T}{T} \tag{9}$$

$S_i =$ partial molal entropy.

Our thermal coupling equations can then be written as

$$I = F(Z_pJ_p + Z_nJ_n) = -F^2[Z_p{}^2L_{11} + Z_n{}^2L_{22} + Z_pZ_n(L_{12} + L_{21})]\Delta\phi$$

$$- F[L_{14}Z_p + L_{24}Z_n - (Z_pL_{11} + Z_nL_{21})TS_p - (Z_nL_{22} + Z_pL_{12})TS_n]\frac{\nabla T}{T} \tag{10}$$

$$J_Q = -F[Z_pL_{14} + Z_nL_{24}]\nabla\phi - [L_{44} - L_{41}TS_p - L_{42}TS_n]\frac{\nabla T}{T}. \tag{11}$$

The quantity $-F[Z_pL_{14}+Z_nL_{24}]\nabla\phi$ appearing in (11) can be interpreted as the heat transported by the ions moving under the influence of the electrical field.

$$-F[Z_pL_{14} + Z_nL_{24}]\nabla\phi = Q_pJ_p + Q_nJ_n. \tag{12}$$

$Q =$ heat of transport.

From the definition of transference number,

$$\tau^+ = FZ_pJ_p/I; \qquad \tau^- = 1 - \tau^+ = FZ_nJ_n/I$$

we have therefore

$$FZ_p L_{14} = Q_p \tau^+ \sigma_{ac}/FZ_p \tag{13}$$

$$FZ_n L_{24} = Q_n \tau^- \sigma_{ac}/FZ_n. \tag{14}$$

We also have from (10)

$$F(Z_p L_{11} + Z_n L_{12}) = \tau^+ \sigma_{ac}/FZ_p \tag{15}$$

$$F(Z_n L_{22} + Z_p L_{21}) = \tau^- \sigma_{ac}/FZ_n. \tag{16}$$

A further simplification of notation is achieved by setting

$$[L_{44} - TS_p L_{41} - TS_n L_{42}] = TK; \qquad K = \text{thermal conductivity.} \tag{17}$$

We can now rewite (10) and (11), using Onsager's relation $L_{ij} = L_{ji}$, as

$$I = - \sigma_{ac} \nabla\phi - \left[(Q_p - TS_p) \frac{\tau^+}{FZ_p} + (Q_n - TS_n) \frac{\tau^-}{FZ_n} \right] \sigma_{ac} \frac{\nabla T}{T} \tag{18}$$

$$J_Q = - \left(Q_p \frac{\tau^+}{FZ_p} + Q_n \frac{\tau^-}{FZ_n} \right) \sigma_{ac} \nabla\phi - K \nabla T. \tag{19}$$

In the steady-state limit $J_q = 0$, and solving for the temperature gradient set up we can obtain the steady-state conductivity.

$$\sigma_{dc} = \sigma_{ac} \left[1 - \frac{\left(\sum Q_i \frac{\tau_i}{FZ_i} \right) \left(\sum (Q_i - TS_i) \frac{\tau_i}{FZ_i} \right) \sigma_{ac}}{TK} \right]. \tag{20}$$

If the time scale is extended, the temperature gradients can also establish concentration gradients (Soret effect) which will modify the current flow because of the diffusion potentials set up. A greater practical difficulty in establishing the magnitudes of these effects is the fact that a measurement of the thermo-electric coefficient

$$\theta = \left(\frac{\nabla\phi}{\nabla T} \right)_{I=0} = - \sum \left(\frac{Q_i - TS_i}{T} \right) \frac{\tau_i}{FZ_i} \tag{21}$$

is not enough to establish the polarization effects of this coupling. In principle one would need to also measure the heat of transport. Such a calorimetric measurement is much more difficult to carry out than the electrical measurement involved in (21).

We can make estimates of the term $\sum Q_i (\tau_i/FZ_i)$ in (20) which are adequate for our purposes here. In most rocks the positive ion transference number is much larger than the negative ion transference number. Thus

$$\theta \cong \frac{Q_p - TS_p}{TFZ_p}. \tag{22}$$

Z_p (13)

$Z_n.$ (14)

$_{ac}/FZ_p$ (15)

$_{ac}/FZ_n.$ (16)

y setting

= thermal conductivity.   (17)

s relation $L_{ij}=L_{ji}$, as

$$\left. {}_n - TS_n)\ \frac{\tau^-}{FZ_n}\right]\sigma_{ac}\ \frac{\nabla T}{T} \quad (18)$$

$'T.$ (19)

or the temperature gradient set

$$\left. - TS_i)\ \frac{\tau_i}{FZ_i}\right)\sigma_{ac}\right] \quad (20)$$

e gradients can also establish
modify the current flow because
al difficulty in establishing the
urement of the thermo-electric

$$\left. TS_i\right)\frac{\tau_i}{FZ_i} \quad (21)$$

of this coupling. In principle
ort. Such a calorimetric meas-
the electrical measurement in-

Z_i) in (20) which are adequate
e ion transference number is
mber. Thus

        (22)

The partial molal entropies for aqueous solutions of ions are known, so that if we can assume similar values for the ions in the pore fluids, (22) would give us an estimate of $\sum Q_i(\tau_i/FZ_i)$. Using KCl solutions typical values of θ ran around 0.3 mv/deg. C. These were measured in a cell where the thermo-electric voltages across the rock samples were bucked against the thermo-electric voltage across a water column (Uhri, 1958). The voltage between the measuring electrodes were then corrected for a semi-theoretical value of the water thermo-electric voltage (Eastman, 1928, and Wirtz, 1948). The partial entropy value for K^+ of 24 entropy units per mole, thus gave from (22) an estimate of Q_{K+} of 3.6 Kcal/mole. The value of $\sum(Q_i - TS_i)\tau_i$ was about 2.3 Kcal/mole, so that we are within the correct order of magnitude to replace $\sum Q_i\tau_i$ by $\sum(Q_i - TS_i)\tau_i$. This allows us to rewrite (20) as

$$\frac{\sigma_{ac}}{\sigma_{dc}} \cong 1 \bigg/ \left(1 - \frac{T\theta^2\sigma_{ac}}{K}\right). \quad (23)$$

In Table III are listed some of the thermo-electric data and the approximate maximum polarization effect possible from such coupling.

TABLE III

MEASURED THERMO-ELECTRIC COUPLING COEFFICIENTS
AND POSSIBLE POLARIZATION EFFECTS

Sample	Thermo-Electric Coef. mv/deg. C	Maximum % Frequency Effect
ss. with clay	.23	.000003
s.s.	.48	.00003
shale	.33	.00004
limestone	.27	.0000002

It is obvious that this coupling is of no importance in causing polarization effects. Actually the thermo-electric coefficients are quite high, but the ratio of electrical conductivity to thermal conductivity is very low, so that from (23) $\sigma_{ac} \cong \sigma_{dc}$. This is also the reason why semi-conductors are being used for thermo-electric power conversion; one must have a very good electrical conductor as well as strong thermo-electric effects.

DIFFUSION COUPLING

It is apparent by now that the cross terms appearing in the matrix describing the flow properties of the medium are not large enough in geologic materials to cause appreciable polarization effect. It is quite a different matter, however, when diffusion flow effects are investigated. This, of course, is because the ions themselves carry the electric current, so that the diffusion gradients and the electrical potential gradients have to appear together as primary driving forces for the ion motion.

If we drop all the off diagonal terms in (1) we are left with

$$J_p = -L_{11}\nabla\mu_p - L_{11}FZ_p\nabla\phi \tag{24}$$

$$J_n = -L_{22}\nabla\mu_n - L_{22}FZ_n\nabla\phi \tag{25}$$

as the flow equations for the anions and the cations. In place of the coefficients L_{ij}, we can introduce the more familiar electrochemical quantities of mobility, diffusion coefficients, and transference numbers. Thus we can rewrite the flow equations, assuming uni-valent ions, as

$$J_p = -D_p\frac{\partial p}{\partial x} + u_p p E \tag{26}$$

$$J_n = -D_n\frac{\partial n}{\partial x} - u_n n E \tag{27}$$

U = mobility　　　　　　　　　　　　p = cation concentration

D = diffusion coef.　　　　　　　　　　n = anion concentration

$t^+ = U_p/(U_p + U_n) = D_p/(D_p + D_n)$　　= cation transference no.

$t^- = 1 - t^+$　　　　　　　　　　　　= anion transference no.

If t^+ should vary along the current path, a divergence will result in the flow of the ions, causing concentration gradients to build up. This is illustrated in Figure 9 where zone II represents a strongly cation selective zone, and zone I represents a zone with no selectivity. Because of its selective transference properties zone II would be called a membrane zone. Since the current in zone II is largely carried by the cations, a surplus of these ions will occur at one end of zone II, and a deficiency at the other end. The anion flow will also be unbalanced, and the buildup of anions will equal that of the cations. The resulting concentration gradients will modify the ion flow until a balance is reached. In this steady-state
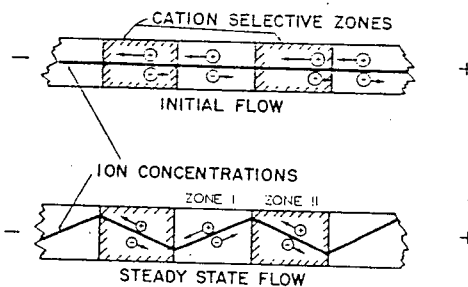
MODEL FOR MEMBRANE POLARIZATION

Fig. 9. Ion motion and concentration changes developed by current flow through a membrane system.

are left with

$$FZ_p\nabla\phi \tag{24}$$

$$FZ_n\nabla\phi \tag{25}$$

ions. In place of the coefficients
chemical quantities of mobility,
. Thus we can rewrite the flow

$$\cdot pE \tag{26}$$

$$\cdot nE \tag{27}$$

= cation concentration

= anion concentration

= cation transference no.

= anion transference no.

nce will result in the flow of the
. This is illustrated in Figure 9
ve zone, and zone I represents
transference properties zone II
nt in zone II is largely carried
at one end of zone II, and a
also be unbalanced, and the
. The resulting concentration
is reached. In this steady-state

} +

} +

LARIZATION

eloped by current flow
.

condition the net flow of cations and anions in zone II will equal that in zone I.

$$J_{pI} = J_{pII} \tag{28}$$

$$J_{nI} = J_{nII}. \tag{29}$$

The impedance of the zones will also be modified, because the concentration gradients developed will have diffusion potentials associated with them. These potentials arise because of a slight unbalance of charge, but since so little charge is needed to develop an electric field, one can say that the cation and anion concentrations are essentially equal.

$$p = n. \tag{30}$$

The electric field is assumed to be constant in each zone, so that the total potential difference across the pair of zones is given by

$$\Delta\phi = -E_I\Delta L_I - E_{II}\Delta L_{II}. \tag{31}$$

The concentrations, p and n, will be continuous across the boundaries, so that if the succeeding zones repeat the same pattern with the same geometry and electrical properties, we can put

$$\Delta p_I = -\Delta p_{II} \tag{32}$$

$$\Delta n_I = -\Delta n_{II}. \tag{33}$$

When it is also assumed that the concentration gradients are constant in each zone, (28), (29), (30), (32), and (33) can be considered as a system of algebraic equations for the unknown electric fields and concentration gradients. Solving these we obtain for the steady-state conductance

$$\sigma_{dc} = \frac{Fu_{pI}C\left(\dfrac{1}{\tau_{II}^-} + \dfrac{A}{B}\dfrac{1}{\tau_I^-}\right)S_IS_{II}}{\Delta L_I\left[S_I\left(1 + \dfrac{B}{A}\right) + S_{II}\left(1 + \dfrac{A}{B}\right)\right]} \tag{34}$$

c = net concentration

$A = \Delta L_I/\Delta L_{II}$

$B = D_{pI}/D_{pII}$

$S_i = \tau_i^-/\tau_i^+.$

At the high frequency limit, no concentration gradients develop, and the only unknowns are the potential gradients. Using the condition that the electric current is the same in the two zones as well as the condition on the total voltage given by (31) allows us to solve for the conductance

$$\sigma_{ac} = Fu_{pI}CA/\Delta L_I(A\tau_I^+ + B\tau_{II}^+). \tag{35}$$

TABLE IV

POLARIZATION OF MEMBRANE MODEL

percent frequency effect $(\tau_I{}^+ = 0.5)$

$\tau_{II}{}^+$	$B =$ $A =$	1 .1	1 1	1 10	3 .1	3 1	3 10	D_P Ratio Length Ratio
.999		4.8	33	81	1.6	14	62	
.990		4.5	32	67	1.6	14	57	
.909		3.3	20	20	1.2	9.6	27	
.667		.7	2.8	1.2	1.9	1.8	2.5	

The maximum frequency effect that diffusion coupling can develop in our model is given as

$$\frac{\sigma_{ac}}{\sigma_{dc}} = \frac{(A + B)\left[\dfrac{A}{\tau_I{}^-\tau_{II}{}^+} + \dfrac{B}{\tau_I{}^+\tau_{II}{}^-}\right]}{\left[\dfrac{A}{\tau_{II}{}^+} + \dfrac{B}{\tau_I{}^+}\right]\left[\dfrac{A}{\tau_I{}^-} + \dfrac{B}{\tau_{II}{}^-}\right]}. \tag{36}$$

Typical values are given in Table IV. It will be observed that there is a finite limit to the frequency effect caused by this form of polarization.

For the time scales to be reasonable, the zones must be very small, and one would not be able to measure the electrical properties of each zone. The presence of membrane zones should make itself known when diffusion measurements are made, because the average transference value for the anions and cations will not be equal, and a diffusion potential will be set up. The information given in Table IV is therefore plotted in Figure 10 in terms of the effective transference number which would be determined from diffusion potential measurements. In Table V are shown the results of diffusion measurements on a few rock samples, and the possible polarizing effects that diffusion coupling could result in.

The values listed above show that these diffusion coupling effects are capable of causing considerable electrical polarization. There are two factors that should be pointed out here. First of all the possible polarization effects could increase without limit if we assumed that zones with positive ion blocking properties

TABLE V

MEASURED TRANSFERENCE VALUES AND POSSIBLE POLARIZATION EFFECTS

Sample	t^+ (Effective)	Maximum % Frequency Effect
tuff	.51	1
tuff	.72	40
tremolite limestone	.87	72
sandstone, medium grained	.48	1
sandstone, medium grained	.49	1
sandstone, fine grained	.89	78
dirty sandstone	.6	20

MODEL
=0.5)

3	3	D_P Ratio
1	10	Length Ratio
14	62	
14	57	
9.6	27	
1.8	2.5	

)ling can develop in our model

$$\frac{B}{\tau_I^+ \tau_{II}^-}$$
$$+\frac{B}{\tau_{II}^-}$$

(36)

)bserved that there is a finite
i polarization.

must be very small, and one
ies of each zone. The presence
n diffusion measurements are
he anions and cations will not
he information given in Table
effective transference number
i measurements. In Table V
. a few rock samples, and the
)uld result in.

n coupling effects are capable
·e are two factors that should
ization effects could increase
:tive ion blocking properties

POLARIZATION EFFECTS

iective)	Maximum % Frequency Effect
51	1
72	40
37	72
18	1
49	1
89	78
6	20

existed as well as those zones which can block negative ions. It is very unlikely that geologic materials will ever include such zones, but synthetic ion exchange resins can be found that do. The second factor that should be pointed out is the dependence of the polarization effect on the length ratio A. If a material has zones of very high t^+ values, but these zones are too numerous, so that most of the conduction path lies within such zones, little polarization will result. If has been
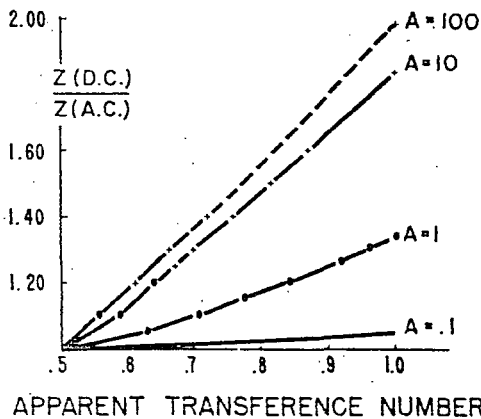
FIG. 10. Effect of the ratio of the zone lengths on the maximum polarization of a membrane system.

noted before that clays, despite their very striking t^+ values, often show extremely little polarization effect, especially if they have been mechanically manipulated. It is believed that this may be due to a tendency for the conduction paths to lie almost entirely within clay zones. Vacquier in his work reported that he could only obtain polarization effects from clays when he coated them on sand grains.

We have advanced no theory here as to why the pores of a rock or clay particles should show much membrane properties. This will involve a microscopic theory of the mineral solution interfaces. It is interesting to point out in this connection, however, that the presence of a surface charge on the minerals does not by itself cause any polarization.

A more detailed study showed that a fixed charge in a system can lead to a very slight polarization, but it is really necessary, if the system is to have a finite polarization effect, that the motion of certain ions be hindered in the system. Thus it appears that the electrostatic and Van der Waal forces that attract the positive ions to the surface of a polarizing clay system must also act to prevent negative ions from moving along the surface.

COMPARISON OF ELECTRODE AND MEMBRANE POLARIZATION

The model given for membrane polarization sets a finite limit to the polarization effect of membrane zones within a rock. The model given in Figure 1 for
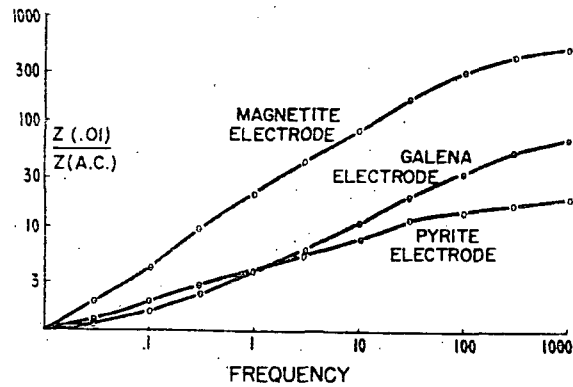
FIG. 11. Impedance of natural electrodes.

electrode polarization is not so limited however. In Figure 11 is shown some data on the interfacial impedance of a few natural electrodes. The frequency effects are much larger than 100 percent. We might expect, therefore, to find a difference between the magnitude of the observed polarization depending on the cause of the polarization. Because of the diluting, mentioned before, that is caused by parallel unpolarized conduction paths, it seems best to compare the metal factors rather than the percentage frequency effects. In Figure 12 there is shown in a somewhat generalized form, the results of laboratory measurements on a large number of rock samples, and field measurements in many areas. These results again indicate the pronounced polarization effects of well-mineralized rocks. However, in rocks with less mineralization, there begins to exist considerable ambiguity. This is especially true in sedimentary rocks of high conductivity. The geometry of the mineralization is also very critical. When the sulphides form connected veinlets
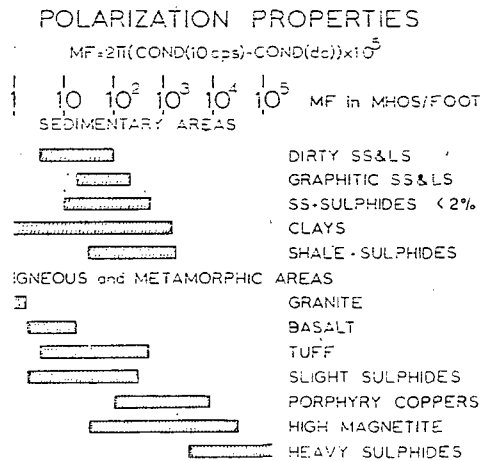
FIG. 12. Distribution of observed metal factor values.

ORE R. MADDEN

ALENA
DE

PYRITE
ECTRODE

100   1000

ctrodes.

Figure 11 is shown some data
trodes. The frequency effects
, therefore, to find a difference
depending on the cause of the
iore, that is caused by parallel
pare the metal factors rather
there is shown in a somewhat
ements on a large number of
:. These results again indicate
ized rocks. However, in rocks
siderable ambiguity. This is
ctivity. The geometry of the
:ides form connected veinlets

ES

HOS/FOOT

.LS
SS&LS
DES ⟨2%

_PHIDES

_PHIDES
COPPERS
IETITE
_PHIDES

ctor values.

their metal factor values are far superior to those of well-disseminated sulphides.

These results, although not eliminating the great usefulness of induced polarization measurements, do point out certain dangers in holding too simple a concept about the causes of the polarization. It also leads one to search for other criteria, besides a magnitude criterion, to help in separating out the various contributing factors.

FREQUENCY BEHAVIOR OF MEMBRANE POLARIZATION

The mechanism involved in membrane polarization appears to be quite different than that pictured in Figure 1 for electrode polarization. It might be hoped, therefore, that the details of the frequency spectrum for the two polarization effects would lead to some means of distinguishing between the different effects. For this reason the study of the membrane model was expanded.

From equations (26) and (27) we can obtain the equations of motion for the ion species.

$$\frac{\partial p}{\partial t} = D_p \frac{\partial^2 p}{\partial x^2} - U_p \frac{\partial}{\partial x}(pE) \tag{37}$$

$$\frac{\partial n}{\partial t} = SD_p \frac{\partial^2 n}{\partial x^2} + SU_p \frac{\partial}{\partial x}(nE). \tag{38}$$

Poisson's equation must also be satisfied

$$\frac{\partial E}{\partial x} = \frac{F}{\epsilon}(p - n). \tag{39}$$

These equations are non-linear but can be linearized for our case since we are interested in very small current densities. For small current densities we can consider the electric fields and the concentration changes to be small

$$P = C + \Delta P$$
$$N = C + \Delta N, \tag{40}$$
$$E = \Delta E.$$

If the product of these small terms is neglected and harmonic time dependence is assumed, (37), (38), and (39) become linear equations for Δp, Δn, and ΔE.

$$i\omega\Delta p = D_p \frac{d^2\Delta p}{dX^2} - U_p C \frac{d\Delta E}{dX} \tag{41}$$

$$i\omega\Delta n = SD_p \frac{d^2\Delta n}{dx^2} + SU_p C \frac{d\Delta E}{dx} \tag{42}$$

$$\frac{d\Delta E}{dx} = \frac{F}{\epsilon}(\Delta p - \Delta n). \tag{43}$$

These equations are the ones usually dealt with in treatments of space charge effects, and appear in discussions of solution-electrode interfaces as well as in this membrane model (MacDonald, 1953). The general solutions are simple exponentials with two characteristic lengths.

$$\Delta p = L_p e^{\pm r_1 x} + M_p e^{\pm r_2 x}$$
$$\Delta n = L_n e^{\pm r_1 x} + M_n e^{\pm r_2 x}. \tag{44}$$

One of these characteristic lengths

$$\frac{1}{r_1} = 1/K \left(1 + \frac{j\omega(S+1)}{DSK^2} \right)^{1/2} \cong 1/K; \quad K^2 = \frac{2CF^2}{\epsilon RT} \gg 1 \tag{45}$$

is essentially frequency independent and represents a space charge set up at the boundaries of a zone. The other characteristic length

$$\frac{1}{r_2} = \left[\frac{2D_p S}{j\omega(S+1)} \right]^{1/2} \tag{46}$$

varies inversely with the square root of the frequency and represents a diffusion phenomenon.

The undetermined constants in the solution are solved for by imposing the boundary conditions. In the membrane model, because of the symmetry imposed by the regular spacing of the zones, there are six constants to be determined, three for each zone. The boundary conditions can be given as the continuity of concentration and of ion flow at the boundary, the continuity of E at the boundary, and the condition that $\int \Delta E dx = -\Delta\phi$, the applied potential. These conditions, when expressed in terms of the general solutions, give us six simultaneous algebraic equations for the undetermined constants. Their solution is straightforward, but laborious, since the system of equations is highly singular and many terms must be carried along. The impedance of the membrane zone can then be determined and is given by

$$Z = \frac{\Delta L_1}{U_{p1}CF} \left\{ t_I^+ + \frac{B}{A} t_{II}^+ + \frac{(S_{II} - S_I)^2}{\dfrac{X_I S_I}{(t_{II}^+)^2 t_I^+ \tanh X_I} + \dfrac{A}{B} \dfrac{X_{II}S_{II}}{t_{II}^+(t_I^+)^2 \tanh X_{II}}} \right\}$$

$$X_i = \left(\frac{j\omega}{2D_{pi}t_i^-} \right)^{1/2} \frac{\Delta L_i}{2}$$

$$A = \Delta L_I / \Delta L_{II} \tag{47}$$

$$B = D_{pI}/D_{pII}$$

$$S_i = t_i^-/t_i^+.$$

Values of the membrane impedance as a function of frequency are shown in Figure 13, where it is assumed that zone I is a neutral zone. The value used for

'DORE R. MADDEN

h in treatments of space charge
trode interfaces as well as in this
:al solutions are simple exponen-

$\pm r_2 x$

$\pm r_2 x$ (44)

$$K^2 = \frac{2CF^2}{\epsilon RT} \gg 1 \qquad (45)$$

nts a space charge set up at the
ngth

/2

(46)

iency and represents a diffusion

are solved for by imposing the
cause of the symmetry imposed
ix constants to be determined,
n be given as the continuity of
ie continuity of E at the bound-
pplied potential.. These condi-
itions, give us six simultaneous
.nts. Their solution is straight-
ons is highly singular and many
he membrane zone can then be

$$\left. \begin{array}{l} \text{:}_1 - S_1)^2 \\ \dfrac{A}{B} \dfrac{X_{II}S_{II}}{t_{II}^{+}(t_{I}^{+})^2 \tanh X_{II}} \end{array} \right\}$$

L_i
—

(47)

ion of frequency are shown in
utral zone. The value used for
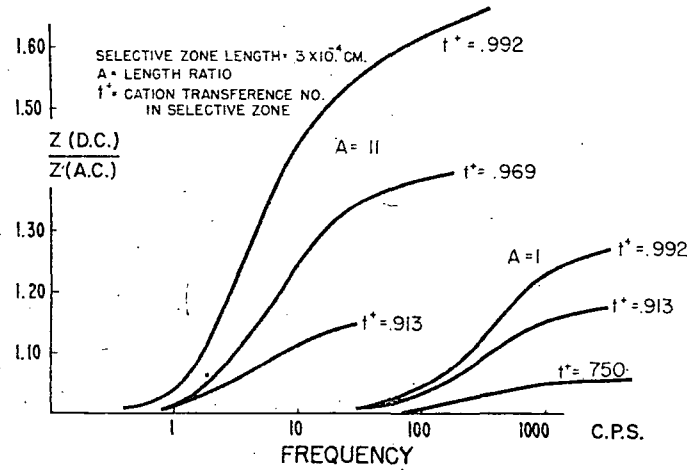
FIG. 13. Details of the impedance of a simple membrane system.

ΔL_2 of 0.3×10^{-3} cm. is typical of the size of clay particles. The frequency response for a given zone size is quite sharp. The frequencies at which the impedance is varying depend on the square of zone length, so that in an actual system with a distribution of zone lengths we can expect the frequency variations to be spread out over a wide range of frequencies. In Figure 14 are shown some impedance measurements on real membrane systems for comparison.

FREQUENCY BEHAVIOR OF ELECTRODE POLARIZATION

To compare electrode polarization to membrane polarization we must extend the simple model of Figure 1. In fact the data shown in Figure 11 are quite different from what we would expect from a simple RC circuit. Therefore, to better under-
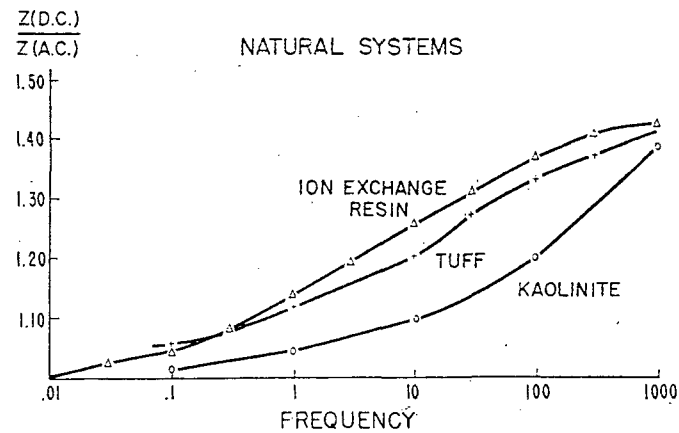

FIG. 14. Details of the impedance of a natural membrane system.

stand the nature of electrode impedances, detailed kinetic calculations were also carried out for the impedance of an electrode-solution interface. Equations (41) (42) and (43) can again be used to describe the ion motions, but the boundary conditions are very different. First of all there can be capacitive coupling between the solution and the electrode. Secondly any Faradaic current involving actual charge transfer must entail chemical reactions, and a whole chain of events may follow depending on the products of these reactions. These events are all reflected in the boundary conditions, and thus modify the electrode impedance (Madden and Marshall, 1959). When typical reaction rate values are used, however, the

NORMAL REACTION RATE VALUES

C_e = ELECTRODE CAPACITANCE
R_s = SOLUTION RESISTANCE
R_I = REACTION RESISTANCE

CATALYZED REACTION

R_2 = CATALYZED REACTION RESISTANCE

W_2 = WARBURG IMPEDANCE = W_2 (FREQ.)$^{-\frac{1}{2}}e^{-i\frac{\pi}{4}}$

C_{C_H} = CHEMICAL CAPACITANCE
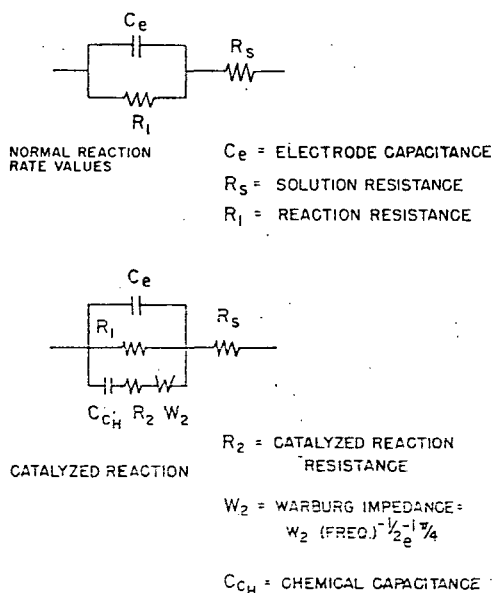
FIG. 15. Equivalent circuits for the impedance of polarized electrodes.

solutions obtained indicate that at audio and sub-audio frequencies the circuit of Figure 1 should well represent the electrode impedance. If a reaction occurring at the surface is well catalysed, a different behavior would be expected. There is little reaction resistance in such a case, but the depletion of the reacting species at the surface would require a diffusion of the ions to or away from the surface. This is responsible for an impedance which has the typical diffusion behavior and depends inversely on the square root of the frequency. It is called a Warburg impedance and is given the symbol W (Grahame 1952). The accumulation of the reaction product will in general tend to oppose any further reaction, and this causes an impedance just like that of a capacitance. We have given this capacitance the symbol C_{ch}. The equivalent circuits for an electrode impedance with normal reactions or with catalyzed reactions are shown in Figure 15.

:d kinetic calculations were also
iution interface. Equations (41)
ion motions, but the boundary
. be capacitive coupling between
radaic current involving actual
nd a whole chain of events may
ns. These events are all reflected
: electrode impedance (Madden
: values are used, however, the

)DE CAPACITANCE

: RESISTANCE

N RESISTANCE

D REACTION
TANCE

IMPEDANCE=
:ɔ.ɩ⁻½₂⁻ⁱ¾

L CAPACITANCE

: of polarized electrodes.

ib-audio frequencies the circuit
pedance. If a reaction occurring
ior would be expected. There is
lepletion of the reacting species
ns to or away from the surface.
e typical diffusion behavior and
juency. It is called a Warburg
ie 1952). The accumulation of
e any further reaction, and this
ice. We have given this capaci-
ir an electrode impedance with
shown in Figure 15.
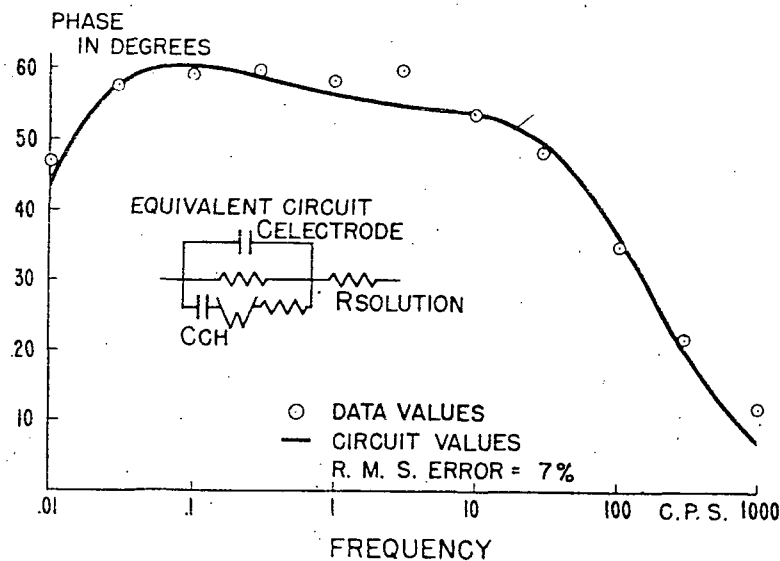
FIG. 16. Phase shift of the impedance of a magnetite electrode, and its comparison with the equivalent circuit.

Measurements were made on a wide variety of electrodes, and data were also obtained from the literature. Equivalent circuits such as those shown in Figure 15 were then adjusted to fit the data. In most cases the circuits could be made to fit the data within the experimental error. An example of such a fit is shown in Figure 16, where only the phase of the impedance is plotted. The magnitude of the impedance for this same electrode is shown in Figure 10, and on this logarithmic scale the errors of the equivalent circuit would not be discernible. The most striking result of these measurements was that in every case a well catalyzed reaction appeared to be taking place and contributed a large part of the current being passed. This means that the impedance was in a large part controlled by a diffusion phenomenon, just as in the membrane model. A summary of these electrode measurements is given in Table VI.

SUMMARY AND CONCLUSIONS

When using induced polarization measurements for the detection of metallic or semi-conducting minerals, one must be aware of other causes of the electrical polarization. An examination of the possible causes of these effects reduced the important factors to electromagnetic coupling effects and membrane polarization as well as the metallic mineral, i.e., electrode polarization that one is usually looking for. The electromagnetic effects can be avoided by using only information at very low frequencies. In typical mining exploration applications, one must work with frequencies of less than 10 cps.

TABLE VI

SUMMARY OF ELECTRODE IMPEDANCES

Values are given for 1 cm² of surface at room temp. Symbols are referred to Fig. 15.

Electrode	Reaction Resistance R_1	Electrode Capacitance C_e	Catalyzed Reaction Resistance R_2	Warburg Impedance W_2	Chemical Capacitance Cch
ST steel	160,000	3.2	11	3,960	247
Ni	8,500	112	3	670	830
Cu	3,080	3.8	19	1,270	55,000
Graphite	49,500	80	26	2,700	170
Pyrite	3,900	15.	60	800	150,000
Galena*	3,800	8.5	6	760	43,000
Magnetite*	222,000	4.8	101	5,870	106

* Area not known accurately.　　　　　　Resistances given in ohms.
　　　　　　　　　　　　　　　　　　　　Capacities given in μf.
　　　　　　　　　　　　　　　　　　　　W_2 calculated at 1 cps.

The effects of membrane polarization are more difficult to separate out. The effects are more limited than the electrode polarization, but may still be significant. Detailed investigations of these two processes were made to look for fundamental differences in their electrical behavior. Unfortunately the investigations showed that the principal factor contributing to the electrode impedance is a diffusion phenomenon, and this is the same factor involved in membrane polarization. Both electrode and membrane impedances show a wide and gentle frequency variation making any discrimination on this basis very difficult. This result was borne out in the measurements on rock and clay samples. The phase shifts of the metal factor, which should represent approximately the phase shift of the blocked conduction paths, were computed from an analysis of transient measurements at one tenth, one and ten cps. for hundreds of samples. Although the results were often quite characteristic for a given rock or clay type, there seemed to be no clear separation between those samples with electrode polarization and those with membrane polarization. Some typical values are shown in Table VII.

This represents of course only a somewhat limited frequency range and a wider frequency analysis might prove to be more discriminating. It is difficult, however, to extend the measurements to higher frequencies in the field because of the electromagnetic coupling effects. The measurements at lower frequencies are in principle possible, but the natural earth currents make the noise problem an important practical factor.

The magnitude of the polarization effects still appears to be the best guide for the detection of electrode polarization in rocks. When the mineralized target is well below the surface, the observed effects are, of course, considerably reduced, and may be hardly different than a small background polarization. The authors are of the opinion that the greatest improvement in interpretation will come from

IMPEDANCES

Symbols are referred to Fig. 15.

lyzed ction stance R_2	Warburg Impedance W_2	Chemical Capacitance Cch
!1	3,960	247
3	670	830
!9	1,270	55,000
!6	2,700	170
!0	800	150,000
6	760	43,000
!1	5,870	106

Resistances given in ohms.
Capacities given in μf.
W_2 calculated at 1 cps.

more difficult to separate out. The
polarization, but may still be sig-
processes were made to look for
navior. Unfortunately the investi-
buting to the electrode impedance
ime factor involved in membrane
npedances show a wide and gentle
n on this basis very difficult. This
rock and clay samples. The phase
ent approximately the phase shift
ted from an analysis of transient
or hundreds of samples. Although
a given rock or clay type, there
e samples with electrode polariza-
ome typical values are shown in

t limited frequency range and a
ore discriminating. It is difficult,
r frequencies in the field because
easurements at lower frequencies
currents make the noise problem

till appears to be the best guide
cks. When the mineralized target
, of course, considerably reduced,
ground polarization. The authors
t in interpretation will come from

TABLE VII
METAL FACTOR PHASE IN DEGREES

Sample Type	Frequency cps.		
	10	1	0.1
Kaolinite	9	14	22
Mica	8	12	19
Ion exchange resins	13	29	51
Sediments from Colorado Plateau			
with sulphides	12	20	30
little or no sulphides	9	15	21
Sedimentary copper ore	12	18	19
Rhodesian copper ore	18	27	41
Field data, porphyry copper body		18	31
Lithic Tuff, little or no sulphides	12	22	34
Graphitic ss	13	16	22
Dirty sands from Dakota, ss sequence	11	17	30
Manganese ore	9	14	22
Highly magnetic altered, ultrabasic	42	-41	47

an accurate handling of this geometric factor, rather than a subtle analysis of
the frequency spectrum of the observed polarization.

Calument and Hecla Mining Co.
National Lead Co.
Nucom Ltd.
Pan American Petroleum Corp.

REFERENCES

Bleil, D. F., 1953, Induced polarization, a method of geophysical prospecting: Geophysics, v. 18, p. 636–661.

Brant, A. A., personal communication.

Casagrande, L., 1952, Electro-osmotic stabilization of soils: Jour. Boston Soc. Divil Eng., v. 39, p. 51.

De Groot, S. R., 1951, Thermodynamics of irreversible processes: New York, Interscience Publishers.

Denbigh, K. G., 1951, The thermodynamics of the steady state: London, Methuen & Co., Ltd.

Eastman, 1928, Electromotive force of electrolyte thermocouples and thermocells and the entropy of transfer and absolute entropy of ions: J. Amer. Chem. Soc., v. 50, p. 292.

Eckart, 1940, Thermodynamics of irreversible processes: Phys. Rev., v. 58, p. 267.

Grahame, D. C., 1952, Mathematical theory of the faradaic admittance: Jour. of Electrochem. Soc., v. 99, p. 370.

Hallof, P., 1957, On the interpretation of resistivity and induced polarization results: Ph.D. thesis, M.I.T. Department of Geology and Geophysics.

Henkel, J. H., and Van Nostrand, R. G., 1957, Experiments in induced polarization: A.I.M.E. Trans., v. 9, p. 355–359.

Kermabon, A. J., 1956, A study of some electro-kinetic properties of rocks: M.S. thesis, M.I.T. Department of Geology and Geophysics.

MacDonald, J. R., 1953, Theory of A.C. space-charge polarization effects in photoconductors, semiconductors, and electrolytes: Phys. Rev., v. 92, p. 4.

Madden, Marshall, Fahlquist, and Neves, 1957, Background effects in the induced polarization method of geophysical exploration: A.E.C. report RME-3150.

Madden, T. R., and Marshall, D. J., 1958, A laboratory investigation of induced polarization: A.E.C. report RME-3156.

——, 1959, Electrode and membrane polarization A.E.C. report RME-3157

Olsen, H., 1958, Personal communication.

Schlumberger, C., 1920, Etude sur la prospection electrique du soussol: Paris, Gauthier-Villars, Chapt. VIII.

Sunde, E. D., 1949, Earth conduction effects in transmission systems: New York, D. Van Nostrand Co., Chapt. IV.

Uhri, D., 1958, Personal communication.

Vacquier, V., Holmes, C. R., Kintzinger, P. R., and Lavergne, M., 1957, Prospecting for ground water by induced electrical polarization: Geophysics, v. 22, p. 660–687.

Wirtz, V. K., 1948, Platzwechselprozesse in Flussigkeiten, Zeit f. Naturforschung, 3a, p. 672.

Wyllie, M. R. J., 1955, The role of clay in well-log interpretation: State of California, Division of Mines, Bulletin 169, p. 282.

IONIC DOUBLE-LAYER CONDUCTIVITY IN RESERVOIR ROCK

W. O. WINSAUER AND W. M. McCARDELL, JUNIOR MEMBERS AIME, HUMBLE OIL AND REFINING CO., HOUSTON, TEX.

ABSTRACT

The abnormal conductivity found in shaly reservoir rocks containing an electrolyte is shown to be a consequence of the electrical double layer in the solution adjacent to charged clay surfaces. This increased conductivity results from a higher concentration of ions in the double layer than in the solution in equilibrium with the double layer. It is shown that the magnitude of the increased conductivity of a shaly reservoir material is influenced by the concentration and type of ions in the equilibrium solution as well as by the colloidal nature of the rock.

INTRODUCTION

An important factor in the quantitative interpretation of the electric log is the resistivity factor of reservoir rock. The resistivity factor is defined as the resistivity of the rock when completely saturated with an electrolyte divided by the resistivity of the electrolyte itself.[1] In the normal case, the resistivity factor for a particular rock sample is independent of the resistivity of the electrolyte and reflects the pore geometry of the rock.[2]

In 1949, Patnode and Wyllie[3] showed that in some cases the resistivity factor is not constant, but instead varies with the resistivity of the electrolytic solution. It was shown that clean sands behave normally—i.e., that the resistivity factor does not vary with resistivity of the electrolyte—but that sands containing shale and clay may exhibit abnormally low resistivity factors when the solution used to saturate them is of fairly high resistivity. At low resistivities of the electrolyte, the resistivity factor for a shaly sand appeared to approach a normal behavior. It is evident that the resistivity factor of a shaly sand is dependent upon factors other than pore geometry when the solution used to saturate it is of high resistivity.

Patnode and Wyllie, and later de Witte,[4] assumed that the conductivity of a shaly sand saturated with an electrolyte could be represented as the sum of two quantities. One of these was assumed, in effect, to be the conductivity which would be expected if the sample were a clean sand, and the other was assumed to be a conductivity inherent in the sample itself. The latter was supposed to be constant for a given rock sample regardless of the solution used to saturate it. The source of this added conductivity was ascribed to "conductive solids."

In actual practice, the effect of the abnormal behavior of shaly sands is of minor importance except when the resistivity of a formation such as a sand is high. Thus the effect is more important when the sand is saturated with a dilute brine than when it contains a more concentrated electrolyte. The effect is also more important when the sample contains oil or gas than when it contains only saline water.

Recently it has been suggested that the porosity of a stratum may be estimated from the electric log by use of the resistivity of the invaded zone.[5] This is the zone flushed with the filtrate from mud used in drilling the well, which is ordinarily very dilute brine. When the method is applied to shaly sands, the effect of abnormal conductivity becomes of importance.

This report describes an investigation of the mechanism responsible for the abnormal behavior of the resistivity of shaly rock saturated with conducting solutions. The investigation

was undertaken to provide a better understanding of the phenomenon in order that allowance may be made for it in the interpretation of the electric log.

MECHANISM OF THE ABNORMAL CONDUCTION

Role of Matrix Material

Despite the unfortunate connotation of the term "conductive solids," it may readily be demonstrated that the conductivity of the matrix material of a shaly sand is negligible. A shaly formation will not conduct in the dry state; conduction is apparent only when the rock contains an electrolyte. Although it is evident that the clay in the matrix plays an essential part in abnormal conduction, it is also evident that it does so only in the presence of an ionic solution. This suggests immediately that the adsorptive properties of the clay may be responsible for the phenomenon.

Conductivity of the Ionic Double Layer

Nature of Double-Layer

The surface property of the colloidal shales and clays found in nature is such that they adsorb more negative ions than positive ions from an ionic solution. This results in the colloidal material being negatively charged with respect to the solution and also results in an electric field which attracts positive ions to the vicinity of the negatively charged surface.

These positive ions form a diffuse ionic layer. The nature of this diffuse layer and the distribution of ions throughout the so-called double layer are described in the classical theories of Helmholtz,[5] Stern,[7] and Gouy.[8] Recently an excellent discussion of the electrical double layer was given in a treatment by Verwey and Overbeek.[9] The existence of the double layer in naturally occurring shales and its role in the development of the logging potential has been discussed by McCardell, *et al.*[10]

It may be shown that one consequence of the ion distribution in the double layer is a higher concentration of mobile positive ions in the immediate vicinity of a shale surface than in the bulk of the solution with which the shale is in equilibrium.

Distribution of Ions in Double Layer

The concentration of ions in a solution adjacent to a charged surface, such as exists in a sand in which there is some clay, may be illustrated in idealized form by Fig. 1.

Several points are exemplified by this figure. First, nearly all of the "fixed" negative charges which reside on the surface of the pore are on the clay. Second, the concentration of mobile positive ions near the charged surface is higher than that of the mobile negative ions. Third, the total numbers of positive and negative charges, both mobile and fixed, in the system are identical. Fourth, if the pore be sufficiently large so that a portion of the solution will be beyond the influence of the surface charge or if no charged surface exists, then part or all of the solution will have equal numbers of positive and negative ions. This "double-layer free" solution is the same as the solution in equilibrium with the rock.

The distance through which the surface charge is operative, the thickness of the double layer, is determined essentially by the concentration and kind of ions in the solution in equilibrium with the surface. The number and distribution of the ions in the double layer are dependent upon the type and concentration of the ions in the equilibrium solution and upon the surface charge.

The distribution of the mobile ions in the double layer may be estimated if the surface potential, temperature, and type of ions are known. From a knowledge of the surface charge, the variation of potential with distance from a flat charged surface may be approximated by application of Poisson's equation.[9] The concentrations of mobile positive and negative ions at any point are related to the potential at that point by Boltzmann's equations

$$n_1 = ne^{\dfrac{-V\varepsilon\phi}{kT}} \qquad \cdots \cdots \cdots \cdots \quad (1)$$

$$n_2 = ne^{\dfrac{V\varepsilon\phi}{kT}} \qquad \cdots \cdots \cdots \cdots \quad (2)$$

where:

  n_1 is the concentration of mobile positive ions

  n_2 is the concentration of mobile negative ions

  n is the concentration of mobile positive or negative ions in the equilibrium solution far away from the charged surface

  k is Boltzmann's constant

  ε is the charge on an electron

  ϕ is the electrical potential at any point referred to the equilibrium solution

  V is the valence of the ions.

To provide an example, the concentrations of univalent positive and negative ions were calculated as a function of the distance from a charged surface for two different assumed values of surface potential. These were −25.6 and −76.8 milli-
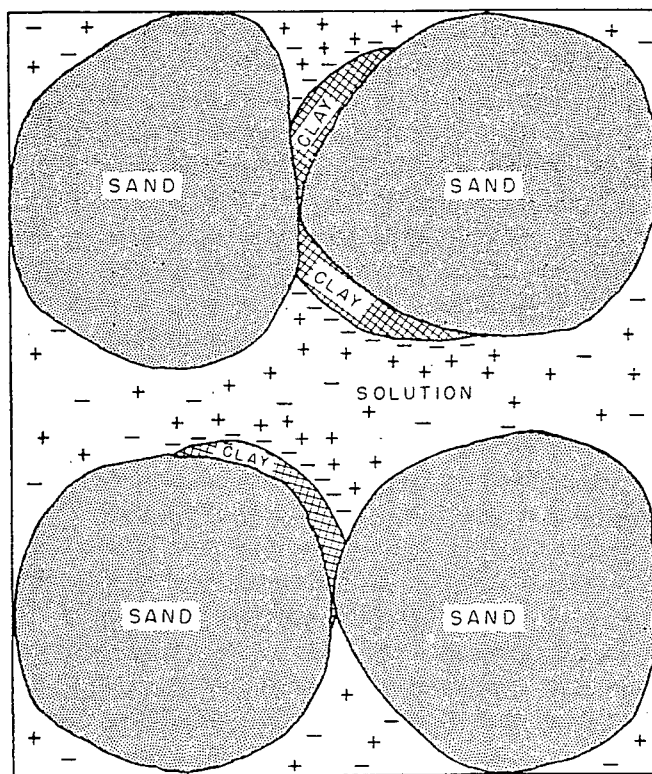

FIG. 1 — SCHEMATIC ILLUSTRATION OF CHARGE DISTRIBUTION IN SHALY SAND.

volts with respect to the equilibrium solution. In this calculation, the solution was assumed to be at 25°C. The results are shown graphically in Fig. 2. In these examples, the negative charges on the surface were assumed to be points so that the layer of negative charges was of zero thickness.

Several important points are illustrated by Fig. 2. First, the number of mobile positive ions per unit volume in the electrical double layer may be much greater than the mobile positive ions in the equilibrium solution. Second, although there are fewer mobile negative ions in the double layer than in the equilibrium solution, the difference in these two negative ion concentrations is not large. Third, the surface potential has a marked effect on the concentration of the positive ions in the double layer. It is this high positive ion concentration in the double layer which causes the increased or excess double-layer conductivity found in argillaceous reservoir material.

Excess Ions in the Double Layer

An examination of Fig. 2 also reveals that the number of mobile ions in the double layer in excess of those in the solution remote from the surface may be approximated by the difference in the mobile positive and negative ions. The equation from which the charge density of the double layer may be obtained is derived in Verwey and Overbeek's[11] work for a flat double layer. It is

$$\sigma = \sqrt{\frac{2n \, D \, kT}{\pi}} \; \sin h \; (V \, \varepsilon \, \phi_a / 2kT) \quad \dots \quad (3)$$

where:

σ is the surface charge per sq cm

D is the dielectric constant

ϕ_a is the surface potential in millivolts referred to the equilibrium solution.

The above equation was derived by assuming that the ions are point charges. Thus, this equation is applicable only to fairly dilute solutions.

If Equation (3) is divided by the valence of the ions and the charge, $V \, \varepsilon$, then the resultant equation

$$n_1 - n_2 = \sqrt{\frac{2n \, D \, kT}{\pi}} \; \frac{\sin h \; (V \, \varepsilon \, \phi_o / 2kT)}{V \, \varepsilon} \quad . \quad (4)$$

indicates the difference in the number of positive and negative ions in the double layer.

On this basis, the excess double-layer conductivity is a function of the product of $(n_1 - n_2)$ and the mobility of the positive ions in the double layer. The magnitude of $(n_1 - n_2)$ is dependent upon the concentration of the equilibrium solution, n, and the surface potential, ϕ_o. Although the concentration of the equilibrium solution may be determined experimentally, the manner in which the surface potential, referred to the equilibrium solution, varies with concentration is not amenable to experimental determination. However, McCardell *et al*[10] have shown that $(n_1 - n_2)$ appears to increase with concentration. This effect seems to be more pronounced in the more dilute than in the more concentrated solutions.

There is considerable uncertainty as to the mobility of the positive ion in the double layer. It should lessen, however, with an increase in concentration. This reduction in positive ion mobility is probably not as great as the increase in $(n_1 - n_2)$ at low concentrations. At high concentrations, it is probable that the mobility decreases faster than $(n_1 - n_2)$ increases. Thus, there is likely to be an increase in excess double-layer conductivity when the solution is dilute and a subsequent decrease when the solution becomes more concentrated.
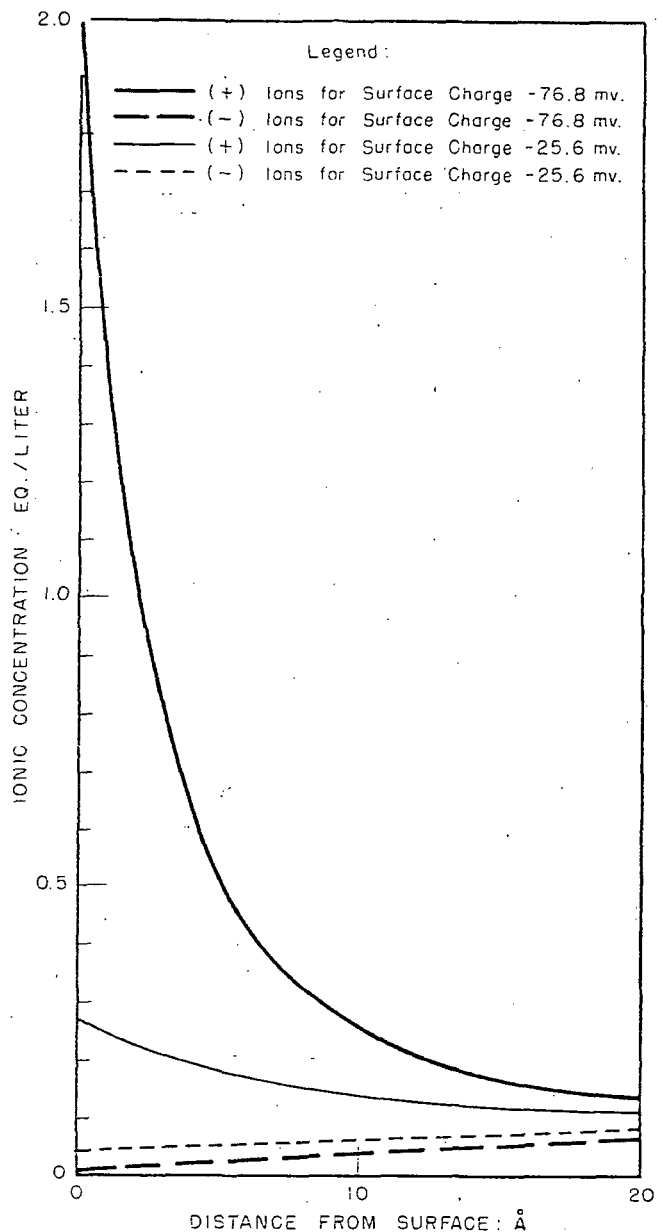

FIG. 2 — DISTRIBUTION OF IONS IN ELECTRICAL DOUBLE LAYER FOR 0.1 *N* EQUILIBRIUM SOLUTION.

The foregoing analysis shows that it is reasonable to expect the excess double-layer conductivity to vary with concentration. This immediately suggests that predictions based on the assumption of constant excess double-layer conductivity, irrespective of the nature and concentration of the solution in contact with the sample, will be in error.

EXPERIMENTAL CORROBORATION OF THEORY

Presence of Excess Ions in Double Layer

It has been stated that a higher concentration of positive ions exists in the solution opposite negatively charged surfaces than in the solution in equilibrium with the sample. This was verified experimentally in the following manner.

Table 1 — Apparent Resistivity Factor and Ion Displacement Data — Stevens Sandstone

Sodium Chloride Solution in Contact with Core	Apparent Resistivity Factor	Concentration of Solution in Core as Computed from Ions Displaced by NH_4NO_3	
		Na^+	Cl
Eq./Liter	Fa	Eq./Liter	Eq./Liter
1.0	19.7	....	....
0.0882	9.8	0.201	0.111
0.00882	4.0	0.103	0.020

A sample which showed abnormal conductivity was obtained from the Stevens sandstone, Elk Hills Field, California. This sample was saturated and flushed with $1N$ $NaCl$ solution. Then the sample was flushed with $0.0882N$ $NaCl$ solution until the resistivity of the core remained constant. After this, the solution in the pores was displaced by flowing at least 50 pore volumes of $1N$ NH_4 NO_3 through the core. When this quantity of ammonium nitrate had been flushed through the core, the chloride ion could not be detected in the effluent solution. The effluent solution then was analyzed for its sodium and chloride content. The results of this determination and a similar one in which $0.00882N$ $NaCl$ was used instead of the $0.0882N$ $NaCl$ are given in Table 1.

An examination of these data reveal that more sodium and chloride ions were displaced from the core than could be accounted for by the pore volume and concentrations of the solution in contact with the core. The excess ions can only be explained by an adsorption phenomenon and consequent concentration of ions in the double layer as discussed previously.

It is apparent that more sodium ions were displaced by the ammonium nitrate solution than were chloride ions. If displacement of sodium by ammonium and chloride by nitrate were quantitative, and if cation exchange in the clay lattice

did not take place, then it might be expected that equal excesses of sodium and chloride ions would be found in the ammonium nitrate effluent. That the excess sodium was greater than the excess chloride was probably due partly to cation exchange and partly to incomplete desorption of chloride, since the chloride ion is notoriously difficult to displace by nitrate.

Although it is not feasible to make quantitative use of these data shown in Table 1 to account for the variation in apparent resistivity factor, the data demonstrate qualitatively the existence of excess ions which comprise the double layer.

Effect of Ion Concentration on Excess Double-Layer Conductivity

To investigate the influence of solution concentration on excess double-layer conductivity, experiments were performed on a sample of shale approximately one-eighth in. in thickness and 1 in. in diameter from the Spraberry formation of West Texas. The Spraberry shale was particularly suitable for this investigation since it showed no tendency to disperse in dilute solutions.

The shale sample was saturated with $5N$ $NaCl$ solution and placed in contact with this solution until the resistivity of the sample remained constant over a period of 72 hours. When constant resistivity had been reached, the solution in contact with the sample was changed to one of lower salinity. The above procedure was repeated for $1N$, $0.1N$, and $0.01N$ $NaCl$ solutions. The results are given in Table 2.

Patnode and Wyllie and de Witte advocated the use of an equation of the form

$$\frac{1}{R_s} = A + \frac{B}{\rho} \qquad \ldots \ldots \ldots \quad (5)$$

where:

R_s is the resistivity of the rock saturated with solution
A and B are constants for a particular rock
ρ is the resistivity of the solution in equilibrium with the rock, to represent the conductivity of brine-saturated shaly materials. To test the validity of this equation, the data on the Spraberry shale given in Table 2 were plotted in the form $1/R_s$ against $1/\rho$. As may be observed in Fig. 3, these data do not give a straight line as Equation (5) indicates. This indicates that Equation (5) is not valid.

The influence of electrolyte concentration on excess double-layer conductivity may be examined by considering, first, a sample in which the double-layer contribution is negligible. The resistivity factor is

$$F = R_s/\rho = \text{Constant} \qquad \ldots \ldots \ldots \quad (6)$$
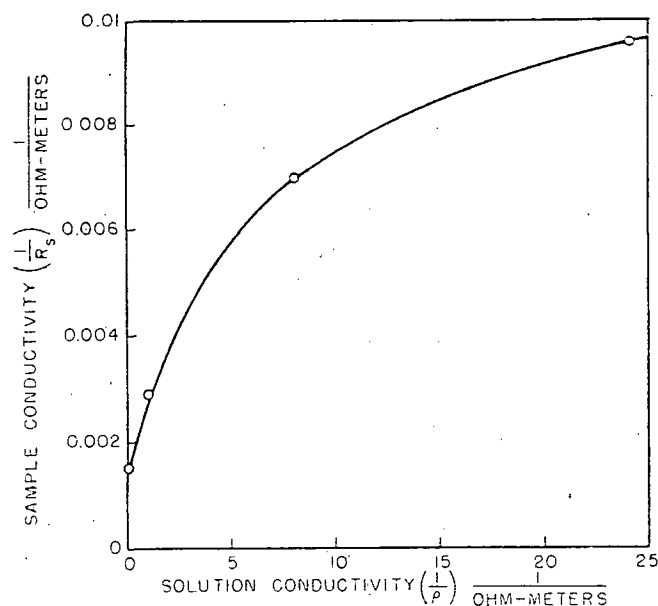
where F is the resistivity factor which is not influenced by the

FIG. 3 — RELATION OF $\left(\dfrac{1}{R_s}\right)$ TO $\left(\dfrac{1}{\rho}\right)$

Table 2 — Resistivity Data — Spraberry Shale

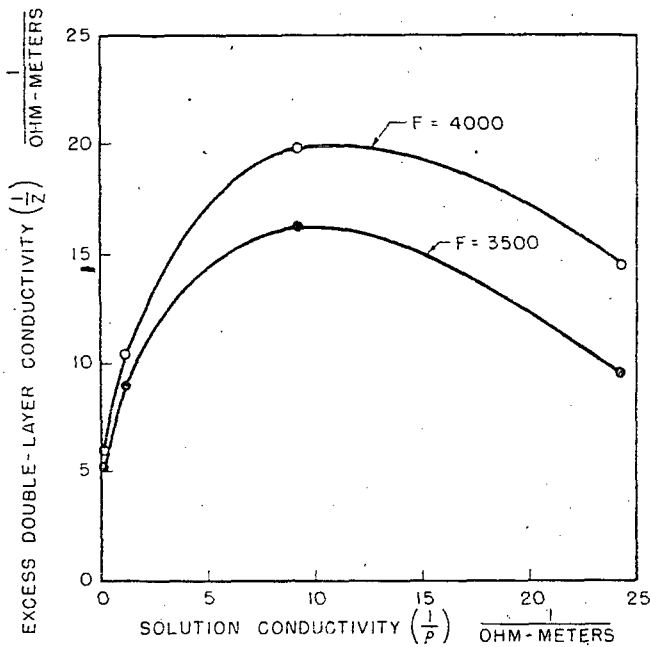| Sodium Chloride Solution in Contact with Sample Eq./Liter	Solution Resistivity (ρ) Ohmeters	Sample Resistivity (R_s) Ohmeters	Apparent Resistivity Factor Fa
5.0	0.0417	104	2,490
1.0	0.120	143	1,190
0.1	0.95	347	365
0.01	8.0	665	83

FIG. 4 — VARIATION OF EXCESS DOUBLE-LAYER CONDUCTIVITY WITH NaCl SOLUTION CONDUCTIVITY, SPRABERRY SHALE.

in another. The results are shown in Fig. 4. From this figure it is manifest that there is some uncertainty as to the actual magnitude of the double-layer conductivity because of uncertainty as to the value of F. This error is minimized as

$\dfrac{1}{\rho}$ decreases.

Whether F is assumed to be 3,500 or 4,000, the shapes of the curves remain the same. In each case there was an increase in double-layer conductivity as the solution concentration increased up to about 1.0 normal. When the solution in equilibrium with the sample was more concentrated than about 1.0 normal, there was a decrease of double-layer conductivity with an increase in solution conductivity. These results confirm those predicted from the theory discussed previously. The results of Berg[32] who worked with kaolin and salt solutions, and more recently Wyllie,[33] also corroborate the observed variation of double-layer conductivity with concentration of dilute solutions.

Effect of Ion Type on Double-Layer Conductivity

Since the double-layer conductivity of a sample is dependent mainly upon the valence and concentration of the ions, the surface potential, and the mobilities of the ions, it would be expected that the type of ions in equilibrium with the sample should influence the double-layer conductivity.

The effect of different solutions on the double-layer conductivity was investigated by use of the Spraberry shale sample discussed previously. The sample was allowed to come to equilibrium with a $5N$ $NaCl$ solution; then the sample was allowed to come to equilibrium in successive experiments, with solutions of $CaCl_2$ of various concentrations. The resistivity of the sample and the resistivity of the solution were measured
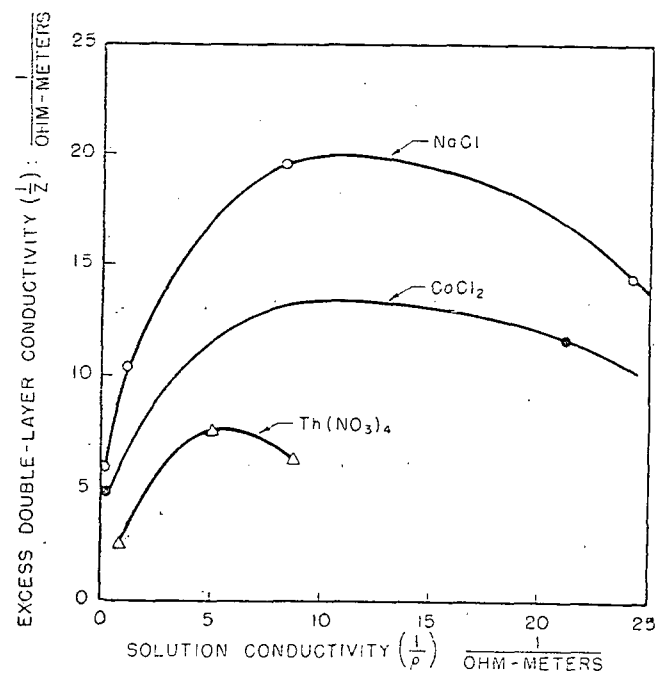
double-layer. The resistivity factor in this case is a measure of the effect of pore geometry upon the flow of an electric current through the sample. Even for very shaly sands or limestones, the apparent resistivity factor approaches a constant value as the concentration of the electrolyte used to saturate it increases. Since the actual pore configuration of a sample may be assumed to undergo no significant change as the concentration of electrolyte changes, even for a shaly sample R_s/F is an indication of the resistivity of the solution in the pores of the sample. Then, Equation (6) may be written

$$R_s/F = \rho_1 \quad \ldots \ldots \ldots \ldots \ldots \quad (6a)$$

in which ρ_1 is the resistivity of the interstitial solution, including the double layer.

The resistivity of this internal solution, ρ_1, may be related to that of the equilibrium solution by

$$\frac{1}{\rho_1} = \frac{1}{\rho} + \frac{1}{Z} \quad \ldots \ldots \ldots \ldots \quad (7)$$

where $\dfrac{1}{Z}$ is the excess double-layer conductivity.

Combination of the above equation with Equation (6a) gives

$$\frac{F}{R_s} = \frac{1}{\rho} + \frac{1}{Z} \quad \ldots \ldots \ldots \ldots \quad (8)$$

For the Spraberry shale sample which was investigated, the effect of double-layer conductivity could not be eliminated even at very high salinities. This is not the case for most shaly sands and limes. For purpose of illustration of excess double-layer conductivity with the Spraberry shale data, the resistivity factor, F, may be assumed to be in the neighborhood of 3,500 or 4,000.

The values of the double-layer conductivity were calculated by Equation (8) for an F of 3,500 in one case and of 4,000

FIG. 5 — EFFECT OF DIFFERENT IONS ON EXCESS DOUBLE-LAYER CONDUCTIVITY, SPRABERRY SHALE. $F = 4,000$.

in each case. Determinations were also made by the same procedure using $Th(NO_3)_4$ as an electrolyte.

The results of this investigation are shown in Fig. 5. From these results it may be observed that the type of ion as well as the number of ions affect the excess double-layer conductivity.

Natural shale, such as the Spraberry shale investigated, is not the only porous material which is sensitive to type of ion and resistivity of the solution in contact with the material. Sollner and Gregor[14,15] have reported results of resistivity measurements on permselective collodion membranes. The results of their investigations indicate that the resistivities of these materials are even more influenced by ion type and concentration than was the Spraberry shale.

CONCLUSIONS

1. The abnormal conductivity of shaly sands and limes containing an electrolyte is a consequence of adsorption on the clay surface and a resultant concentration of ions adjacent to the surface.

2. The magnitude of the abnormal or excess double-layer conductivity varies with the concentration of the electrolyte.

3. The excess double-layer conductivity is dependent upon the particular ions in the electrolyte, as well as upon their concentration.

ACKNOWLEDGMENT

The writers acknowledge their indebtedness to M. Williams of Humble Oil and Refining Co., under whose supervision this work was performed, for his helpful suggestions in the planning and preparation of the paper.

REFERENCES

1. Sundberg, K.: "Effect of Impregnating Waters on Electrical Conductivity of Soils and Rocks," *Trans.* AIME, Geophysical Prospecting, (1932) 367.

2. Winsauer, W. O., Shearin, H. M., Masson, P. H., and Williams, M.: "Resistivity of Brine-Saturated Sands in Relation to Pore Geometry," *Bull.* AAPG, (1952) **36**, 253.

3. Patnode, H. W., and Wyllie, M. R. J.: "The Presence of Conductive Solids in Reservoir Rock as a Factor in Electric Log Interpretation," *Trans.* AIME, (1950) **189**, 47.

4. de Witte, L.: "Relations Between Resistivities and Fluid Contents of Porous Rock," *Oil and Gas Jour.*, (Aug. 24, 1950) **49**, 120.

5. Tixier, M. P.: Personal Communication. 1952.

6. Helmholtz, H.: "Studien Uber Electrische Grenzschichten," *Wied. Ann.*, (1879) **7**, 337.

7. Stern, O.: "Zur Theorian Der Elektrolytischen Doppelschischt," *Z. Electro-chem.*, (1924) **30**, 508.

8. Gouy, G.: "Sur La Fonction Electrocapillaire," *Ann. d. Phys.*, (1917) (9) **7**, 129.

9. Verwey, E. J. W., and Overbeek, J. T. G.: *Theory of the Stability of Lyophobic Colloids*, Elsevier, New York, (1948).

10. McCardell, W. M., Winsauer, W. O., and Williams, M.: "Origin of the Electric Potential Observed in Wells," *Trans.* AIME, (1953) **198**, 41.

11. Verwey, E. J. W., and Overbeek, J. T. G.: *Theory of the Stability of Lyophobic Colloids*, Elsevier, New York, (1948), 32.

12. Berg, J. W., Jr.: "Conductivity Study of Aqueous Kaolin *NaCl* Mixtures," *Producers Monthly*, (1952) (3) **16**, 36.

13. Wyllie, M. R. J.: "Clay Technology in Well Log Interpretation," presented at National Conference on Clays and Clay Technology, Berkeley, Calif., July, 1952.

14. Sollner, K., and Gregor, H. P.: "The Electrochemistry of Permselective Membranes," *J. Colloid Sci.*, (1951) **6**, 557.

15. Sollner, K., and Gregor, H. P.: "The Electro-chemistry of Permselective Protamine Collodion Membranes," *J. Colloid Sci.*, (1952) **7**, 37.   ★ ★ ★

EFFECT of CLAY and WATER SALINITY on ELECTROCHEMICAL BEHAVIOR of RESERVOIR ROCKS

H. J. HILL
J. D. MILBURN
MEMBERS AIME

SHELL OIL CO.
HOUSTON, TEX.

T. P. 4223

ABSTRACT

In quantitative interpretation of electrical logs the presence of clay minerals introduces an additional variable which further complicates an already complex problem. Although recognizing the difficulties introduced as a result of the heterogeneity of natural sediments and despite the present incomplete state of knowledge regarding electrochemical behavior of shales, disseminated clay minerals and concentrated electrolytes, it was felt that useful empirical correlations might be obtained from experimental investigation.

Six typical sandstone formations, having a wide variety of petrophysical properties, were selected for the study. Approximately 45 samples from each formation were selected to satisfactorily represent the range of pore size distribution within the particular formation. As a matter of general interest, four limestone formations were also included in the investigation.

Previously proposed equations relating to resistivity, SP and interrelationship of the two phenomena have, where possible, been tested with data obtained in this investigation. These equations do not satisfactorily describe experimental behavior of samples through all degrees of shaliness or throughout the range of brine solution resistivities normally encountered in logging practice.

An empirical equation has been developed which quantitatively relates formation resistivity factor to saturating solution resistivity, porosity, and "effective clay content." This relation is indicated to be uniformly applicable to clean or shaly reservoir rocks.

It is shown that both the SP and resistivity phenomena of shaly samples are related to the sample cation exchange capacity per unit pore volume. The independent chemical determination of this parameter is thus a means of determining the "effective clay content" of samples.

Some implications regarding theory and electric log interpretation of shaly sands are discussed.

INTRODUCTION

The use of electrical resistivity logs as a means for estimating formation porosity is based upon the original work of Archie[1]. It was shown by empirical methods that the resistivity of a rock, when 100 per cent saturated with brine solution, could be related to rock porosity through the equation,

$$F = R_o/R_w = f^{-m} \qquad (1)$$

where F, the formation resistivity factor, is defined as the ratio of the resistivity of the 100 per cent water saturated rock, R_o, to the saturating solution resistivity, R_w; f is the ratio of pore volume to bulk volume; and m is the slope of the average line when the data are plotted on log-log paper. This relation was established for relatively shale-free formations containing water having high salt concentrations, and under these conditions F may be considered constant for a given rock sample. Applications of Eq. 1 to interpretation of logs of shale-free formations has been quite successful when satisfactory formation water resistivity data could be obtained.

The most readily available means of estimating formation water resistivity is the self-potential log. Conventional methods of SP log interpretation involve correct-

[1]References given at end of paper.

ing the total potential for streaming potential contribution, then estimating R_w from an equation of the type originally proposed by the Schlumbergers and Leonardon[2]. The form most commonly used is,

$$E_c = K \log R_{mf}/R_w \quad . . . . . . (2)$$

where E_c is the electrochemical component of the SP, R_{mf} is the mud filtrate resistivity, and K is a constant for a given temperature. Again, this technique has been reasonably successful when applied to logs of formations containing very little clay mineral.

Interpretation of electrical logs of shaly and fresh water-bearing sands has, however, been difficult or impossible because of insufficient quantitative knowledge regarding the effect of clay minerals on the electrical properties of reservoir rocks. Examples of the complications which may be encountered are: (1) clean water-bearing sands may, for the same formation water salinity, be more resistive than oil-bearing shaly sands; and (2) conventional interpretation of the SP curve for shaly formations results in erroneous salinities of interstitial waters, particularly when waters are relatively fresh.

That the oil industry has long recognized the importance of these problems is indicated by publication of numerous papers since 1949. Outstanding contributions are those of Wyllie and co-workers[3,5,6], Doll[4], de Witte[7], Winsauer and co-workers[8,9,10], and Poupon, Loy and Tixier[11]. Many of these contributions have been based on theoretical developments for some particular model.

Although improvement in interpretation has been made possible as a result of the many contributions, it is believed that quantitative interrelation of resistivity and SP phenomena and continued improvement in electrical log interpretation can best be accomplished by relatively large scale experimental studies of the electrochemical properties of reservoir rocks. It is the purpose of this paper to present the experimental relations obtained from one such investigation. It is believed that these relations can form a basis for quantitative interpretation of shaly formations.

LABORATORY INVESTIGATION

Six sandstone formations having different general properties were chosen for study. As a matter of general interest, four limestone formations were included. Table 1 gives general characteristics of the formations included in the investigation and it should be noted that these vary from clean sandstone and limestone to very shaly sandstone. A sufficiently large number of samples was used in the experimental program to cover each formation's characteristic range of porosity, permeability, grain size and degree of shaliness.

Three general types of data — resistivity, electrochemical potential, and "effective clay content" — were obtained from the selected samples. The general flow diagram of the experimental program is given in Table 2.

METHODS AND APPARATUS

RESISTIVITY

When the samples had been flushed with the appropriate solution, resistivities were determined in the cell shown schematically in Fig. 1. Cell electrodes are platinized platinum as found in conventional conductivity cells. Contact between solution in the rock pores and electrodes was achieved by means of the solution with which the cores had been flushed and in which they had been soaking. Bulk solution resistivity was obtained by use of a conventional conductivity cell. All resistance measurements were made with a commercial Leeds and Northup 60-cycle wheatstone bridge and galvanometer. Laboratory temperature was controlled to 77° F, ±3°.

After the initial determination of resistivities for a particular group of samples, the samples were sealed in containers under the salt solution with which they had been saturated and were allowed to soak an additional period of time. Resistivities were again determined and the process repeated until successive determinations indicated no further change of resistivities with time of soaking. The time required for obtaining constant resistivities varied from a few weeks to several months, depending on characteristics of the samples and salinity of the saturating solution.

ELECTROCHEMICAL POTENTIAL

Fig. 2 is a simplified flow system for one of the cells used for measuring electrochemical potentials. Since the concentrated solution in this cell was always in the bottom portion, it was usually possible to maintain a fairly

TABLE 1 — DESCRIPTION AND PETROPHYSICAL CHARACTERISTICS OF ROCKS INVESTIGATED

Type of Formation	Suite Number	Description	Age, Locality	No. of Samples	Characteristic Range				
					Perm. (md)	Porosity (%)	$F_{.01} = f^{-m}$ "m"	$F_{.01} = af^{-m}$ "a"	"m"
Clean Sandstones	1	Clean, medium to fine grained friable quartz sand. Major cement material present is calcite and quartz.	Miocene Weeks Island, Louisiana	35	0.2-1500	11-26	1.76	0.78	1.92
	2	Clean, fine grained friable quartz sand. Somewhat argillaceous.	Cretaceous Paluxy sand, Quitman, Texas; and Mitchell Creek, Texas	50	0.1-1500	8-26	1.78	0.47	2.23
	3	Clean, fine to very fine grained consolidated quartz sand.	Ordovician Simpson sand, Marshall, Oklahoma	44	0.1-300	7-15	1.82	1.3	1.71
Shaly Sandstones	4	Micaceous, shaly, fine grained to silty hard quartz sand. Cementing material is chiefly quartz.	Eocene Lower Wilcox sand, Sheridan, Texas	72 (Two Groups)	0.1-100	9-22	1.96	1.8	1.64
	5	Highly calcareous, shaly, medium to fine grained arkosic sandstone. Cementing material is chiefly calcite.	Oligocene Frio sand, Seeligson, Texas	63 (Two Groups)	0.1-1500	7-26	1.98	1.7	1.65
Very Shaly Sandstones	6	Very shaly, very fine grained to silty, consolidated quartz sand.	Cretaceous, Taylor sand, Big Foot, Texas	36	0.1-15	7-31	2.15	1.7	1.80
Limestones[12] Type I/III A and III/I B and C	7	Medium grained fossiliferous, oolitic, limestone.	Cretaceous Pettit Limestone, Chapel Hill, Texas	13	0.1-80	7-19	2.02	2.3	1.64
Type III and III/I	8	Coarse to fine grained oolitic limestone.	Jurassic Smackover Limestone, Magnolia, Arkansas	42	0.3-2500	9-26	1.93	0.73	2.10
Type II A and B	9	Chalky siliceous limestone.	Devonian Crossett, Texas	58	0.1-15	7-30	1.96	1.2	1.88
Type III F/VF C/B I/III F/VF A	10	Fine to very fine grained fossiliferous limestone containing a small quantity of dolomite and some siliceous material.	Cretaceous Rodessa Limestone, Tennessee Colony, Texas	37	0.1-70	8-30	2.08	2.2	1.65
TOTAL				450	0.1-2500	7-30	1.93	1.40	1.78

$F_{.01} = af^{-m}$

"a"	"m"
0.78	1.92
0.47	2.23
1.3	1.71
1.8	1.64
1.7	1.65
1.7	1.90
2.3	1.64
0.73	2.10
1.2	1.88
2.2	1.65
1.40	1.78

TABLE 2 — GENERALIZED FLOW DIAGRAM

CORE SAMPLE

1-in. × ¾-in. cylindrical plug

Determine total porosity, permeability, mount in Lucite[21], saturate and flush with distilled water.

Dry, saturate with dilute salt solution and obtain equilibrium core resistivity (R_o).

Measure electrochemical potential (E_c) using equilibrium solution from R_o determination as one solution.

Flush with next higher concentration salt solution and obtain equilibrium resistivity.
Obtain E_c at new solution resistivity ratio.

Repeat previous step until several values are obtained.

Cation Exchange Capacity
(Selected samples only.)

---

sharp transition zone inside the core sample. Experience with this apparatus emphasized the necessity of carefully balancing the respective solution heads so that the point of equal head was near the center of the core sample. Solution flow was maintained through use of a Sign-mamotor pump. A sample was placed in the cell and a slow flow of solution started past the core faces. Solution heads were adjusted to equalize near the core center. Potentials were measured at time intervals until a constant reading was obtained. This value was taken as the equilibrium electrochemical potential.

Potential measurements were made with a Beckmann Ultrohmmeter, a vacuum tube DC millivoltmeter having a variable input resistance. In the usual experiments, 10^5 ohms was found satisfactory as an input resistance. The meter was calibrated against a Leeds and Northup type K-2 potentiometer and found to be accurate to within ±3 per cent.

CATION EXCHANGE CAPACITY

Measurement of cation exchange capacity of samples was carried out using the mounted core as an ion exchange column. Standardized ammonium acetate solution was flowed through the core and the effluent solution analyzed for ammonium ion. A slow flow of solution through the core was continued until the concentration of ammonium ion in the effluent solution and the input solution were equal. Total loss of ammonium ion to the sample was then calculated by mass balance and cation exchange capacity was calculated in milliequivalents per cubic centimeter of pore volume.
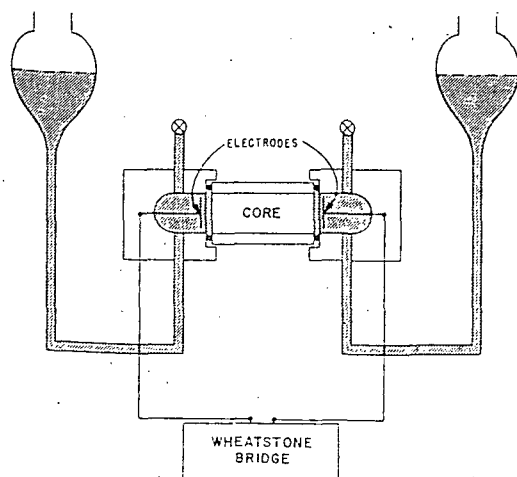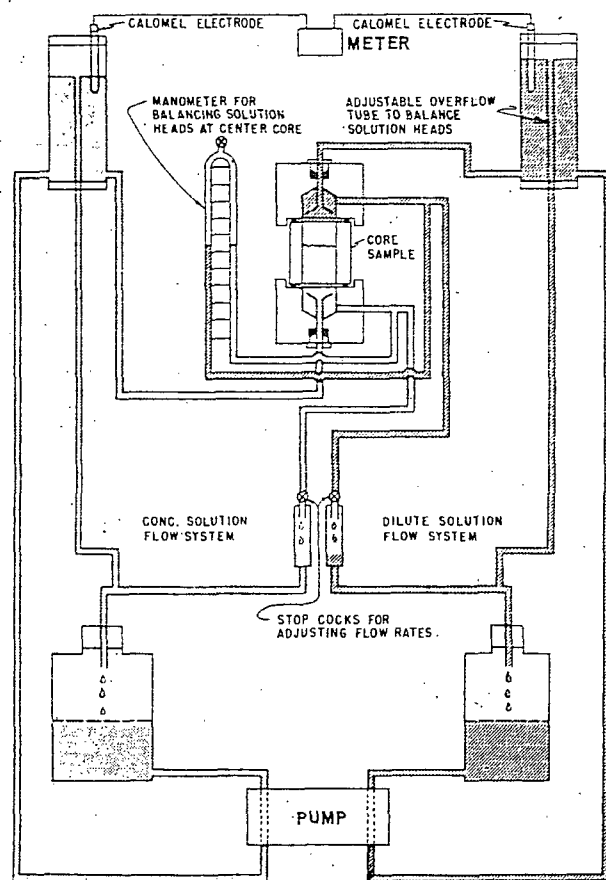

FIG. 1 — CORE RESISTIVITY CELL.

FIG. 2 — ELECTROCHEMICAL POTENTIAL SYSTEM.

DISCUSSION OF DATA

RESISTIVITY DATA

Core Resistivity vs Resistivity of Saturating Solution: Variation of core resistivity, R_o, with saturating solution resistivity, R_w, for 10 typical samples is shown in Figs. 3 and 4. Inspection of these data shows that for *each sample* a regular relationship exists between the two variables and thus the data should be amenable to mathematical expression.

It has been previously suggested by Patnode and Wyllie[2] and de Witte[7] that the resistivity of reservoir rocks can be expressed by an equation of the type:

$$1/R_o = C + 1/(F\,R_w) \quad . \quad . \quad . \quad . \quad (3)$$

where C is a constant related to the clay mineral of the formation and R_o, F, and R_w have their usual significance.

If Eq. 3 is multiplied by R_w and rewritten as:

$$1/F_a = C\,R_w + 1/F \quad . \quad . \quad . \quad . \quad (4)$$

it is evident that a graph of the reciprocal of the apparent formation factor (F_a) vs R_w will be linear if Eq. 3 and 4 are valid. Fig. 5 is a graph of $1/F_a$ vs R_w for four of the samples shown in Figs. 3 and 4. As indicated by Wyllie[6] and Wyllie[5], et al, the predicted linear behavior resistivities encountered in logging practice. The data thus confirm the conclusion of Winsauer[3], et al, that the experimental effect of a given quantity and distribution of clay mineral is not constant but must be considered to be a function of the saturating solution resistivity.

Review of the data from this investigation revealed that a suitable equation could be written as:

$$R_o/R_r = A(R_w/R_r)^{1-b\,\log\,R_w/R_r} \quad . \quad . \quad . \quad (5)$$

where R_r is 1 ohm-cm and may be described as the resistivity of an arbitrarily chosen hypothetical reference solution. A is a constant, equal to R_o/R_r when R_w/R_r is
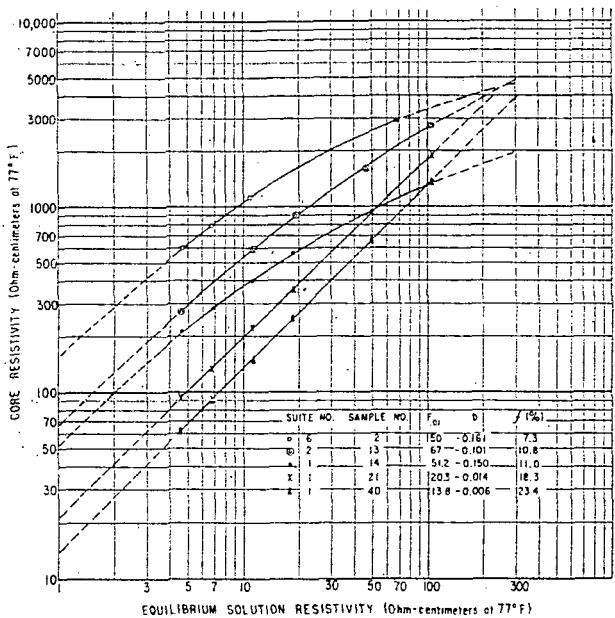
FIG. 3—CORE RESISTIVITY VS EQUILIBRIUM SOLUTION RESISTIVITY.

SUITE NO.	SAMPLE NO.	$F_{.01}$	b	f(%)
6	2	150	-0.181	7.3
10	13	67	-0.101	10.8
1	14	54.2	-0.150	11.0
X	21	203	-0.014	18.3
4	40	13.8	-0.006	23.4

unity, and b is a constant which, for formation samples, has a negative sign. Curves shown in Figs. 3 and 4 are calculated by Eq. 5, and it is apparent that the experimental data are accurately described. It should be emphasized that the equation describes experimental data only when a reference resistivity of 1 ohm-cm is used.

Eq. 5 can be divided by R_w/R_r to yield:

$$R_o/R_w = F_a = A(R_w/R_r)^{b \log R_w/R_r} \quad . \quad (6)$$

As is customary in logging literature, the experimental ratio, $\frac{R_o}{R_w}$, has been given the symbol F_a and will be referred to as the apparent formation resistivity factor. Eq. 6 reduces to:

$$R_o/R_w = F_a = A \quad . \quad . \quad . \quad . \quad . \quad (7)$$

when b is set equal to zero or when b has a finite value but the ratio (R_w/R_r) is unity. It is thus evident that clean sands and limestones may be expected to have b values of zero. Further, A may be interpreted as a formation resistivity factor at a hypothetical saturating solution resistivity of 1 ohm-cm.

As it is common logging practice to express resistivities in ohm-meters, Eq. 6 is re-written:

$$F_a = F_{.01}(R_w/0.01)^{b \log (R_w/0.01)} \quad . \quad . \quad . \quad (8)$$

or

$$F_a = F_{.01}(100 R_w)^{b \log (100 R_w)} \quad . \quad . \quad . \quad (9)$$

where A is replaced by $F_{.01}$, the formation resistivity factor extrapolated to a hypothetical saturating solution resistivity of 0.01 ohm-m (77° F). Fig. 6 presents the ratio of F_a to $F_{.01}$ for various typical values of b, as a function of saturating solution resistivity.

Eq. 9 has been statistically tested with data from 450 samples (2,154 individual resistivity factors) and has been found to describe the experimental data with a standard deviation of approximately ±1 per cent. Fig. 7 shows the distribution of per cent deviation. Since the 10 formations included in the investigation are of widely different characteristics, it seems reasonable to expect Eq. 9 to be widely applicable. It should be emphasized that the validity of Eq. 9 is dependent on experimental data which were obtained using a range of solution resistivities varying from 0.045 ohm-m to approximately 2 ohm-m at 77° F. As this range includes the resistivi-

ties normally encountered in logging practice, it is readily apparent that the equation constitutes a firm basis for describing the variation of apparent formation resistivity factor with resistivity of saturating solution. Further, data presented by Perkins, et al[10], which can be satisfactorily described by the equation, indicate that the applicable range of solution resistivities can be extended to approximately 16 ohm-m. Eq. 5 predicts that core resistivities go through a maximum and thereafter decrease as R_w increases. As this behavior seems unlikely, it may be that the *maximum* solution resistivity for which the equation is applicable is,

$$R_w = R_r(10)^{-\frac{1}{2}b} \quad . \quad . \quad . \quad . \quad . \quad (10)$$

determined by setting the first derivative of Eq. 5 equal to zero and solving for R_w.

Relation of $F_{.01}$ to Porosity: The work of Archie[1,14] has emphasized the necessity of utilizing data from a large number of samples to establish formation resistivity factor-porosity relationships, for a given formation. It was also indicated that different values of m (Eq. 1) for different formations were to be expected. Fig. 8 presents $F_{.01} - f$ data for four typical formations included in this investigation. It is apparent that a usable relation exists between $F_{.01}$ and porosity. As it has been previously shown that $F_{.01}$ is equivalent to a formation resistivity factor extrapolated to a solution resistivity of 0.01 ohm-m at 77° F and as it is generally recognized that clay mineral resistivity effects are minimized by using low resistivity saturating solutions, it seems reasonable to interpret $F_{.01}$ as being principally dependent on pore geometry.

It has been suggested by Winsauer, et al[15], that Eq. 1 should best be written in the form:

$$F = a f^{-\overline{m}} \quad . \quad . \quad . \quad . \quad . \quad . \quad (11)$$

where a and $\overline{m}$ determined from their data have the values of 0.62 and −2.15 respectively. For comparison, the method of least mean squares has been used to determine values of a and $\overline{m}$ and values of m (Eq. 1: $a = 1$) for the formations included in this investigation. These constants are given in Table 1 and on Fig. 8. It is apparent that the best straight line log-log relation between $F_{.01}$ and porosity takes the form of Eq. 11. It should, however, be noted that not only does the value
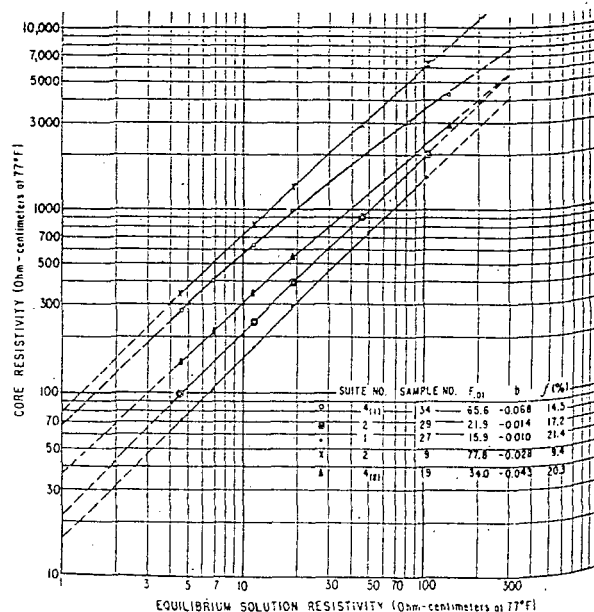

SUITE NO.	SAMPLE NO.	$F_{.01}$	b	f(%)
4(11)	34	65.6	-0.068	14.5
2	29	21.9	-0.014	17.2
1	27	15.9	-0.010	21.4
2		77.6	-0.028	9.4
4(8)	19	340	-0.043	20.3

FIG. 4—CORE RESISTIVITY VS EQUILIBRIUM SOLUTION RESISTIVITY.
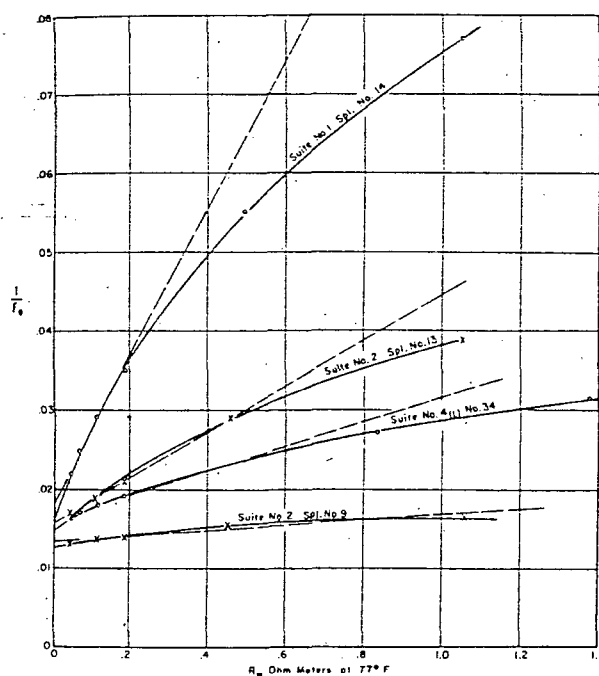
FIG. 5—TEST OF EQUATION $\dfrac{1}{F_a} = CR_w + \dfrac{1}{F}$.

of $\overline{m}$ vary for each formation, but values of a ranging from 0.47 to 1.8 were obtained.

As a matter of general interest Fig. 9 presents $F_{.01}$-porosity data for the 450 samples used in this investigation. Statistical determination of the best straight line representing all data yields:

$$F_{.01} = 1.4\,f^{-1.78} \quad . \quad . \quad . \quad . \quad (12)$$

If this line is restricted to $a = 1$, Eq. 12 becomes:

$$F_{.01} = f^{-1.93} \quad . \quad . \quad . \quad . \quad (13)$$

Relation of b to Cation Exchange Capacity:

Examination of the samples used in this investigation indicated that a broad qualitative relation existed between quantity of clay and the value of b. As this relation was only slightly improved by determining clay content using various techniques, measurement of cation exchange capacity was chosen as an independent chemical method of determining "effective clay content."

Fig. 10 presents data for some 34 samples and clearly illustrates that b is a function of cation exchange capacity per unit pore volume. Although the available data constitute only a fair statistical sample over the full range of b values and there is some indication of non-linearity, the relation can reasonably be represented by the equation:

$$b = -0.135\,\frac{CEC}{PV} - 0.0055 \quad . \quad . \quad . \quad (14)$$

where CEC/PV is expressed as milliequivalents exchange capacity per cubic centimeter of pore volume. This relation should be of considerable aid in log interpretation when representative samples of the formation of interest are available for cation exchange measurements.

Although it seems conceivable that the consolidated core technique might yield data which reflect clay distribution, some small amount of data obtained for crushed samples indicates such is not the case. It therefore appears that cation exchange capacity per unit pore volume is a measure of "effective clay content" and that knowledge of clay type, quantity, and distribution is not required for prediction of resistivity behavior of shaly samples.

ELECTROCHEMICAL POTENTIAL DATA

Typical data for 10 sandstones and two shale samples are presented in Fig. 11. These data were obtained using a reference solution having a constant resistivity of 0.045 ohm-m at 77° F and are plotted as electrochemical potential vs resistivity of the second solution. For comparison, potentials calculated from the equation:

$$E = 59.1\,\log\frac{a_{\pm 2}}{a_{\pm 1}} \quad . \quad . \quad . \quad . \quad (15)$$

where $a_{\pm 1}$ and $a_{\pm 2}$ are the mean ionic activities of the two solutions, and *experimental* liquid-liquid junction potentials are also presented.

It is immediately apparent that Eq. 15 ("Nernst" potential or "perfect membrane" potential equation) does not describe the experimental behavior of shale samples throughout the solution resistivity range. For resistivities above about 0.30 ohm-m, Eq. 15 becomes approximately parallel with experimental data and through this part of the resistivity range the equation will satisfactorily describe the data. Practically, the failure of Eq. 15 to describe experimental behavior may be of little importance insofar as log interpretation is concerned since it is shown by experimental data for shale No. 1 that the equation:

$$E = 55\,\log R_{w_1}/R_{w_2} \quad . \quad . \quad . \quad . \quad (16)$$

is satisfactory throughout the solution resistivity range normally encountered in logging. In view of the recognized assumptions involved in theoretical derivations of Eq. 15, it is believed that experimental data on carefully selected shale samples form a more positive basis for SP interpretation.

Reference to the data for formation samples reveals that a more complex relation involving "effective clay content" exists between electrochemical potential and solution resistivities for these samples. The data are in qualitative accord with current membrane potential theory but cannot be expressed quantitatively by the various theoretical equations thus far proposed. Again, it seems probable that assumptions made in deriving theoretical equations may account for departure of these equations from experimental behavior.

Because of the obvious relation between potential behavior and b and the difficulty of expressing this relation in a useful mathematical form, electrochemical potential data were grouped by b value ranges, and all data within a particular group and for a particular "second" solution resistivity were averaged to obtain Fig. 12, a graph of electrochemical potential vs log of $-b$ for
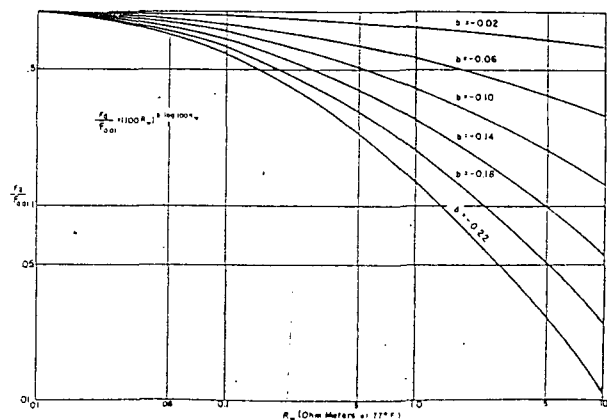

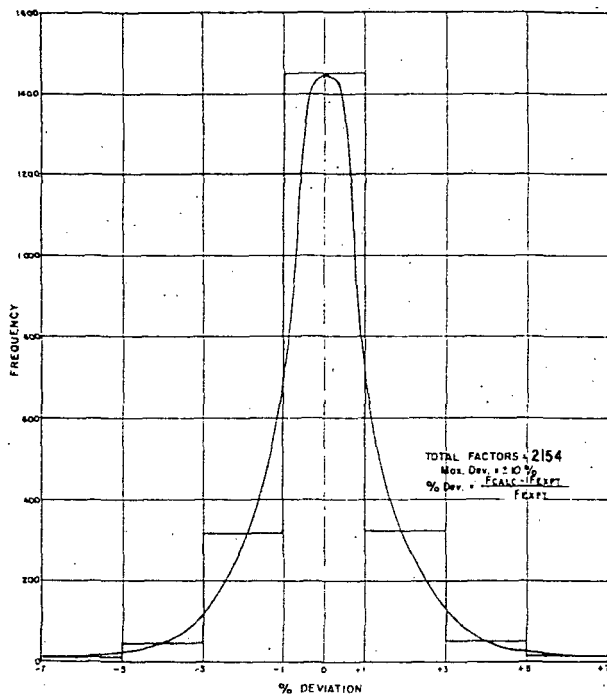FIG. 6—RATIO OF EXPERIMENTAL TO EXTRAPOLATED FACTOR FOR VARIOUS VALUES OF b.

FIG. 7—DISTRIBUTION OF PER CENT DEVIATION.

FIG. 9—FORMATION RESISTIVITY FACTOR $(F_{0.1})$ VS TOTAL POROSITY.

various solution resistivities. Values obtained from this graph were then used to construct Fig. 13, a graph of sample potential vs second solution resistivity for samples of various "effective clay content." This figure also shows the relation for the theoretically perfect membrane and the two shales.

From the resistivities of two sodium chloride solutions, the electrochemical potential of a sample of known b value can be obtained with Fig. 13. Also, if the relation for the shale is known, the total electrochemical potential of a shale and sand in series can be obtained. Assume that the resistivities of the two solutions are 0.08 and 1.0 ohm-m, the sample has a b value of -0.06, and the shale is identical to shale No. 1. The difference in potential between the intersections of the curve for a b value of -0.06 and the ordinates of 0.08 and 1.0 is 12 mv, the electrochemical potential of the sand. The electrochemical potential of the shale, found in the same way, is 63 mv. Because these two potentials oppose each other in the SP circuit, the difference between them, 51 mv, is the potential of the system. The sign of the potential depends on which solution is considered the reference solution.

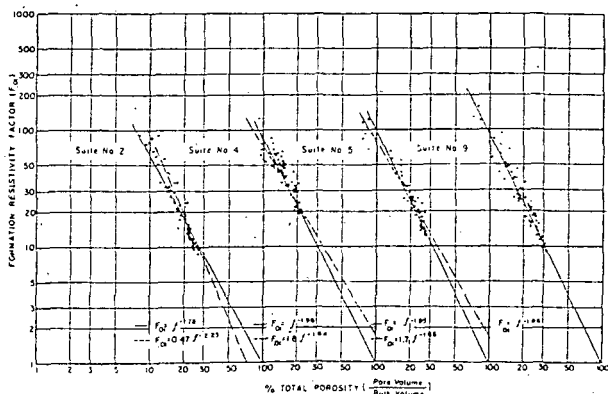Inspection of Fig. 13 reveals that as the resistivity of

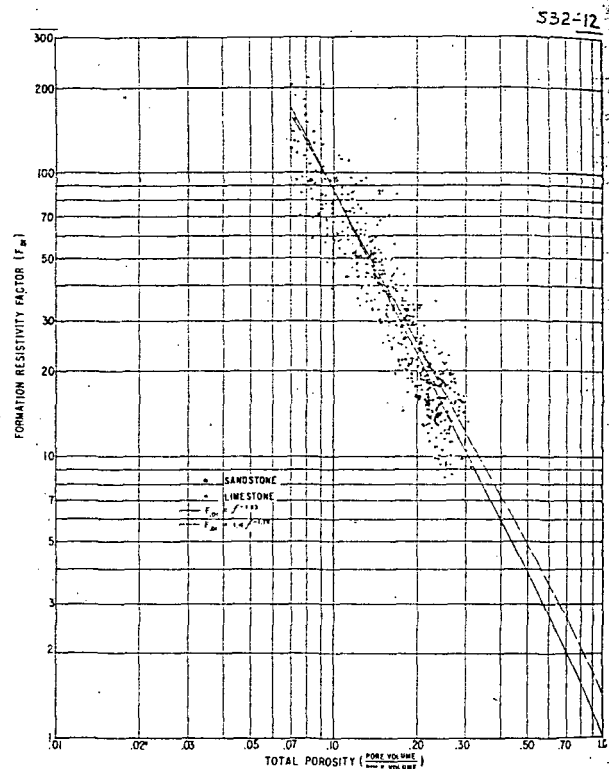FIG. 8—FORMATION RESISTIVITY FACTOR $(F_{0.1})$ VS TOTAL POROSITY.

the second solution increases, the slope of the lines increases and approaches the slope of the curve for the shales. This is especially true for samples having higher b values. Therefore, shaly sand potential behavior may approach shale potential behavior for high solution resistivities. Over the range of solution resistivities where the slope of the sample potential curve is nearly parallel to the shale potential curve, the potentials would be almost equal and would, therefore, cancel each other even though the resistivities of the two solutions differed by a factor of 10 or more.

Wyllie[5] et al, Perkins[10] et al, and Poupon[11] et al, have suggested equations for interpretation of logs from shaly sands. Each of these authors concludes that an equation of the form

$$PSP = K \log (R_{xo}/R_o) \quad . \quad . \quad . \quad . \quad (17)$$

can be satisfactorily used to describe the electrochemical potential behavior of shaly sands which are completely saturated with salt solutions.

The electrochemical potential data presented in Fig. 11 and resistivity data presented in Figs. 3 and 4 have been used to calculate values of E_c and R_{xo}/R_o for four samples of widely different degrees of shaliness. Fig. 14 shows these data for the assumption of shale behavior as represented by data for Shale No. 1. Fig. 15 presents similar data for shale behavior predicted from Eq. 15. In both cases, it is assumed that the invading filtrate has a resistivity of 1 ohm-m at 77°F and formation water resisitivities are varied from 0.045 to 2 ohm-m. Inspection of the figures indicates conclusively that the linear behavior predicted by Eq. 17 is not realized experimentally.

APPLICATION TO LOG INTERPRETATION

Methods of application to field problems will vary widely and will, of necessity, be controlled by the amount of data available relative to the total number of
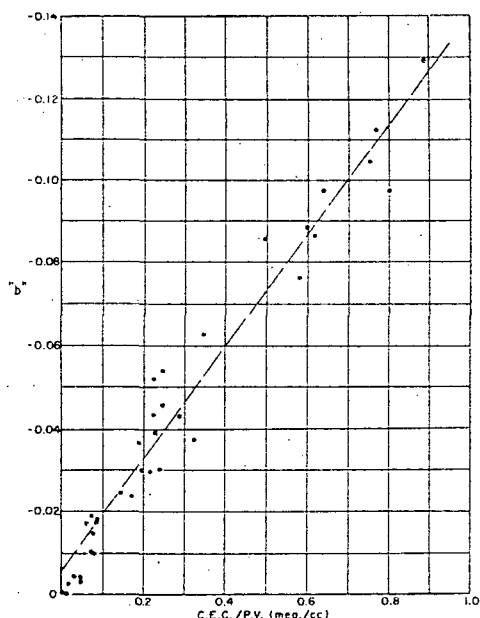
FIG. 10 — b FROM $F_a = F_{.01}(100 R_w)^{b \log R_w}$ VS
CATION EXCHANGE CAPACITY.

variables. If samples are available a distinct advantage is realized from the fact that a definite clay parameter can be determined by any of three different methods. The parameter b for the sand can be obtained either by direct measurement of the cation exchange capacity, the electrochemical potential, or formation resistivity factors with a number of solutions of different concentrations.

After determining b it is then possible to estimate resistivity of formation water from charts similar to Fig. 13. Using R_t, b and R_w, $F_{.01}$ can be calculated and porosity estimated from the appropriate $F_{.01}$-porosity relation.

In the event R_w is known but samples are not available for estimating b, Fig. 13 can be used to estimate b from the electrochemical component of the SP. Eq. 9 can then be used to calculate a value of $F_{.01}$ from which an approximation of porosity may be obtained. In addition, when R_w is known and both R_0 and R_t are available from appropriate logs, both $F_{.01}$ and b can be calculated from Eq. 9.

Since the relations and application techniques outlined are valid only for 100 per cent water saturated formations, the necessary parameters for solution of Eq. 9 and for use in the interpretation charts cannot be obtained directly from electrical logs of oil-bearing formations. However, when the formation factor at any salinity, the average b value, and the connate water salinity can be obtained from samples or other sources, the equation permits accurate determination of resistivity of shaly formations when 100 per cent saturated with water. As this is the basis for determining the presence of hydrocarbons by the electrical log, it represents a fundamental advance in log interpretation.

Experimental study of the effect of clay and saturating solution resistivity on the resistivity ratio-connate water saturation relation, together with experimental data regarding the effect of oil saturation on the electrochemical component of the SP are required before full benefit can be derived from the established relations. It is of interest, however, to recall that b appears to be directly related to cation exchange capacity per unit pore volume. Since both conductivity and potential phenomena occur in the water phase, it is implicit that
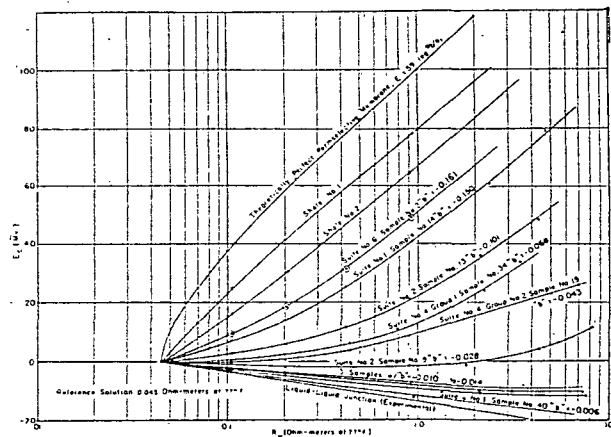

FIG. 11 — ELECTROCHEMICAL POTENTIAL OF SELECTED
FORMATION SAMPLES, E_c VS SOLUTION RESISTIVITY.

a decrease in volume of pore space filled with water should, in effect, increase the applicable b value by an amount related to the decrease in water saturation. Thus, the SP would be decreased opposite oil-bearing formations by an amount related to the "effective clay content" and the connate water saturation. When considering the effect of oil on the resistivity relation, it is apparent that two factors are involved. The pore geometry factor, represented as $F_{.01}$ for 100 per cent water-bearing formations, can be expected to increase as oil saturation increases since water-filled pore geometry will become increasingly complicated. On the other hand, the *reduction* in resistivity due to "effective clay content" can also be expected to increase with increasing oil saturation.

CONCLUSIONS

Experimental relations for solving the basic problem of fresh water bearing argillaceous rocks have been presented. These relations are believed to be of general applicability because of the large number of samples, wide variety of sedimentary rock used for samples, and the wide range of solution salinities used in the experi-
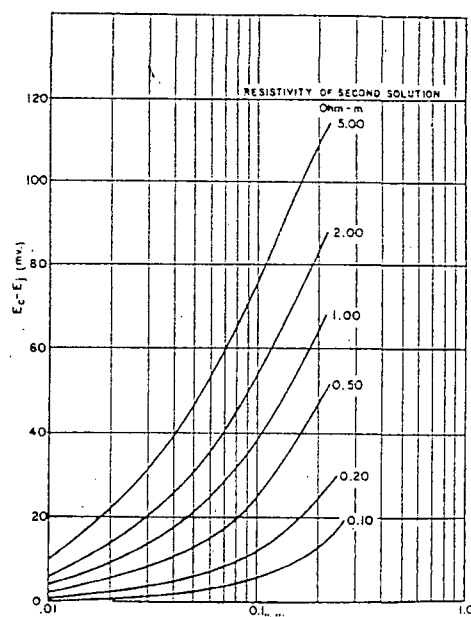

FIG. 12 — AVERAGE ELECTROCHEMICAL POTENTIAL
MINUS JUNCTION POTENTIAL VS AVERAGE b FROM
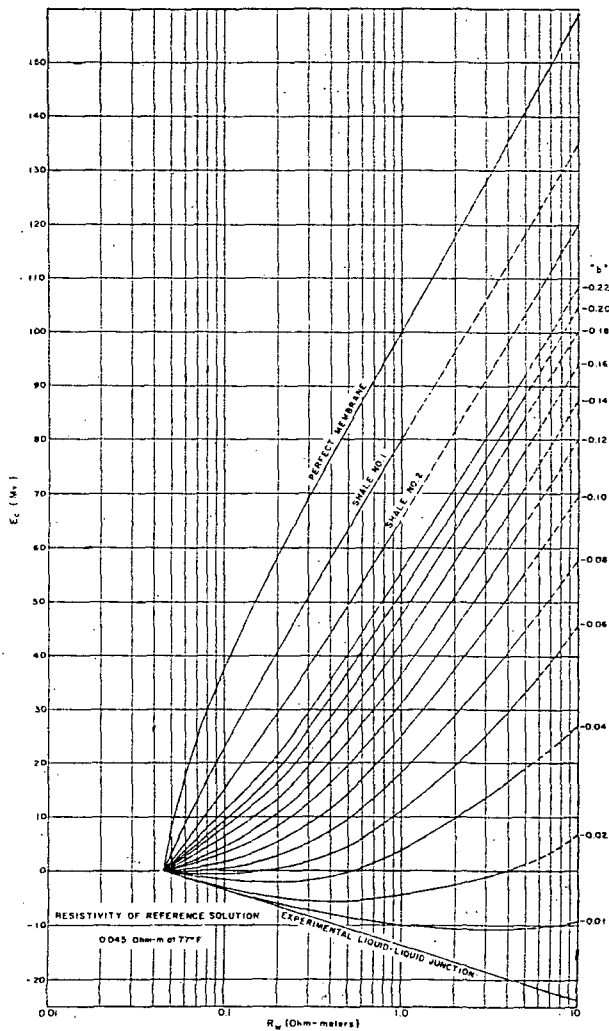$F_a = F_{.01} (100 R_w)^{b \log 100 R_w}$.

FIG. 13—AVERAGE ELECTROCHEMICAL POTENTIAL VS RESISTIVITY OF SECOND SOLUTION.

mental program. The relations are confined to water-saturated formations, thus limiting their application in quantitative log interpretation. In spite of this limitation they represent an experimental basis for determining the resistivity of shaly sands from the resistivity of formation water and measurable characteristics of the formation. Further, it has been shown that the effect of clay
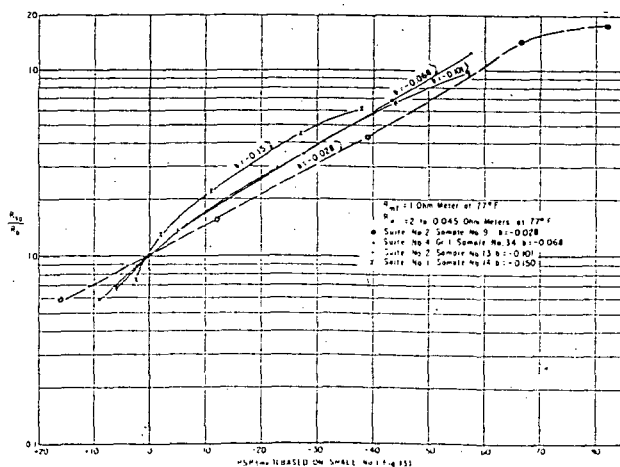

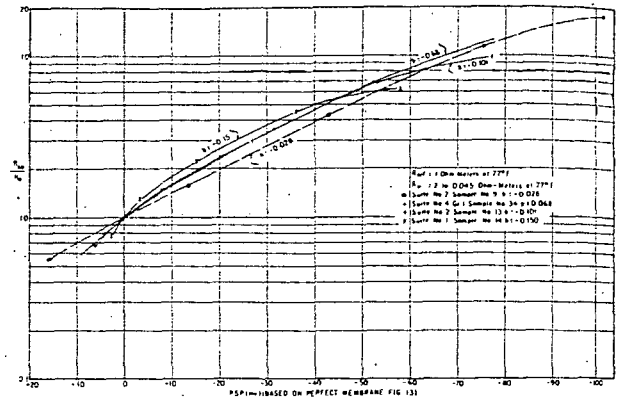FIG. 14—TEST OF EQUATION PSP $= K \log \dfrac{R_{xo}}{R_o}$.

FIG. 15—TEST OF EQUATION PSP $= K \log \dfrac{R_{xo}}{R_o}$.

mineral on the electrochemical properties of reservoir rocks is definitely related to the cation exchange capacity per unit pore volume. Therefore, the measurement of this parameter is an independent chemical method of determining quantitatively the "effective clay content."

It is implicit in the relations that the effect of clay on electrochemical properties of reservoir rocks increases as the ratio of clay to water content increases. It is probable, therefore, that hydrocarbon saturation increases the effect of clay on both resistivity and SP. The investigation thus constitutes the basis for further research concerning shaly sands.

ACKNOWLEDGMENT

REFERENCES

1. Archie, G. E.: *Trans.* AIME (1942), **146**, 54.
2. Schlumberger, C. and M., and Leonardon, E. G.: *Trans.* AIME (1934), **110**, 237.
3. Patnode, H. W., and Wyllie, M. R. J.: *Trans.* AIME (1950), **189**, 47.
4. Doll, H. G.: *Trans.* AIME (1950), **189**, 205.
5. Wyllie, M. R. J., and Southwick, P. F.: *Trans.* AIME (1954), **201**, 43.
6. Wyllie, M. R. J.: Report No. 24, Geology Division Gulf Research and Development Co., National Conference on Clay and Clay Technology, Berkeley, Calif. (1952).
7. de Witte, L.: *Oil and Gas Jour.* (1950), **49**, No. 16, 120.
8. Winsauer, W. O., and McCardell, W. M.: *Trans.* AIME (1953), **198**, 129.
9. McCardell, W. M., Winsauer, W. O., and Williams, M.: *Trans.* AIME (1953), **198**, 41.
10. Perkins, F. M., Jr., Brannon, H. R., Jr., and Winsauer, W. O.: *Trans.* AIME (1954), **201**, 176.
11. Poupon, A. Loy, M. E., and Tixier, M. P.: *Trans.* AIME (1954), **201**, 138.
12. Archie, G. E.: *Bull.* AAPG (1952), **36**, No. 2, 278.
13. Schowalter, W. E.: *Jour. Pet. Tech.* (1950), **11**, No. 12, 8.
14. Archie, G. E.: *Bull.* AAPG (1947), **31**, No. 2.
15. Winsauer, W. O., Shearin, A. M., Jr., Masson, P. H., and Williams, M.: *Bull.* AAPG (1952), **36**, No. 2, 253. ★★★

EXTENDED VERSION OF GOUY-CHAPMAN ELECTROSTATIC THEORY AS APPLIED TO THE EXCHANGE BEHAVIOR OF CLAY IN NATURAL WATERS

C. NEAL AND D. M. COOPER

Institute of Hydrology, Maclean Building, Crowmarsh Gifford
Wallingford, Oxon OX10 8BB, United Kingdom

Abstract—A model based on Gouy-Chapman theory, describing the ion exchange behavior of clays in mixed electrolyte solutions is presented. Computed ionic distributions, taking into account variations in relative permittivity, ion activity, and closeness of approach of ions to clay surfaces, are compared with experimental data for smectite and kaolinite in contact with river and saline waters. To obtain reasonable agreement between theoretical prediction and observation the most important extension of Gouy-Chapman theory involves the introduction of a closeness of approach term. Furthermore, the aggregated nature of smectites plays an important part in controlling its exchange properties, whereas a fixed-charge model provides a poor description for the ion exchange properties of kaolinite.

Key Words—Electrolyte, Gouy-Chapman theory, Ion exchange, Kaolinite, Smectite, Water.

INTRODUCTION

Electrostatic theory can be used to describe element exchange behavior for many clay-water mixtures of environmental and theoretical importance, including soil salinization, pollutant transport through soil and groundwaters, major element budgets in the hydrosphere, soil and sediment stabilities, the structure of water and clay surfaces, and ion hydration. Here, the value of electrostatic theory is that it gives without prior determination of selectivity coefficients, the distribution of cations, anions, and neutral molecules in solution near clay surfaces on a molecular scale. This information can be compared with experimental evidence to provide insight into the molecular structure of clay surfaces, the hydration state of ions, and the structure of water in the intense electric fields near clay surfaces. Electrostatic theory also eliminates the need for arbitrary and limiting definitions of ion-exchange parameters and the experimentally unjustifiable simplification to monolayer adsorption of commonly used mechanistic models (Bolt, 1967; Sposito, 1981; Neal et al., 1982; Thomas et al., 1982; Truesdale et al., 1982). Furthermore, electrostatic theory is complementary to, but distinct from, the well-developed, mass-action type, thermodynamic view of clay-electrolyte systems (cf. Bolt, 1967, 1979; Sposito, 1981a, 1981b); the latter is much simpler to evaluate than the former but can only be related on macroscopic scale in a non-mechanistic fashion to ion exchange (Neal et al., 1982; Sposito, 1981).

Despite much progress (e.g., Bolt, 1955a, 1979; Bolt and Warkentin, 1958; Bolt and de Haan, 1965, 1979; Edwards and Quirk, 1962; Helmy et al., 1980; Schofield, 1949), electrostatic models are not yet either sufficiently well developed or tested to describe clay-electrolyte solutions. For example, homovalent selectivity coefficients are not close to unity for many clays in a wide variety of mixed electrolyte solutions (Bruggenwert and Kamphorst, 1979) in contradiction to Gouy-Chapman theory where ions are described as point charges (Joshi and Parsons, 1961; Bolt, 1979; Sposito, 1981). In addition, the Gouy-Chapman model does not allow for changes in the water structure near clay surfaces which can significantly affect the distribution both of neutral and charged molecules (Davis and Worrall, 1971; Bolt, 1979). Consequently the predictive capacity of the Gouy-Chapman model can be improved.

In an attempt to overcome some weaknesses of existing theory, an extended version of the Gouy-Chapman model is developed here. Predictions from this model are compared with experimental data for smectite and kaolinite in contact with mixed river and marine waters. The extended Gouy-Chapman model incorporates terms describing variations in the activity and hydration of ions and in the relative permittivity of water (Bolt, 1955a, 1955b, 1979; Grahame, 1952; Sparnaay, 1958; Ravina and Gur, 1978); these terms allow for ion-ion and ion-surface interactions to improve the prediction given by the basic Gouy-Chapman model. Following closely Oldham's (1975) analysis for a simplified Gouy-Chapman model for ion exchangers in contact with estuarine and marine waters, we show that the experimental and analytical results are compatible, provided that the closeness of approach of ions to the clay surface is considered.

DEFINITIONS OF EXCHANGE PARAMETERS

Most of the variables which are of interest cannot be measured directly; the model predicts significant

367

changes in the concentration of ions and field strength within a region only a few tens of Ångströms from a charged surface, and these cannot be directly sampled. Consequently, an assessment of model performance can only be made indirectly by comparing experimentally determined "notional interfacial contents" (NIC) and computed G values as defined below.

For the laboratory studies the variables measured, NICs, are related to commonly used terms in the clay literature such as adsorbed and exchangeable cations (see Neal et al., 1982, for discussion of the usage of NICs). NIC variables are defined by the general equation.

$$NIC_{i(j)} = T_i - T_j{}^ic_j,$$

where $NIC_{i(j)}$ is the notional interfacial content of species i with respect to a reference species j, T_i is the total amount of any species i in the system (both in units of meq/kg clay) and ${}^ic_j$ is the concentration of i with respect to j in the bulk solution outside the influence of the clay charge (a dimensionless unit). For the laboratory study the reference species (j) chosen was water; the subscript j is omitted, without ambiguity, in the remaining text, thus $NIC_{i(H_2O)} \equiv NIC_i$. For the theoretical studies the quantities calculated (G) are similar to surface excesses defined by Bolt (1967) and are defined here by

$$G_i = \int (c_i - c_i{}^b) \, dx,$$

where c_i is the concentration of component i and x is the distance from the clay surface. As x tends to infinity $c_i \equiv c_i{}^b$, the bulk solution concentration of species i. The lower limit of integration is zero; when the upper limit is infinite, $G_i \equiv G_i{}^b$, the "overall ion excess."

An important feature of the experimental and theoretical results is that while the former refer to components related to water as a reference, the latter refer to molal concentrations. To make both sets of results comparable we have assumed the concentrations of water to be constant within the solution volume. Under this assumption the $G_i{}^b$ values can be regarded as theoretical values of the observed NIC_i.

CHEMICAL ANALYSIS

Materials and methods

Samples of kaolinite (English china clay) and smectite (Wyoming bentonite), supplied by BDH Chemicals (UK) Ltd., were purified to give homoionic Na forms with a particle size of <2 μm using the method described by Neal (1977). They were converted to their "river" and "saline" counterparts by repeatedly washing (~30 times) and storing the clays (~2 days/wash) with mixtures of filtered water from the River Thames and artificial seawater prepared using the recipe of Lyman and Fleming (1940).

The notional interfacial content of the clays was determined for the treated clays using a multiple salt leach based on the method described by Neal (1977). To minimize analytical error, excess pore solution was removed using a porous asbestos tile, and subsequent determinations were made on well-mixed samples of the damp clay remaining. Exposure of the clay to the atmosphere was minimized to ensure that evaporative effects would be insignificant.

The total equivalents of cations (Na, K, Mg, Ca) per unit weight of dry clay, T_i, were determined by treating an accurately weighed sample of damp clay (~0.2 and 0.5 g portions of smectite and kaolinite, respectively) six or more times, depending upon extraction efficiency, with 10-ml portions of a 60% alcohol solution containing 0.25 M CsCl and 0.75 M LiCl. For each treatment the clay was continuously suspended for ~2 hr in the extracting solution to maximize cation release. The major cation concentration of each solution was then determined by standard atomic absorption and emission spectroscopy (Slavin, 1968) and the T_i values calculated.

The water content T_{H_2O} was determined by drying weighed samples of damp clay at 60°C to constant weight and determining the weight loss (in accord with Thomas et al., 1983). Drying times were ~6 days. The amount of Cl (T_{Cl} — meq/kg of dry clay) was determined with the washing technique used for the cations except that the extraction solution contained no leaching salt. The concentration of Cl in each extract was determined using an automated colorimetric version of the method of Zall et al. (1956). Three washing steps were required to complete the extraction.

NIC values for Na, K, Mg, Ca, and Cl were subsequently determined for the saline and fresh-water clays by first determining the river and seawater molal end-member compositions and then calculating ${}^ic_{H_2O}$.

Experimental results

Except for chloride, the variations in NIC_i values with changing salinity are similar for both clays (Table 1). Considering first, cation variations, with increasing salinity, NIC_{Ca} decreases and NIC_{Na} and NIC_K increase. NIC_{Mg} increases up to a salinity of ~4‰ and then decreases slightly at higher salinities. For all cations the largest variation is in the 0 to 10‰ salinity range.

Cation NIC data for both clays are consistent with previous theoretical and experimental evidence for two reasons: (1) Because the river water contains mainly Ca in solution and the seawater contains relatively low Ca and high Na, Mg, and K concentrations, NIC_{Ca} should decrease with increasing salinity relative to NIC_{Na}, NIC_K, and NIC_{Mg}. Such a trend has been observed for several studies of fresh and saline clays (Sayles and Manglesdorf, 1977, 1979; Zaytseva, 1966); (2) Be-

Table 1. NIC$_i$ values for smectite and kaolinite in fresh and saline waters.

Salinity (‰)	Na	K	Mg	Ca	Cl	Total
			Smectite			
0.36	15	8	63	1039	0.0	1126
0.83	55	12	220	885	3.7	1169
1.30	72	15	275	521	1.5	1162
2.25	93	20	350	726	-2.5	1192
3.22	146	24	390	661	-9.7	1236
4.15	164	29	432	893	-19.3	1538
5.09	182	30	433	667	-19.1	1331
6.04	192	30	415	544	-20.0	1202
7.00	203	34	436	530	-27.3	1231
7.93	225	32	411	473	-35.2	1176
8.88	243	41	414	463	-38.8	1200
9.83	247	33	413	641	-42.3	1376
14.60	303	42	390	516	-63.4	1315
19.30	293	55	349	392	-82.9	1173
24.00	314	53	345	491	-85.6	1289
28.80	286	49	310	382	-116.1	1143
33.50	331	57	311	404	-130.2	1232
			Kaolinite			
0.36	0.0	2.1	7.3	49.3	2.8	55.9
0.83	4.6	3.2	14.6	46.4	1.9	66.9
1.30	6.5	3.0	15.8	45.0	1.7	68.6
2.25	10.8	4.3	24.2	48.1	-0.1	87.6
3.22	11.2	5.1	23.7	40.3	-1.2	81.5
4.15	15.0	7.9	24.8	39.1	-1.8	88.6
5.09	14.9	6.4	26.3	26.6	0.6	73.6
6.04	13.8	6.9	25.7	20.4	0.6	66.1
7.00	17.8	7.5	28.2	28.0	-1.3	88.3
7.93	21.5	8.3	26.1	21.8	1.5	76.1
8.88	17.7	7.4	24.7	16.4	0.6	67.0
9.83	19.4	7.0	23.8	9.6	0.5	59.3
14.6	24.5	9.5	24.5	15.3	5.8	68.0
24.0	22.3	9.4	21.5	7.9	4.3	56.8
28.8	38.6	11.0	27.4	20.1	17.9	79.1
33.5	30.0	10.0	23.7	6.1	12.8	56.9

Table 2. Bulk solution chemical concentrations.

	River water	Mixedwater		Artificial seawater
Salinity (%)	0.36	10	20	33.5
Ionic concentrations (mmole/liter)				
Na	1.72	136.0	276.0	464.0
K	0.087	2.89	5.78	9.7
Mg	0.215	15.3	31.0	52.3
Ca	2.60	4.75	6.98	10.0
Cl	1.75	157.0	318.0	535.0
HCO$_3$	3.70	3.32	2.93	2.4
SO$_4$	1.42	9.04	16.9	27.6
Ionic ratios				
Na/K	19.8	47.1	47.8	47.8
Na/Mg	8.0	8.9	8.9	8.9
Na/Ca	0.66	28.6	39.5	46.4
Na/Cl	0.983	0.866	0.868	0.867

trast, the anion values differ for the two clays. For smectite, as previously noted by Thomas et al. (1982), NIC$_{Cl}$ decreases uniformly with increasing salinity. For kaolinite, the variations were unexpectedly complicated because NIC$_{Cl}$ decreases at very low salinities from a positive to a negative value and increases again to positive values at high salinities; as for the cations, the data do not vary smoothly, again probably due to analytical error.

MODELING FRAMEWORK

Theoretical G-values have been computed for several models which are modified versions of the Gouy-Chapman model. The necessary additional notation is given in Table 3. The Poisson-Bolzmann equations of the basic Gouy-Chapman model for a system containing n ion species, are

$$c_i = c_i{}^b \exp\{z_i F\phi/RT\} \qquad (1a)$$

$$i = 1, \ldots, n, \quad \text{and}$$

$$d^2\phi/dx^2 = -F \sum z_i c_i/\epsilon_0\epsilon, \qquad (1b)$$

Table 3. Notation used for the mathematical analysis.

Symbol	Meaning	Units	Value of constant
F	Faraday constant	C mole^{-1}	9.65×10^4
ϵ	Relative permittivity		
ϵ_0	Permittivity of free space	Fm^{-1}	8.85×10^{-12}
z_i	Charge number of ith ion		
R	Gas constant	J K^{-1} mole^{-1}	8.32
T	Temperature	K	
ϕ	Potential	V	
E	Field strength	V m^{-1}	
σ	Charge density	C m^{-2}	
x	Distance	m	
I	Ionic strength	mole m^{-3}	

cause the main change in the proportion of cations in the bulk solution occurs in the 0 to 10‰ salinity range, the maximum change in NIC$_i$ should also be in this range due to the freshwater salt component providing an insignificant contribution to the total salt content at high salinities. This prediction can be judged by comparing the proportions of ions at different salinities (Table 2); for example, the ratio of Na/K is 19.8 in the river water and 47.1 to 47.8 at salinities of 10‰ and above.

Despite these consistencies, the data are in part fairly variable. For smectite, NIC$_{Na}$, NIC$_K$, and NIC$_{Mg}$ change smoothly as salinity increases whilst NIC$_{Ca}$ fluctuates. For kaolinite, the variations are probably due in part to the difficulty in analyzing for materials of low cation-exchange capacity in contact with solutions of high salt content; because both T$_i$ and the product of T$_{H_2O}$ and $^ic_{H_2O}$ will be of a similar size, NIC$_i$ will be small and particularly sensitive to analytical errors in the component terms. For smectite, however, such errors are much less important because T$_i \gg$ T$_{H_2O}{}^ic_{H_2O}$. In con-

where $C_i \equiv C$ species i, the alternative notations being unambiguous. These equations have been modified in three different ways. First, the relative permittivity in the Poisson equation (1b) was allowed to vary with field strength. The functional relationship used was

$$\epsilon(e) = a_1/(1 + a_2E^2) + a_3,$$

where a_1, a_2 and a_3 are constants taking values $a_1 = -5.5$, $a_2 = 1.2 \times 10^{-17}$ m²v⁻², $a_3 = 5.5$. This choice of $\epsilon(E)$ was suggested by Grahame (1951). Secondly, an activity term was introduced, modifying the exponent in the Bolzmann equation (1a). The full equation is

$$c_i = c_i{}^b\exp\{f_i\ (E,\phi,c_1\ \ldots\ c_n)\},$$

with

$$\begin{aligned}f_i(\cdot) = &\ z_iF\phi/RT \\ &- Az_i{}^2\sqrt{I}/(1 + BL\sqrt{I}) \\ &+ Az_i{}^2\sqrt{I^b}/(1 + BL\sqrt{I^b}),\end{aligned}$$

where L is an ion-size parameter.

The additional extended Debye-Hückel activity terms approximate the difference in activity coefficients between ions in the bulk solution and those closer to the charged surface. Some justification for the choice of this functional form has been given by others (Berner, 1971; Pytkowicz, 1979a, 1979b; Whitfield, 1979; Moore 1968). Strictly, A and B should be regarded as functions of relative permittivity: here, this case was considered, but we also allowed A and B to be constant. Thirdly, certain ions were excluded from a region near the charged surface. If the charge on an ion is regarded as present at a point at its center, it cannot approach the surface closer than the radius of the ion. The surface concentration of any ion is therefore zero, unless it enters the structure of the clay surface. The effect of constraining ions to a position no closer than their hydrated radius is to increase the predicted concentration of smaller ions near the surface, compared with those given by models without this constraint. In the mathematical analysis the constraint was introduced by allowing the activity coefficient of each ion to be infinite in the exclusion zone. This third modification was included to allow for the selectivity of ions which is observed experimentally but not accounted for by the Gouy-Chapman model. It is an alternative to ideas suggested by other authors. The Stern triple layer model (Heald *et al.*, 1964; Bolt *et al.*, 1967; Westall and Hohl, 1980; Sposito, 1981b), for example, combines an adsorbed surface layer with given selectivity coefficient and a diffuse region extending into the bulk solution.

In summary, the models used were:

(1) The Gouy-Chapman model.
(2) The Gouy-Chapman model with the relative permittivity in the Poisson equation allowed to vary with field strength.

(3a) As in model (2), but with the extended Debye-Hückel activity term (A and B taken as constants) included in the exponent of the Boltzmann equations as described above.
(3b) As in model (3a), but with the terms A and B taken as functions of the relative permittivity.
(4) The Gouy-Chapman model with a minimum distance of approach for the ions introduced, with relative permittivity dependent on field strength. The minimum distances of approach for the ions in solution are taken to be 3 Å for K⁺, and 4 Å for Na⁺, Ca²⁺, Mg²⁺, and all anions. These values correspond approximately to the hydrated radii of the ions.
(5a) As in model (4), but using more appropriate values for the closeness of approach (McConnell, 1964; Grim, 1968; Berner, 1971). For kaolinite, Na⁺ and K⁺ = 2 Å, Ca²⁺ = 3 Å, Mg²⁺ and all anions = 4 Å; for smectite the values are the same except for K where a value of 0 Å is used to allow for this ion entering the surface of smectite particles (Dolcater *et al.*, 1968; Grim, 1968; Bruggenwert and Kamphorst, 1979).
(5b) As in model (5) for smectite, except the distances of approach are taken as zero for K and 4 Å for all other ions.

The method of computing G-values for each of the above models closely followed that of Oldham (1975). The surface potential ϕ^s and surface field strength E^s were computed using the appropriate modified versions of Eq. (1a) and (1b) and the known value of the total charge density σ^b. First, E^s was found using the relationship.

$$d\sigma/dx = -\epsilon_0\epsilon(E)\ dE/dx.$$

For simple functions $\epsilon(E)$ this equation can be integrated analytically over $[0,\sigma^b]$ to give a non-linear equation in E^s. For example, when $\epsilon(E) = a_1/(1 + a_2E^2) + a_3$, the relevant equation is

$$\sigma^b = \epsilon_0[a_1a_2{}^{-1/2}\tan^{-1}(a_2{}^{-1/2}E^s) + a_3E^s]. \tag{2}$$

The surface potential ϕ^s was found by solving numerically the equation

$$d\phi/d\{E^2\} = [-2F\sum z_iC_i/(\epsilon_0\epsilon(E))]^{-1}.$$

Initially $\phi \equiv \phi^b = 0$, and numerical integration was carried out over the interval $E^2 = [0,\{E^s\}]^2$, giving at end point the surface potential ϕ^s. Values of c_i were needed for this integration and were found by solving numerically the set of non-linear equations

$$c_i = c_i{}^b\exp\{f_i(1)\} \qquad i = 1, \ldots, n.$$

Having computed ϕ^s and E^s, the equations
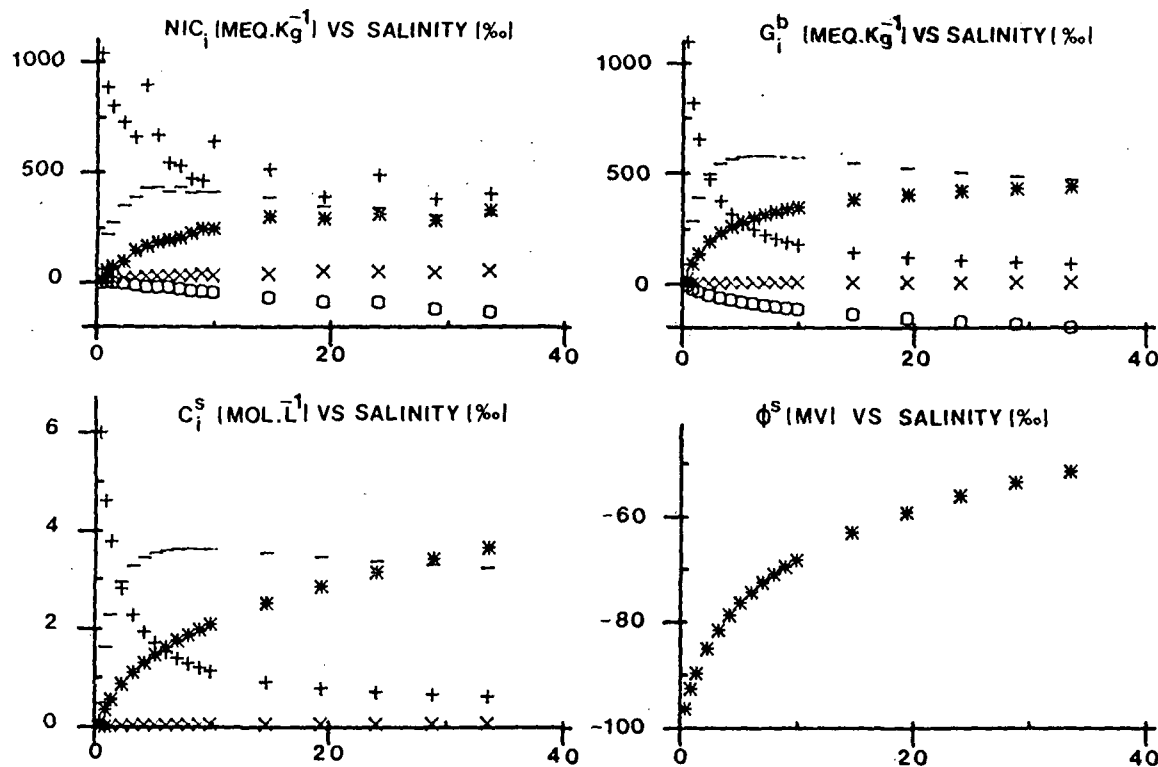
$$dG_i/dx = c_i - c_i{}^b,$$

$$d\phi/dx = E, \text{ and}$$

Figure 1.　The variation in G_i, surface concentration, and surface potential as predicted by Gouy-Chapman theory (model 1) and NIC_i with change in salinity for smectite (+ = Ca, − = Mg, * = Na, × = K, □ = Cl).

$$dE/dx = -F \sum z_i c_i / \epsilon_0 \epsilon(E)$$

can be solved numerically as an initial value problem, giving a profile of G_i, ϕ, and E adjacent to the charged surface. A more detailed account of a special case of our analysis is given by Oldham (1975).

RESULTS

Results given here are for kaolinite and smectite in mixtures of river and seawater containing the ions Na^+, K^+, Mg^{2+}, Ca^{2+}, Cl^-, SO_4^{2-}. The salinity of the mixture is in the range 0 to 35‰. Three sets of results are presented: (1) For the basic Gouy-Chapman model, G_i^b, and NIC_i values, surface concentrations of ions and surface potential are given for each mixture; (2) Values of these variables for the more complex models are given for seawater and fresh water only; (3) Profiles of G-values, ionic concentrations, and potential and field strength near a clay surface are given for smectite in seawater.

A comparison of G_i^b and NIC_i values for each mixture of waters (shown in Figures 1 and 2) is of interest because these are theoretical and observed measures of the same variable. A striking feature is the discrepancy for K^+ throughout the range of salinities for both clays. The low G_i^b values are to be expected because

the ratio of K^+ to Na^+ in the bulk solution was low, and in the Gouy-Chapman model this ratio was preserved throughout the double layer. For smectite, the G_{Ca}^b and NIC_{Ca} values also show discrepancies at high salinities which may be due to aggregation and the related difficulty of extracting Ca^{2+} from the clay. The remaining important difference between theoretical and observed results is observed in the G_i^b and NIC_i values for both clays, particularly at high salinities. This difference could be explained by the presence of positively charged sites on the clay surface, especially for kaolinite, and aggregation, especially for smectite. Some evidence for this was given by Hofmann et al. (1958) and Grim (1968) Difficulties in providing a standard (fiduciary) drying temperature for damp clays (Thomas et al., 1982) and complexation/hydrolysis of divalent ions near clay surfaces (Bache, 1976; Steger, 1973) may also be complicating factors.

Results for the more complex models are given in Tables 4–7. Although predicted surface concentrations are quite different for models 1 to 3, the G-values are much the same for any given ion. Comparison between predicted and measured values shows that the predictions are of variable quality; particularly poor are those for K^+ for both clays at both solution strengths, and also Ca^{2+} for smectite in seawater. Of these models,
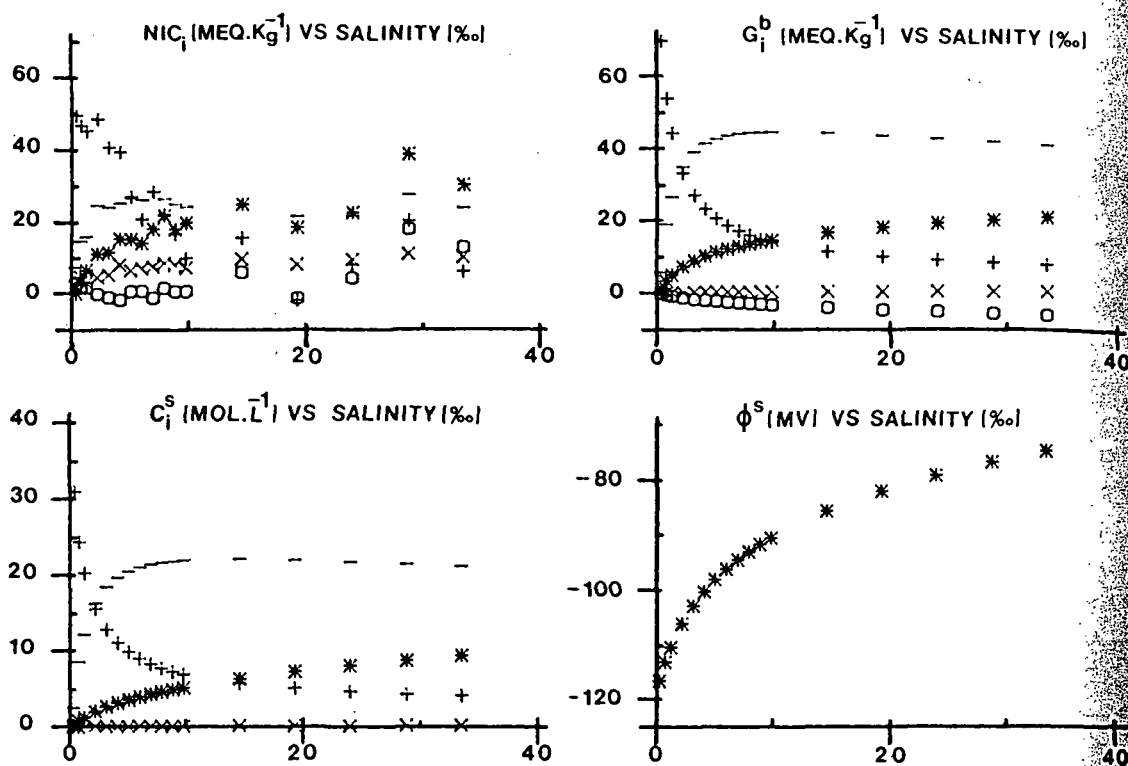
Figure 2. The variation in G_i, surface concentration, and surface potential as predicted by the basic Gouy-Chapman theory (Model 1) and NIC_i with change in salinity for kaolinite ($+ = Ca$, $- = Mg$, $* = Na$, $\times = K$, $\square = Cl$).

the one which included terms for relative permittivity in the activity equation (Model 3b) was unsatisfactory because unrealistic values of activity coefficients and surface concentrations were obtained. Indeed, for kaolinite, G values could not be determined for the seawater example owing to this effect; surface ion concentrations were in excess of 1000 M. This concentration arose because within the model ϵ varied by ~14 fold ($\epsilon \sim 6$ near the clay surface, ~80 in the bulk solution) resulting in 52- and 4-fold changes, re-

Table 4. Smectite G_i^b-values for river and marine end members determined by various models.

Model	Na	K	Mg	Ca	Cl	SO₄	HCO₃
				River water			
1	24.5	1.3	90.3	1096.2	−4.7	−11.0	−9.8
2	22.4	1.2	89.4	1084.4	−3.3	−6.9	−8.8
3a	19.0	1.1	66.4	1131.1	−3.5	−8.4	−7.5
3b	17.8	1.0	60.1	1140.3	−3.5	−8.5	−7.5
4	22.3	1.7	89.2	1082.9	−4.2	−9.0	−8.8
5a	33.7	8.2	45.3	1099.0	−3.7	−7.8	−7.8
5b	22.4	20.1	88.0	1068.4	−4.3	−9.3	−9.1
Measured	15.2	7.7	66.3	1039.5	0.0	—	—
				Seawater			
1	422.9	9.3	474.3	90.7	−190.8	−29.7	−0.85
2	441.1	9.2	479.4	91.7	−189.5	−29.6	−0.84
3a	451.9	10.2	481.9	106.7	−162.3	−25.7	−0.74
3b	428.9	10.1	504.0	131.6	−141.3	−22.4	−0.70
4	282.0	16.8	435.9	83.4	−353.8	−45.8	−1.58
5a	600.6	75.5	135.0	68.3	−302.1	−40.3	−1.35
5b	234.2	187.0	342.4	65.5	−347.6	−45.2	−1.56
Measured	330.9	57.0	310.6	403.6	−130.2	—	—

Table 5. Kaolinite G_i^b-values for river and marine end members determined by various models.

Model	Na	K	Mg	Ca	Cl	SO$_4$	HCO$_3$
				River water			
1	0.8	0.04	5.8	69.8	−0.13	−0.30	−0.28
2	0.8	0.04	5.7	69.5	−0.09	−0.19	−0.19
3a	0.6	0.04	3.9	72.2	−0.09	−0.20	−0.19
3b	0.5	0.03	2.1	76.8	−0.09	2.59	−0.20
4	0.7	1.7	5.5	66.3	−0.08	−0.15	−0.16
5a	7.1	4.4	1.5	61.1	−0.07	−0.15	−0.16
Measured	1.0	2.1	7.3	49.3	2.8	—	—
				Seawater			
1	20.9	0.43	41.0	7.8	−6.0	−0.90	−0.03
2	19.7	0.41	42.6	8.0	−5.7	−0.90	−0.03
3a	20.5	0.48	40.7	9.8	−5.0	−0.80	−0.02
3b	—	—	—	—	—	—	—
4	14.6	9.4	34.5	6.6	−10.5	−1.4	−0.05
5a	48.4	6.2	7.3	4.8	−9.3	−1.4	−0.05
Measured	30.0	10.0	23.7	6.1	12.8	—	—

Table 6. Ratio of G_i^b/NIC_i values for smectite.

Salinity	Na	K	Mg	Ca	Cl
	Basic Gouy-Chapman model				
0.36	1.60	0.16	1.43	1.05	−∞
0.83	1.65	0.21	1.31	0.92	−5.68
1.30	1.87	0.22	1.43	1.26	−21.6
2.25	2.08	0.22	1.43	0.65	19.6
3.22	1.58	0.21	1.40	0.57	6.3
4.15	1.58	0.20	1.31	0.35	3.7
5.09	1.54	0.20	1.33	0.41	4.2
6.04	1.56	0.21	1.40	0.45	4.4
7.00	1.55	0.20	1.32	0.42	3.5
7.93	1.45	0.22	1.41	0.43	2.9
8.88	1.39	0.18	1.39	0.41	2.7
9.83	1.40	0.22	1.38	0.29	2.7
14.60	1.27	0.19	1.41	0.27	2.1
19.30	1.39	0.15	1.51	0.31	1.8
24.00	1.34	0.17	1.18	0.22	2.0
28.00	1.52	0.19	1.58	0.26	1.6
33.50	1.33	0.16	1.52	0.22	1.5
	Alternative models				
	(a) River water				
Model					
1	1.60	0.16	1.43	1.05	−∞
2	1.49	0.15	1.42	1.04	−∞
3a	1.27	0.14	1.05	1.09	−∞
3b	1.17	0.13	0.94	1.00	−∞
4	1.49	0.21	1.41	1.04	−∞
5a	2.25	1.02	0.71	1.06	−∞
5b	1.49	2.51	1.39	1.03	−∞
	(b) Seawater				
Model					
1	1.33	0.16	1.52	0.22	1.5
2	1.33	0.16	1.54	0.22	1.5
3	1.36	0.18	1.55	0.26	1.2
3a	1.30	0.18	1.62	0.33	1.1
4	0.85	0.29	1.40	0.21	2.7
5a	1.81	1.32	0.43	0.17	2.3
5b	0.71	3.20	1.10	0.16	2.7

Table 7. Ratio of G_i^b/NIC_i values for kaolinite.

Salinity	Na	K	Mg	Ca	Cl
	Basic Gouy-Chapman model				
0.36	—	0.02	0.79	1.41	−0.1
0.83	0.69	0.03	1.30	1.14	−0.5
1.30	0.76	0.04	1.79	0.98	−0.6
2.25	0.66	0.04	1.43	0.68	14.0
3.22	0.79	0.04	1.63	0.67	1.4
4.15	0.67	0.03	1.67	0.59	1.2
5.09	0.74	0.04	1.80	0.77	−3.8
6.04	0.86	0.04	1.69	0.90	−4.3
7.00	0.71	0.04	1.56	0.60	2.1
7.93	0.62	0.03	1.70	0.72	−2.0
8.88	0.79	0.04	1.80	0.90	−5.2
9.83	0.74	0.04	1.87	1.46	−5.6
14.60	0.67	0.04	1.80	0.74	−0.7
24.00	0.86	0.04	1.98	1.13	−1.2
28.80	0.52	0.04	1.53	0.41	−0.3
33.50	0.70	0.04	1.73	1.29	−0.5
	Alternative models				
	(a) River water				
Model					
1	0.8	0.02	0.79	1.41	−0.04
2	0.8	0.02	0.79	1.41	−0.03
3a	0.6	0.02	0.53	1.46	−0.03
3b	0.5	0.01	0.29	1.56	−0.03
4	0.7	0.81	0.75	1.34	−0.03
5a	7.1	2.10	0.20	1.24	−0.03
	(b) Seawater				
Model					
1	0.70	0.04	1.73	1.29	−0.5
2	0.66	0.04	1.80	1.31	0.4
3a	0.68	0.05	1.71	1.61	0.4
3b	—	—	—	—	—
4	0.49	0.94	1.46	1.08	0.8
5a	1.61	0.62	0.31	0.79	0.7

EXAMPLE 1   EXAMPLE 2   EXAMPLE 3

G_i (MEQ.Kg^{-1}) VS DISTANCE (Å)

C_i (MOL.L^{-1}) VS DISTANCE (Å)

POTENTIAL (*)(MV) AND FIELD STRENGTH (X)(MV.Å^{-1}) VS DISTANCE (Å)
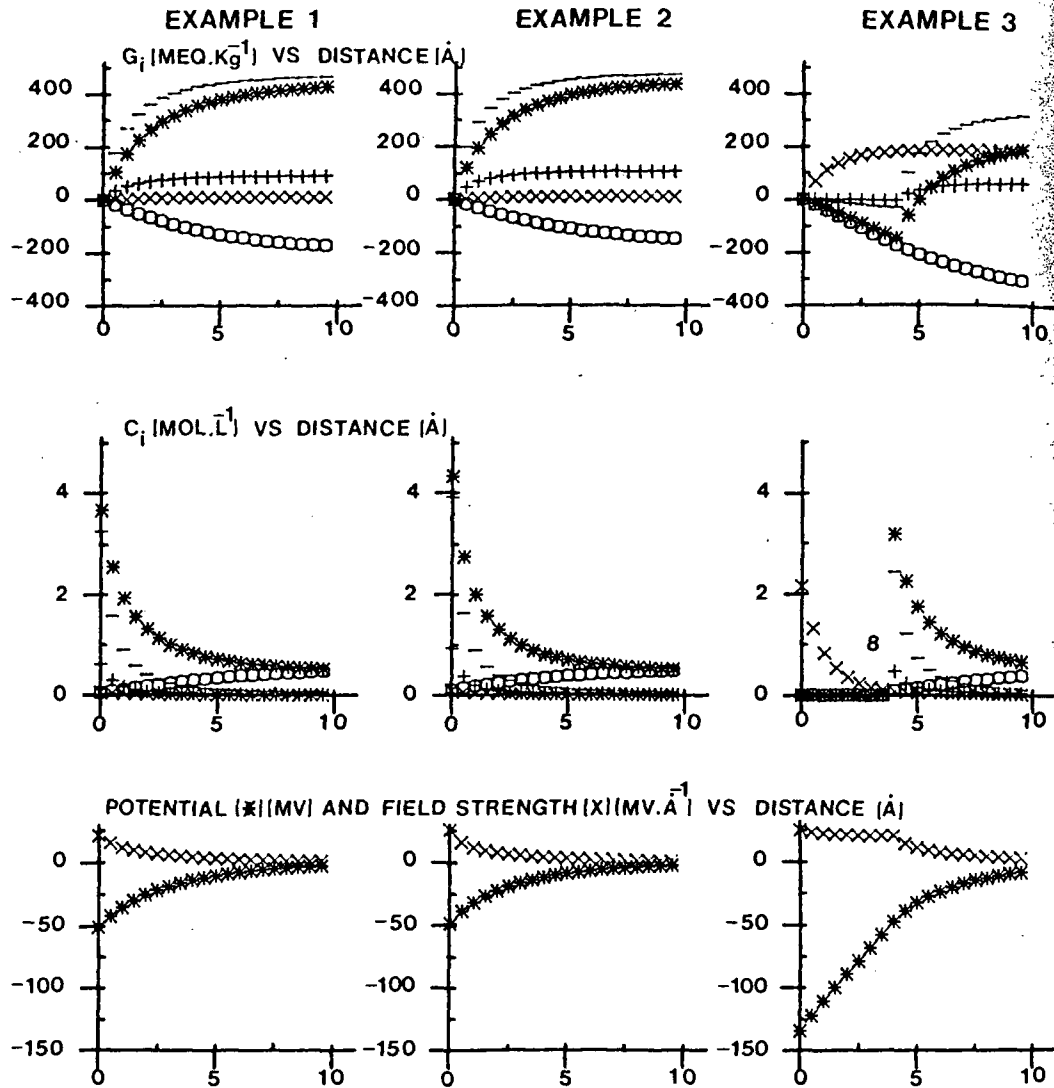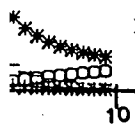
Figure 3. Numerical solutions to three electrostatic models for smectite in seawater. Example 1 = basic Gouy-Chapman model; example 2 = Gouy-Chapman model with dependence of the relative permittivity on field strength in the Poisson equation and an extended Debye-Hückel activity term included; example 3 = Gouy-Chapman model with all ions except potassium restricted to be at least 4 Å from the surface; potassium is unrestricted (+ = Ca, − = Mg, * = Na, × = K, □ = Cl).

spectively, in the A and B terms in the activity coefficient expression. For example, within one molecular diameter of the clay surface, estimates of γ_i for monovalent and divalent ions (I = 4, L = 4) were 2×10^{-5} and 1×10^{-19}, respectively; these values compare with bulk solution values of 5×10^{-1} and 7×10^{-2}, respectively.

Models 4 and 5 show that large changes in G-values can be produced by using minimum distance constraints. For kaolinite, Model 4 gave G_K values which are considerably closer to observations than those for Models 1 to 3, whereas those for other cations were still of the correct order. Model 4 also gave quite good predictions for cation G-values for smectite, apart from

Ca. One effect of introducing distance constraints without also allowing the concentration of water to vary, however, was that G-values for anions became increasingly negative. This effect is clearly shown for Models 4 and 5, where the difference between experimental and predicted values were quite marked for both clays. The models certainly took no account of the possible presence of positively-charged sites on kaolinite which led to NIC_{Cl} values greater than zero, and aggregation in smectite which led to reductions in $|NIC_{Cl}|$. Models 5a and 5b showed that G-values may vary considerably when small changes are made in minimum distance constraints. The relative merits of these sub-models are difficult to judge. Surface concentrations of ions

given by Models 1, 2, and 3 were rather variable and in many cases unrealistic (e.g., 65 molar Ca). Models 4 and 5 gave zero surface concentrations in general, by definition.

Figure 3 shows profiles of ionic concentrations, G-values, potential, and field strength for smectite in seawater for a selection of the models used, namely Models 1, 3a, and 5b. The examples were chosen for the clarity with which the results could be presented graphically. The profiles show that the region in which there was most change in concentrations and G-values is for Models 1 to 3, of the order of 2 or 3 Å; smaller than most hydrated ionic radii.

CONCLUSIONS

The incorporation of variable relative permittivity and activity coefficient terms in the basic Poisson-Boltzmann equations has little effect on G-values determined except where the relative permittivity term is inserted into the activity equation. Here, the large variation in relative permittivity results in extremely large variations in activity coefficients and surface concentrations which are unrealistic. Consequently, our results suggest that the incorporation of extra terms for relative permittivity and activity does not lead to a significant improvement in the performance of the model.

The inclusion of a closeness of approach constraint alters the determined G_i^b values to a far greater extent than any of the other modifications we tested and provides a better fit for the cation data. Indeed, the variation in closeness of approach may provide a sensitive means of adjusting the model to fit the observed data. Thus, inasmuch as our theoretical results were made more compatible by the incorporation of an ion hydration term and hydration effects were shown to be critical in controlling ion selectivity, this modification is an important extension to the Gouy Chapman model.

The more elaborate models, while providing better predictions of the clay-electrolyte system, show important differences between theory and observation which provide an insight on how the electrolyte-clay exchange system operates. Thus, it seems that the aggregated nature of smectite clays plays an important part in controlling its exchange properties. Correspondingly, for kaolinite it seems that a variable surface charge model is needed to describe its ion-exchange properties.

ACKNOWLEDGMENT

REFERENCES

Bache, B. W. (1976) The measurement of cation exchange capacity of soils: *Jour. Sci. Fd. Agric.* **27**, 273–280.

Berner, R. A. (1971) *Principles of Chemical Sedimentology:* McGraw-Hill, New York, 240 pp.

Bolt, G. H. (1955a) Ion adsorption by clays. *Soil Sci.* **79**, 267–276.

Bolt, G. H. (1955b) Analysis of the validity of the Gouy-Chapman theory of the electric double layer: *Jour. Colloid Sci.* **10**, 206–218.

Bolt, G. H. (1967) Cation-exchange equations used in soil science—a review: *Neth. Jour. Agric. Sci.* **15**, 81–103.

Bolt, G. H. (1979) The ionic distribution of the diffuse double layer: in *Soil Chemistry B. Physico-Chemical Models,* G. H. Bolt, ed., Elsevier, Amsterdam, 1–76.

Bolt, G. H. and de Haan, F. A. M. (1965) Interactions between anions and soil constituents: *IAEA, Vienna, Tech. Rep. Ser.* **44**, 94–110.

Bolt, G. H. and de Haan, F. A. M. (1979) Anion exclusion in soil: in *Soil Chemistry B. Physico-Chemical Models,* G. H. Bolt, ed., Elsevier, Amsterdam, 233–257.

Bolt, G. H., Shainberg I., and Kemper W. D. (1967) Discussion of the paper by I. Shainberg and W. D. Kemper entitled "Ion exchange equilibria on montmorillonite": *Soil Sci.* **104**, 444–453.

Bolt, G. H. and Warkentin, B. P. (1958) The negative adsorption of anions by clay suspensions: *Kolloid Z.* **156**, 41–46.

Bruggenwert, M. G. M. and Kamphorst, A. (1979) Survey of experimental information on cation exchange in soil systems: in *Soil Chemistry B. Physico-Chemical models,* G. H. Bolt, ed., Elsevier, Amsterdam, 141–203.

Davis, G. A. and Worrall, W. E. (1971) The adsorption of water by clays: *Trans. Brit. Ceram. Soc.* **70**, 71–75.

Dolcater, D. L., Lotse, E. G., Syers, J. K., and Jackson, M. L. (1968) Cation exchange selectivity of some clay-sized minerals and soil materials: *Soil Sci. Soc. Amer. Proc.* **32**, 795–798.

Edwards, D. G. and Quirk, J. P. (1962) Repulsion of chloride by montmorillonite: *J. Colloid Sci.* **17**, 872–882.

Grahame, D. C. (1947) The electrical double layer and the theory of electrocapillarity: *Chem. Rev.* 441–502.

Grahame, D. C. (1952) Diffuse double layer theory for electrolytes of unsymmetrical valency type: *J. Chemical Physics* **21**, 1054–1060.

Grim, R. E. (1968) *Clay Mineralogy:* McGraw-Hill, New York, 596 pp.

Guggenheim, E. A. (1967) *Thermodynamics:* North-Holland Publishing Co. Amsterdam, 390 pp.

Helmy, A. K., Natale, I. M., and Mandolesi, M. E. (1980) Negative adsorption in clay water systems: *Clays & Clay Minerals* **28**, 262–266.

Heald, W. R., Frere, M. H., and De Wit, C. T. (1964) Ion adsorption on charged surfaces: *Soil Sci. Soc. Amer. Proc.* **28**, 622–627.

Hofmann, U., Weiss, A., Koch, G., Mehler, A., and Scholz, A. (1958) Intracrystalline swelling, cation exchange, and anion exchange of minerals of the montmorillonite group and of kaolinite: in *Clays and Clay Minerals, Proc. 4th Natl. Conf., University Park, Pennsylvania, 1956,* Ada Swineford, ed., Natl. Acad. Sci., Natl. Res. Counc., Publ. 456, Washington, D.C., 273–287.

Joshi, K. M. and Parsons, R. (1961) The diffuse double layer in mixed electrolytes: *Electrochimica Acta* **4**, 129–140.

Lyman, J. and Fleming, R. H. (1940) Composition of seawater: *J. Marine Res.* **3**, 134–146.

McConnell, B. L., Williams, K. C., Daniel, J. L., Stanton, J. H., Irby, B. M., Dugger, D. L., and Maatman, R. W. (1964) A geometric effect at the solution surface interface and its relationship to ion solvation. *Jour. Physical Chem.* **68**, 2941–2946.

Moore, W. J. (1968) *Physical Chemistry:* Longmans, London, 944 pp.

Neal, C. (1977) The determination of adsorbed Na, K, Mg,

and Ca on sediments containing $CaCO_3$ and $MgCO_3$: *Clays & Clay Minerals* **25**, 253–258.

Norrish, K. (1954) The swelling of montmorillonite: *Discuss. Faraday Soc.* **18**, 120–134.

Oldham, K. B. (1975) Composition of the diffuse double layer in sea water or other media containing ionic species of +2, +1, −1 and −2 charge types: *J. Electroanalytical Chem.* **63**, 139–156.

van Olphen, H. (1977) *Clay Colloid Chemistry:* Wiley, New York, 318 pp.

Pytkowicz, R. M., ed. (1979a) *Activity Coefficients in Natural Waters:* Vol. 1, CRC Press, Boca Raton, Florida, 304 pp.

Pytkowicz, R. M., ed. (1979b) *Activity Coefficients in Natural Waters:* Vol. 2, CRC Press, Boca Raton, Florida, 336 pp.

Ravina, I. and Gur, Y. (1978) Application of the electrical double layer theory to predict ion adsorption in mixed ionic systems: *Soil Sci.* **125**, 204–209.

Sayles, F. L. and Manglesdorf, P. C., Jr. (1977) The equilibrium of clay minerals with sea water: exchange reactions: *Geochim. Cosmochim. Acta* **41**, 951–960.

Sayles, F. L. and Manglesdorf, P. C., Jr. (1979) Cation exchange characteristics of Amazon River suspended sediment and its reaction in sea water: *Geochim. Cosmochim. Acta* **43**, 767–779.

Schofield, R. K. (1949) Calculation of surface areas of clays from measurements of negative adsorption: *Trans. Brit. Ceram. Soc.* **48**, 207–213.

Slavin, W. (1968) *Atomic Absorption Spectroscopy:* Wiley-Interscience, New York, 307 pp.

Sparnaay, M. J. (1958) Corrections of the theory of the flat diffuse double layer: *Rec. Trav. Chim.* **77**, 872–888.

Sposito, G. (1981a) *The Thermodyanics of Soil Solutions:* Clarendon Press, Oxford, 155–186.

Sposito, G. (1981b) Cation exchange in soils: an historical

and theoretical perspective: in *Chemistry in the Soil Environment,* Amer. Soc. Agronomy Special Publ. 40, 13–31.

Steger, H. F. (1973) On the mechanism of the adsorption of trace copper by bentonite: *Clays & Clay Minerals* 21, 429–436.

Thomas, A. G., Truesdale, V. W., and Neal, C. (1982) The heterogeneous distribution of anions and water around a clay surface with special reference to estuarine systems: in *Transfer Processes in Cohesive Sediments,* R. Parker and D. J. J. Kinsman, eds., Plenum Press, London, (in press).

Thomas, H. C. (1965) Toward a connection between ionic equilibrium and ionic migration in clay gels: *Int. Atomic Energy Agency, Tech. Rep.* No. **48**, Vienna, 4–19.

Truesdale, V. W., Neal, C., and Thomas, A. G. (1982) A rationalisation of several approaches to clay/electrolyte studies: in *Transfer Processes in Cohesive Sediments,* R. Parker and D. J. J. Kingsman, eds., Plenum Press, London (in press).

Westall, J. and Hohl, H. (1980) A comparison of electrostatic models for oxide/solution interface: *Adv. Coll. Int. Sci.* **12**, 265–294.

Whitfield, M. (1979) Activity coefficients in natural waters: in *Activity Coefficients in Electrolyte Solutions,* Vol. 2, R. M. Pytkowicz, ed., CRC Press, Boca Raton, Florida, 153–299.

Wiklander, L. (1964) Cation and anion exchange phenomena: in *Chemistry of the Soil,* F. Bear, ed., Van Nostrand Reinhold Co., New York, 163–205.

Zall, D. M., Fisher, D., and Garner, M. Q. (1956) Photometric determinations of chlorides in water: *Anal. Chem.* **28**, 1665–1668.

Zaytseva, E. D. (1966) Exchange capacity and cations of sediments of the Pacific Ocean: in *Khimiya Tikhogo Okeana,* (*Chemistry of the Pacific Ocean*), S. V. Brujewicz, ed., Izd. Nauka, 273–290.

Резюме—На основе теории Гуя-Чапмана представлена модель, описывающая ионообменное поведение глин в растворах смешанных электролитов. Принимая во внимание изменения диэлектрической проницаемости, активности ионов и близость доступа ионов к глинистым поверхностям, были рассчитаны ионовые распределения, которые сравнивались с экспериментальными данными для смектита и каолинита, находившимися в контакте с речной и соленой водой. Наиболее значительное расширение теории Гуя-Чапмана включает в себя введение члена "близость доступа," чтобы получить достаточное согласие между теоретическими предсказаниями и наблюдениями. Кроме того, сложная натура смектитов играет значительную роль в контролировании свойств обмена, тогда как модель постоянного заряда неполностью описывает свойства обмена ионов для каолинита. [E.G.]

Resümee—Es wird ein Modell vorgestellt, das auf der Gouy-Chapman Theorie beruht, mit dem das Ionenaustauschverhalten von Tonen in gemischten Elektrolytlösungen beschrieben wird. Mittels Computerberechnete Ionenverteilungen, die Variationen der relativen Durlässigkeit, der Ionenaktivität und der Annäherung der Ionen an die Tonoberflächen berücksichtigen, wurden mit experimentellen Daten für Smektit und Kaolinit, die in Kontakt mit Flußwässern und salinen Wässern waren, verglichen. Um eine brauchbare Übereinstimmung zwischen der theoretischen Vorhersage und den Beobachtungen zu erzielen, war die Einführung eines Annäherungsterms die wichtigste Erweiterung der Gouy-Chapman Theorie. Darüberhinaus spielt das Aggregat-förmige Auftreten der Smektite eine wichtige Rolle, indem es die Austauscheigenschaften beeinflußt, während ein Modell mit definierter Ladung nur eine ungenügende Beschreibung für die Ionenaustauscheigenschaften des Kaolinits liefert. [U.W.]

Résumé—On présente un modèle, basé sur la théorie Gouy-Chapman, décrivant le comportement d'échange d'ions d'argiles dans des solutions d'électrolytes melangés. Des distributions ioniques computées, qui tiennent compte des variations de permittivité relative, d'activité ionique et de la proximité d'approche des ions des surfaces argileuses, sont comparées avec des données expérimentales pour la smectite et la kaolinite en contact avec des eaux fraîches et salées. Pour obtenir un accord raisonnable entre la prédiction théorique et l'observation, l'extension la plus importante de la théorie de Gouy-Chapman implique le terme de proximité d'approche. De plus, la nature aggrégate des smectites joue un role important dans le contrôle de ses propriétés d'échange, tandis qu'un modèle à charge fixe fourni une description pauvre pour les propriétés d'échange d'ions de la kaolinite. [D.J.]

DEPARTMENTS

DISCUSSIONS AND COMMUNICATIONS

CATION EXCHANGE AND INDUCED ELECTRICAL POLARIZATION

J. A. SCHUFLE[†]

INTRODUCTION

A report has been made by Vacquier et al. (1957) on the detection of ground water by induced electrical polarization (I.P.). Direct current is introduced into the ground at two points for a short period of time. The current is then interrupted and a small induced voltage, which may take several minutes to decay, appears between another pair of electrodes. Vacquier suggested that the I.P. might be pictured as being due to local electrodialysis of the clay across semi-permeable membranes formed by adjacent sand grains. When the current is shut off, the induced potential dies away as the exchangeable ions slowly redistribute themselves along the clay.

It should be possible to test such a proposed mechanism by measuring the I.P. in the presence of different cations. The more firmly bound the cation to the exchange material, the less it should migrate under a given potential and the lower should be the I.P. obtained. All other factors being equal, the higher the valence on the cation, the more firmly bound it is to the exchanger. Thus the higher the valence on the cation, the lower should be the I.P. obtained.

Some difficulty was encountered in forming reproducible clay-sand beds for measuring the I.P. To eliminate variations due to the clay it was proposed to replace the clay with ion exchange resin. Similar substitution of resin for clay has been made, for example, by McKelvey et al. (1955) in preparing "synthetic dirty sands" for studying the resistivity of oil sands. Reproducible mixtures of resin and sand in the presence of specific cation concentrations are more readily prepared than is the case with clay-sand mixtures.

EXPERIMENTAL PROCEDURE

A mixture of 5-percent resin and 95-percent sand by volume was arbitrarily taken as the bed to be used. The particle size of both sand and resin was 20–30 mesh. This mixture was found to give satisfactorily large I.P. values and had a decay time in excess of 60 seconds. Pure resin beds give high initial potentials but decay in a second or less. The resin used was a cation exchange resin of high capacity, Permutit Q, a sulfonated polystyrene resin of high stability. The resin was first saturated with the cation under investigation, then brought into equilibrium with the particular concentration of salt to be tested. All salts used were in the form of nitrates in order to eliminate possible variations due to anion

† New Mexico Institute of Mining and Technology, Socorro, New Mexico.

ICATIONS

CAL POLARIZATION

ı on the detection of ground
ırect current is introduced
f time. The current is then
ay take several minutes to
Vacquier suggested that the
lysis of the clay across semi-
ıs. When the current is shut
ıble ions slowly redistribute

echanism by measuring the
firmly bound the cation to
er a given potential and the
being equal, the higher the
:o the exchanger. Thus the
ɛ the I.P. obtained.
oducible clay-sand beds for
:he clay it was proposed to
titution of resin for clay has
ı preparing "synthetic dirty
ıroducible mixtures of resin
ıtions are more readily pre-

ɛ

ı by volume was arbitrarily
h sand and resin was 20–30
large I.P. values and had a
⁊e high initial potentials but
tion exchange resin of high
of high stability. The resin
on, then brought into equi-
e tested. All salts used were
ıle variations due to anion

New Mexico.

effects. The sand also was rinsed several times with the solution to be tested. The proper volumes of resin and sand were measured in a graduated cylinder, drained of excess solution, and thoroughly mixed. The mixture was then transferred to the cell. The mixture normally retained a volume of solution equal to 25 percent of the total volume of mixture.

The cell consisted of a hemicylindrical container fabricated from inert plastic material. The cell had interior dimensions of 22.1 cm in length and 3.8 cm in diameter. The current was applied through two platinum electrodes mounted in the ends of the cell. The potential electrodes were two silver-silver chloride electrodes in porous pots, mounted 4.8 cm from each end of the cell and 12.5 cm apart. The I.P. was measured at two different voltages, approximately 1 volt and 5 volts, as a check. The integrated I.P. value was measured as the area under the decay curve in millivolt-seconds per volt. The 1-volt and 5-volt I.P. values usually check each other within less than 5 percent. The current was applied for a period of 20 seconds, after which the I.P. decay curve was recorded. The electrical circuit was the same as that used by Vacquier.

The integrated I.P. values obtained for four different salts, $NaNO_3$, $Ca(NO_3)_2$, $La(NO_3)_3$, and $Th(NO_3)_4$, at different concentrations are shown in Table 1. The valences of the cations in these salts are one, two, three, and four, respectively. The I.P. values for the different salts are plotted against resistivities of the bed in Figure 1.

TABLE 1

Salt	Conc. (equivs./L)	I.P. (mv-sec/v)	Resistivity (ohm-m)
$NaNO_3$	0.005	568 ± 34	9.1
	0.001	541 27	49.1
	0.0002	559 19	104.5
$Ca(NO_3)_2$	0.01	352 32	4.2
	0.005	421 14	8.9
	0.002	471 40	19.4
	0.001	420 29	35.9
	0.0004	579 30	73.9
	0.0002	561 21	117
$La(NO_3)_3$	0.005	200 22	9.3
	0.001	408 20	38.1
	0.0002	536 33	125
$Th(NO_3)_4$	0.005	9 4	7.0
	0.001	8 2	21.5
	0.0002	16 5	52.5
	0.00004	37 5	122

DISCUSSION

The results show a decrease in I.P. with increase in valence of the cation for the highest concentration, 0.005 normal, as predicted from the cation exchange mechanism. As concentration decreases, the I.P. values for Na, Ca, and La appear to approach a common value of about 560 mv-sec/v. The I.P. value for thorium, however, remains at a low value even at the lowest concentrations.

The cation exchange mechanism leads one to consider that the I.P. produced may be due to a concentration gradient built up across the cell as suggested by Vacquier. Work by Spiegler et al. (1956) suggests that the initial potential could be calculated from their equation for a plug potential, $E = 2RT/nF \log c_2/c_1$, for dilute solutions. From the amount of current moving through the cell during the time the potential is applied one can calculate the amount of electrolyte moved and obtain an estimate of the concentration gradient to be expected. Using this value and the equation for a plug potential one obtains values in substantial agreement with experimental values, but only in the case of the thorium solutions.
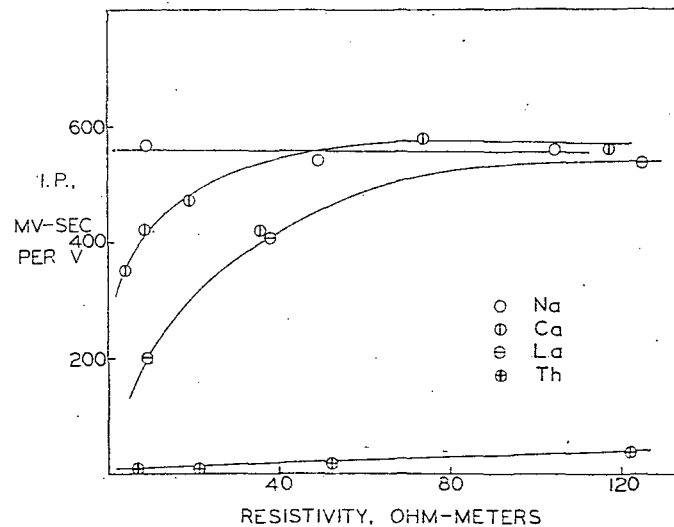
FIG. 1. Induced polarization versus resistivity.

In the case of the other salts the observed potential is higher than the calculated one by two orders of magnitude.

The present experiments, then, particularly in the case of the thorium solutions, give some support to the cation exchange mechanism for the I.P. However, the inconsistencies in the results are sufficient to suggest that there are perhaps factors involved other than those suggested by this simple mechanism.

REFERENCES

McKelvey, J. G., Jr., Southwick, P. F., Spiegler, K. S., and Wyllie, M. R. J., 1955, The application of a three-element model to the s.p. and resistivity phenomena evinced by dirty sands: Geophysics, v. 20, p. 913–931.

Spiegler, K. S., Yoest, R. L., and Wyllie, M. R. J., 1956, Electrical potentials across porous plugs and membranes: Discussions of the Faraday Society, n. 21, p. 174–185.

Vacquier, Victor, Holmes, Charles R., Kintzinger, Paul R., and LaVergne, Michel, 1957, Prospecting for ground water by induced electrical polarization: Geophysics, v. 22, p. 660–687.

$$R_0 = \frac{F^* R_w}{1 + BQ_v R_w}$$

Know R_0 only

- smectites cause increase in conductivity
- seems to be a relation between conductivity and % smectite
- suspect continuous attach smectite for low % of
  samples
- smectites usually have large CEC

$$\boxed{Q_v = \frac{(1 - \phi)\, \rho_{ma}\, CEC}{100\, \phi}}$$

$\rho_{ma} = $ grain density

$$\boxed{Q_v = IC\, CEC}$$

- how does CEC relate to IP? in this case?

Table 21. Resistivity of Solutions with
Various Concentrations of NaCl [8]

Concentration, g/liter	Resistivity, Ω-cm	Concentration	Resistivity, Ω-cm
0.005	$1.05 \cdot 10^5$	1.0	$5.8 \cdot 10^2$
0.05	$1.1 \cdot 10^4$	10.0	$6.5 \cdot 10$
0.5	$1.2 \cdot 10^3$	50.0	15

conditions, and on the relief of the terrain. In platform areas, the salinity varies in going from north to south from 0.1 to 0.5 g/liter (Baltic Shield) to 3 to 5 g/liter (Azov Massif) [8].

Lower resistivities are found for water in ore deposits and in tectonically active zones. In mountainous regions, ground waters have low salinities and high resistivities. Triple-distilled water has the highest resistivity, about 10^7 Ω-cm.

High-Resistivity Dense Rocks. The water content in igneous, metamorphic, and dense sedimentary rocks commonly is no more than 3%, and frequently is less than 1%. However, even this amount of moisture is enough that small variations in the amount will cause large variations in resistivity. Values for resistivity of various rocks as a function of water content, obtained by the author and from reference [125], are listed in Table 22.

It may be seen from these data that decreasing the moisture by a few tenths of a percent causes a change in ρ of an order of magnitude or more. Results of measurements by the author indicate that the slope of the line $\rho = f(w)$ is not the same for rocks of different genesis and petrographic composition (Fig. 29).

Resistivity increases most rapidly with decreasing water content in granites, and less rapidly in dolomite and basalt. It should be noted that experimental data points do not always lie along a straight line, but they rarely deviate very much from such a line. This reflects the fact that the rate of change of resistivity with water content varies not only with the nature but also with the size of grains, the structure of the pore volume, and the content of conductive minerals. In peridotite, for example, the low

Table 22. Resistivities of Rocks with Various Water Contents

Rock	Water content, %	Resistivity, Ω-cm	Rock	Water content, %	Resistivity, Ω-cm
Siltstone	0.54	$1.5 \cdot 10^6$	Diorite	0.02	$5.8 \cdot 10^7$
	0.5	$7.3 \cdot 10^7$		0	$6.0 \cdot 10^8$
	0.44	$8.4 \cdot 10^8$	Peridotite	0.03	$2.2 \cdot 10^6$
	0.38	$5.6 \cdot 10^{10}$		0.016	$1.1 \cdot 10^8$
				0	$1.8 \cdot 10^9$
Coarse-grained sandstone	0.34	$9.6 \cdot 10^7$			
	0.18	10^{10}	Olivene-pyroxenite	0.028	$0.7 \cdot 10^7$
				0.014	$0.39 \cdot 10^8$
Medium-grained sandstone	1.0	$4.2 \cdot 10^5$		0	$0.56 \cdot 10^{10}$
	1.67	$3.18 \cdot 10^8$	Basalt	0.95	$4.1 \cdot 10^6$
	0.1	$1.4 \cdot 10^{10}$		0.49	$9.0 \cdot 10^7$
Pyrophyllite	0.76	$6.1 \cdot 10^9$		0.26	$3.1 \cdot 10^9$
	0.72	$4.9 \cdot 10^9$		0	$1.26 \cdot 10^{10}$
	0.7	$2.1 \cdot 10^{10}$	Peridotite	0.1	$3.07 \cdot 10^5$
	0	$\sim 10^{13}$		0.003	$4.0 \cdot 10^5$
Granite	0.31	$4.4 \cdot 10^5$		0	$6.5 \cdot 10^5$
	0.19	$1.8 \cdot 10^8$			
	0.06	$1.3 \cdot 10^{10}$			
	0	10^{12}			

resistivity as water is removed probably is caused by the presence of significant amounts of metallic minerals.

The relationship between rock resistivity and water content is well-developed only over the range 0-2 to 4% water content. At higher water contents, the resistivity of a rock is less affected by changes in water content. The large effect small amounts of water have on conductivity may be explained as follows: the water forms thin, continuous films over the grains; as a result, we have a system in which water acts as a conductive matrix, and the resistant, rock-forming minerals are merely inclusions. Thus, according to Semenov's theory [91], a small increase in the conductive component must cause a large change in resistivity, as is observed experimentally.

Resistivity of Water-Saturated Clay-Free Rocks. Carbonate rocks, sandstones, and sand are included in this group of rocks. Because the rock framework in such rocks is made up of highly resistive mineral grains, the resistivity is
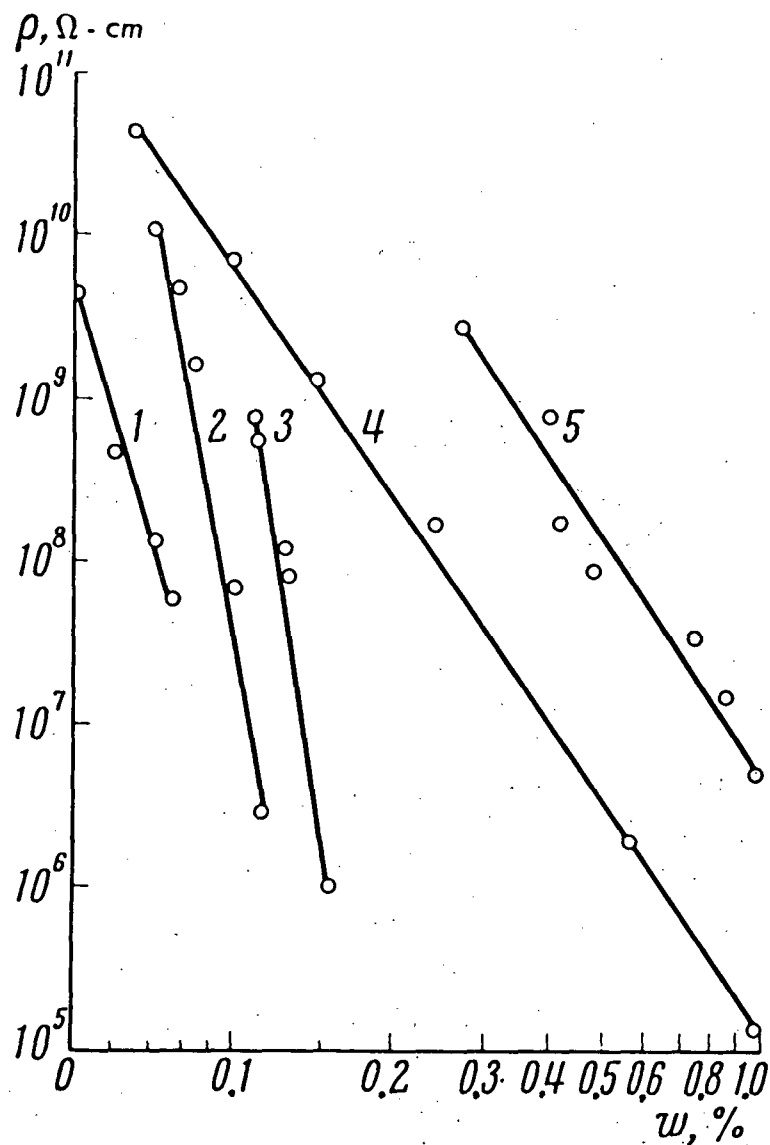
Fig. 29. Relationships between resistivity and moisture content: (1) andesite-basalt, (2,3) granite,(4) dolomite, (5) basalt.

determined mainly by the amount of water present, its salinity, and by the way the water is distributed through the rock.

The amount of water that can be held in a rock at full saturation is limited by the available porosity. The greater the porosity, k, the greater will be the water content, w. Therefore, for this group of rocks, the relationship between resistivity and porosity is the same as the relationship between resistivity and water content. Actually, in practice the relationship $\rho = f(k)$ is used.

This is done because the porosity is an important property describing the reservoir characteristics of a rock.

With complete saturation of the pore volume, the resistivity of a rock is a function of the salinity of the water in the pores. However, for the same salinity and for the same water contents, the resistivities of two rocks may still differ significantly. Both theoretical and experimental studies have shown that there should be a linear relationship between the bulk resistivity of a rock, ρ_{vp}, and the resistivity of the water saturating the rock, ρ_v. Therefore, in order to have a parameter which does not depend on the salinity of the saturating solution, the formation factor P_p is defined as the ratio of bulk resistivity, ρ_{vp}, to the resistivity of the water filling the pores, ρ_v.

Theoretical studies for various simplified rock models, such as collections of cubes, spheres, ellipsoids, and so on, have provided a number of equations relating the formation factor to porosity [86, 139, 140-144]. Mathematical evaluations of experimental data have shown that the most satisfactory expression $P_p = f(k)$ for an inhomogeneous rock over the porosity range from 3-5% to 20-40% as follows:

$$P_p = \frac{a_p}{k^m},\qquad\qquad\text{(III.8)}$$

where a_p is an empirically defined parameter ranging between 0.4 and 1.4 and m is an empirically defined exponent, related to the structure of the pore volume and the degree of cementation of the rock. The exponent may vary from a value of 1.3 for loose sands and oolitic limestones to $2.0-2.2$ for well-cemented, low-porosity sandstones.

In graphical presentations of the function $P_p = f(k)$, experimental data are usually grouped according to petrology, grain sizes, and the amount of cementation of the rock-forming minerals; grouping of experimental data by rock type only partially eliminates the effect of pore shape. As may be seen from Fig. 30, the porosity may vary widely in a number of rock types.

Based on a statistical study of a great volume of data reported by investigators both in the Soviet Union and in other countries for limestones and sandstones, Dakhnov [139] has constructed the average curves shown in Fig. 31, which are of the form of equation
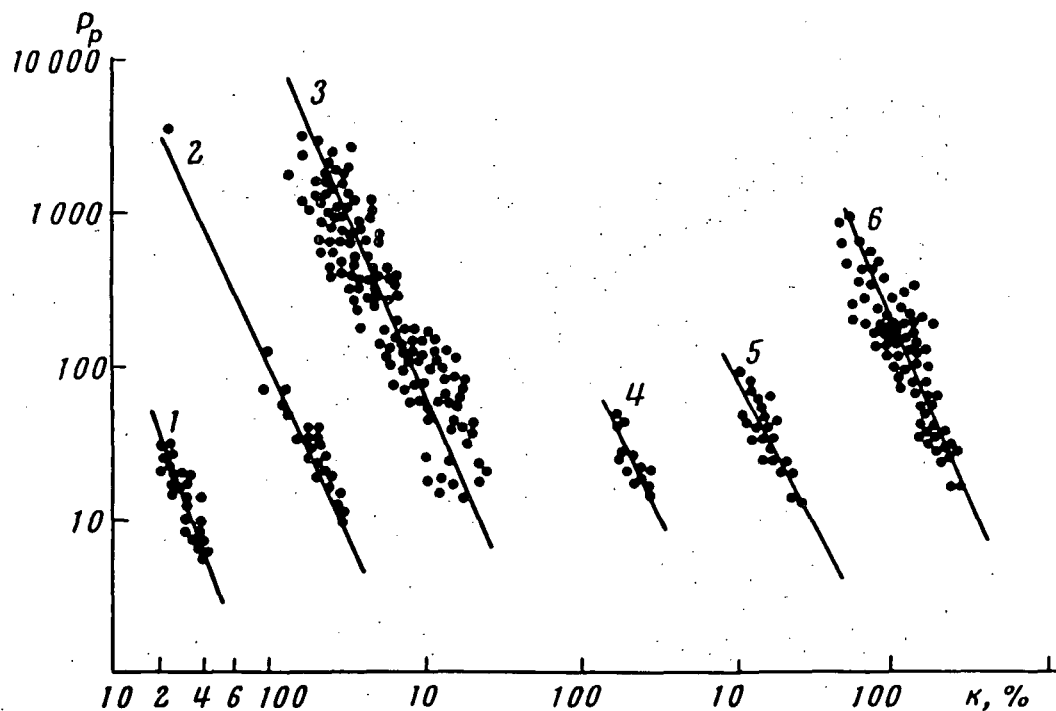
Fig. 30. Relationship of the formation factor, P_p, to the coefficient of porosity, k, for carbonate (limestone) sedimentary rocks in the USSR and the USA: (1) limestones from Kazakhstan (from Sigal), (2) limestones from the Kuibyshev area, Bashkiria (from Kachurina) (3) carboniferous limestones from the Saratov Basin (from Eidman), (4) devonian limestone from Crosset, Texas, (5) oolitic limestone, Smackover formation, (6) Permian limestone, San Andreas Basin, Texas (from Archie).

(III.8). Values for the parameters a_p and m for these curves are listed in Table 23.

These curves indicate that the greater the degree of cementation of a rock, the larger will be the formation factor, as well as resistivity, for a given water content. With increasing cementation, pore shape becomes progressively more important in determining the resistivity. With increasing cementation, the added material reduces the cross section of portions of the pore structure and increases the tortuosity. The tortuosity of a pore structure is defined as the statistical length of the pore structure between two parallel planes, in relation to the actual distance between these planes. The effect of tortuosity on the electrical conductivity of a rock is fundamental because two rocks saturated with the same amounts of a solution with the same salinity, but with different
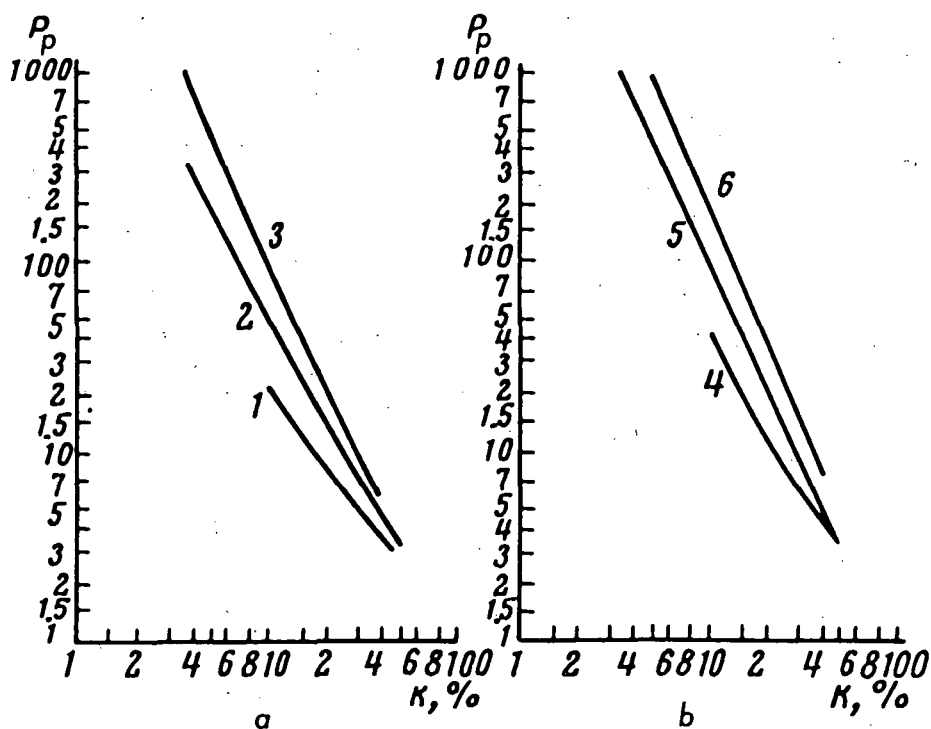
Fig. 31. Averaged relationships between formation factor P_p and the coefficient of porosity (water content by volume) for sandstones and carbonate rocks (from (Dakhnov): a-sandy-shaly rocks, b-carbonate rocks. (1) Loose sand, (2) weakly cemented sand, (3) moderately cemented sandstone, (4) unconsolidated limestone grains, (5) coarsely crystalline dense limestone and dolomite of moderate density, (6) finely crystalline.

Table 23. Values a_p and m for Curves of the Form $P_p = a_p/k^m$

Curve number on Fig. 31	a_p	m
1	1	1.3
2	0.7	1.9
3	0.5	2.2
4	0.55	1.85
5	0.6	2.15
6	0.8	2.3

textures, may have quite a different resistivities [145-148]. The effect of pore geometry becomes particularly important in well-cemented rocks. As a result, in many rocks the correlation between resistivity and permeability is much better than the correlation between resistivity and porosity [149-152].

In cases in which the complete pore structure is saturated with an electrolyte and contributes to conduction, the formation factor is related to tortuosity, T, and porosity, k, by the equation [139]

$$P_p = \frac{T^2}{k}.$$

Published data are in good agreement with this expression. Knowing the resistivity of a rock from an electric log, and knowing the resistivity of the formation water, it is a simple matter to determine the porosity using the curves $P_p = f(k)$ for the appropriate rock type [143, 144]. The inverse problem may also be solved — that of estimating the resistivity of a rock when the porosity and water resistivity are known. In addition, knowledge of the relationship between formation factor and porosity has a further value, in that it may be possible to estimate the lithologic composition of a rock using resistivity data.

Shaly Rocks. In shaly rocks, in addition to nonconducting minerals, zeolites and clay minerals which serve as current conductors are found. As a result, the resistivity of a shaly rock is a function not only of the resistivity of the pore water, but also of the amount of clay present, its properties, and the manner in which it is distributed in the rock [153, 154]. Clay may occur as aggregates between grains in a rock, or it may occur as a coating over the grain surfaces. Significant amounts of clay in a rock lead to a number of peculiar effects. In the first place, with increasing clay content, the water saturation may exceed the porosity because of interactions between the clay minerals and the water [155]. Secondly, the linear relation between bulk resistivity and water resistivity no longer holds. A highly saline solution increases the formation factor of a shaly rock, while a dilute brine reduces the formation factor. Graphs of the relation between formation factor and brine salinity, given by Éidman [146], are shown in Fig. 32. A similar group of curves $P_p = f(C_1)$ for rocks with varying amounts of
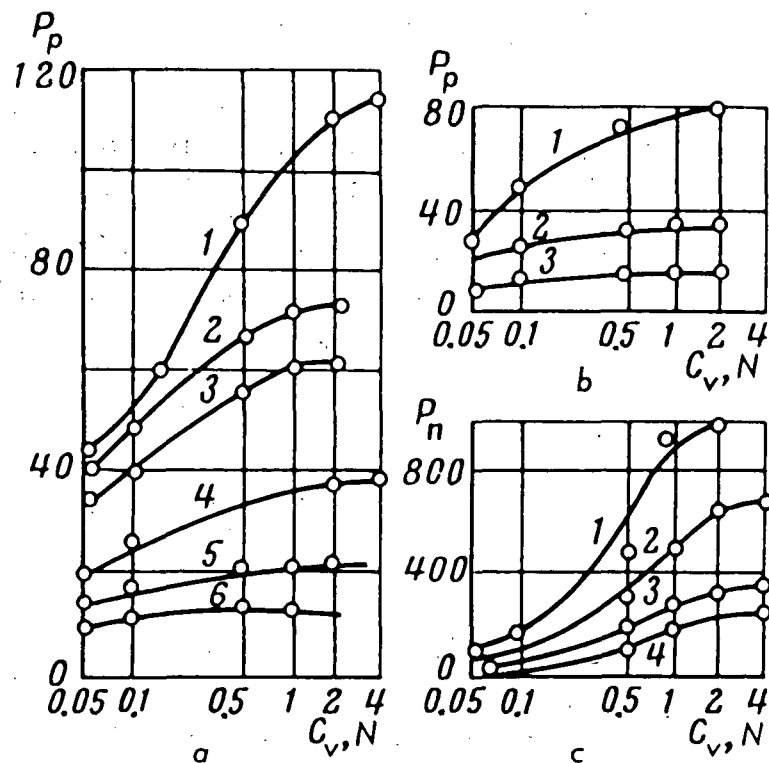
Fig. 32. Relationship between formation factor P_p and the concentration C_v of a solution of sodium chloride saturating shaly-sandy rocks: a — sandstones, (1, 2) shaly, (3, 4) slighly shaly or silty, (5, 6) clean; b — siltstones with varying degrees of shaliness; c — siltstones.

clay has been given by Vendel'shtein [156]. It is obvious that the effect — the change in formation factor with salinity — is more pronounced in clay-rich rocks. The effect of salinity on the formation factor of shaly rocks is accompanied by a variation in resistivity for rocks as a function of grain size. The resistivity of fine-grained rocks saturated with a high salinity brine is always greater than the resistivity of medium- or fine-grained rocks saturated with the same brine. With low salinities, the opposite is true.

These phenomena have been explained by Dakhnov as follows. For a highly saline electrolyte, a portion of the ions leave the solution and enter an electrical double layer. Ions in the double layer have a lower mobility than free ions in response to an externally applied electric field; therefore, the resistivity is increased. Thus, the greater the amount of clay in a rock, the larger will be the surface area over which the double layer forms, and the

greater will be the relative increase in the resistivity of the rock. Lowering of the resistivity of shaly rocks when they are saturated by dilute solutions is explained by the effects of surface conductance, which arises from partial hydrolysis of clay minerals. The results of this hydrolysis contribute to conductivity. The higher the shaliness, the greater will be the number of ions released in hydrolysis and, therefore, the lower will be the resistivity of the rock.

Surface conductivity depends on the existence of a high-conductivity double layer, which becomes thinner with increasing salinity and finally becomes insignificant [157].

In considering the effect of surface conductance, a special parameter related to the percent clay content in a rock is defined by the ratio of the formation factor for a clayey rock saturated with an electrolyte of a given salinity to the formation factor for the same rock in a clay-free condition. The effect of shaliness is to increase this parameter with increasing water resistivity. The relationship between resistivity in shaly rocks and porosity is quite complicated in detail [24, 139].

The presence of shaly material in oil-bearing rocks reduces their resistivities markedly, so that the resistivities of such rocks may be moderate or low.

Electrical Resistivity of Oil-Bearing Rocks

It has been indicated in the preceding section that the resistivity of a rock which is completely saturated with a brine is determined by the porosity to a first approximation. However, the pore spaces in a rock may not always be saturated with an aqueous electrolyte. Sedimentary rocks above the water table or forming gas reservoirs may be only partially saturated with water. Also, in oil reservoirs, oil may partially replace water in the pore spaces. The presence of oil, natural gas, or air in the pore structure of a rock may increase the resistivity significantly over what it would be in a completely water-saturated rock. Dry rock, oil, and gas have practically infinite resistivities. The higher the oil or gas saturation in a rock, the higher will be the resistivity. However, for a given oil or gas saturation, the resistivity of a rock may vary widely, depending on the salinity of the residual water in the pores, the distribution of fluids in the pores, and so on.

The Effect of Pressure on the Electrical Resistivity of Water-Saturated Crystalline Rocks

W. F. Brace

Department of Geology and Geophysics
Massachusetts Institute of Technology, Cambridge

A. S. Orange

Geoscience, Incorporated, Cambridge, Massachusetts

T. R. Madden

Department of Geology and Geophysics
Massachusetts Institute of Technology, Cambridge

Abstract. Electrical resistivity of eight igneous rocks and two crystalline limestones was measured at pressures to 10 kb. The rocks were saturated with tap water or salt solution, and the pore pressure was maintained near zero. The dependence of resistivity on temperature, porosity, and pore fluid salinity suggested that conduction was primarily electrolytic throughout the entire pressure range, even though the porosity of some rocks was less than 0.001. Resistivity increased with increasing pressure. The average increase over the 10-kb range amounted to a factor of 250. The changes of resistivity with pressure parallel changes of compressibility with pressure, being rapid over the first 2 kb and tapering off more gradually at higher pressures. The data suggest that the electrical conduction of these rocks consists of (1) conduction along cracks, below a few kilobars pressures, and (2) volume and surface conduction along a network of pores which persist throughout the entire pressure range. Surface conduction of the rocks saturated with tap water was 10 to 20 times greater than the volume conduction of the pores. The dependence of conductivity on porosity for all the samples saturated with saline solution followed the same empirical law that is observed for porous sedimentary rocks, $\sigma(\text{rock}) = \sigma(\text{solution}) \times \eta^2$.

Introduction. A great deal is known about the electrical resistivity of rocks having a porosity of 5% or more, under conditions of interest in petroleum exploration [see *Wyllie*, 1963, for example]. The effects of porosity itself, temperature, clay content, and degree of saturation on resistivity seem to be well understood. Considerably less is known about the resistivity of crystalline rocks like granite or diabase, particularly under conditions likely to prevail at deeper levels in the crust. A few observations have been reported of the effects of elevated temperature and pressure on the resistivity of dry rocks. *Parkhomenko and Bondarenko* [1963] found that a diabase or amphibolite at 10 kb pressure had a resistivity of 10^8 to 10^9 ohm meters and that resistivity decreased up to 70% in 40 kb. The same rocks under low confining pressure and saturated with water may have a resistivity of 10^4 or 10^5 ohm meters. Near-surface rocks probably approach this latter condition, and it is of some interest to determine just how quickly characteristics more nearly akin to the dry state are attained as pressure is increased. As most typical crustal rocks have only a minute porosity, this transition might occur under only moderate pressure. But if minute water films persist within interstices in spite of fairly high pressure, the resistivity might remain orders of magnitude below the dry values up to pressures corresponding to levels deep in the crust. In the present exploratory study, the resistivity of saturated crystalline rocks has been measured, particularly as a function of pressure, in order to gain a better understanding of the electrical characteristics as pore fluids are expelled.

In recent studies of the effect of pressure on elastic properties of rocks, the role of porosity for rocks like granite was found to be very important [*Birch*, 1961; *Brace*, 1965]; this was surprising because porosity of granite may be

only a few tenths of a per cent. The reason is that certain of the interstitial openings are not rounded as they are in typical limestone or sandstone but are in the form of cracks. In contrast to round openings, which require a pressure of the order of Young's modulus to be closed [Walsh, 1965a], cracks change shape and even close under slight pressure. Crack closure leads to a big change in apparent elastic modulus or compressional wave velocity. This is reflected in a very rapid increase in elastic modulus or velocity with confining pressure up to about 3 to 4 kb, which is the pressure at which most cracks in rocks are closed.

Because of the importance of crack porosity and crack closure in elastic and even thermal behavior [Walsh, 1965b] under pressure, it was natural to suspect that electrical resistivity might be similarly affected, if cracks did in fact serve as conduction paths. With this possibility in mind, we selected rocks from previous studies of elasticity, to see if resistivity and elastic properties underwent parallel changes with confining pressure.

Although the primary emphasis of the study was on effects of pressure and on comparison of electrical with mechanical characteristics, a few measurements were made as a function of temperature.

Experimental procedure. The general procedure was as follows: A cylindrical sample was prepared from a core or large block and then saturated with water or a salt solution. Resistance of the specimen was then measured as the jacketed sample was subjected to changes in confining pressure and temperature. Various physical properties such as linear compressibility and porosity were measured on the same specimen or on material adjacent to the specimen.

Thoughout this study, the term *pressure* can be taken to mean effective confining pressure [Handin et al., 1963], or overpressure, because pressure was applied to the sample through an impervious jacket and, although the rocks were

TABLE 1. Description of Rocks

Rock	Density g/cm^3	d, mm	Porosity			Modal Analysis
			η_c	η_p	η	
Granite, Casco, Maine	2.626	5.0	0.0045	0.002	0.007	45 or, 28 qu, 22 an$_{15}$, 5 mica
Granite, Stone Mt., Georgia	2.631	2.5	0.0035	0.002	0.006	30 qu, 24 mi, 42 an$_{10}$, 4 mica
Quartzite, Rutland, Vermont	2.643	0.30	0.0012	0.004	0.005	91 qu, 7 or, 2 mi
Granite, Westerly, Rhode Island	2.646	0.75	0.002	0.007	0.009	27.5 qu, 35.4 mi, 31.4 an$_{17}$, 4.9 mica
Limestone, Solenhofen	2.663	0.01	0	0.048	0.048	99 ca
Limestone, Oak Hall, Pennsylvania	2.712	0.075	0	0.002	0.002	99 ca
Granodiorite, Cape Cod, Massachusetts	2.715	6.5	0.001	0.003	0.004	42 or, 28 qu, 18 an$_{18}$, 12 mica
Anorthosite, Wadhams, New York	2.748	7.0	0	0.002	0.002	90 an$_{60}$, 7 au, 2 mica
Diabase, Frederick, Maryland	3.020	0.175	0	0.001	0.001	48 an$_{67}$, 49 au, 1 mica
Dunite, Addie, North Carolina	3.255	1.0	0.002	0.001	0.003	80 fa$_{12}$, 19(?) serp

Abbreviations:
qu	quartz
or	orthoclase
mi	microcline
ca	calcite
an	plagioclase with anorthite content
fa	olivine with fayalite content
au	augite-hypersthene
mica	muscovite, biotite, chlorite
serp	serpentine

initially saturated, pore pressure was maintained near zero.

Physical properties of the rocks studied are listed in Table 1. Several of the rocks were used in a previous study: Stone Mountain granite, Rutland quartzite, Westerly granite, Oak Hall limestone, and Maryland diabase [*Brace*, 1965] and Addie dunite [*Birch*, 1961]. The Solenhofen limestone is similar to the rock studied by *Robertson* [1955].

Of the new materials, the granodiorite comes from a core taken 256 m below the surface at Tubman, Cape Cod, Massachusetts. The anorthosite comes from a core taken at 455 m depth in no. 2 hole, Wadhams, New York. The Casco granite was collected by E. Decker from a core taken 262 m below the surface near Casco, Maine.

Mineral density, average grain diameter d, and crack prosity η_c, were determined as described elsewhere [*Brace*, 1965]. Total porosity η was found by immersion in CCl_4 and is the value used in the resistivity measurement. Pore porosity η_p is obtained from the relationship $\eta = \eta_c + \eta_p$. Differences between the values of η and η_p in Table 1 and those previously published arise from several sources. Total porosity of a rock such as Westerly granite is somewhat dependent on the ratio of sample area to volume. Different samples were used here and in the previous study [*Brace*, 1965]. Here, η_p was found from $\eta - \eta_c$; previously it was found by comparing calculated and measured intrinsic compressibilities. Uncertainty in crack porosity is ±0.0005, in the pore porosity reported here it is ±0.001.

Duplicate samples of each rock were prepared. Diameter was 2.5 cm and length varied from 1.6 cm for the fine-grained material, such as Solenhofen limestone or Westerly granite, to 4 cm for the coarse-grained anorthosite or granodiorite. Length was held to a minimum to keep resistance within easily measurable limits; a lower limit was placed by grain size. Unless the sample length was greater than about 10 grain diameters, the measured resistivity would probably not be representative of the rock as a whole.

Samples were next cleaned of cutting oil and other foreign material by soaking them in acetone for several days. This was followed by

determinations were usually made at this stage.

Complete saturation of the samples proved to be one of the more difficult operations. The method finally adopted was as follows: The dried sample was suspended above a pan of tap water or salt solution in a vacuum chamber. A pressure close to the boiling point of the water (about 25 mm Hg) was maintained for several hours, and then the sample was dropped into the water. Next, the vacuum was broken and the immersed sample placed in a pressure vessel and subjected to an N_2 pressure of 15 bars for a day or so. After slight warming to boil off dissolved N_2 the specimen was ready for measurement of resistivity. The important feature in the above operation is that air in the pores is removed before the fluid is introduced. Completeness of saturation was judged by repeatability of the resistance measurement. Early attempts at saturation by simply placing the sample in water for long periods of time, for example, were evidently unsuccessful; successive measurements of resistance might differ by a factor of 5 or 10. With the method described above, resistance at any pressure could be duplicated to within 10 to 15%. This was no assurance, of course, that the rock was 100% saturated, but most interconnected pores, including 'dead-ends,' were probably reached.

The experimental arrangement is shown in Figure 1. At each end of the specimen, which is a precisely ground right cylinder, is first a thin layer (about ½ mm) of 100-mesh ZrC.
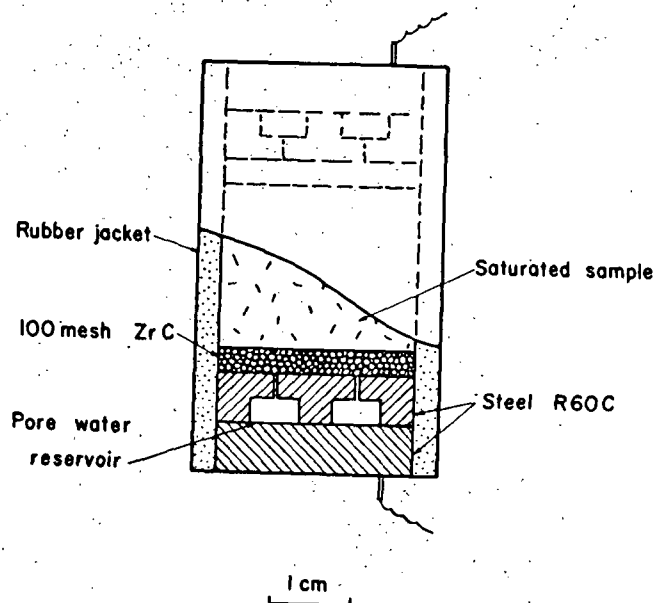

Fig. 1. Arrangement of specimen for resistivity

This hard material, which is also a good conductor, remains porous even under extreme pressure and allows movement of water outward from the sample. Next to the carbide powder is a hardened steel electrode in two parts; the inner part has holes to accommodate pore water driven out of the rock by the externally applied pressure. The holes in the steel remain open under pressure and are of greater volume than the pores in the rock, so that pore pressure in the sample remains approximately zero, regardless of the externally applied confining pressure. The entire assembly, specimen and electrodes, is covered by 3-mm-thick gum rubber tubing which keeps out the pressure medium (kerosene and petroleum ether).

Two samples could be accommodated at once in the pressure vessel, which was a standard piston-cylinder type. Pressure above 1 kb was measured by a manganin coil and by a Heise bourbon tube gage at lower pressure. Accuracy of measured pressure was better than $\frac{1}{2}\%$. The temperature of the pressure vessel, pressure medium, and samples was maintained by an external bath to a variation of less than 1°. Leakage resistance between electric leads and pressure vessel was 10^9 to 10^{10} ohms.

Absolute accuracy of the resistance measurement was no better than 10 to 15%, so that no correction was made for changes in dimension of the samples due to compressibility. Frequency dependence of resistance was small. For example, for six different specimens, resistance at 25 cps ranged from 5 to 10% less than resistance at 0.25 cps.

When the pressure was changed, some time was required for resistance to reach a constant value; for relatively porous rocks, such as Westerly granite or Solenhofen limestone, half an hour was required. For the tighter rocks, such as the dunite or anorthosite, an hour was required. An entire pressure run therefore required 6 to 12 hours, depending upon the rock.

The resistance of the sample was also measured at constant pressure for different temperatures.

Numerical observations. All the observations are listed in Table 2. The number given at any pressure is the average resistivity ρ for two or more runs on each of two samples. For example, the resistivity of Stone Mountain granite in tap water at 1 kb was 3.3×10^4 ohm meters; all of the measurements at this pressure (in this case 5) were within 18% of this value. No range is given when only a single measurement was made.
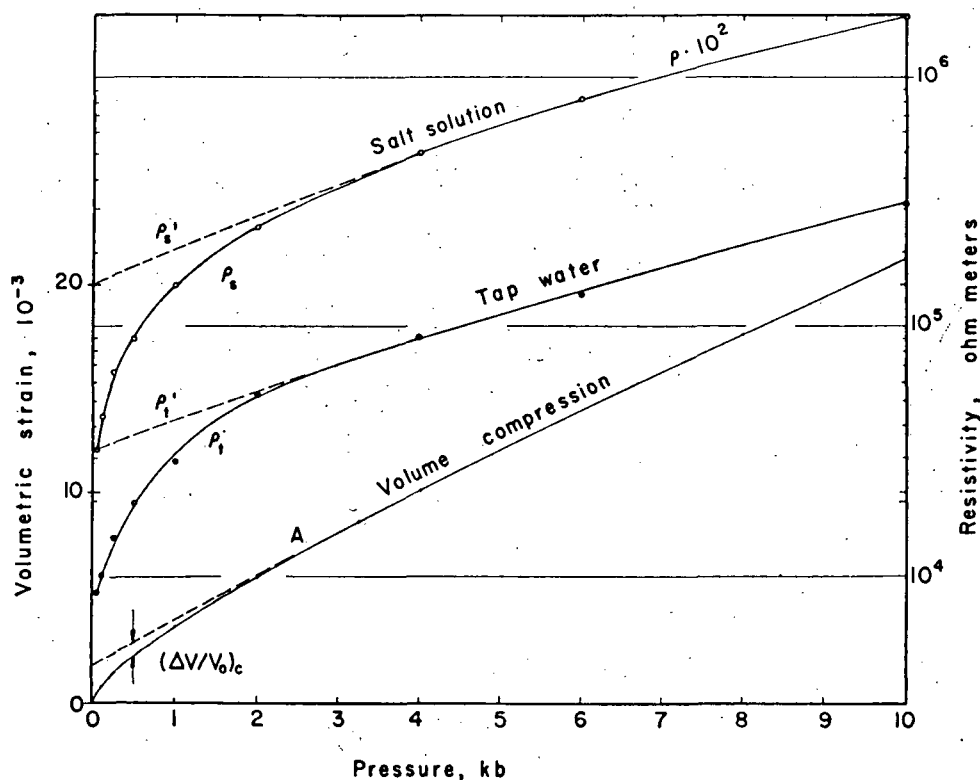

Fig. 2. Volume change and resistivity of Westerly granite as a function of pressure. Curves marked ρ_s' and ρ_t' are extrapolated from the region of high pressure.

TABLE 2. Resistivity and Volume Change as a Function of Pressure and Temperature

Resistivities are in ohm meters, volume compressions, $^3\Delta V/V_0 \times 10^3$. ρ_t is the resistivity in tap water, ρ_s in salt solution. ρ_c is explained in text. The exponent given is the power of 10 and the number in parentheses half the range of all measured values expressed as a per cent of the mean. Measurements were made at 10 cps.

	Pressure, kb								
	0.05	0.1	0.25	0.5	1	2	4	6	10
Granite, Casco									
ρ_t 20°	$8.5^3(40)$	$1.2^4(40)$	$2.4^4(35)$	$3.5^4(35)$	$6.8^4(30)$	$1.4^5(28)$	$2.8^5(35)$	$5.3^5(30)$	$1.3^6(28)$
ρ_s 20°	5.2^2	7.5^2	1.5^3	2.9^3	5.9^3	1.2^4	2.8^4		1.1^5
ρ_c 20°	5.6^2	8.4^2	1.9^3	4.5^3	1.2^4	8.8^4			
$\Delta V/V_0$	1.21	2.13	3.48	4.53	5.91	8.22	12.45		
$(\Delta V/V_0)_c$	2.91	2.21	1.20	0.66	0.26	0.09	0		
Granite, Stone Mountain									
ρ_t 20°	$4.4^3(20)$	$5.7^3(18)$	$9.5^3(11)$	$1.6^4(15)$	$3.3^4(18)$	$8.2^4(24)$	$3.2^5(28)$	$7.0^5(30)$	$1.6^6(25)$
ρ_s 20°	$2.5^2(10)$	$3.6^2(10)$	$6.9^2(12)$	$1.3^3(10)$	$2.8^3(8)$	$7.4^3(8)$	$2.8^4(5)$	$8.0^4(6)$	2.0^5
$\Delta V/V_0$	0.80	1.29	2.26	3.34	4.74	7.12	11.23		
$(\Delta V/V_0)_c$	2.38	2.00	1.36	0.79	0.43	0.08	0		
Quartzite, Rutland									
ρ_t 20°	$4.9^3(22)$	$6.0^3(25)$	$9.5^3(20)$	$1.4^4(20)$	$2.4^4(18)$	$4.1^4(15)$	$8.4^4(13)$	$1.4^5(5)$	$2.9^5(5)$
ρ_s 20°	$4.0^2(5)$	$5.9^2(5)$	$1.1^3(5)$	$1.8^3(5)$	$3.2^3(5)$	$6.0^3(5)$	$1.2^4(5)$	$2.0^4(5)$	$4.5^4(5)$
ρ_c 20°	4.5^2	7.2^2	1.5^3	3.3^3	6.3^3				
$\Delta V/V_0$	0.39	0.68	1.37	2.20	3.66	6.27			
$(\Delta V/V_0)_c$	0.90	0.74	0.44	0.24	0.04	0			
Granite, Westerly									
ρ_t 20°	$8.5^3(20)$	$1.0^4(20)$	$1.4^4(20)$	$1.9^4(20)$	$2.8^4(22)$	$5.2^4(24)$	$9.0^4(22)$	$1.3^5(12)$	$3.2^5(20)$
ρ_t 40°					2.0^4			8.6^4	
ρ_t 65°					1.6^4			6.3^4	
ρ_s 20°	$3.1^2(5)$	$4.2^2(5)$	$6.5^2(5)$	$9.3^2(5)$	$1.4^3(5)$	$2.5^3(5)$	$4.9^3(5)$	$8.2^3(5)$	$1.8^4(5)$
ρ_c 20°	3.9^2	5.7^2	1.1^3	1.9^3	4.5^3	1.8^4			
$\Delta V/V_0$	0.42	0.76	1.41	2.19	3.57	5.89	10.15		
$(\Delta V/V_0)_c$	1.43	1.24	0.88	0.67	0.32	0.04	0		
Limestone, Solenhofen									
ρ_t 20°	$1.1^3(5)$	$1.1^3(5)$			$1.1^3(5)$	$1.2^3(5)$	$1.4^3(5)$		
ρ_s 20°	4.6^1				5.8^1	6.4^1	7.7^1		
Limestone, Oak Hall									
ρ_t 20°	$1.4^4(40)$	$2.3^4(40)$	$9.0^4(50)$	$2.0^5(35)$	$2.5^5(30)$	$3.9^5(37)$	$7.0^5(45)$		$2.8^6(40)$
Granodiorite, Cape Cod									
ρ_t 20°	$1.4^4(7)$	$1.8^4(3)$	$2.4^4(1)$	$3.1^4(7)$	$4.4^4(16)$	$6.2^4(10)$	$9.8^4(6)$	$1.6^5(4)$	$2.8^5(5)$
ρ_t 40°					2.8^4			9.3^4	
ρ_t 65°					$1.9^4(10)$			6.0^4	
ρ_s 20°	$2.1^3(6)$	$3.1^3(13)$	$6.3^3(6)$	$8.8^3(5)$	$1.3^4(5)$	$1.9^4(5)$	$2.9^4(5)$	$3.8^4(5)$	$7.0^4(5)$
ρ_c 20°	2.4^3	3.9^3	1.0^4	2.0^4	4.4^4	3.2^5			
$\Delta V/V_0$	0.42	0.66	1.14	1.74	2.82	4.86	8.64		
$(\Delta V/V_0)_c$	0.96	0.78	0.60	0.39	0.30	0.10	0		
Anorthosite, Wadhams									
ρ_t 20°	$8.0^4(25)$	$9.0^4(30)$	$1.2^5(20)$	$1.4^5(18)$	$1.8^5(17)$	$2.4^5(20)$	$5.1^5(20)$	$9.5^5(20)$	$3.6^6(25)$
ρ_t 40°					1.3^5			6.0^5	
ρ_t 65°					$8.2^4(12)$			4.0^5	
ρ_s 20°	$2.7^3(12)$	$5.4^3(15)$	$1.1^4(10)$	$1.6^4(8)$	$2.3^4(5)$	$3.5^4(7)$	$6.7^4(1)$	$1.2^5(4)$	$3.3^5(1)$
Diabase, Maryland									
ρ_t 20°	$1.1^5(10)$	$2.6^5(5)$	$3.3^5(9)$	$3.9^5(15)$	$5.0^5(13)$	$8.9^5(13)$	$2.5^6(18)$	$5.5^6(10)$	$1.6^7(5)$
ρ_t 40°					2.8^5			3.2^6	
ρ_t 65°					$1.5^5(20)$			1.8^6	
ρ_s 20°	4.1^3	1.2^4	2.3^4	3.0^4	4.3^4	7.3^4	1.9^5		1.7^6
Dunite, Addie									
ρ_t 20°	$1.5^4(7)$	$3.5^4(5)$	$1.0^5(2)$	$2.0^5(1)$	$3.0^5(2)$	$5.1^5(2)$	$9.6^5(4)$	$1.3^6(6)$	$1.9^6(9)$
ρ_s 20°	2.7^3	6.7^3	1.6^4	2.7^4	4.6^4	8.7^4	1.9^5	3.3^5	7.6^5

The tap water had a resistivity of 40 to 50 ohm meters; the NaCl solution, a resistivity of 0.30 ohm meters.

The volume compressions were obtained using methods described by *Brace* [1965]. Although expressed in that paper as $\beta = -(1/V_0)(dV/dP)$, the quantity $-\Delta V/V_0$ is given here; both quantities were found from the same experiment. Several new determinations were made for the present study, for Casco granite, the granodiorite, and the anorthosite.

The quantity $(\Delta V/V_0)_c$ is the volume compression due to crack closure. For example, in Figure 2, $-\Delta V/V_0$ for Westerly granite is plotted as a function of pressure. As discussed by *Brace* [1965] and *Walsh* [1965a], the marked curvature between zero and about 3 kb may be interpreted as due to crack closure in this rock.
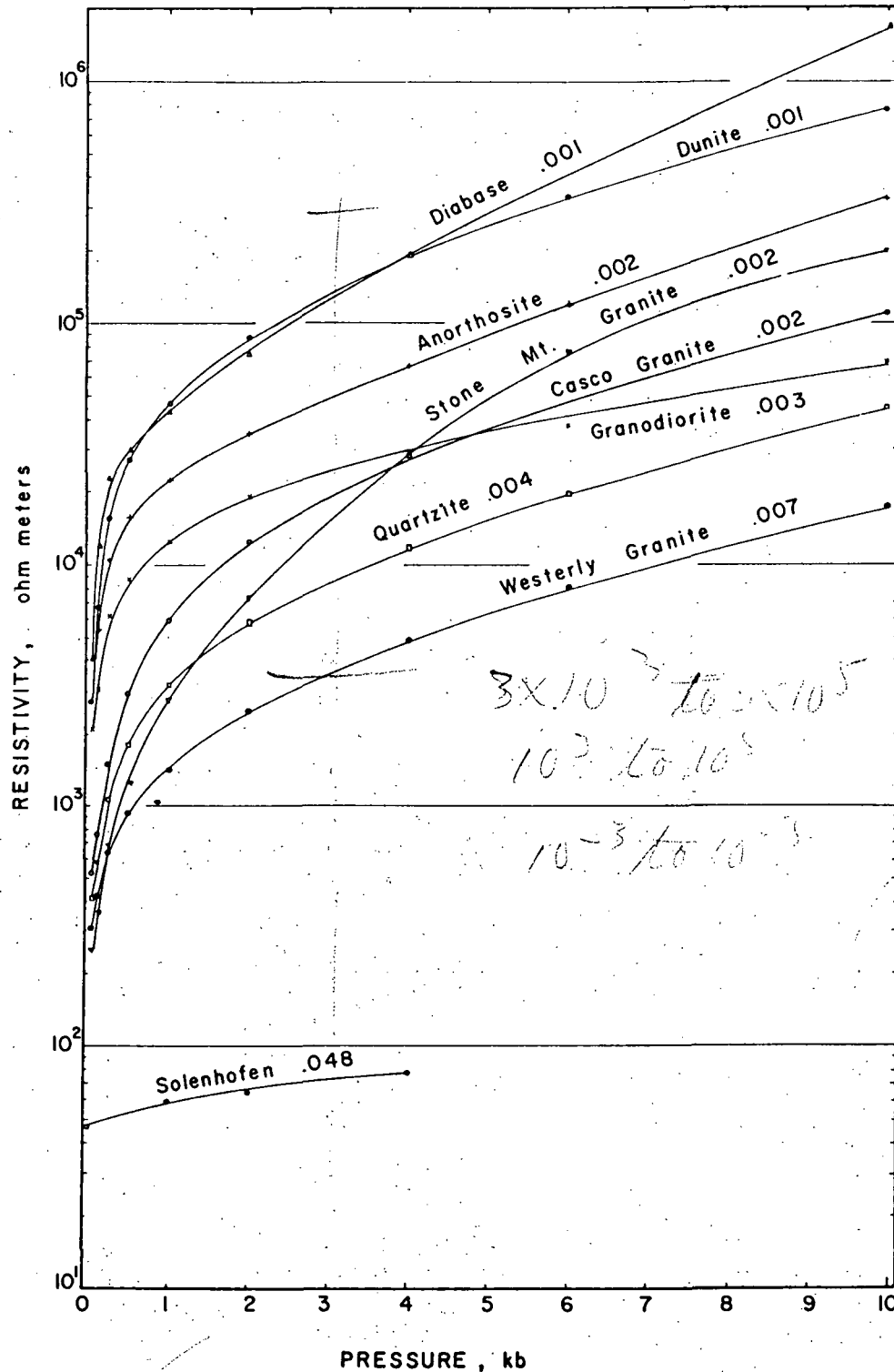
Fig. 3. Resistivity as a function of pressure in salt solution at 20°C.

Above about 3 kb the curve reflects essentially the intrinsic elastic compressibility of the minerals in the rock. Projecting the straight part of the curve back to zero pressure gives the compression which the rock would have were there no cracks. *Crack porosity* $(\Delta V/V_0)_c$, then, is the difference at any pressure between the actual and projected curves, as shown in Figure 2. Above point A, crack porosity is zero. Crack porosity and total volume compression are given in Table 2 for certain of the rocks up to the pressure at which cracks are apparently closed. At zero pressure the value of crack porosity is called η_c; this is the quantity given in Table 1.

Measurements on Solenhofen limestone were made only to 4 kb pressure. Above this pressure the rock undergoes permanent volume change.

Discussion. Resistivity of the rocks saturated with salt solution is plotted in Figure 3. The curves for tap water are similar in form. Several general characteristics are evident. Resistivity of all the rocks increases with pressure, by as much as 10^3. For all except Solenhofen, the increase is in two stages: a very rapid initial increase followed, above approximately 2 kb, by a more gradual nearly linear increase. The relative change of ρ from zero to about 2 kb increases with crack porosity of the rock (compare curves in Figure 3 with values of η_c in Table 1). Above about 2 kb, the absolute value of ρ increases systematically with decreasing pore porosity (the value of η_p is shown above each curve in Figure 3). From Table 2, the maximum resistivity of any of the rocks, at the highest pressure, is still several orders of magnitude below the resistivity (10^9 to 10^{10} ohm meters) of quartz, feldspar, and other common minerals. Although there appears to be some grouping according to mineralogy in Figure 3 (acid rocks with low and basic rocks with high resistivity), this is probably fortuitous. Almost certainly, resistivity at all pressures in these rocks is determined principally by pore geometry and resistivity of the pore fluids.

It is of interest to examine several of these observations in more detail. Some of the measurements as a function of temperature are shown in Figure 4. A change in temperature appears to change resistivity by an amount that is independent of pressure. The change of resistivity of four of the rocks at a single pressure

is shown in Figure 5. Decrease of resistivity over this temperature interval is about the same for these different rocks and is about the same as the relative decrease in viscosity of water *Bridgman*, 1952, p. 346] over the same temperature interval. A similar result obtained at 6 kb pressure suggests that, over the entire pressure range studied here, conduction is by flow of ions in the pore fluids. Ionic conduction has generally been assumed for rocks at atmospheric pressure [*Birch et al.*, 1942, p. 300; *Madden and Marshall*, 1959, p. 47].

Since most of the current flows through the interstitial fluids, it ought to be possible to separate conduction along cracks (which close under a few kilobars pressure) from conduction through pores (which remain open under pressure), just as it is possible [*Brace*, 1965; *Walsh*, 1965a] to differentiate crack from pore porosity. In addition, we might expect, in rocks which have narrow water-filled interstices a third conduction path, namely *surface conduction* [*Overbeek*, 1952].

These three contributions can be separated as follows. Cracks in these rocks are closed at pressures higher than about 3 kb, so that conduction at higher pressure will be through a network of pores, assisted perhaps by surface conduction. Measured values of conductivity (equal to ρ^{-1}) at 4 kb (from Table 2) are plotted as a function of pore porosity (from Table 1) in Figure 6. The values for the rocks saturated with salt solution fall very close to a straight line of slope +2. At 10 kb the values fall near a line of slope +2.1. For the rocks saturated with tap water, data points are more widely scattered but roughly follow the curve
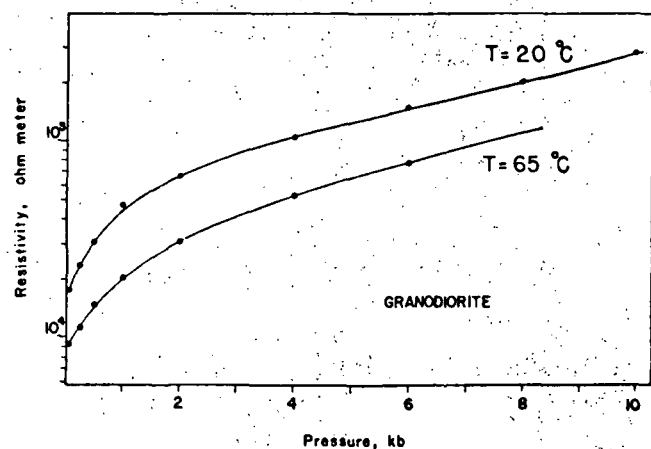

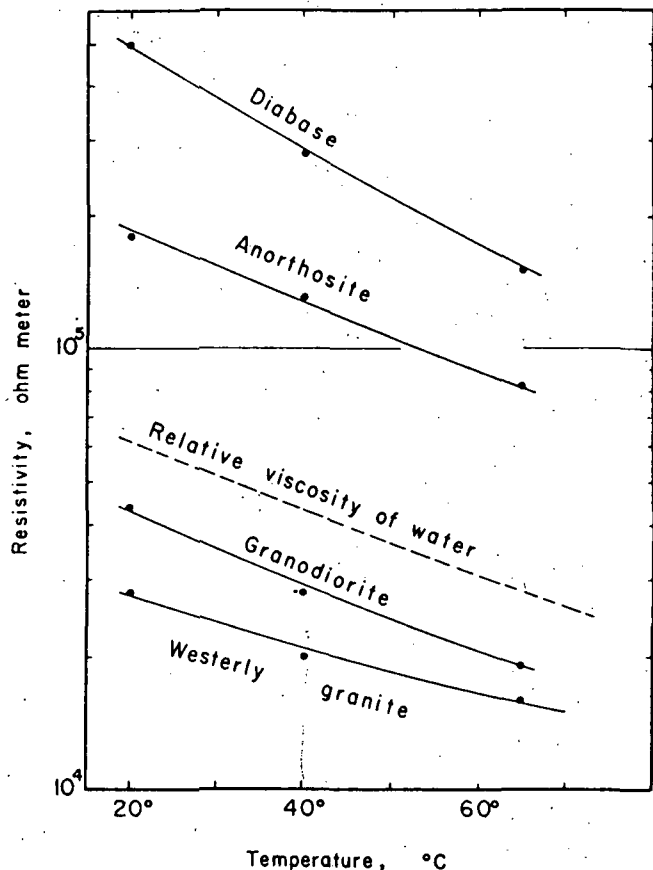Fig. 4. Resistivity as a function of pressure and temperature for granodiorite in tap water.

Fig. 5. Resistivity as a function of temperature at 1 kb.

Fig. 6. Conductivity at 4 kb as a function of pore porosity in tap water and in salt solution.

shown. From the known conductivities of the tap water (45 ohm meters) and salt solution (0.30 ohm meters) the samples in tap water ought to fall along the second lower line of slope $+2$. They do not, and conductivity is 10 to 20 times greater than if conduction were solely through the bulk of the pore water. This increase is probably due to surface conduction [*Madden and Marshall*, 1959, p. 55], which in turn is due to an excess of ions electrically attracted to the vicinity of the solid-liquid interfaces. It adds considerably to the conduction through narrow pores in dilute solutions, but its effect is apparently drowned out by the bulk conductivity of saline solutions. The difference between the two lower curves in Figure 6 gives a measure of surface conductivity; a convenient way of expressing this, using a ratio of resistivity of tap water to salt solution of 150, is $150\rho_s/\rho_i$. This quantity is readily calculated from the data in Table 2 for any pressure above that necessary to close cracks. This is done for 4 and 10 kb (Table 3); the calculation for 50 bars is explained below.

In a plot of 4 kb conductivity versus pore porosity (Figure 6) the data points lie very close to the line

$$\sigma_s/\sigma_0 = \rho_0/\rho_s = \eta_p^2 \qquad (1)$$

where σ is conductivity, ρ is resistivity, the subscript s refers to rock saturated with salt solution and the subscript o refers to salt solution alone. It is rather remarkable to find that this same empirical relationship is followed by typical sandstone and limestone from oil-bearing formations [*Wyllie*, 1963, p. 30], where porosity ranges from 5 to 20%. It is also remarkable because it suggests that tortuosity of all rocks of the same (pore) porosity must be about the same. This is seen from the general relationship [*Madden and Marshall*, 1959, p. 51]

$$\sigma_s/\sigma_0 \approx \tau^{-2}\eta$$

which, when combined with (1), implies that τ is proportional to $\eta^{-1/2}$. This does not seem un-

TABLE 3. Surface Conductivity
The value shown is the ratio $150\rho_s/\rho_t$. ρ_s' and ρ_t'
are obtained as explained in the text;
units are ohm meters.

Rock	ρ_s'	ρ_t'	$150\rho_s/\rho_t$ Pressure, kb		
			0.05	4	10
Granite, Westerly	1.5^3	4.1^4	6	8	8
Limestone, Solenhofen	5.2^1	1.1^3	7	8	
Diabase, Maryland	3.0^4	3.4^5	13	13	16
Granite, Casco	7.0^3	7.5^4	14	15	13
Quartzite, Rutland	3.6^3	2.7^4	20	21	23
Anorthosite	1.8^4	1.3^5	21	20	14
Granodiorite, Cape Cod	1.5^4	5.6^4	40	44	38

reasonable, for we might expect tortuosity to increase as porosity decreases.

Resistivity of most of the rocks increases uniformly with pressure in the range 4 to 10 kb (Figure 3). This increase could be explained in a number of ways. One passageway after another might be cut off as pressure increases and the walls of passageways meet at the narrowest points, or the increase might be due simply to elastic distortion of tubular passageways. This second possibility can be evaluated from knowledge of the elastic properties of the rock. If we assume that tubular passageways have a circular cross section, the resistivity of the rock ρ will be related to pressure P in the following way:

$$d \ln \rho/dP = a\beta$$

where β is compressibility and a is a constant equal to about 5/3 for a circular cross section. For Westerly granite $d \ln \rho/dP$ is about 10^{-4} bar^{-1}; using β of 2 mb^{-1}, calculated $d\ln \rho/dP$ is about 3×10^{-6} bar^{-1}. Evidently elastic distortion gives far too small a change, at least for openings that are more or less equidimensional in cross section.

Turning next to conduction at pressures less than 4 kb, we first need to separate the contribution of cracks from that of pores. In Figure 2, point A is approximately the pressure at which cracks have closed in this rock; it coin-
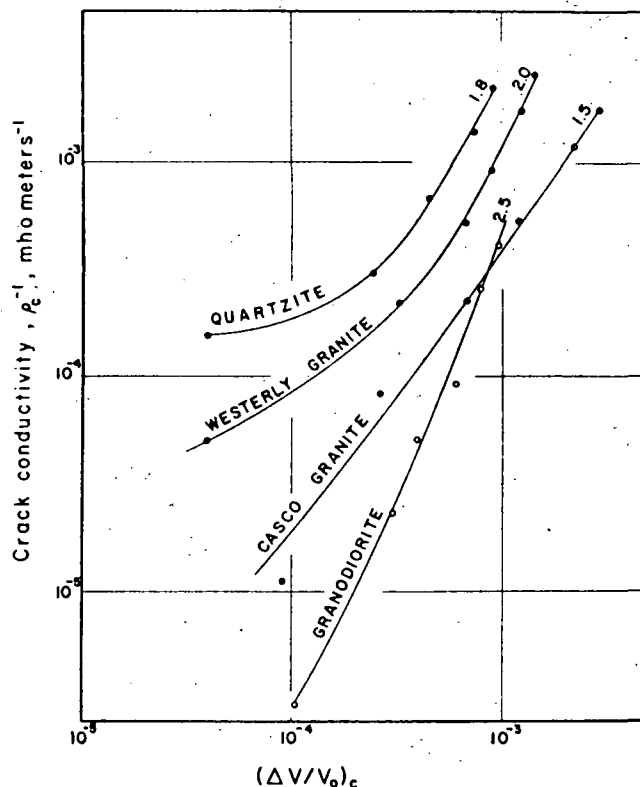

Fig. 7. Crack conductivity as a function of crack porosity in salt solution at 20°C. The number at the top of each curve is the slope.

cides roughly with the point at which resistivity assumes a more gradual increase with pressure. This suggests that conduction along cracks occurs below A and is eliminated as cracks are closed. Of course, some conduction paths must remain above about 3 kb to provide so-called pore conductivity. The continued increase of resistivity with pressure suggests that pore cross sections change also with pressure, although in a less drastic fashion than the change of crack cross sections at low pressure.

The magnitude of conduction through cracks alone is found as follows. Although the plot of resistivity versus pressure above 4 kb (Figure 2) is slightly curved, it can be approximately extended (the dotted line in Figure 2), keeping curvature constant, back to zero pressure. This dotted line represents the resistivity the rock would have were there no cracks. The difference between this line and the actual curve of ρ versus pressure can be considered a measure of crack conductivity. The magnitude, calculated by assuming that pores and cracks form parallel conduction paths, is given (as a resistivity, ρ_c) in Table 2.

Crack conductivity can be determined with some confidence for four rocks (Figure 7). Al-

though the uncertainty in both parameters plotted in Figure 7 is quite large (at least a factor of 2 near the lower ends of the curves), the curves have certain features in common. They are nearly straight at the upper ends (where the greatest changes in crack porosity occur), with slopes suggestive of the same relationship (equation 1) found above for pore conductivity. At the lower ends the curves flatten in a transition to conduction which is primarily through pores.

Returning to surface conductivity, we calculate the value the rock would have had were there no cracks. We call the resistivities of such a rock ρ_s' and ρ_t' for tap water and salt solution, respectively. ρ_s' and ρ_t' are obtained from curves (see Figure 2) which have been extended back to zero from the region of 3 to 5 kb. The ratio $150\rho_s'/\rho_t'$ is shown in Table 3 for 50 bars, for comparison with the same quantity calculated at the higher pressures.

Apparently the ratio $150\rho_s/\rho_t$ varies little with pressure in these rocks. This indicates that surface conduction decreases with pressure in about the same way as pore conduction. This would seem to suggest that the cross section of pores is not being decreased gradually, but that, as pressure is increased, some passages are being completely cut off, together with the surface films which provide surface conduction.

References

Birch, F., The velocity of compressional waves in rocks to 10 kilobars, 1, *J. Geophys. Res., 65,* 1083–1102; 1960; 2, *66,* 2199–2224, 1961.

Birch, F., J. F. Schairer, and H. C. Spicer, Handbook of physical constants, *Geol. Soc. Am. Spec. Paper 36,* 325 pp., 1942.

Brace, W. F., Some new measurements of linear compressibility of rocks, *J. Geophys. Res., 70,* 391–398, 1965.

Bridgman, P. W., *The Physics of High Pressure,* 445 pp., T. Bell and Sons, London, 1952.

Handin, John, R. V. Hager, Jr., M. Friedman, and J. N. Feather, Experimental deformation of sedimentary rocks under confining pressure: pore pressure tests, *Bull. Am. Assoc. Petrol. Geologists, 47,* 717–755, 1963.

Madden, T. R., and D. J. Marshall, Induced polarization, *U. S. At. Energy Comm. Rept. RME-3160,* 80 pp., 1959.

Overbeek, J. Th. G., Electrochemistry of the double layer, in *Colloid Science,* edited by H. R. Kruyt, pp. 115–190, Elsevier Publishing Company, New York, 1952.

Parkhomenko, E. I., and A. T. Bondarenko, An investigation of the electric resistivity of rocks at pressures up to 40,000 kg/cm^2 and temperatures up to 400°C, *Izv. Akad. Nauk SSSR, Geofiz. Ser.,* no. 12, 1106–1111, 1963.

Robertson, E. C., Experimental study of the strength of rocks, *Bull. Geol. Soc. Am., 66,* 1275–1314, 1955.

Walsh, J. B., The effect of cracks on the compressibility of rocks, *J. Geophys. Res., 70,* 381–389, 1965a.

Walsh, J. B., The effect of cracks on the thermal conductivity of rocks (abstract), *Trans. Am. Geophys. Union, 46,* 176, 1965b.

Wyllie, M. R. J., *The Fundamentals of Well Log Interpretation,* 3rd ed., 238 pp., Academic Press, New York, 1963

Further Studies of the Effects of Pressure on Electrical Resistivity of Rocks

W. F. Brace

Department of Geology and Geophysics, Massachusetts Institute of Technology
Cambridge, Massachusetts 02139

A. S. Orange

Geoscience, Inc., Cambridge, Massachusetts 02139

The effects of pressure of up to 10 kb on the electrical resistivity of 30 widely differing crystalline rocks is analyzed. For rocks of low porosity (0.01–0.001), degree of saturation affects both resistivity and the effect of pressure on resistivity. At low pressure the difference in the effect of pressure is particularly marked: a partially saturated rock becomes less resistive, whereas saturated rock becomes more resistive as the pressure increases. Porosity is the sole property which determines the high pressure resistivity of water-saturated rocks composed of nonconducting minerals. Grain size, mineralogy, and degree of alteration, when considered apart from porosity, have almost no effect. Variation in resistivity within one formation or rock type is as great as that among widely different rock types.

At pressures above about 3 kb, we found close agreement with two empirical laws connecting resistivity, ρ, pressure, P, and porosity, η: $\rho_{rock}/\rho_{fluid} = \eta^{-2}$ and $1/\rho \, (d\rho/dP) = 0.10$ kb^{-1}. With the first relation, resistivity of a rock of known porosity can be calculated relative to fluid resistivity, and with the second, the effect of pressure of up to 10 kb.

For a rock composed of conductive minerals, pressure at first decreases resistivity sharply and, then, has almost no effect. For rocks in which pressure causes collapse of pores, resistivity may either increase or decrease with pressure depending on initial connectivity of pores; an increase is the more common. Coarse-grained rocks containing calcite became abnormally resistive at high pressure owing to, we believe, flow of the mineral calcite, with sealing off of interstices. This would suggest the presence of local shearing stress in our hydrostatic experiments. There was no indication of flow in rocks containing dolomite, mica, or serpentine.

Introduction

In an earlier paper [*Brace et al.*, 1965; referred to below as '*BOM*'] we described the pronounced effect of confining pressure on the electrical resistivity of ten water-saturated crystalline rocks. Resistivity increased by as much as three orders of magnitude in 10 kb pressure; much of the change took place during application of the first few kilobars. We attributed this not to changes in resistivity of the minerals, but rather to changes in cross-section of water-filled pore spaces. In water-saturated crystalline rocks, conduction is almost wholly through the pore fluids. The pore spaces change shape when a rock is subjected to pressure, particularly at low pressure. The drastic increase in resistivity observed at low pressures is reflected in the closure of cracklike pore spaces known to be present in rocks from studies of elastic properties [*Adams and Williamson*, 1923; *Birch*, 1961; *Walsh and Brace*, 1966].

Although our observations seemed to be consistent with the general behavior of crystalline rocks under pressure, a number of questions were raised. For one thing, the effect of pressure we reported (increased resistivity with pressure) was just the opposite of that observed elsewhere [*Parkhomenko*, 1967]. The difference may have been due to the degree of saturation of the rocks [*Brace and Orange*, 1968], but additional experiments were needed to test this possibility. In addition to partial saturation, we also wished to study the effect of pressure on a rock containing minerals which were partly conducting. Would pressure still cause the resistivity to increase?

We were concerned about the generality of our results. Would a wider sampling of rock types, perhaps including porous or altered rocks, reveal important departures from what seemed like general characteristics? Would the relation we had found between resistivity and porosity

continue to hold if we widened our selection of rocks? Finally, we wished to explore one phenomenon observed during our study of the effects of stress on resistivity [*Brace and Orange*, 1968]. Under stress, marble became virtually nonconducting, apparently owing to the sealing off of pore spaces owing in turn to flow of calcite. Would other ductile rocks behave in this way, and would pressure as well as stress produce this effect? We studied the effects of pressure on twenty-two additional rocks, selected so as to throw light on these questions.

EXPERIMENTAL PROCEDURE

The physical properties of the rocks studied are listed in Table 1. The source of the specimens and their connection to other studies is given in the appendix.

It will be recalled from *BOM* that crack porosity, η_c, is obtained from compressibility. It was not feasible to measure compressibility for all our materials, so that the data for porosity in Table 1 are incomplete. Zero crack porosity is indicated by the lack of a pronounced low pressure toe in a resistivity-pressure curve, as shown, for example, by Solenhofen limestone and Maryland diabase in *BOM*. Among the present rocks such a toe was absent for Oak Hall limestone II, San Marcos gabbro, Twin Sisters dunite, Lynn felsite, and Jersey gabbro. We, therefore, assumed that the crack porosity of these rocks was zero.

Sample preparation, the experimental arrangement, and procedure were identical with those given in *BOM*. In one new procedure, rock samples of Westerly granite were partially saturated. After weighing the dry sample, it was first saturated in the usual manner. It was then placed on a balance and allowed to dry until a predetermined amount of water had evaporated. The sample was then quickly jacketed and resistivity measured in the normal manner.

Measurements of a 'dry' sample were made after drying in vacuo at 75° for 24 hours.

All of the observations are listed in Table 2, with the same notation used in *BOM*. Some of the measurements were made with tap water (50 ohm meters) and some with an NaCl solution (0.25 ohm meters). Many of the runs are plotted in Figures 1 and 2.

Measurements for dry, partially saturated (43%) and saturated Westerly granite are shown in Figure 3. The values for saturated rock are from *BOM*. The resistivities of the dry rock were at or beyond the limits of measurement in our system and the values shown are probably much less than the true values. Dry rock values given by *Parkhomenko* [1967] often reach 10^{10} for granite and 10^8 for diabase; resistivity of dry minerals such as quartz, mica and feldspar is in the vicinity of 10^{12} ohm-meters.

DISCUSSION

Effect of moisture content. The effect of moisture content on resistivity of a typical granite (Figure 3) is striking. At very low pressure even partial saturation, representing a few parts per thousand by weight of water, greatly reduces resistivity. If we take the true dry rock value to be 10^{10} ohm meters [*Parkhomenko*, 1967], then this reduction in resistivity amounts to a factor of 10^4. Complete saturation reduces the resistivity by an additional factor of 10^2, so that we could conclude that pore water lowers the resistivity of granite at very low pressure by about 10^6.

The effect of pressure on resistivity differs in an interesting way for partial and complete saturation. For complete saturation, resistivity ρ_t increases with pressure, at first rapidly and then, more gradually at higher pressure. For partial saturation, the rock is quite resistive at low pressure; the resistivity ρ_{tt} at first drops, then becomes constant, and finally, increases with pressure. Between 6 and 10 kb, the slope is about the same as for complete saturation. The values of resistivity for the two cases are, at pressures above 6 kb, within the variation we found for duplicate saturated samples in *BOM*. We conclude, therefore, that saturated and partially saturated samples here reached about the same resistivity above 6 kb.

Qualitatively, the three curves in Figure 3 may be considered characteristic of crystalline rocks that are dry, partially saturated, or completely saturated with a conducting fluid. Much detailed work reported by *Parkhomenko* [1967] indicates that pressure has very little effect on the resistivity of dry rocks up to the highest temperatures (500°–800°) applied. The curve of ρ_t versus pressure, on the other hand, is typical of practically all the water-saturated crystalline rocks we have studied. The only exceptions are rocks like Nahant gabbro (Fig-

TABLE 1. Description of Rocks

Rock	Density, g/cm^3	d, mm	Porosity, %			Modal Analysis
			η_c	η_p	η	
Rhyolite tuff, Castle Rock, Colo.	2.45	0.5	0	40	40	33 gl, 20 qu, 40 or, 4 an$_{10}$, 2 ox
Pottsville sandstone, Spring City, Tenn.	2.620	0.20	0.3	2.6	2.9	46 qu, 41 or, 11 mica, 2 ox
Limestone, Bedford, Ind.	2.620	1.0	0	12	12	99 ca?
Granite, Lanesville, Mass.	2.627	6.0	?	?	0.6	47 qu, 52 or, 2 am
Lynn felsite, Saugus, Mass.	2.673	0.1	0.1	0.2	0.3	40 or, 35 an$_{30}$, 25 qu, 2 ox, 1 mica
White marble, source unknown	2.715	0.20	0.1	0.2	0.3	99 ca
Limestone, Oak Hall, Pa., I	2.712	0.08	0	0.2	0.2	99 ca
Limestone, Oak Hall, Pa., II	2.746	0.10	0	0.6	0.6	98 ca-do, 1 qu, 1 ox
Grenville marble, St. Jovite, Quebec	2.748	2.5	?	?	0.4	90 ca, 4 pyr, 2 ol, 2 an$_{10}$, 2 ox
Black slate, source unknown	2.776	0.020	0.2	1.0	1.2	55 mica, 30 qu, 15 ca
Gabbro, San Marcos, Calif.	2.819	2.0	0	0.2	0.2	70 an$_{42}$, 12 mica, 8 pyr, 7 am, 3 ox
Blair dolomite, W. Virginia	2.847	0.075	0.1	0.1	0.2	85 do, 6 ca, 9 insol. res.
Dolomite, Chittenden, Vt.	2.861	5.0	?	?	1.0	98 do, 2 mica
Dolomite, Webatuck, Dover Plains, N. Y.	2.867	0.66	0.1	0.5	0.6	99 do, 1 ox
Chlorite schist, Chester, Vt.	2.874	0.6	?	?	?	99 mica (clinochlore)
Diabase I, Frederick, Md.	3.020	0.18	0	0.1	0.1	48 an$_{67}$, 49 pyr, 1 mica
Diabase II, Frederick, Md.	3.033	0.2	0	0.1	0.1	49 an$_{45}$, 46 pyr, 3 ox, 2 mica
Gabbro, Nahant, Mass.	3.084	5.0	?	?	0.1	40 pyr, 20 se, 15 ol, 10 an$_{70}$, 10 mica, 3 ox
Gabbro, Jersey City, N. J.	3.098	5.5	0.1	0.2	0.3	60 pyr, 15 an$_{40}$, 15 mica, 10 qu
Dunite, Spruce Pine, N. Carolina	3.262	0.50	?	?	0.2	96 ol, 3 se, 1 ox
Peridotite, Mt. Albert, Gaspé, Quebec	3.307	1.0	0.1	0.1	0.2	89 ol, 10 pyr, 1 ox
Dunite, Twin Sisters Mt., Wash.	3.320	10.0	0	0.1	0.1	99 ol, 1 ox

Abbreviations

qu	quartz		ox	oxides
or	orthoclase, microperthite		do	dolomite
ca	calcite		gl	glass
se	serpentine		d	average grain diameter
pyr	pyroxene		η_c	crack porosity
an	plagioclase with anorthite content		η_p	pore porosity
mica	muscovite, chlorite, biotite		η	total porosity
am	amphibole			

TABLE 2. Resistivity as a Function of Pressure

Resistivities are in ohm meters. ρ_t is resistivity in 50-ohm meter tap water, ρ_s in 0.25-ohm meter salt solution, ρ_d is dry, and ρ_{tt} is partially saturated. The exponent given is the power of 10. Frequency was 10 Hz, and temperature 20°C.

	Pressure, kb								
	0.05	0.1	0.25	0.5	1	2	4	6	10
Colorado Tuff									
ρ_t	2.9^1	2.9^1	2.8^1	2.9^1	2.9^1	2.8^1	2.12^1	1.94^1	1.80^1
ρ_s	1.1^1	1.1^1	1.1^1	1.1^1	1.1^1	1.1^1	1.02^1	9.1^0	9.1^0
Pottsville Sandstone									
ρ_t	2.5^3	3.1^3	5.0^3	8.4^3	1.54^4	2.85^4	5.2^4	8.4^4	1.7^5
ρ_s	1.17^2	1.56^2	2.75^2	5.5^2	1.12^3	2.4^3	4.2^3	7.8^3	1.18^4
Bedford Limestone									
ρ_t	9.4^1	9.5^1	9.9^1	9.9^1	1.01^2				
ρ_s	1.47^1	1.47^1	1.6^1	1.6^1	1.6^1	2.0^1	3.1^1	3.5^1	4.4^1
Lanesville Granite									
ρ_t	1.1^4	1.6^4	2.6^4	4.3^4	7.0^4	1.16^5	2.15^5	3.6^5	7.0^5
ρ_d	$>8^6$				$>7^6$	$>8^6$	$>8^6$	$>8^6$	$>8^6$
Westerly Granite									
ρ_t	8.5^3	1.0^4	1.4^4	1.9^4	2.8^4	5.2^4	9.0^4	1.3^5	3.2^5
ρ_{tt}	1.29^6	4.4^5	1.95^5	1.03^5	6.6^4	5.6^4	5.6^4	6.1^4	1.45^5
ρ_d	$>8^6$			$>8^6$					$>8^6$
Lynn Felsite									
ρ_t	4.1^4	5.4^4	6.6^4	7.9^4	9.6^4	1.36^5	2.3^5	3.9^5	8.6^5
ρ_s	5.3^3	6.0^3	9.0^3	1.15^4	1.58^4	2.32^4	3.9^4	6.5^4	1.75^5
White Marble									
ρ_s	1.73^2	2.06^2	3.6^2	6.3^2	1.18^3	2.3^3	5.7^3	1.2^4	$>8^4$
Oak Hall Limestone II									
ρ_t	2.0^3	2.0^3	2.18^3	2.40^3	2.9^3	4.0^3	7.2^3	1.24^4	2.5^4
ρ_s	6.0^2	6.6^2	8.3^2	9.8^2	1.15^3	1.53^3	2.5^3	3.9^3	8.1^3
Grenville Marble									
ρ_s	6.2^2	9.3^2	1.76^3	2.6^3	4.6^3	1.0^4	2.6^4	7.0^4	$>2.4^5$
Black Slate, Parallel to Cleavage									
ρ_t	2.3^2	2.7^2	3.4^2	5.0^2	9.0^2	1.45^3	3.0^3	5.1^3	1.0^4
ρ_s	9.0^1	1.0^2	1.26^2	1.95^2	3.3^2	6.0^2	1.28^3	2.5^3	5.3^3
Black Slate, Perpendicular to Cleavage									
ρ_t	9.7^2	1.08^3	1.26^3	1.50^3	1.90^3	2.6^3	4.5^3	7.7^3	1.25^4
ρ_s	5.0^2	5.7^2	6.8^2	8.3^2	1.13^3	1.6^3	2.7^3	4.2^3	7.7^3
San Marcos Gabbro									
ρ_t	1.32^4	1.36^4	1.49^4	1.79^4	2.3^4	3.2^4	6.8^4	1.22^5	3.4^5
ρ_s	1.20^3	3.0^3	5.7^3	8.2^3	1.07^4	1.54^4	2.8^4	4.6^4	1.25^5
ρ_d	$>1.2^7$				$>4^6$	$>4^6$	$>1.2^7$	$>1.6^7$	$>1.2^7$
Blair Dolomite									
ρ_s	4.5^3	9.5^3	2.5^4	5.2^4	8.7^4	1.42^5	2.46^5	3.5^5	5.7^5
Chittenden Dolomite									
ρ_s	1.03^2	1.27^2	1.78^2	2.6^2	3.7^2	5.6^2	1.03^3	1.85^3	4.6^3

TABLE 2 *(continued)*

	Pressure, kb								
	0.05	0.1	0.25	0.5	1	2	4	6	10
	Webatuck Dolomite								
ρ_t	1.45^4	3.2^4	7.2^4	1.67^5	8.5^5	2.0^6	4.6^6	7.3^6	1.06^7
ρ_s	3.4^2	5.2^2	1.08^3	1.90^3	3.3^3	5.3^3	9.3^3	1.41^4	2.8^4
	Chlorite Schist								
ρ_s	1.9^2	3.0^2	5.6^2	8.5^2	1.55^3	3.5^3	6.1^3	1.0^4	1.95^4
	Maryland Diabase II								
ρ_t	2.7^4	3.6^4	3.9^4	4.8^4	5.8^4	1.05^5	3.7^5	8.7^5	3.3^6
	Nahant Gabbro								
ρ_t	8.7^0	3.1^0	6.5^0	6.4^0	6.3^0	6.1^0	6.0^0	5.8^0	5.4^0
	New Jersey Gabbro								
ρ_t	3.3^4	3.4^4	3.7^4	3.9^4	4.5^4	6.3^4	1.3^5	2.7^5	1.3^6
ρ_s	1.0^4	1.15^4	1.62^4	2.4^4	3.3^4	5.2^4	1.08^5	2.3^5	7.8^5
	Spruce Pine Dunite								
ρ_t	1.45^4	2.7^4	5.2^4	7.7^4	1.25^5	2.0^5	3.1^5	3.4^5	3.6^5
	Mt. Albert Peridotite								
ρ_t	2.3^6	2.5^6	2.7^6	2.9^6	3.2^6	3.8^6	4.6^6	5.3^6	6.2^6
ρ_s	2.1^4	2.8^4	6.6^4	1.9^5	3.5^5	4.9^5	7.7^5	1.08^6	1.9^6
	Twin Sisters Dunite								
ρ_t	2.2^4	2.7^4	3.5^4	4.3^4	5.6^4	8.3^4	1.75^5	3.4^5	1.10^6
ρ_s	1.94^3	4.4^3	6.8^3	9.5^3	1.15^4	1.59^4	2.8^4	4.9^4	1.28^5

ure 1) in which conduction through the minerals is important, Solenhofen limestone (Figure 2) in which crack porosity is negligible, or the rhyolite tuff (Figure 1) in which isolated pores collapse under pressure. The third curve, ρ_{ts} versus pressure, contains features reported elsewhere for partially saturated rocks. Rocks of low porosity [*Parkhomenko*, 1967], as well as rocks with porosity of 0.30–0.50 [*Yamazaki*, 1965, 1966], showed the sharp decrease of resistivity with pressure at low pressure found here.

Our observations of the effect of saturation on resistivity of granite (Figure 3) support the explanation advanced in *Brace and Orange* [1968] for differences that have been reported for the effect of pressure. The explanation, in brief, is based on the differing role of water in cracks in the two cases. At low pressure, as known from elastic studies, open cracks are present in most crystalline rocks. If the rock is saturated, these cracks are filled with water. As pressure is increased, water is expelled and resistivity increases. If the rock is only partially saturated, these cracks are only partially filled and some potential conduction paths cannot be utilized. Under pressure, however, as porosity is reduced, some isolated water films become interconnected and resistivity drops. With increasing pressure (and further decrease in porosity) the rock becomes effectively saturated and then with further increase in pressure behaves like initially saturated rock.

Mineral conduction. How will pressure affect the resistivity of a rock composed of minerals that, rather than being insulators, are partially conducting? If we assume that cracks are present initially, pressure will first tend to close cracks. This closing of the cracks will bring grains into closer contact and decrease resistiv-
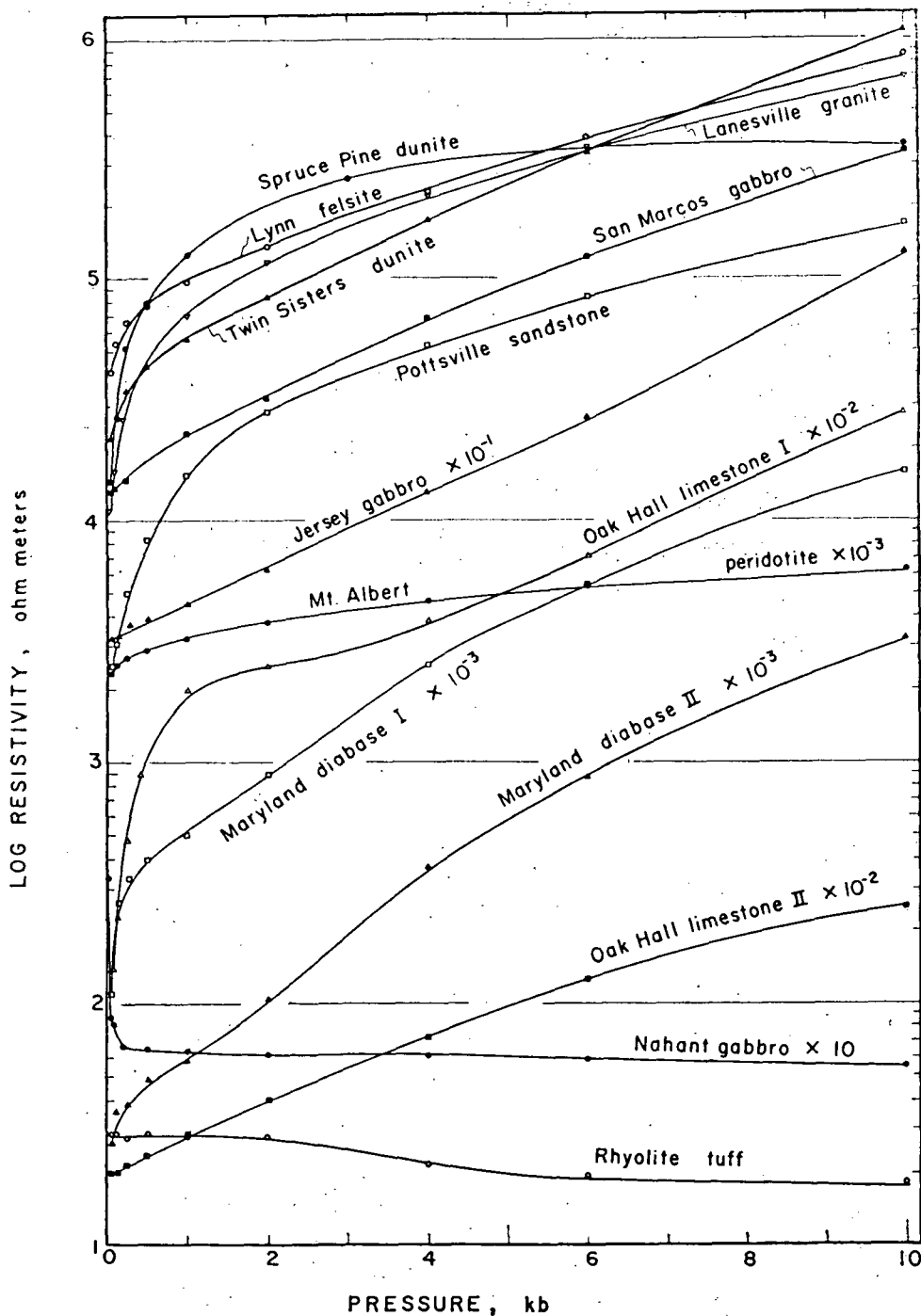
Fig. 1. Resistivity as a function of pressure for samples saturated with tap water.

ity, in much the same way as thermal resistivity is lowered with the first application of pressure [*Walsh and Decker*, 1966]. Beyond the pressure at which crack porosity is eliminated, we would expect, based on *Parkhomenko*'s work [1967], little further change with pressure. Thus, behavior of a rock composed of conducting minerals should differ from all three cases shown in Figure 3.

It seems clear that mineral conduction was important in the Nahant gabbro (Figure 1) for several reasons. First, the resistivity was abnormally low. Second, the resistivity was not greatly

different if the rock was wet or dry. For example, resistivity of a saturated sample was 39 ohm meters, whereas resistivity of the same sample dried in the vacuum oven was 73 ohm meters. Finally, unlike all of the other rocks, the resistivity of Nahant gabbro varied markedly with frequency. The wet and dry values of 93 and 73 ohm meters, respectively, reported above were measured at 10 Hz. When the measurement was repeated at 3 H, both wet and dry values increased to about 150 ohm meters. This higher value is probably due to increased capacitive impedance between adjacent grains at the lower
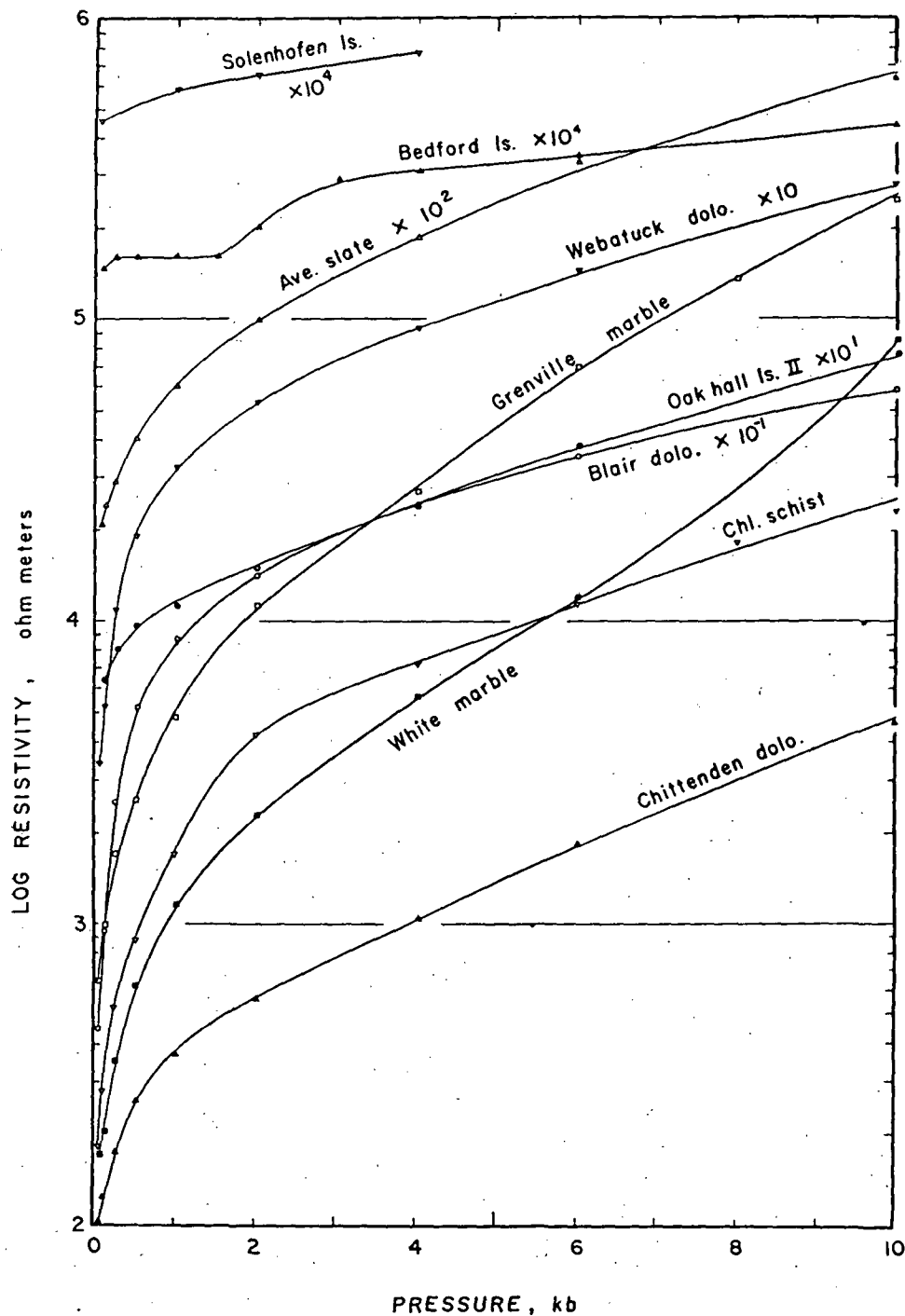
Fig. 2.   Resistivity as a function of pressure for samples saturated with salt solution.

frequency. The effect is probably not the usual induced polarization effect, which depends on a conductive pore fluid and the resultant electronic conductor–ionic conductor interface.

Our prediction above regarding the effect of pressure seems to be supported by the behavior of Nahant gabbro (Figure 1). A very rapid initial decrease in resistivity was followed by little further change. Unfortunately, it is not clear which mineral in this rock is so strongly conducting. The oxides (Table 1) are no more abundant than in the Maryland diabase or San Mar-

cos gabbro, although they may be somewhat more widely dispersed in the Nahant gabbro.

Effect of mineral content, grain size, and alteration.   With the data at hand, here and in *BOM*, we now have a good opportunity to examine the influence of various petrographic features on the resistivity of water-saturated rocks. Here, we will consider mineral content, mineral alteration, and grain size. Porosity is given special attention in the next section.

With the sole exception of Nahant gabbro, mineral content seems to play a very minor
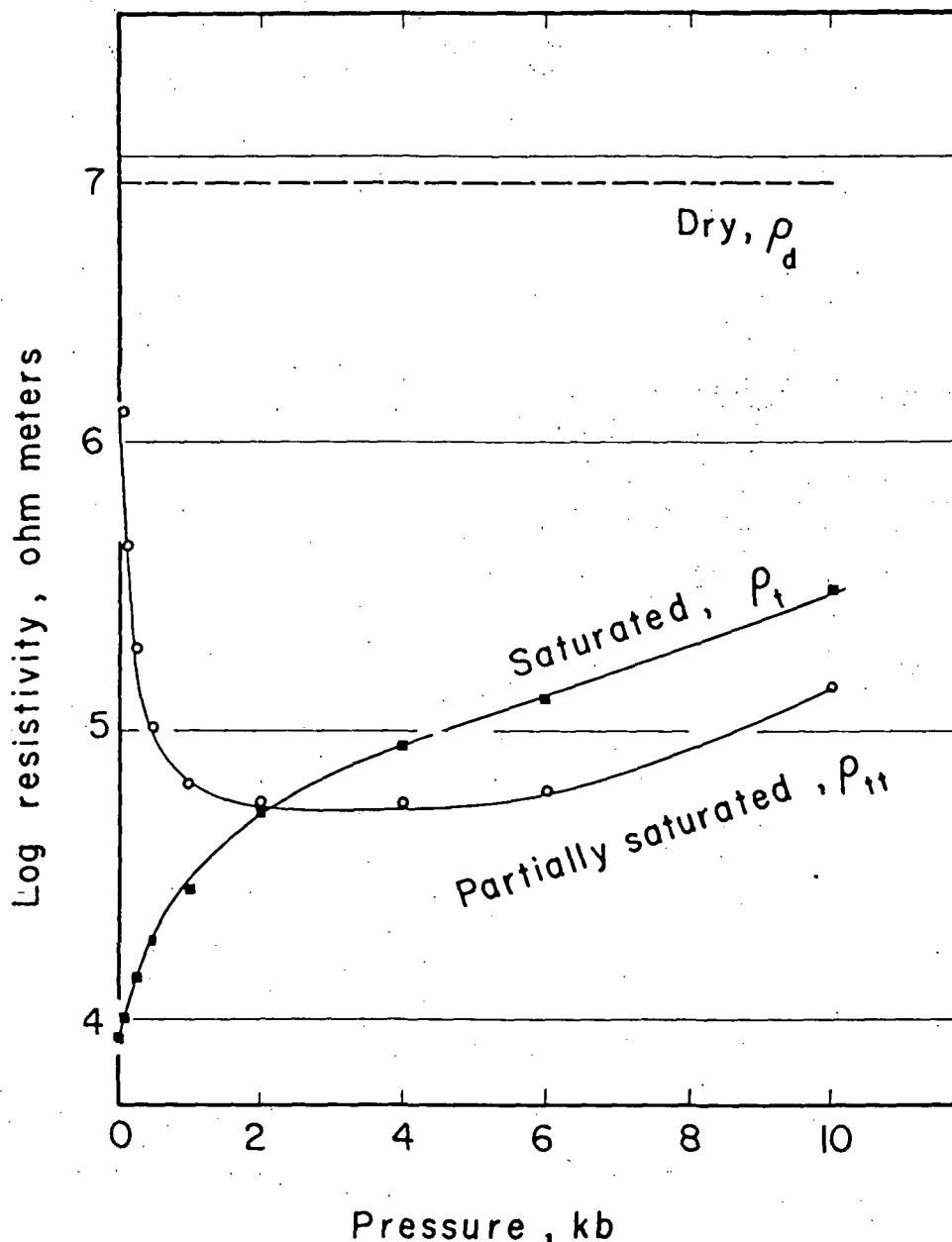
Fig. 3. Effect of saturation on resistivity of Westerly granite in tap water. The dry curve represents a minimum value for it is near the limit of our measurement of resistivity. The partially saturated sample had 43% of the pore space filled with water at 1 bar.

role. For example, Lanesville granite and Lynn felsite are nearly the same mineralogically as Oak Hall limestone, Twin Sisters dunite, and San Marcos gabbro. Content of oxides such as magnetite and ilmenite ranges in this group from zero to about 3%. Alteration also seems to have little influence on resistivity, although further study of the highly altered Nahant gabbro might reveal an influence. Twin Sisters dunite is free of serpentine; Adie dunite (with the same resistivity) contains as much as 19%. Jersey gabbro has abundant alteration to chlorite and sericite; fresh diabase, dunite, and granite have, however, about the same resistivity. Black slate (the color is evidently not due

to graphite) is in no sense anomalous in this group of crystalline igneous rocks.

It is difficult to separate the effect of grain size from the effect of porosity and mineral plasticity, which we further discuss below. Among pairs of rocks of similar mineralogy and porosity, however, grain size seems to have little effect: Lanesville granite (6 mm) and Lynn felsite (0.10 mm) have about the same resistivity, as Maryland diabase (0.2 mm) and Mt. Albert (1.0 mm) peridotite. Among the dolomites (Figure 2) large grain size and porosity increase together; as a result the resistivity falls with grain size. This relation is less clear with the calcite rocks: Oak Hall limestone I is more

resistive than the two marbles, whereas the coarser Grenville marble is more resistive than the finer white marble.

Thus, mineral content, grain size, and alteration, when compared among rocks of the same porosity, have little influence on resistivity. Of course, it is no surprise that mineralogy has little effect. Most of the minerals, including alteration products, in the present rocks are effectively insulators with resistivities many orders of magnitude greater than the water that fills the pore spaces. It is possible that with closer study an independent effect of grain size might become apparent. Even the lack of an effect is rather interesting and, if proved, could lead to a clearer understanding of the mechanics of electrical conduction in rocks.

Porosity, pore crushing. Data for twenty-two rocks are given in Figure 4, which is a plot of pore porosity (Table 1) versus resistivity in 0.25 ohm meter NaCl solution. As discussed in *BOM*, the use of salt solution eliminates surface conduction, so that Figure 4 gives a measure of bulk conduction through pore water as a function of porosity. At the pressure for which the data apply (4 kb) crack porosity is presumably eliminated, so that all porosity in the rock is pore porosity.

The remarkable relation between pore porosity η_p and resistivity ρ_s reported in *BOM*, namely that

$$\rho_0/\rho_s = \eta_p{}^2 \qquad (1)$$

still seems to hold, although there are several exceptions apparent in Figure 4. Although such diverse rocks as oolitic limestone, sandstone, slate (average of directions parallel and perpendicular to cleavage), granite, and dunite all fall close to a common line, agreement is now somewhat less perfect than with the eight samples previously available. There is marked scatter at porosities of 0.001 and 0.002. Presumably, this is because of the large probable error in the measurement of porosity at these low porosities; the error in porosity is about 0.001 and, in view of this, it is almost surprising that agreement is as close as it is. The point that falls farthest from the line (at about 10 ohm meters) corresponds to the rhyolite tuff. This rock has a porosity close to 40%; much of the porosity is in the form of round holes enclosed in volcanic glass. As it is unlikely that

these are all interconnected, perhaps a good part of the porosity in this rock does not contribute to conduction the way all the pore space in, say, the Bedford limestone does. This might account for the fact that the rhyolite tuff is only about as conductive as a normal rock of around 12% porosity.

The physical basis for the above relation between porosity and resistivity is still obscure. If has been recognized as an empirical law in the petroleum industry, where in a more general form it is often referred to as Archie's [1942] law. From our work, this law would appear to have wide application and, one might suppose, to be based on some very general properties of rocks: on characteristics shared by rocks as diverse as anorthosite and slate. Unfortunately, an explanation of this tantalizingly simple law must await further study.

Certain of the more porous rocks show an irreversible reduction of porosity with application of a high confining pressure. Two of these rocks show effects that seem to contradict and yet are, in fact, consistent. At about 1.5 kb pressure, Bedford limestone (Figure 2) abruptly increased in resistivity; above this pressure the rock was actually found to be denser. By contrast, the resistivity of rhyolite tuff decreased with pressure, although this rock also became denser as some pores were collapsed by the external pressure. We would regard the behavior of the Bedford limestone as normal; that of the tuff, as abnormal. An increase of resistivity with pressure is normal because it is consistent with the increase that accompanies crack closure under pressure and the increase that one finds in going from more to less porous rocks. The abnormal behavior of the tuff must be due to the unique pore geometry of this rock. As suggested above, there could be appreciable dead-end pore space in this rock; some crushing of the rock might increase the connectivity of water films and thus lower resistivity.

Effect of pressure at high pressure. Another general relationship is apparent if changes in resistivity of the dense crystalline rocks (we eliminate all rocks in which pores collapse under pressure, as well as Nahant gabbro) are compared in the high-pressure region, in which cracks have closed. For comparison, the curves have been normalized to the 4-kb value of resistivity in NaCl solution (Figure 5).
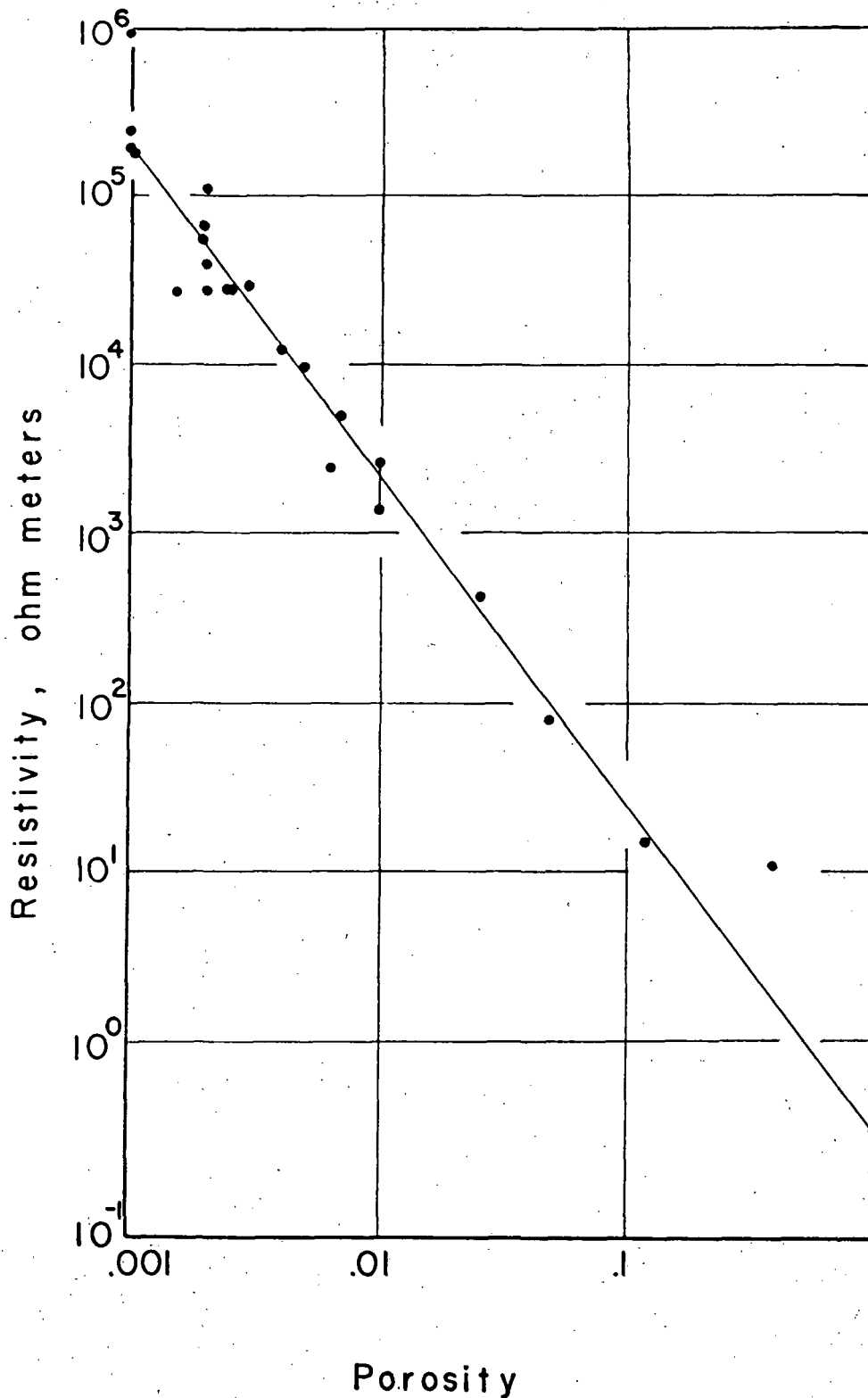
Fig. 4. Resistivity at 4 kb as a function of pore porosity in salt solution. Data are from Table 2 and from *BOM*. The two points joined by a bar are the values in two directions for black slate.

Evidently the effect of pressure is similar for the various rocks; all but four of the nineteen curves are at an angle to the pressure axis of $17° \pm 5°$. At the average angle,

$$\Delta \log \left(\frac{\rho}{\rho_4} \right) = 0.10 \, (\Delta P) \qquad 2 \leq P \leq 10$$

where ρ_4 is the 4-kb value of resistivity and P is pressure in kilobars. Or, simply,

$$1/\rho \, dP/dP = 0.10 \, \text{kb}^{-1} \qquad (2)$$

Once again, we have what appears to be a very general relationship, one that holds for peridotite and granite as well as for slate and
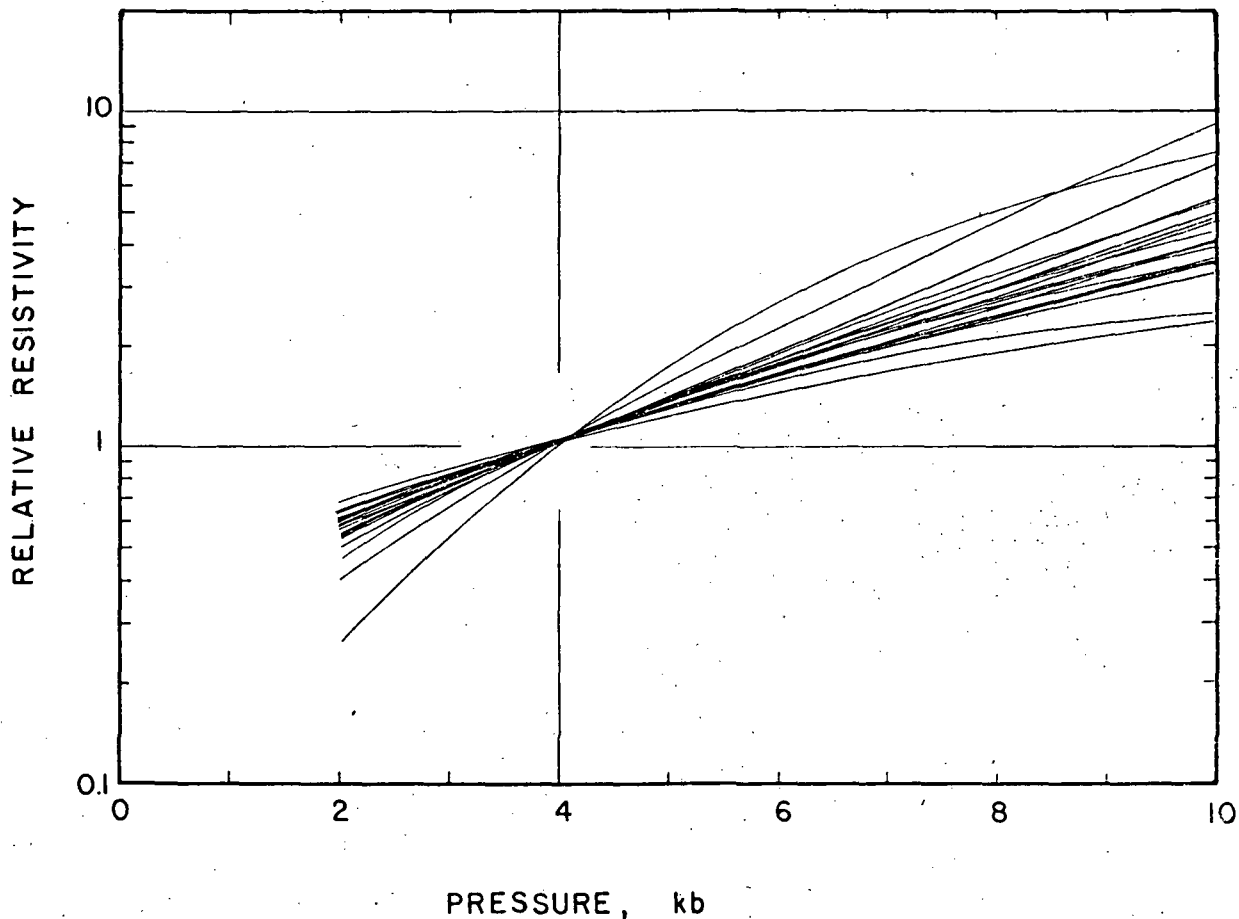
Fig. 5. Effect of pressure on resistivity at high pressure. Values are given for salt solution relative to the 4-kb value. Data from Table 2 and from *BOM*.

one that, rather curiously, is independent of initial porosity, as long as the initial porosity is 0.01 or less. We might infer from this that, at high pressure, all pores in crystalline rocks have the same cross-sectional form; then, elastic changes in cross section would be the same per unit of pressure. It seems unlikely, however, that this relation is true, that the pores in slate, for example, have the same form as the pores in diabase. In any event, the pores are not circular, as we proved in *BOM*.

With (1) and (2) and the effects of temperature, one can now predict fairly closely the electrical resistivity of an arbitary crystalline rock to 10 kb and 100° and by extrapolation to perhaps twice these limits. All that is required is a knowledge of the pore porosity of the rock and the resistivity of pore fluid. Equation 1 will give the resistivity at 4 kb, 20°; equation 2 will then give resistivity at any different pressure. The effect of temperature can be estimated from Figure 5, *BOM*. Under natural conditions, pore fluids might be under pressure. Then, P in (2) will become the *effective pressure*, the dif-

ference between total pressure and pore pressure. Experiments with pore pressure [*Brace and Orange*, 1968] showed that resistivity depended on effective rather than total pressure, just as many mechanical properties do.

It is of interest to estimate from (2) the pressure that would raise the resistivity of typical saturated rocks to the dry rock values. With a dry rock value of 10^{10} ohm meters, we obtain a pressure of 40–60 kb, corresponding to a depth of about 200 km in the earth. At these depths in the earth, however, it is unlikely that rocks will have such high resistivity, owing to the additional effect of high temperature. Although little is known about the effect of high temperature on other than dry rocks, it is probably safe to assume that regardless of the role of water intracrystalline conduction will be significant. To judge from work reported by *Parkhomenko* [1967] as well as results given here for Nahant gabbro, pressure would then have a much more diminished effect on resistivity. Even within the earth's crust, where we might assume that temperatures are still

	Pressure, kb		
	0.05	3	9
$\rho_\perp$	5.0^2	2.1^3	6.6^3
$\rho_\parallel$	9.0^1	8.9^2	4.5^3
$\rho_\perp/\rho_\parallel$	5.5	2.4	1.5
$\beta_\perp$	1.46	1.23	0.78
$\beta_\parallel$	0.57	0.59	0.50
$\beta_\perp/\beta_\parallel$	2.5	2.1	1.6

fairly low, pressure (which may reach 10–15 kb) is clearly insufficient to raise resistivity of saturated rock to within the orders of magnitude of the dry rock values.

Anisotropy and inhomogeneity. The black slate offers an interesting example of a high degree of anisotropy in electrical resistivity. Values at three pressures are compared in Table 3. At the pressures chosen (0.05, 3, and 9 kb) we can compare changes in resistivity with changes in linear compressibility from *Brace* [1965]. Note that at the two high pressures, the ratio of properties in the two directions (parallel and perpendicular to cleavage) are very nearly the same. Since linear compressibility is an expression of elastic response to pressure, we have a further indication of the close connection between elastic and electrical behavior in the high-pressure region. In *BOM* we indicated the close connection between electrical changes and elastic volume changes under pressure during crack closure.

It is also interesting to note in Table 3 the decreasing anisotropy of slate with pressure, with respect to both linear compressibility and electrical resistivity. This may be a general feature of rocks containing mica. *Birch* [1961] reported a similar decrease in anisotropy in compressional wave velocity, and we have observed this for linear compressibility both for micaceous rocks and for single crystals of biotite.

We have two examples of rocks that come from different parts of the same formation, the Oak Hall limestone, I and II, and the Maryland diabase, I and II. Each pair is petrographically

very similar, and yet resistivity differs by one (diabase) or two (limestone) orders of magnitude, as shown in Figure 1. The cause of the difference is apparently minute differences in porosity in each pair (see Table 1). These differences in resistivity within a single rock formation are more pronounced than between rocks of widely differing mineral content and grain size. Clearly, resistivity differences will be of little use in telling one subsurface rock type from another, if one has to deal with the types of rocks considered here. The single dominating factor here is porosity. Of course, on a larger scale, crystalline rocks may be jointed in characteristic ways and, as a result, have electrical properties that are more definitive than the electrical properties observed in our small samples.

Effects due to mineral plasticity. An interesting effect was reported in our study of the changes in resistivity due to stress [*Brace and Orange*, 1968]. Under stress, calcite marble became highly resistive; all other rocks, including some with ductile stress-strain curves like that for marble, became more conducting. Our interpretation was that the marble had become 'sealed off' under stress, owing to intracrystalline gliding of the calcite grains. It was of interest to see if the same phenomenon occurred under pressure as well as under stress, and whether it occurred for other rocks in which intracrystalline gliding might take place. Even though, in principle, hydrostatic pressure ought to cause no macroscopic shearing stress, shearing stress probably does exist across grain boundaries, owing to the fact that we are forcing grains together which do not quite fit.

The minerals in the present suite of rocks most likely to glide at room temperature are calcite, dolomite, serpentine and the micas. Neither the Adie dunite, nor the slate, nor the chlorite schist shows an anomalous increase in resistivity at high pressure (Figure 2). An anomalous increase would be readily apparent in Figure 5 in which both slate and schist are plotted. Similarly, none of the three dolomite rocks are anomalous. Among the six calcite-rich rocks, however, two stand out. They are the coarsest-grained members, the white marble and the Grenville marble; resistivity of both increases much more rapidly than is normal. During the experiments on these rocks it was noted that

at 10 kb, resistivity did not reach a constant value, as is normal; resistivity continued to drift upward, and the value in Table 2 is simply the value reached in what was the normal time period for a measurement. We suggest that sealing off began in these two rocks, just as it did much more strongly under stress; here a *pressure* of 8–10 kb was required, whereas a *stress* of only 1 kb produced a striking effect. It is interesting that sealing off depends as much on grain size as on mineral content; sealing off was observed in none of the fine-grained limestones. This could be explained in two ways: On the one hand, shearing stress might be higher in the coarser-grained rocks owing to a greater misfit; crack porosity is nearly zero for the fine-grained rocks, and it could be inferred from this that the grains fit rather perfectly from the start. On the other hand, one might assume that shearing stress is about the same in these rocks but that the stress at which flow occurs, the yield point, depends on grain diameter. For metals such a dependence is well known [*Cottrell*, p. 118, 1964]; the yield point of fine-grained metals is higher than for coarse-grained ones. This is in the right direction to explain the differences indicated in Figure 2.

In any event, we infer that gliding in calcite has occurred in these hydrostatic pressure tests and that it is, for whatever reason, more pronounced in coarse- than in fine-grained rocks. Sealing off and, by inference, gliding were not apparent in rocks containing serpentine, mica, or dolomite.

APPENDIX

Most of the rocks used here have been studied previously, although some were collected for this study.

The new rocks were collected as follows: Rhyolite tuff and Jersey gabbro (obtained from Wards Inc., Rochester, New York), Lanesville granite (collected at Pigeon Cove, Lanesville, Cape Ann, Massachusetts), Lynn felsite (collected from Griswold Pond area, Saugus-Melrose town line, Massachusetts), Oak Hall limestone II (from the quarry of the Neidigh Bros. Limestone Co. of Oak Hall, near State College, Pennsylvania), Grenville marble (collected at the 1962 New England Intercollegiate Geological Conference field trip stop 8, St. Jovite,

Quebec), San Marcos gabbro (obtained from cut stone dealer in Los Angeles), Chittenden dolomite (collected from area mapped as Precambrian, about 1 mile north of Deer's Leap, east of Rutland, Vermont), chlorite schist (collected from dump at Chester talc quarry, Chester, Vermont), Nahant gabbro (collected from shore outcrop on northwest side of big island of Nahant, Massachusetts), peridotite (collected by R. H. McNutt near Mt. Albert Inn, 25 miles south of Ste. Ann des Mont, Gaspé, Quebec), and Twin Sisters dunite (obtained by *Birch* [1961] from Twin Sisters Peak, Washington). The rocks that have been studied before were: Pottsville sandstone [*Brace and Orange*, 1968; *Brace and Martin*, 1968], White marble [*Brace*, 1964; *Brace and Orange*, 1968; *Brace, Paulding and Scholz*, 1966], Maryland diabase II [*Brace and Orange*, 1968], black slate [*Brace*, 1965], Blair and Webatuck dolomites [*Brace*, 1964], chlorite schist [*Brace*, 1965], and Spruce Pine dunite [*Brace and Orange*, 1968]. Many of these rocks have been studied by Byerlee and Scholz whose results will appear in forthcoming publications.

REFERENCES

Adams, L. H., and E. D. Williamson, On the compressibility of minerals and rocks at high pressures, *J. Franklin Inst., 195*, 475–529, 1923.

Archie, G. E., The electrical resistivity log as an aid in determining some reservoir characteristics, *Trans. AIME, Petrol. Br., 146*, 54–62, 1942.

Birch, F., The velocity of compressional waves in rocks to 10 kilobars, 2, *J. Geophys. Res., 66*, 2199–2224, 1961.

Brace, W. F., Brittle fracture of rocks, in *State of Stress in the Earth's Crust*, edited by W. R. Judd, pp. 110–178, American Elsevier, New York, 1964.

Brace, W. F., Relation of elastic properties of rocks to fabric, *J. Geophys. Res., 70*, 5657–5667, 1965.

Brace, W. F., and R. J. Martin, III, A test of the law of effective stress for crystalline rocks of low porosity, *Intern. J. Rock. Mech. Mining, Sci.*, in press, 1968.

Brace, W. F., and A. S. Orange, Electrical re-

sistivity changes in saturated rocks during fracture and frictional sliding, *J. Geophys. Res.*, *73*, 1433–1445, 1968.

Brace, W. F., A. S. Orange, and T. R. Madden, The effect of pressure on the electrical resistivity of water-saturated crystalline rocks, *J. Geophys. Res.*, *70*, 5669–5678, 1965.

Brace, W. F., B. W. Paulding, Jr., and C. Scholz, Dilatancy in the fracture of crystalline rocks, *J. Geophys. Res.*, *71*, 3939–3953, 1966.

Cottrell, A. H., *The Mechanical Properties of Matter*, 430 pp. John Wiley, New York, 1964.

Parkhomenko, E. I., *Electrical Properties of Rocks*, Plenum Press, New York, 1967.

Walsh, J. B., and W. F. Brace, Cracks and pores in rocks, *Intern. Congr. Rock Mech., Lisbon*, 643–646, 1966.

Walsh, J. B., and E. R. Decker, Effect of pressure and saturating fluid on the thermal conductivity of compact rock, *J. Geophys. Res.*, *71*, 3053–3061, 1966.

Yamazaki, Y., Electrical conductivity of strained rocks, 1, *Bull. Earthquake Res. Inst. Univ. Tokyo*, *43*, 783–802, 1965.

Yamazaki, Y., Electrical conductivity of strained rocks, 2, *Bull. Earthquake Res. Inst. Univ. Tokyo*, *44*, 1553–1570, 1966.

A STUDY IN INDUCED POLARIZATION†

L. A. ANDERSON* AND G. V. KELLER‡

Induced polarization in pyritic sandstone arises in part from overvoltage effects and in part from electrolytic polarization. Because induced-polarization measurements are commonly used to search for sulfides, the electrolytic polarization is an undesirable background effect. Pyrite in sandstone can be located only when overvoltage polarization substantially exceeds electrolytic polarization. Laboratory measurements indicate this is true only if there is ten percent or more pyrite in a rock. However, overvoltage polarization is much larger when low current densities are used, particularly if the matrix resistivity is high. Field measurements indicate that at low current densities as little as one or two percent pyrite may provide sufficient overvoltage polarization to be recognizable in the presence of electrolytic polarization.

INTRODUCTION

The principal characteristic of induced polarization is that following the abrupt ending of current flow in a rock, a prolonged transient voltage may be observed. This transient is most pronounced in rocks containing graphite and disseminated sulfide minerals; moderately large transients may also be observed in clay-bearing rocks.

The principal causes of induced polarization in rocks have been recognized: overvoltage phenomena where metallic mineral grains are in contact with electrolytic solutions, and electrolytic polarization in rocks which have ion-exchange capacity due to distributed fixed charges (Seigel, 1959; Mayper, 1959). Induced-polarization methods are useful in locating sulfides in rocks in which electrolytic polarization is small. These rocks are usually those with low porosities and low ion-exchange capacities, such as granodiorite or quartz monzonite porphyry. It has not been demonstrated that induced-polarization methods may be used in locating sulfides in rocks where the electrolytic polarization is large, such as in shaly sandstone.

Electrolytic polarization at charged membranes

Keller and Licastro (1959) and Keller (1960) have proposed the concept of anion traps to explain polarization in clay-bearing rocks: negatively charged clay anions, fixed in the pore struc-

ture of a rock, alter the apparent mobility of the ions in the solution by blocking some pores to anion migration and by increasing the path length for anions in other pores. Because the anions must generally travel farther than if no fixed charges were present, and because the field added by the fixed charges increases the potential gradient in some areas while decreasing it in others, ions travel at different velocities in various portions of the rock. This results in concentration of anions or cations in the area of velocity increase. If the current flow is interrupted, ions diffuse away from the zones of high concentration toward the zones of low concentration.

The diffusion of ions is discussed at length by Jost (1952). Diffusion of ions through the pores of a rock might be represented crudely by diffusion through a straight capillary tube. According to Jost, the equation describing diffusion in a simple one-dimensional case as expressed in cartesian coordinates with the initial and boundary conditions,

$$C(x, t) = C_0 \quad \text{at } t = 0, \quad x = 0$$

$$C(x, t) = 0 \quad \text{for all } x \text{ at } t \gg 0,$$

can be described by the equation

$$C(x, t) = C_0/2 \left[1 - \text{erf} \left(\frac{x}{2\sqrt{Dt}} \right) \right], \quad (1)$$

* U. S. Geological Survey, Denver, Colorado.

‡ Colorado School of Mines, Department of Geophysics, Golden, Colorado.

where $C(x, t)$ is the increase above normal concentration written as a function of the variables x and t, x being the distance from the concentration buildup in the direction of diffusion, and t the elapsed time from the instant the ions started diffusing. The time rate of change of the ion concentration at the distance, x, is the current at that point.

C_0 is the initial excess concentration where the anions have accumulated.

D is the diffusion coefficient.

We may obtain the transient voltage, $e(t)$, by taking the ratio of product of current density, j, and unit length, Δl, to the conductivity, σ, in the capillary:

$$e(t) = j\Delta l/\sigma. \qquad (2)$$

From Fick's law of diffusion, given by Jost (1952, p. 2) as

$$J = - D \frac{\partial C(x, t)}{\partial x}, \qquad (3)$$

where J is the diffusion current (quantity of substance per cm²-second), the current density through the capillary can be written as

$$j = nFD \frac{\partial C(x, t)}{\partial x}, \qquad (4)$$

where n is the number of charge units involved in the diffusion process and F is the Faraday expressed in coulombs per mole. Differentiating and substituting equation (4) in equation (2), we have:

$$e(t) = - \frac{nFC_0\Delta lD}{2\sigma\sqrt{\pi tD}}\exp -\frac{x^2}{4Dt}. \qquad (5)$$

The negative sign in equation (5) implies that the diffusion current is in the direction opposite the concentration gradient.

There are many individual zones of ion accumulation in a rock which has been electrically polarized, and each polarization center should discharge approximately as shown by equations (1) and (5). The total amount of polarization in the rock should increase with increasing cation-exchange capacity, and, as a first approximation, we may say that the number of polarization centers will be proportional to the density of fixed charges on the rock framework, a_0/ϕ, where ϕ is the vol-

ume fraction of pore spaces. However, if all the negative charges were fixed, there would be no mobile anions in solution to collect at the anion traps, and no polarization could occur. Therefore, we expect the polarization to be proportional to the fraction of anions in solution, $(a-a_0)/a$. When these two factors are combined, the charge, q, stored per unit volume, v, should be approximately:

$$q/v\alpha(a_0/\phi)(a - a_0)/a. \qquad (6)$$

The expression on the right side of equation (6) has a maximum value when

$$a_0 = a/2, \qquad (7)$$

or when half the negative charge is fixed in the form of ion-exchange capacity, and half is in the form of free ions in solution. When more of the charge is fixed, there are few free anions available to collect at the ion traps, and when less of the charge is fixed, there are few traps available to collect the ions.

It should be noted that the number of ion traps can be directly related to clay concentration only when the clay is uniformly distributed through the pore structure. Using cation-exchange capacities reported for various minerals (Grim, 1953, p. 129) and assuming uniform distribution of clay in the pores, we may estimate the clay content required for maximum polarization. Curves showing the relation between the factor $a_0(a-a_0)/a^2$ and the amount of clay in a rock are shown in Figure 1.

Three clays were considered: illite, montmorillonite, and kaolinite. An ion content of 100 parts per million (ppm) was assumed. Maximum polarization under these conditions would occur with relatively small amounts of montmorillonite, from 0.1 to 0.4 percent. For kaolinite, which has a much lower exchange capacity than montmorillonite, maximum polarization would be caused by 3- to 12-percent clay, other conditions being the same. Maximum polarization would be observed for larger amounts of clay, if a higher salinity were assumed.

Polarization at metal-electrolyte interfaces

When a metal is placed in an electrolytic solution, a potential difference, V_0, develops almost instantaneously between the metal and the electrolyte. When an external voltage is applied across

the metal-electrolyte contact so that current flows, polarization occurs at the interface, opposing current flow. The difference between the voltage (V_d) at which electrolysis actually takes place at the electrode and the voltage (V_0) is defined as the overvoltage (η) of the electrode process:

$$\eta = V_d - V_0 \qquad (8)$$

The overvoltage depends on the current density at which it is measured. Experimental work indicates a linear relation between overvoltage and the logarithm of current density (Butler, 1952, p. 161–166). The overvoltage (η) has been observed to satisfy the expression:

$$\eta = \alpha - \beta \log j \qquad (9)$$

where the parameters α and β are constants determined by the nature of the electrode and the solution, and j is the current density.

There are at least three mechanisms which contribute to overvoltage:

(1) Electrolysis may change the concentrations of ions near the electrodes, so that a concentration cell is set up between these zones and the rest of the solution. The voltage developed by this concentration cell is termed concentration polarization or concentration overvoltage.

(2) The rate at which the chemical reaction occurs at an electrode may be so slow as to limit the current flowing from the electrode. In such an event, an additional voltage drop at the electrode may be required to accelerate the chemical reaction at the electrode. This phenomenon is known as activation overvoltage.

(3) An oxide or grease film may cause a large ohmic drop in potential at an electrode surface. Though this is treated as an experimental error in chemical literature, it is probably of considerable importance in geologic applications.

In a sulfide-bearing rock, the amount of current which flows through the sulfide grains depends on the way in which the sulfide grains are situated in the pores. Consider a simple model consisting of conducting spheres distributed in a uniform matrix, with polarization taking place at a resistant shell around each of these spheres. For simplicity, assume that polarization voltages decay exponentially. Each grain is assumed to be a perfectly conducting sphere enclosed in a shell with a specified resistance and capacity per unit area.

The problem of the coated sphere has been considered many times, but a solution by Wait (1959) is probably the most appropriate for the problem at hand. However, it must be realized that the model of a spherical grain is far too simple to rep-
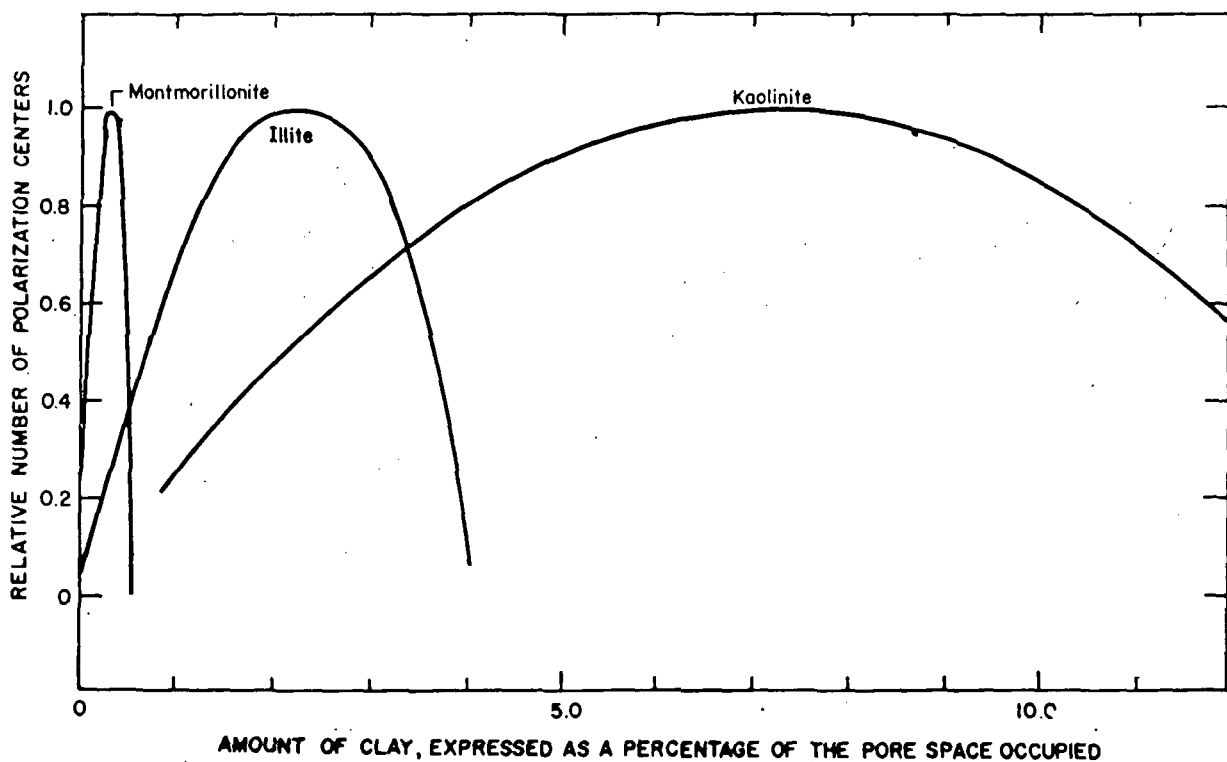

FIG. 1. Predicted effect of various amounts of clay distributed uniformly through a rock saturated with water having a salinity of 100 ppm.
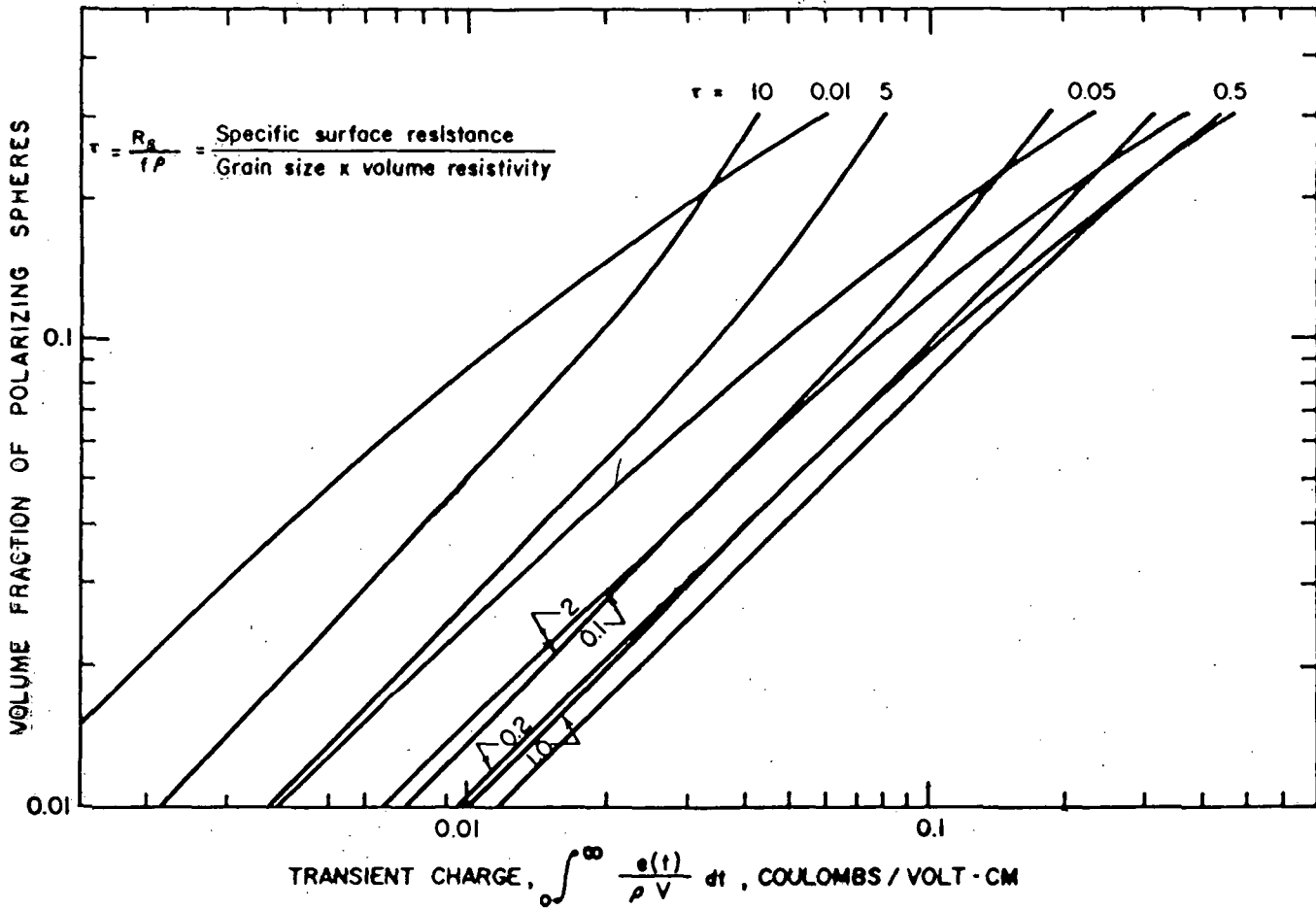
FIG. 2. Predicted relation between induced polarization and the volume fraction of conducting spheres for values of the parameter τ.

resent conditions in a real rock. Therefore, only qualitative conclusions can be drawn from mathematical results based on an assumption of spherical grains.

When conductive spheres are distributed so that the distances between the spheres are large compared with their radii, the transient voltage following the abrupt termination of current flow will be:

$$e(t)/V = \frac{9k\tau}{1 + 2\tau} \exp\left[-W_0(1 + 2\tau)\right], \quad (10)$$

where

$e(t)$ is the transient voltage drop between two points in the medium,

k is the fraction of the total volume occupied by the spherical particles,

W_0 is the relaxation constant of the interface in inverse seconds, and $\tau = R_s/f\rho$, where f is the radius of the spheres, ρ is the resistivity of the medium in which they are imbedded, and R_s is the specific surface resistance in ohm-m^2. Equation (10) is a close approxi-

mation if the volume of the spheres does not exceed several percent of the total volume.

V is the primary field in volts.

The charge, Q, for a given length, l, represented by the transient voltage can be computed by integrating the expression for the transient voltage and dividing by the composite resistivity of the medium:

$$Q = \int_0^\infty \frac{e(t)l}{\rho} \, dt$$

$$Q = \frac{9k\tau Vl}{\rho_c W_0^{(1+2\tau)^2}}, \quad (11)$$

where the composite resistivity, ρ_c, can be taken as nearly equal to the resistivity of the medium without the spheres, ρ, as we have already assumed the concentration of spheres to be quite small. Figure 2 is a graph with curves showing the relation between the volume of conducting spheres and the transient charge for values of the parameter, τ. The transient charge has a maxi-

mum value when $\tau = 0.5$. Therefore, because $\tau = R_s/f\rho$, maximum charge will be stored when the radius, f, of the spheres is $2R_s/\rho$. The dependence of induced polarization on the size of the spheres plotted in terms of values of τ, is shown in Figure 3.

Induced polarization will be a maximum when $R_s = f\rho/2$, if other factors remain constant. This is a rather interesting phenomenon, for the largest polarizations are not contributed by grains with extremely high surface resistances or overvoltage. If grains with a very high overvoltage are inserted in a conductive medium, their high surface resistance will cause the current to flow around the grains, rather than through them.

So far, we have assumed no interaction between the fields of the spheres. When a sphere is polarized, positive charges will accumulate on the face opposite the direction of the applied field, and negative charges will accumulate on the other face, forming a multipole field opposed to the applied field. This will increase the field strength polarizing neighboring spheres, causing a higher total polarization than is indicated in equation (11) (see Frohlich, 1949, chap. II, p. 15–48).

Although the theory outlined in the preceding paragraphs is sketchy and includes many ap-

proximations, it is useful in predicting the effect of various parameters in controlling induced polarization. In summarization, we might expect induced polarization to behave in the following ways:

a) Electrolytic polarization should increase linearly with current density and follow the decay curve shown in equation (5).

b) Electrolytic polarization should be a maximum when half the negative charge is fixed in the form of cation-exchange capacity and half is in the form of anions in solution. In rocks saturated with fresh water, the amount of induced polarization should decrease with increasing shaliness, whereas in rocks saturated with brackish or saline water, the amount of induced polarization should increase with increasing shaliness.

c) Overvoltage polarization is not linearly proportional to current density. At high current densities through a metal-electrolyte interface, there is relatively less polarization than at low-current densities.

d) When polarizing particles are distributed in a conductive matrix, there is an optimum particle size, depending on the contact resistance at the particle surfaces and the matrix resistivity, which will yield maximum induced polarization.
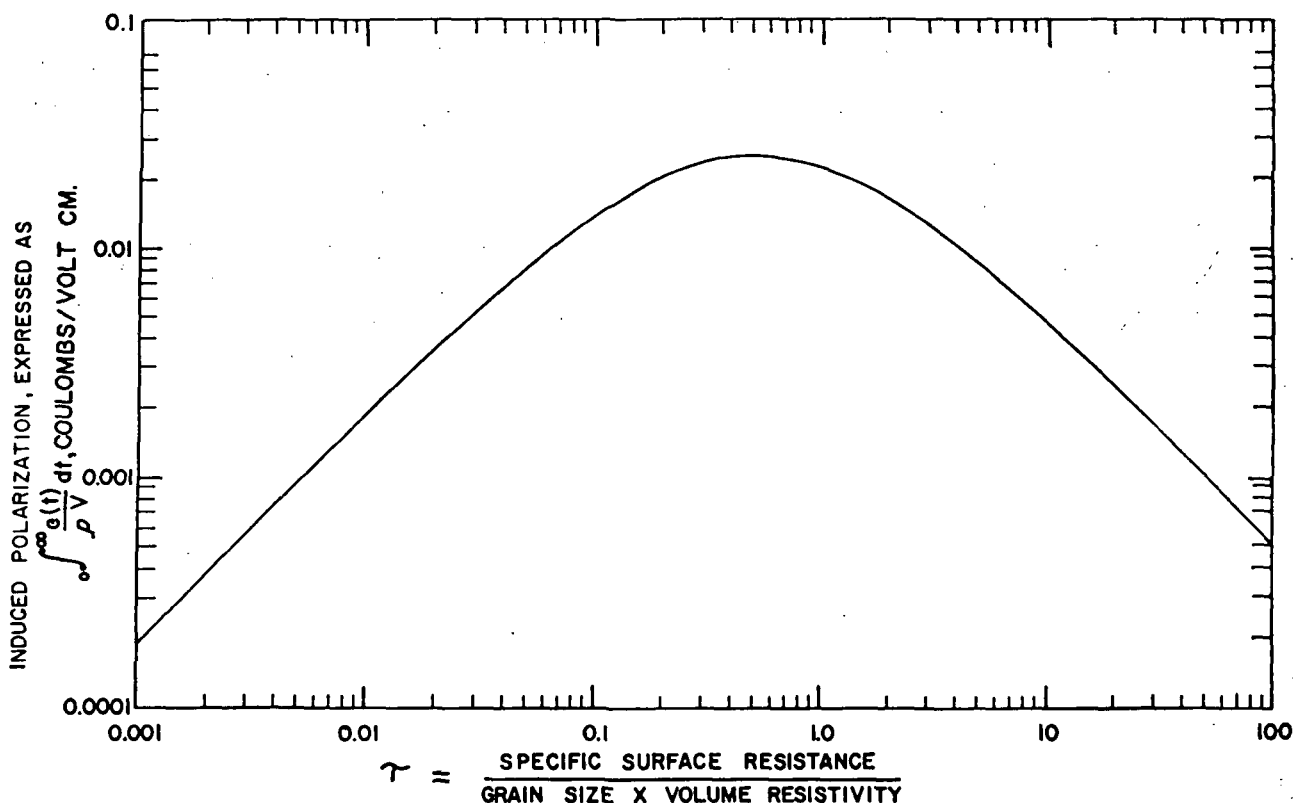

FIG. 3. Predicted relation between induced polarization and τ with τ varying only in grain size and the volume fraction of conducting spheres remaining constant.
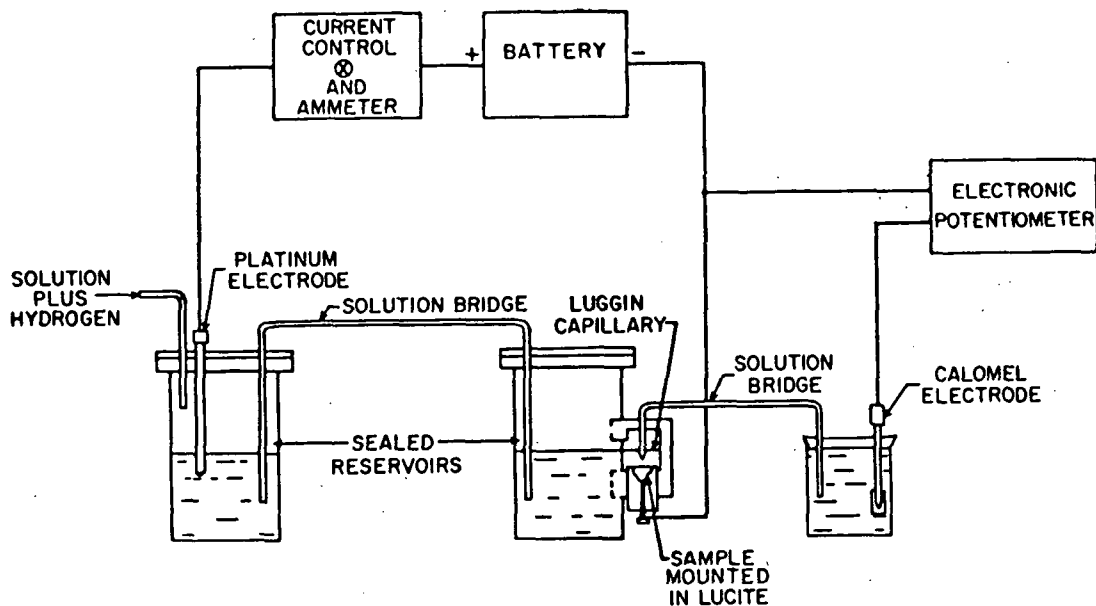
FIG. 4. Laboratory apparatus for overvoltage measurements.

e) Decreasing the resistivity of the matrix in which metallic particles are distributed will increase the amount of polarization if the resistivity is very high, but will decrease it if the resistivity is initially very low.

f) Increasing the current density may either increase or decrease the induced polarization, depending on whether the matrix resistivity is low or high, respectively.

g) Induced polarization should increase somewhat more rapidly than in direct proportion to the amount of conductive mineral present, other factors being equal. At high concentrations of a conductive mineral, when current may flow directly from grain to grain without polarization taking place, the amount of induced polarization may be sharply decreased.

EXPERIMENTAL WORK

Experiments were conducted to test the theory outlined in the preceding section and, in particular, to evaluate the relative importance of the various factors affecting induced polarization. The study was restricted to the system: sandstone-pyrite-sodium chloride-electrolyte. Overvoltage measurements were made on single crystals of pyrite; polarization measurements were made on mixtures of clean quartz sand and pyrite and on natural sandstone samples containing pyrite. At the end of the investigation, a brief field study was carried out over a quartz-pyrite tailings pile which contained two percent pyrite by weight to determine the effectiveness of the induced-polar-

ization method in detecting small sulfide concentrations.

Overvoltage measurements

Several large crystals of pyrite were obtained from the Gilman mine, Colorado. The measurements consisted of placing a pyrite crystal in an electrolytic solution and measuring the electrode potential as a function of current density. The classic description of overvoltage measurements was given by Bowden and Rideal (1928).

Overvoltage measurements are subject to a number of experimental difficulties. The presence of oxygen in the electrolyte interferes with the electrode reaction, causing overvoltages to be erratic and nonreproducible. For this reason, it is important that overvoltages be measured in an oxygen-free atmosphere. In order to avoid spurious ohmic overvoltages caused by surface coatings, a freshly polished mineral face must be used.

The experimental setup we used is shown in Figure 4. A fresh mineral surface was obtained by mounting a crystal in lucite and then cutting the crystal in half and polishing. The sample was then placed in a holder from which air had been displaced by hydrogen. The electrolyte used in the experiment was prepared from triple-distilled water and sulfuric acid, boiled for a long period in a nitrogen atmosphere, and then forced into the hydrogen-filled reservoir, using nitrogen as a pressure agent. The face of the crystal was again polished, using a remotely controlled grinder.

Electrical contact to the pyrite crystal was

made through a brass screw threaded through the side of the lucite sample mount. Current was passed through the pyrite sample to a platinum electrode with a large surface area in a second reservoir; the two reservoirs were connected by a capillary salt bridge. The voltage drop between the pyrite crystal and a calomel electrode was measured with an electronic potentiometer with an input impedance of 100 megohms. The calomel electrode was located in a third reservoir, connected to the sample reservoir by a Luggin capillary whose point was placed very close to the polished surface of the sample so that a minimum amount of voltage drop due to current flow through the solution was included in the measurement.

Overvoltage was measured in a quiescent solution, no attempt being made to distinguish between concentration and activation overvoltage. Overvoltages were measured with current densities ranging from 10^{-4} to 10 amp/m². The upper limit of current density was usually determined by the point at which hydrogen gas was visible at the surface of the pyrite.

Data obtained by using one sample of pyrite are shown in Figure 5. These data are plotted as specific surface resistance: overvoltage divided by current density. At very low current densities, the

specific surface resistance seems to be independent of current density, having a value of 0.25 ohm-m². The surface resistance increases rapidly as the current density is increased from 0.1 to 0.25 amp/m². As the current density is increased further, the surface resistance decreases. This part of the data may be described by the empirical equation:

$$\frac{1}{R} = \frac{1}{R_0}\left[1 + \left(\frac{j}{J_0}\right)^{-m}\right], \qquad (12)$$

where

R is the specific surface resistance, as a function of current density, in ohm-m,²

R_0 is the specific surface resistance, at very low current densities, in ohm-m²,

j is the current density in amp/m²,

J_0 is the current density for a specific surface resistance of one ohm-m², obtained by extrapolating the linear portion of the curve in Figure 5,

m is the slope of the linear portion of the curve.

Equation (12) differs in form from equation (9). To compare our measurements with equation (9), we plotted the overvoltage data as functions of current density (Figure 6).
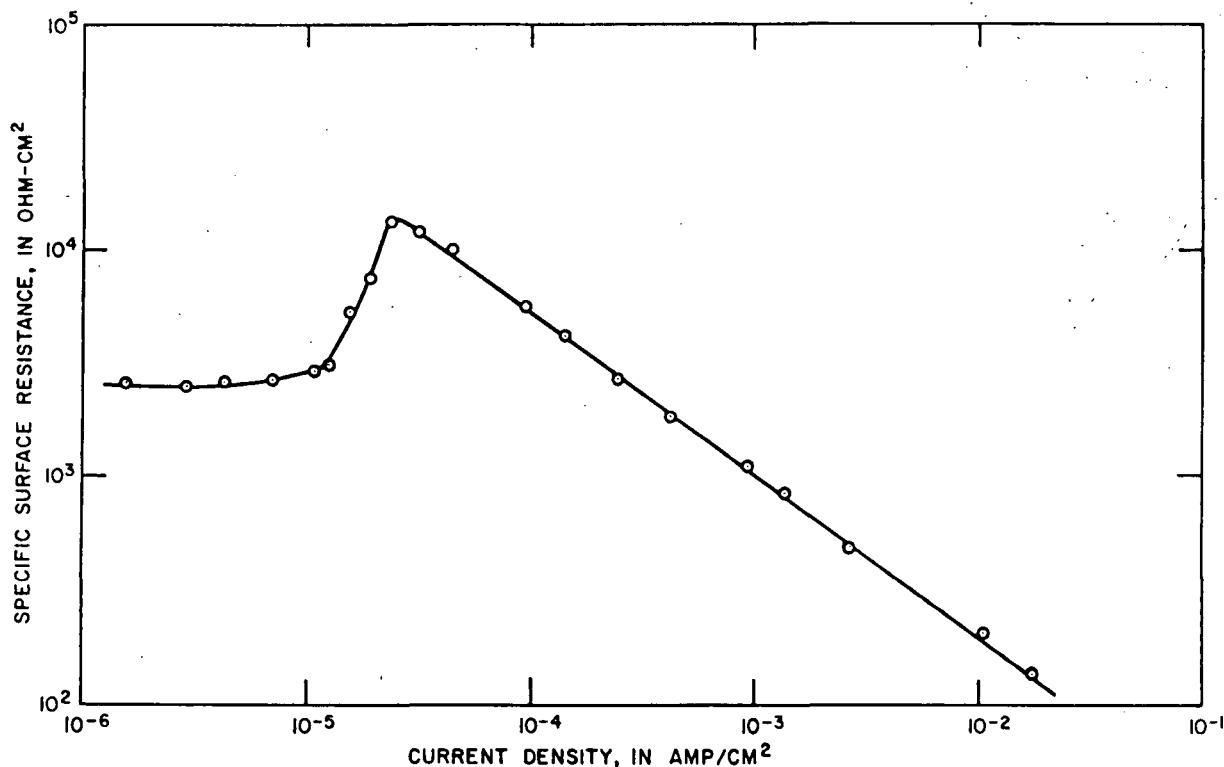

FIG. 5. Specific surface resistance measured as a function of current density for a sample of pyrite from Gilman, Colorado.
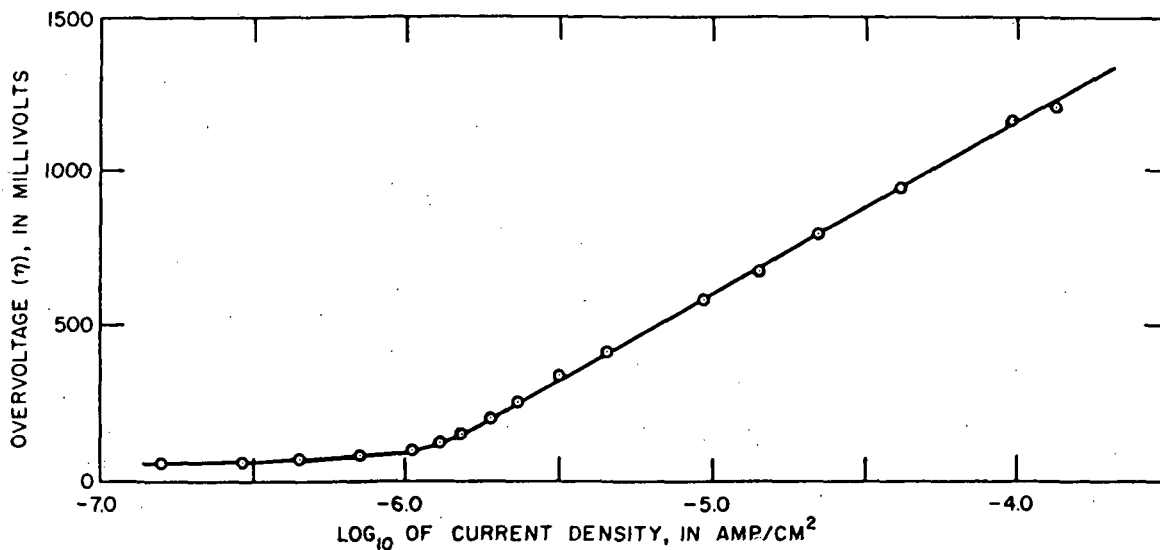
FIG. 6. Overvoltage measured as a function of current density for a sample of pyrite from Gilman, Colorado.

Our overvoltage data may be represented by either equation (9) or equation (12), within the limits of experimental error.

The measured values for the specific surface resistance of pyrite were substituted in equation (11) in order to determine the charge that should be stored by disseminated pyrite as a function of current density. Assuming a constant volume of pyrite spheres and a matrix resistivity of 50 ohm-m, we obtain the curves shown in Figure 7.

We see that the polarization should be greater when a low current density is combined with a large grain size. For very small grain sizes, the polarization is nearly the same at all current densities. The grain size which results in maximum polarization depends on the current density assumed. The amplitudes of these maxima increase as the current density decreases, since the surface resistance of the spheres decreases. This results in a short time constant and a proportionately small amount of charge represented by the transient response.

We should also note the relation between polarization and grain size for constant values of current density. At very small current densities the polarization increases with increasing grain size throughout the range of grain size used in this calculation. At high-current densities a maximum polarization charge is stored with relatively small grains, polarization decreasing as the grain size increases further.

All the curves shown in Figure 7 were calculated for a constant matrix resistivity of 50 ohm-m. Similar curves are obtained if other val-

ues are assumed, lower maxima being found for lower values of matrix resistivity. The opposite would be true for an increase in matrix resistivity. Optimum conditions for maximum induced polarization seem to be low current density, high volume resistivity, and moderately large grain size.

Induced-polarization measurements on mixtures of quartz and pyrite

Induced-polarization measurements were made on mixtures of quartz and pyrite to check the effects of grain size and concentration predicted in the preceding sections. Samples were prepared by combining a clean quartz sand of uniform grain size with varying percentages of pyrite. The mixture was placed in a troughlike holder, water was added, and the mixture was compressed under moderate pressure.

The equipment used in measuring polarization of cores has been described in part in an earlier publication (Keller, 1960, p. 113–115). An electronic timer which can be set for intervals between 15 millisec and 150 sec was used to operate a pair of relays that provided a pulse of current to the sample. At the conclusion of the pulse, another relay connected a pair of pickup electrodes to the recording circuit, which consisted of an integrating network, a pair of dc amplifiers, and a four-channel oscillograph. The oscillograph recorded the applied voltage and transient voltage across the pickup electrodes, the time integral of the transient, and the current.

For analysis of the data obtained in this man-

ner, a graph showing the relation between the integrated transient voltage and the duration of the exciting pulse was prepared for each set of measurements. An example of such a curve is shown in Figure 8. The charge stored by a sample, per volt applied, may be computed from the integrated transient voltage:

$$Q/V = \int_0^\infty \frac{e(t)}{RV} \, dt, \qquad (13)$$

where R is the electrical resistance of the sample and V is the steady-state voltage drop. Specific capacity, ζ, may be computed if this charge per volt is divided by the geometric factor for the sample:

$$\zeta = Q/KV, \qquad (14)$$

where $K = A/l$; l is the length of the sample and A is the cross-sectional area through which the current is passed.

Data for samples of pure sand and sand with 15, 20, and 33 percent pyrite (by weight) are
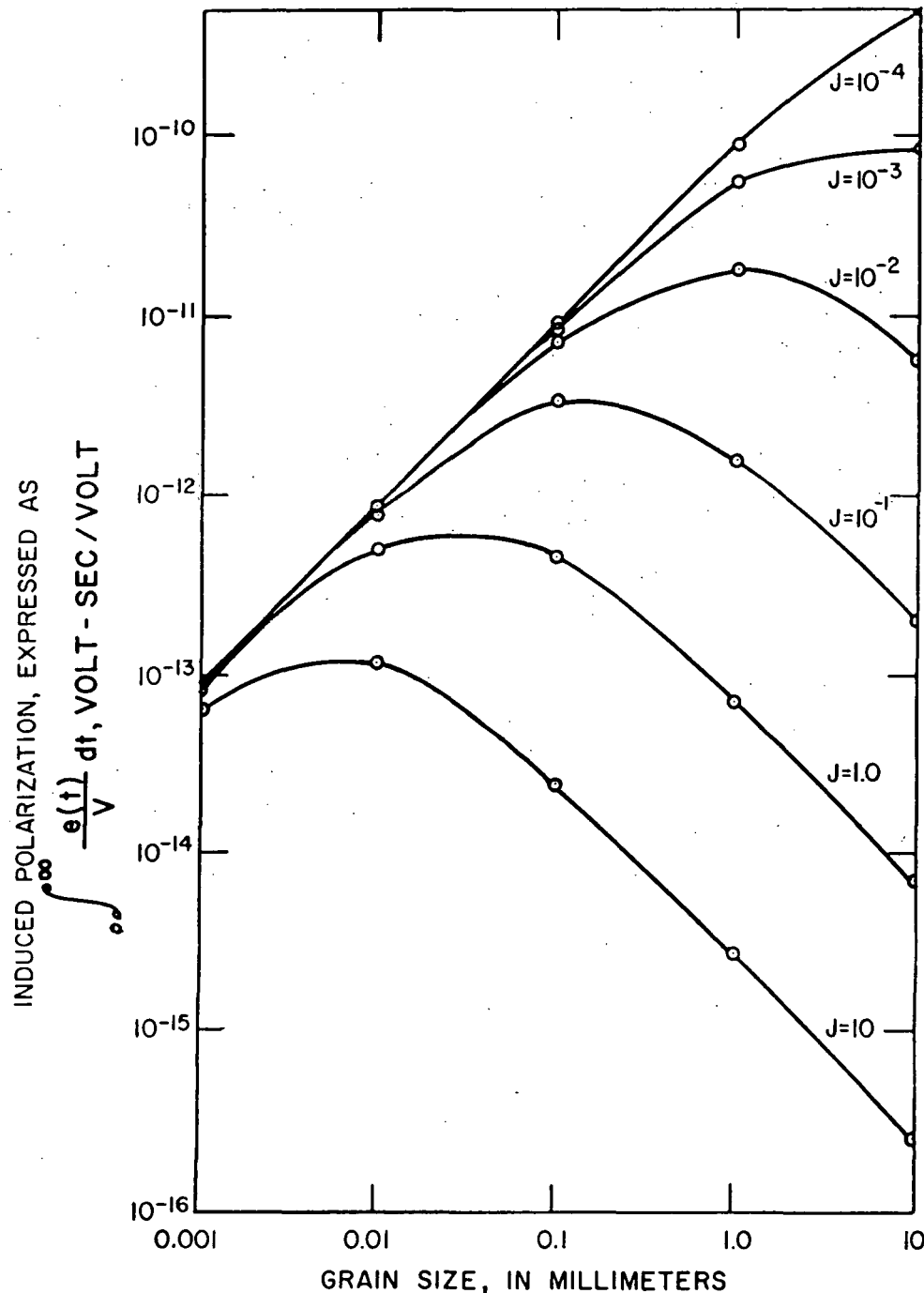

FIG. 7. Predicted relation between grain size and induced polarization for a distribution of pyrite particles in a uniform matrix.
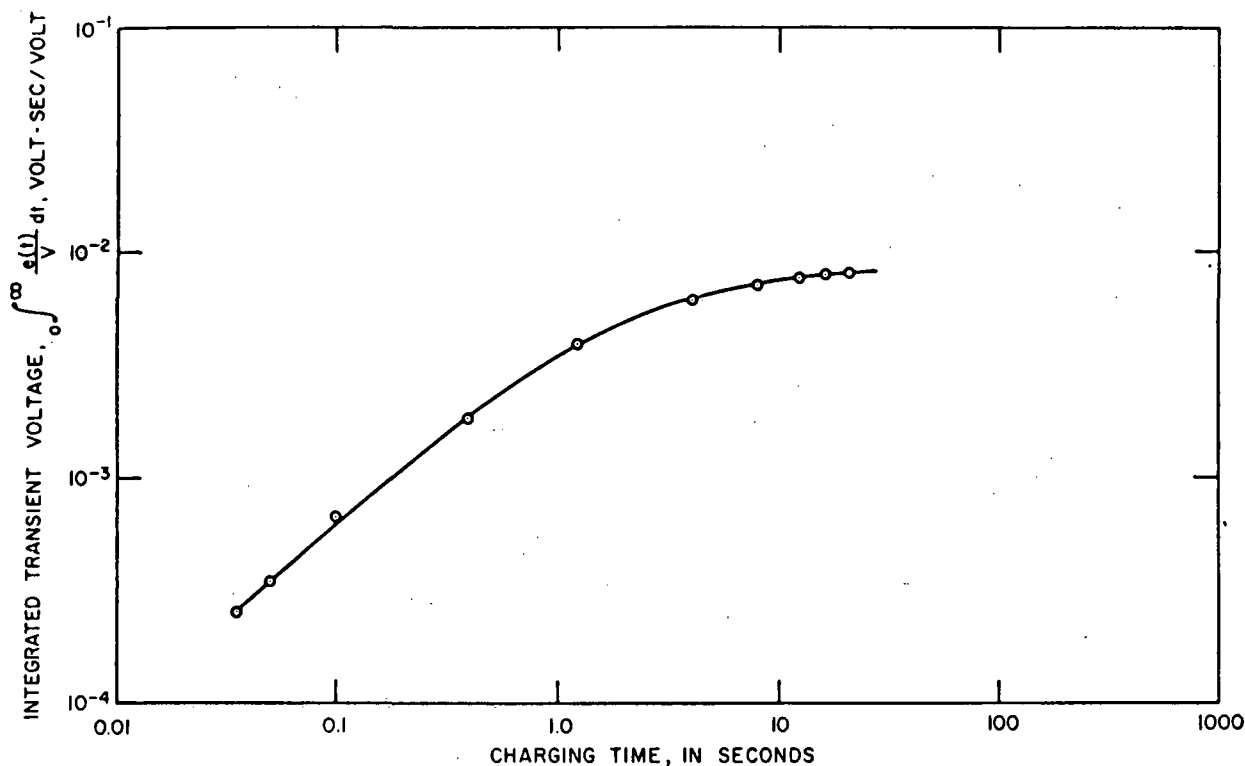
FIG. 8. Measured relation between integrated transient voltage and pulse duration for a sample of pyritic sandstone.

shown in Figure 9. Pyrite concentrations of more than 10 percent were required before polarization became greater than that for a pure-quartz sand.

For long charging periods, the polarization charge stored by the pure-sand sample is greater than that stored by the pyrite-sand mixture with 15 percent pyrite. The polarization charge stored by the sand increases linearly with charging time up to about 60 sec. The charge stored by pyrite-bearing sands reaches an asymptotic value for charging times of 10 to 20 sec.

A factor which must be considered is that the packed sand provides a low-resistivity matrix due to its high porosity, so that most of the current bypasses the pyrite grains. According to the calculations on which the curves in Figure 7 are based, low volume resistivity causes relatively little polarization.

All the measurements on the sand-pyrite mixtures were made with a current density of approximately 100 amp/m² because it was not possible to obtain measurable transient voltages in the laboratory with lower current densities. At this current density, equation (9) is not generally true, as an irreversible chemical reaction at the surface of the pyrite alters the composition at the crystal surface. No attempt was made to measure polarization as a function of current density.

Assuming that the polarization will increase at lower current densities as predicted by equation (9), at a current density of 10^{-1} amp/m², we would expect the polarization contributed by pyrite to increase eightfold, and the electrolytic polarization for the pure sand to remain the same.

The effect of grain size was also studied, using mixtures of pyrite and sand. The samples consisted of sand mixed with 15 percent uniformly sized pyrite grains. Figure 10 shows the results of these measurements, with polarization charge plotted as a function of the pyrite grain size in the range 0.05 mm to 5 mm diameter.

Maximum polarization charge was stored by the sample containing pyrite grains 0.2 mm in diameter.

Measurements on pyrite-bearing sandstone samples

In the sand-pyrite mixtures, the pyrite grains were scattered uniformly through the medium. It is unlikely that such a uniform dispersion would be found in nature. Polarization measurements were made on 24 natural sandstone samples taken from drill holes in the Shinarump Member of the Chinle Formation from northern Arizona. Of the
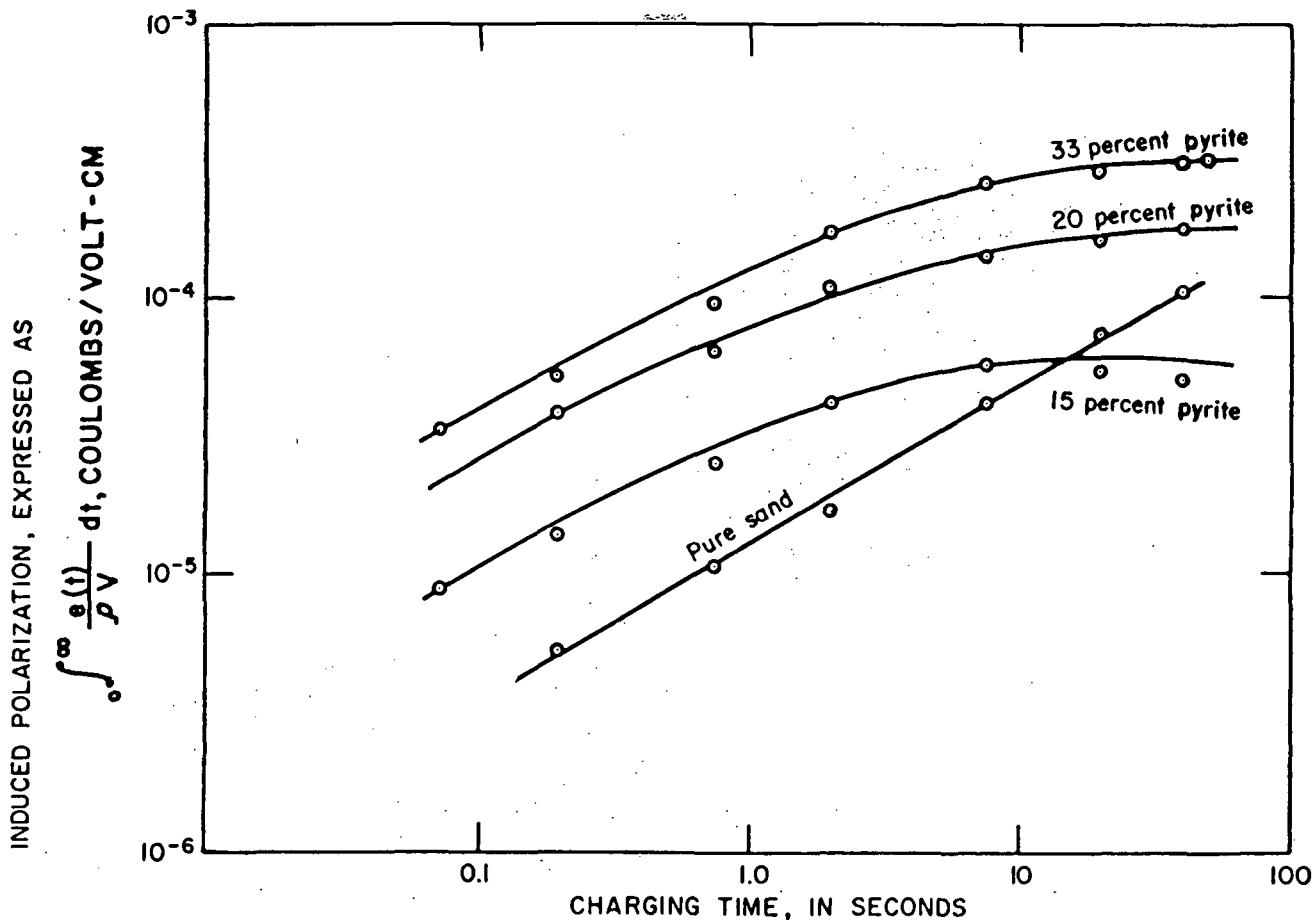
FIG. 9. Observed relation between induced polarization and pyrite content for mixtures of pyrite and sand.

24 samples used, five contained pyrite in amounts from 0.66 to 21.6 percent by weight, and the remainder contained only traces.

The samples were prepared by cutting them into discs having diameters of two inches and thicknesses of one-third inch. In recording electric transients on these core samples, a disc was

placed in a core holder consisting of two circular silver plates which served as current contacts. Separate silver strips were used as pickup electrodes to avoid electrode polarization. Contact between a core and the silver plates was made through sheets of blotting paper soaked in a dilute silver nitrate solution.

In addition to polarization measurements, electrochemical EMF's were measured by placing a core sample between two reservoirs containing aqueous solutions of sodium chloride with concentrations of 50,000 ppm and 5,000 ppm. The potential drop across the sample caused by ion diffusion was measured by a potentiometer from a pair of calomel electrodes inserted in the reservoirs. Voltage readings were taken repeatedly until equilibrium was reached.

The electrochemical-electromotive force (EMF) measurements were used to calculate the number of immobilized negative charges in the rock structure (McCardell, Winsauer, and Williams, 1953). Table 1 lists the electrochemical EMF measured for each sample when saturated with fresh water, and the calculated corresponding value of immobilized charge concentration. The pyrite-bearing
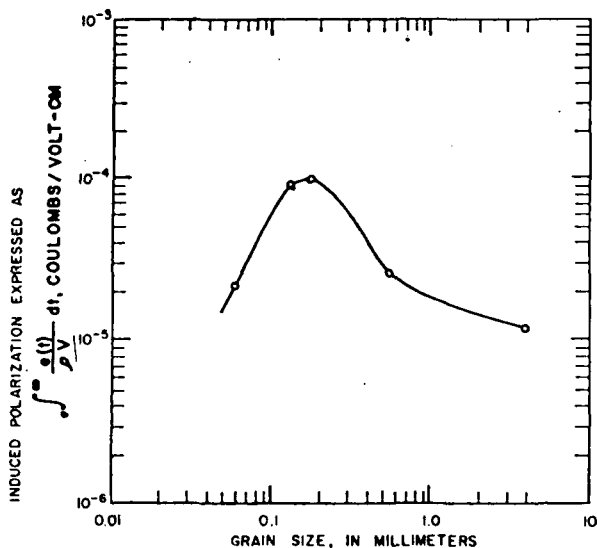

FIG. 10. Observed relation between induced polarization and pyrite grain size for mixtures of pyrite and sand.

Table 1. Electrochemical EMF's measured on sandstone samples saturated by distilled water

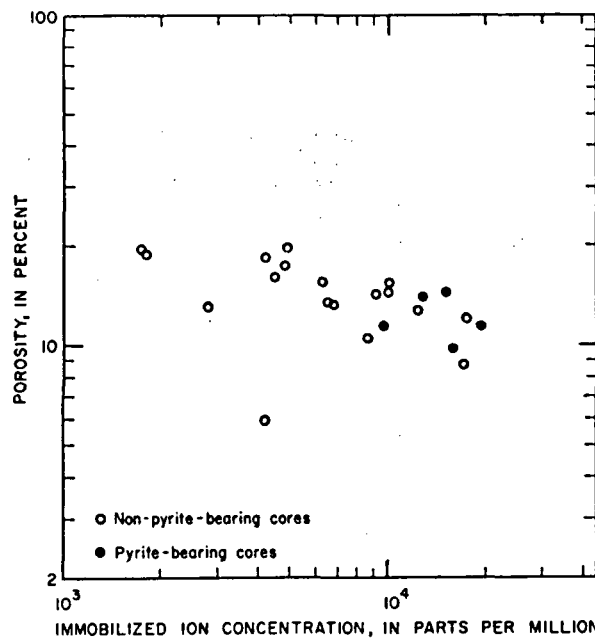| Sample	Self-potential in mv	Immobilized ion concentration
237	7.1	4,200
238	12.3	0
239	7.7	3,750
240	6.5	4,500
241	10.5	1,000
243	4.2	5,900
244	9.3	2,280
245	12.8	0
247	9.3	2,280
248	1.2	7,350
249	7.1	4,200
253	−11.7	17,500
258	− 2.0	9,700
259	1.6	7,000
260	2.5	6,750
261	− 0.3	8,400
262	− 6.8	13,800
263	− 3.8	11,200
264	− 1.3	9,100
265	− 9.2	14,500
266	− 1.3	9,100
267	− 1.0	8,800
268	− 8.0	15,000
269	− 4.0	11,300

Fig. 11. Relation between porosity and fixed ion concentration calculated from electrochemical EMF measurements.

cores (Table 2) show a high value of immobilized charge and a trend toward lower immobilized ion concentration with increasing porosity (see Figure 11). The high value of immobilized charge in the pyritic cores is questionable in that an oxidation-reduction EMF may add to the effect of the electrochemical EMF.

The core samples were disaggregated to separate the heavy minerals from the grains comprising the matrix. The bulk of the heavy minerals was found to be pyrite, though small quantities of

Table 2. Physical characteristics of natural-sandstone samples

Sample	Effective porosity in % after saturation by 50,000 ppm saline solution	Grain size of matrix in mm	% pyrite by wt	Grain size of pyrite in mm	% carbon by wt
237	13.4	0.4–0.7			
238	16.12	0.1–0.25			
239	20.37	0.05–0.1			
240	6.08	0.1 –0.7			
241	5.94	0.0 –0.25			
243	14.1	0.1 –0.2			
244	20.1	0.13–0.25			
245	19.45	0.12–0.24			
247	10.1	0.12–0.25			
248	18.66	0.13–0.25			
249	18.4	0.12–0.25			
253	8.1	0.06–0.12			
258	15.92	0.09–0.2			
259	14.94	0.12–0.25			
260	13.8	0.03–0.11			
261	14.5	0.1 –0.7	5.18	.001–0.05	6.1
262	13.8	0.1 –0.7	0.66	.005–0.4	2.68
263	11.7	0.1 –0.25	21.6	.001–0.1	3.2
264	11.0	0.05–0.1	5.12	.001–0.8	0.45
265	10.0	0.1 –0.75	2.65	.001–0.3	2.3
266	10.8	0.05–0.25			
267	15.8	0.1 –0.5			
268	10.1	0.1 –0.25			
269	12.9	0.05–5.0			

uraninite, sphalerite, and galena were also present. Table 2 lists the range in grain size of the matrix and the pyrite, and the amount of pyrite and carbon in the samples containing measurable amounts of pyrite. Other samples contained some carbon, but in very small quantities.

Previous work (Keller, 1960, p. 121) has indicated that the transient discharge curves can be fitted by an equation of the form:

$$q(t) = E_0 C_g \frac{\gamma b}{T_0 \sqrt{\pi}} \int_0^{\Delta t}$$

$$\cdot \int_{-\infty}^{\infty} [\exp(-b^2 z^2 - z - t/T_0 e^{-z})] dz dt, \quad (15)$$

where

   γ is the constant of proportionality,

   b is related to the reciprocal of the standard deviation of the distribution of time constants in the transient,

  T_0 is the principal time constant,

   t is all possible values of time constants, from 0 to ∞,

   $z = \ln t/T_0$,

  E_0 is the initial voltage,

  C_g is the geometric capacity of the system, and

  Δt is the time which determines the length of the pulse.

The discharge rate parameter b and the principal time constant T_0 were determined by use of a graphical technique described by Keller (1960). These values are listed in Table 3 along with other electrical properties of the sandstone samples. The value of b varied for the pyrite-bearing sandstones from 0.37 to 0.88 and from 0.2 to 1.29 for the nonpyritic sandstones. The principal time-constant variation ranged from 10.2 to 47.8 sec for the pyritic samples and from 7.4 to 269 sec for the nonpyritic samples. For neither parameter was there a significant difference between the pyritic and nonpyritic samples, but the range of values for the principal time constant was the same as that found by other investigators and summarized by Keller (1959).

An excellent inverse correlation was found between induced polarization and resistivity, as shown in Figure 12. With one exception, the resistivities of the pyritic samples were in the same range as that for the nonpyritic samples. The exception was core sample 263 which had the highest percentage of pyrite and the highest polarization. The values for percentage of pyrite are listed in Table 2 and the values for amount of polarization are listed in Table 3. An ion-trap number, which is a measure of the number of pores blocked by anion barriers, was defined as follows:

Table 3. Electrical properties of sandstone samples

| Sample	Discharge rate parameter b	Principal time constant T_0 in sec	Resistivity in ohm-m	Specific capacity in farads/cm	Ion trap number
237	0.39	37.2	582	0.549×10^{-6}	3.56×10^{-3}
238	0.54	20.0	262	0.685×10^{-6}	6.82×10^{-3}
239	0.23	7.4	236	0.506×10^{-6}	9.17×10^{-3}
240	1.1	15.1	2,870	0.030×10^{-6}	2.4×10^{-3}
241	0.35	64.6	1,660	0.194×10^{-6}	0.57×10^{-3}
243	0.65	15.9	450	0.76×10^{-6}	8.26×10^{-3}
244	0.62	26.3	2,370	1.35×10^{-6}	3.39×10^{-3}
245	0.6	23.9	175	3.04×10^{-6}	3.37×10^{-3}
247	0.5	14.5	197	0.792×10^{-6}	7.33×10^{-3}
248	1.1	10.7	437	0.281×10^{-6}	11.7×10^{-3}
249	1.29	39.8	265	2.61×10^{-6}	8.02×10^{-3}
253	0.2	269	201	1.72×10^{-6}	11.2×10^{-3}
258	0.46	135	117	4.38×10^{-6}	8.97×10^{-3}
259	0.57	17.0	111	3.67×10^{-6}	11.7×10^{-3}
260	0.37	19.1	270	1.17×10^{-6}	8.4×10^{-3}
261	0.42	29.5	173	4.86×10^{-6}	15.3×10^{-3}
262	0.74	22.4	144	2.86×10^{-6}	16.8×10^{-3}
263	0.37	47.8	97.2	8.94×10^{-6}	9.99×10^{-3}
264	0.88	10.2	212	1.67×10^{-6}	16.5×10^{-3}
265	0.60	13.8	218	1.35×10^{-6}	12.5×10^{-3}
266	0.36	41.7	384	0.637×10^{-6}	8.31×10^{-3}
267	0.45	15.1	124	1.66×10^{-6}	13.9×10^{-3}
268	0.68	44.6	115	2.27×10^{-6}	14.3×10^{-3}
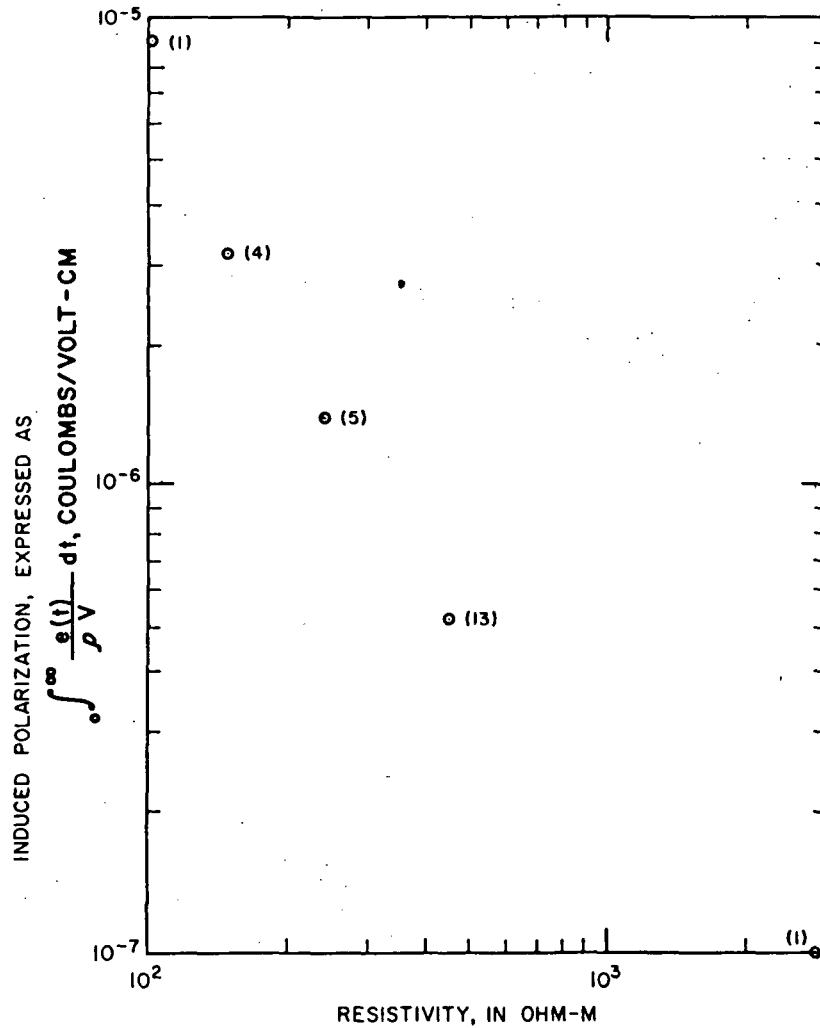
FIG. 12. Observed correlation between induced polarization and resistivity for natural-sandstone samples. Number by a point indicates number of samples.

$$N = \frac{a_0}{a}\left(\frac{a - a_0}{2a - a_0}\right), \qquad (16)$$

where a and a_0 have the same meanings as for equation (5).

A correlation between induced polarization and ion-trap number is shown in Figure 13. The pyritic samples were omitted because we doubt the values determined for immobilized ion charge are significant when pyrite is present in a sample. The correlation supports the theory that the ion-trap phenomenon is an important part of the total polarization effect.

The induced polarizations determined for both natural and synthetic pyritic samples are shown plotted as a function of pyrite content in Figure 14. The induced polarization is approximately proportional to the volume percentage of pyrite, except for the natural-sandstone samples containing less than 6-percent pyrite, in which it is anomalously low. These differences, which we think

are caused by the pyrite distribution within the sandstone, become less apparent as the amount of pyrite in the rock increases. The polarizations of the natural and synthetic samples containing approximately 20 percent pyrite vary by a factor of only two.

Field measurements

The laboratory measurements indicated that relatively large amounts of pyrite are needed to add appreciably to the background level of electrolytic polarization. On the basis of the laboratory measurements of polarization data, we would expect that pyritic sandstone would be difficult to distinguish from nonpyritic sandstone. However, our theory, which requires that overvoltage polarization becomes relatively more important at low current densities, implies that laboratory measurements underestimate the utility of polarization measurements.
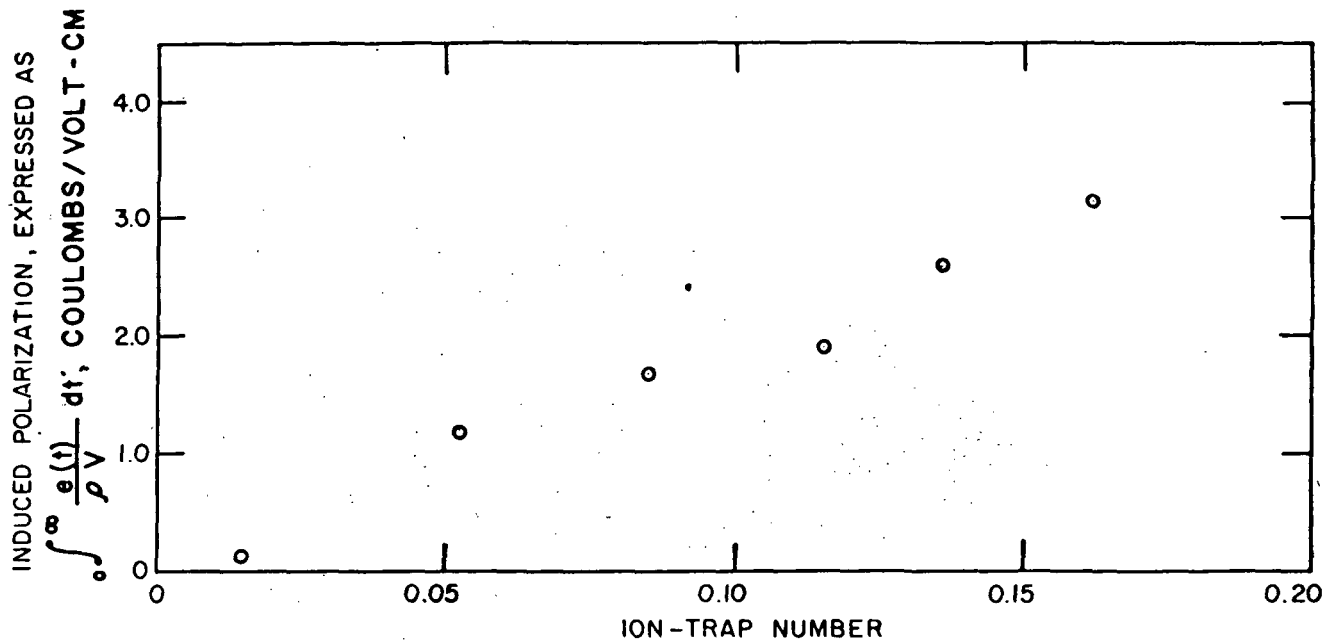
A brief program of field measurements was

FIG. 13. Observed correlation between induced polarization and ion-trap number for natural-sandstone samples.

carried out at an old tailings pond near Idaho Springs, Colorado. Pyritic sandstone was abundant, but no locality was found where we could easily obtain adequate geologic information on the occurrence of the pyrite in sandstone. The tailings pond provided a quartz-pyrite medium in which there was precise information both on the pyrite content and on the extent of the medium.

A single-pole electrode array was used in profiling across the tailings pond. Two electrodes, one for current and one for pickup, were placed several hundred feet apart, a moderate distance from the edge of the pond. The profile was made with two moving electrodes, one for current and one for potential, separated by a distance of 5 ft. A manually operated switch was used to provide current pulses and to separate the transient from the in-phase voltage. Current and in-phase voltages were recorded on meters, and the transient voltage was integrated with a ballistic fluxmeter.

In making the profiles, two currents were used, one of 300 milliamperes and the other 30 milliamperes. These correspond to current densities through the pores of 2.1×10^{-3} and 2.1×10^{-4} amp/m^2, respectively, at a distance of 5 ft from the current electrode, assuming the water content of the medium to be 33 percent. Two sets of data are shown in Figure 15. The survey could not be extended beyond the left boundary of the pond, so the polarization contrast between barren ground and the pyrite mixture is apparent

only on the right side of the figure. It is significant that a two-percent concentration of pyrite was sufficient to cause a detectable polarization response, particularly inasmuch as polarization should be less in a highly conductive medium such as this than in a more resistive medium.
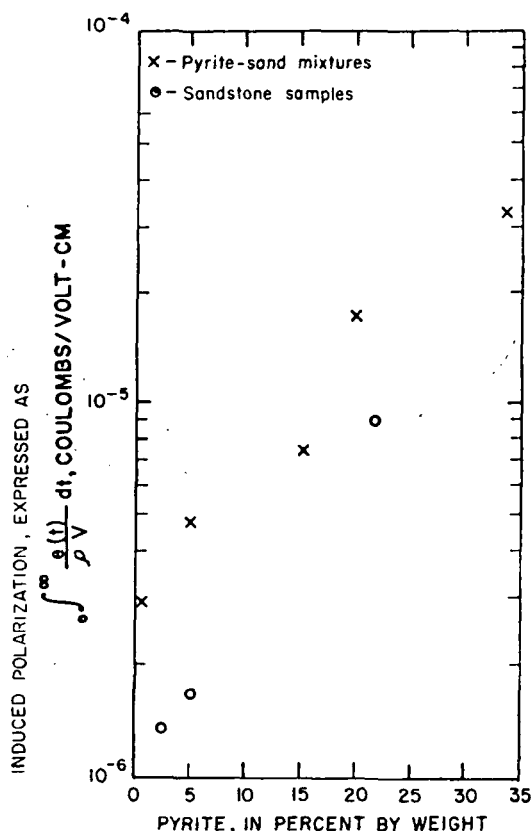

FIG. 14. Observed correlation between induced polarization and pyrite content for both sandstone samples and sand-pyrite mixtures.
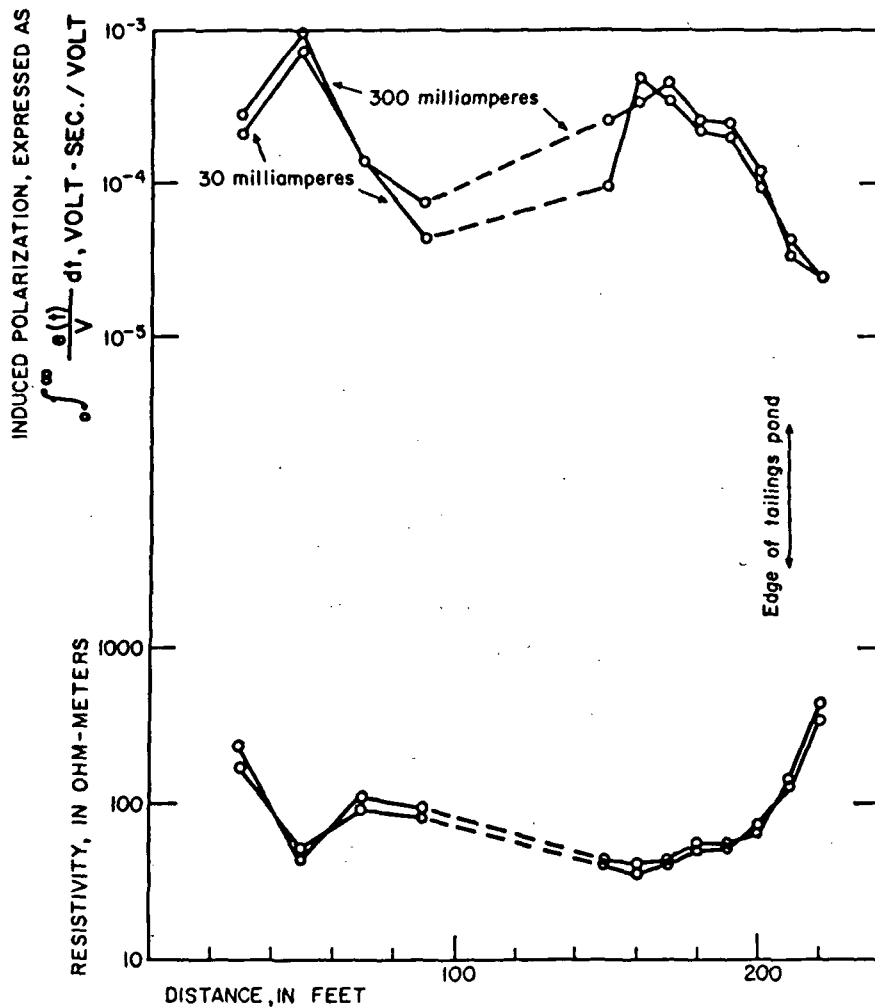
FIG. 15. Field measurements of resistivity and induced polarization over a tailings
pond containing two-percent pyrite.

The curves shown in Figure 7 predict no change in polarization due to variations in current density below approximately 10^{-5} amp/cm². The polarization curves in Figure 15 show this prediction to be true. The transient voltage was proportional to the applied voltage.

SUMMARY AND CONCLUSIONS

From theoretical considerations, it is evident that induced polarization contributed by overvoltage effects should depend upon the current density, the size of the sulfide particles, the resistivity of the matrix, and the distribution of the sulfide grains, as well as the total sulfide content. Laboratory studies have shown that all of these variables do affect polarization as expected. Single-crystal overvoltage measurements on pyrite showed that the specific surface resistance of the crystal does decrease rapidly as current density is increased. Measurements made on mixtures of sand and pyrite showed that polarization does depend on sulfide grain size. Measure-

ments on natural samples indicated that pyrite occurring in nodules or in association with carbon may be ineffective in polarizing, and fairly large amounts of pyrite are necessary to provide polarization in excess of the background level caused by electrolytic polarization. A field survey over a tailings pond showed that the laboratory measurements would lead to a pessimistic estimate of how much pyrite was needed to be detectable.

Pyrite in sandstone probably causes a comparatively more difficult problem in induced-polarization prospecting than does sulfide mineralization in limestone or igneous rocks; in the latter rock types, the high matrix resistivity assures current flow through the sulfide grains even when their surface resistances are high.

It is important to point out that for any rock, laboratory measurements of polarization will show values that are much lower than those obtained in the field, as the current densities used in the two situations are so different. Perhaps the most re-

liable approach to polarization analysis is through overvoltage measurements, which provide the basic data necessary for distinguishing between electrometallic and electrolytic polarization. Laboratory studies of induced polarization, in which high current densities are used, may provide highly misleading results.

REFERENCES

Bowden, F. P., and Rideal, E. K., 1928, Electrolytic behavior of thin films. Part I-Hydrogen: Royal Soc. (London) Proc., ser. A., v. 120, p. 59–79.

Butler, J. A. V., ed., 1952, Electrical phenomena at interfaces; in chemistry, physics, and biology: New York, MacMillan Co., 318 p.

Frohlich, Herbert, 1949, Theory of dielectrics; dielectric constant and dielectric loss: Oxford, Oxford Univ. Press, 180 p.

Grim, R. E., 1953, Clay mineralogy: New York, McGraw-Hill Book Co., Inc., 384 p.

Jost, W., 1952, Diffusion in solids, liquids, gases: New York, Academic Press, Inc., 558 p.

Keller, G. V., 1959, Analysis of some electrical transient measurements on igneous, sedimentary, and metamorphic rocks, Chap. 7, *in* Wait, J. R., ed., Overvoltage research and geophysical applications: New York, Pergamon Press, Inc., p. 92–111.

——— 1960, Pulse-transient behavior of brine-saturated sandstones: U. S. Geol. Survey Bull. 1083-D, p. 111–129, Figs. 36–44.

——— and Licastro, P. H., 1959, Dielectric constant and electrical resistivity of natural-state cores: U. S. Geol. Survey Bull. 1052-H, p. 257–285, Figs. 68–88.

Mayper, V., Jr., 1959, The normal effect, Chap. 10, *in* Wait, J. R., ed., Overvoltage research and geophysical applications: New York, Pergamon Press, Inc., p. 125–158.

McCardell, W. M., Winsauer, W. O., and Williams, M., 1953, Origin of electrical potential observed in wells: Trans. Am. Inst. Mining Metall. Petroleum Engineers, v. 198, p. 41–50.

Seigel, H. O., 1959, A theory of induced polarization effects (for step-function excitation), Chap. 2, *in* Wait, J. R., ed., Overvoltage research and geophysical applications: New York, Pergamon Press, Inc., p. 4–21.

Wait, J. R., 1959, A phenomenological theory of overvoltage for metallic particles, Chap. 3, *in* Wait, J. R., ed., Overvoltage research and geophysical applications: New York, Pergamon Press, Inc., p. 22–28.

Electrical Methods
in Geophysical Prospecting

by

GEORGE V. KELLER

Colorado School of Mines,
Golden, Colorado, U.S.A.

and

FRANK C. FRISCHKNECHT

U.S. Geological Survey,
Denver, Colorado, U.S.A.

TABLE 8

Expressions for Archie's law which have been reported in the literature

Formations for which equations were developed	Porosity range	Number of measurements	Equation
Frio sandstone (Oligocene) Bradford sandstone (Devonian) Woodbine sand (Cretaceous) Wilcox sand (Eocene)	0·15–0·37	30	$F = 0·62\,\varphi^{-2·15}$
Pennsylvanian sandstone, Oklahoma	0·08–0·20	97	$F = 0·65\,\varphi^{-1·91}$
Morrison sandstone (Jurassic), Colorado	0·14–0·23	243	$F = 0·62\,\varphi^{-2·10}$
Clean Miocene sandstone, Weeks Island, Louisiana	0·11–0·26	35	$F = 0·78\,\varphi^{-1·92}$
Clean Cretaceous sandstone, Paluxy sand, Texas	0·08–0·25	50	$F = 0·47\,\varphi^{-2·23}$
Clean Ordovician sandstone, Simpson sand, Oklahoma	0·07–0·15	44	$F = 1·3\,\varphi^{-1·71}$
Shaley sandstone (Eocene), Wilcox formation, Texas	0·09–0·22	72	$F = 1·8\,\varphi^{-1·64}$
Shaley sandstone (Oligocene), Frio sands, Texas	0·07–0·26	63	$F = 1·7\,\varphi^{-1·65}$
Shaley sandstone (Cretaceous), Taylor sand, Texas	0·07–0·31	36	$F = 1·7\,\varphi^{-1·80}$
Oolitic limestone (Cretaceous), Pettit limestone, Texas	0·07–0·19	13	$F = 2·3\,\varphi^{-1·64}$
Oolitic limestone (Jurassic), Smackover limestone, Ark.	0·09–0·26	42	$F = 0·73\,\varphi^{-2·10}$
Siliceous limestone (Devonian), Texas	0·07–0·30	58	$F = 1·2\,\varphi^{-1·88}$
Limestone (Cretaceous), Rodessa limestone, Texas	0·08–0·30	37	$F = 2·2\,\varphi^{-1·65}$

ing to Archie's law in Fig. 9. In practice the uncertainty in knowledge of the proper numerical values for a and m is less serious than the uncertainty in the choice of the proper value for ϱ_w, the resistivity of the water in the pores. Unless water samples are available from wells, vague relationships such as those presented earlier for the dependence of water salinity on geologic age and environment must be used. Even when water samples can be obtained, it is not always certain that the conductivity of the water is the same after the water is removed from the rock as before.

5b. Interaction between electrolytic solutions and the rock framework

In using Eq. (7) to relate the bulk resistivity of a rock to the porosity and the resistivity of the water in the pore space, the appropriate value for the water resistivity is not always the same as that which would be measured on a

been reported in the literature

Number of measurements	Equation
30	$F = 0.62\,\varphi^{-2.15}$
97	$F = 0.65\,\varphi^{-1.91}$
243	$F = 0.62\,\varphi^{-2.10}$
35	$F = 0.78\,\varphi^{-1.92}$
50	$F = 0.47\,\varphi^{-2.23}$
44	$F = 1.3\,\varphi^{-1.71}$
72	$F = 1.8\,\varphi^{-1.64}$
63	$F = 1.7\,\varphi^{-1.65}$
36	$F = 1.7\,\varphi^{-1.80}$
13	$F = 2.3\,\varphi^{-1.64}$
42	$F = 0.73\,\varphi^{-2.10}$
58	$F = 1.2\,\varphi^{-1.88}$
37	$F = 2.2\,\varphi^{-1.65}$

uncertainty in knowledge of the
ious than the uncertainty in the
vity of the water in the pores.
ls, vague relationships such as
water salinity on geologic age
er samples can be obtained, it is
he water is the same after the

nd the rock framework

y of a rock to the porosity and
, the appropriate value for the
which would be measured on a

sample extracted from the pore space. Equation (7) indicates that the ratio of bulk resistivity to water resistivity should be a constant for a given porosity; that it should not depend on the resistivity of the water in the rocks. This ratio is called the *formation factor*. However, it is usually found that this ratio is less

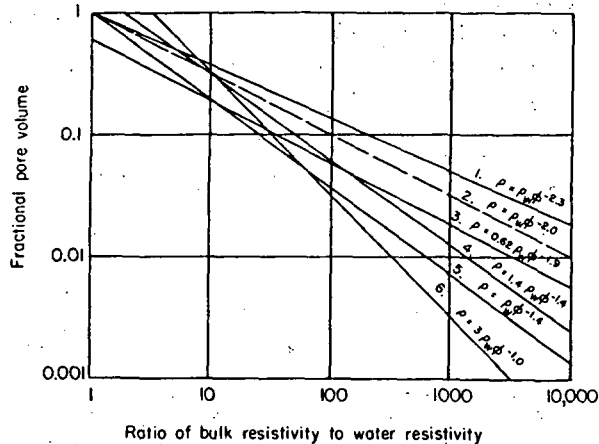Ratio of bulk resistivity to water resistivity

FIG. 9. Graphical presentation of the various forms of Archie's law. The dashed curve is a simple inverse square relationship between resistivity and porosity which is usually a good approximation to the more exact expressions. Curve 6 applies to a model consisting of three sets of straight tubular pores, each set of pores being at right angles to the directions of the other two sets.

when a rock is saturated with a dilute solution than when the rock is saturated with a highly-saline solution. This may be explained by considering that the conductivity of the water distributed through the pore space is usually increased by two phenomena: ionization of clay minerals and surface conductance.

Clay minerals, such as kaolinite, halloysite, montmorillonite, vermiculite, illite, chlorite and others, have the property of sorbing certain anions and cations and retaining these in an *exchangeable state* (see Grim, 1953). The common exchangeable ions adsorbed on clay are Ca, Mg, H, K, Na and NH_3, in order of decreasing abundance. The quantity of exchangeable ions attached to a clay is usually expressed in terms of the weight of ions in milliequivalents absorbed per 100 g of clay. The exchange capacities of some common clays are:

Kaolinite	3 to 15 m-equiv/100 g
Halloysite . $2H_2O$	5 to 10
Halloysite . $4H_2O$	40 to 50
Montmorillonite	80 to 150
Illite	10 to 40
Vermiculite	100 to 150
Chlorite	10 to 40
Attapulgite	20 to 30

Clay minerals are not the only materials exhibiting cation exchange capacity. All fine-grained minerals including quartz have an appreciable cation exchange capacity resulting from unsatisfied crystal bonds along the edges of grains. Exchange capacity is larger for finer grained particles. Zeolite minerals which are common in some volcanic rocks have cation exchange capacities of the order of 100 to 300 m-equiv per 100 g.

There are two principle causes for cation exchange properties in clays:

1. *Broken bonds* around the edges of the silica–alumina units in the crystal lattice contain unsatisfied ionic charges which are balanced by adsorbed ions. A single cation may be adsorbed on a clay mineral with a wide range of bonding energies.

2. Trivalent aluminium may *substitute* for quadrivalent silicon in the tetrahedral sheet structure of a clay mineral, leaving an unbalanced charge in the crystal. Ions of lower valence, such as magnesium, may substitute for aluminium in the lattice with the same effect. Exchangeable ions adsorbed by the unbalanced charges resulting from such substitution are usually found on the cleavage surfaces of the clay mineral.

In clay–water mixtures where there is more water than needed to make the clay plastic, the exchange ions may separate from the clay mineral in a process resembling ionization. The desorbed cations form a mobile cloud around the now negatively-charged clay particle, or *micelle*, as it is sometimes called. Only a portion of the adsorbed ions are likely to be desorbed, with the percentage desorbed depending on the particular clay mineral, the concentration of clay in water, the particular cation involved in the desorption and the concentration of ions already in the solution.

Since all rocks possess some exchange capacity, the conductivity of an electrolyte in a pore structure will always be increased by ions supplied by desorption. As an example, if a sandstone with 20 per cent pore volume contains 0·1 per cent by weight of sodium-charged montmorillonite clay with an exchange capacity of 100 m-equiv per 100 g, the resistivity of the pore water would be determined as follows if the rock were initially saturated with distilled water:

1. Determination of the weight of clay per cm³ of rock:

$$w = 0 \cdot 001 \times (1 - \varphi)\, \delta_m$$
$$= 0 \cdot 001 \times (1 - 0 \cdot 2) \times 2 \cdot 76$$
$$= 0 \cdot 0022 \text{ g}$$

where φ is the porosity and δ_m is the density of the minerals forming the rock framework.

2. Determination of the quantity of exchangeable ions:

$$q = cw$$
$$= \frac{100 \times 0 \cdot 0022}{100 \text{ g}}$$
$$= 0 \cdot 0022 \text{ m-equiv}$$

ting cation exchange capacity
n appreciable cation exchange
ds along the edges of grains
rticles. Zeolite minerals which
n exchange capacities of the

ange properties in clays:

mina units in the crystal lattice
adsorbed ions. A single cation may
ding energies.
nt silicon in the tetrahedral sheet
arge in the crystal. Ions of lower
ium in the lattice with the same
charges resulting from such sub-
he clay mineral.

water than needed to make
e from the clay mineral in a
as form a mobile cloud around
elle, as it is sometimes called
be desorbed, with the percen
mineral, the concentration of
e desorption and the concen-

, the conductivity of an elec-
d by *ions* supplied by desorp-
cent pore volume contains
morillonite clay with an ex-
ivity of the pore water would
aturated with distilled water
of rock:

m

$\times 2.76$

of the minerals forming the

le ions:

where c is the exchange capacity. Since one milliequivalent of sodium ion weighs 23·0 mg, the weight of sodium ion present is 0·508 mg.

3. Determination of the concentration of sodium ion in the pore water:

$$q/\varphi = 0.0508/0.2 = 0.254 \text{ m-equiv/ml}$$

4. Conversion of sodium ion content to an equivalent concentration of sodium chloride, using data on ion mobilities:

$$\frac{m_{Na}}{m_{Na} + m_{Cl}} \times \frac{q}{\varphi} = \frac{4.35 \times 10^{-8}}{4.35 \times 10^{-8} + 6.55 \times 10^{-8}} \times 0.254$$

$$= 0.102 \text{ mg per ml equivalent NaCl concentration}$$

Referring to Fig. 7, the resistivity of this equivalent solution is found to be about 6·0 ohm-m at a temperature of 18°C.

Not all the exchangeable cations would necessarily be desorbed from the clay, so that in fact, the conductivity of the pore water might be less than the value computed in this example. Moreover, the mobility of the desorbed ions is less than the mobility of the same ions in a free solution since they remain close to the negatively charged clay particle. The example does serve to show how little exchange capacity is required to lower the pore-water resistivity significantly. Even in rocks with very low exchange capacities, pore water resistivity rarely exceeds 10 ohm-m. In fine-grained rocks, such as shale, apparent pore water resistivities are always much lower than would be expected on the basis of a chemical analysis of water extracted from the rock. The added salinity is relatively unimportant if the normal salinity of the pore water is high, but if the pore water is dilute, it is practically impossible to predict the resistivity of the water in the pores unless the cation exchange capacity of the rock is known.

The nature of surface conduction is less well known, but the phenomenon is important in water-bearing rocks. Rock-forming minerals usually fracture in such a way that one species of ion in the crystal is commonly closer to the surface than others. In silicates, the oxygen ions are usually closest to the surface (see Fig. 10). When an electrolyte is in contact with such a surface, it will seem to the ions in solution that the surface is charged negatively. Cations will be attracted to the surface by coulomb forces and adsorbed, while anions will be repelled. A similar effect takes place with water molecules, which are *polar*. The water molecule is not symmetrically constructed from an oxygen atom and two hydrogen atoms; rather, there is an angle of 105° between the bonds from the oxygen to the two hydrogen atoms, as shown schematically in Fig. 11. As a result, the center of mass of the positive charges (the hydrogen atoms) does not coincide with the center of mass of the negative charges (the oxygen atom). When viewed from the oxygen side, the water molecule appears to carry a negative charge; when viewed from the hydrogen side, it appears to carry a positive charge.
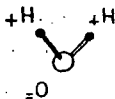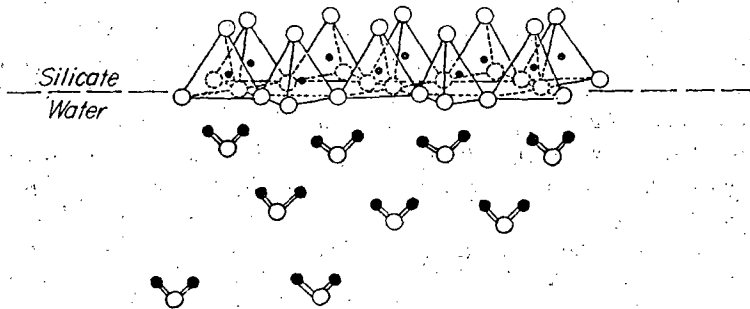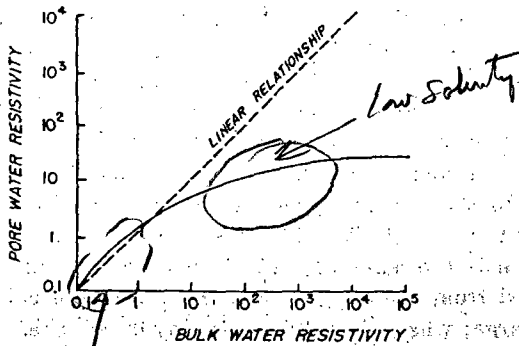
2 BMG
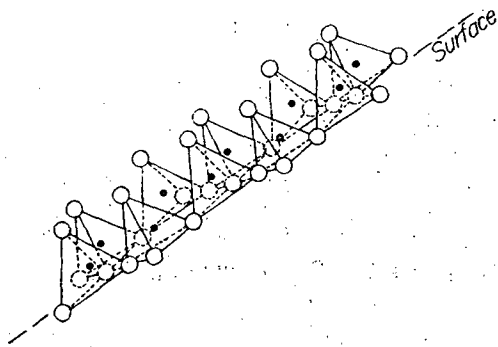
○ Oxygen

• Silicon

FIG. 10.

FIG. 11.

FIG. 12.

$\rho_b = a \rho_w \phi^{-m}$
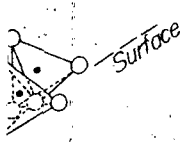
archies law

$a \phi^{-m} = F = $ formation factor
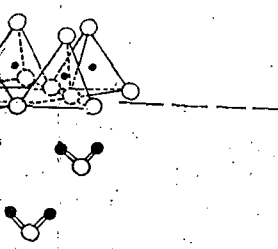
i.e. $\boxed{\rho_b = F \rho_w}$
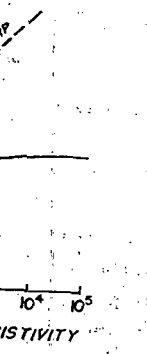

FIG. 13.

high salinity
low ρ

When an electrolyte is in contact with a surface such as that shown in Fig. 10, several layers of water molecules will become adsorbed to the surface, as shown in Fig. 12. This layer may be several molecules thick, if there are relatively few ions in the electrolyte, since each layer of oriented water molecules will absorb other water molecules. A single adsorbed cation will neutralize a surface charge which otherwise would hold several water molecules in a chain.

The conductivity of water in this oriented adsorbed phase is higher than the conductivity of free water, and so contributes to the overall conductivity of a rock. However, the increased pressure in the adsorbed layers increases the viscosity of the water and decreases the mobility of ions. If many ions are adsorbed, the conductivity of the electrolyte may be significantly reduced.

If all these factors that affect the conductivity of water in the pores of a rock are considered, the conductivity might behave as indicated in Fig. 13. The dotted curve shows the relationship which would hold between rock resistivity and water resistivity if there were no interaction between the water and the rock framework; the bulk resistivity of the rock should be directly proportional to the resistivity of the water placed in the pores. The solid curve shows the more probable relation between rock resistivity and water resistivity when interaction between the water and the solid minerals takes place; at high salinities (low resistivity), the resistivity of the electrolyte in the pores is increased slightly by the greater viscosity of the water adsorbed on the grains; at lower salinities (higher resistivities), the resistivity of the pore water approaches a maximum value rather than increasing indefinitely. The resistivity of the pore water cannot exceed some fairly low value, determined by the amount of interaction. Both the increase in resistivity at high salinities and the decrease in resistivity at low salinities is more pronounced in fine-grained rocks than in coarse-grained rocks. A limiting value of 10 ohm-m would be characteristic of a rock with a low cation exchange capacity, while the limiting value in a clay-rich rock may be as low as 0·1 ohm-m.

5c. Resistivity of rocks only partially saturated with water

The pore space of a rock need not necessarily be filled with an electrolyte; in oil reservoir rocks, some of the pore space may be filled with oil or petroleum gas, while in near-surface rocks, part of the pore space may be filled with air. The second case is more common than the first.

Although the term *water table* has no precise scientific definition, it is usually used to indicate the depth at which the pore spaces remain fully saturated. The expression and its usage are misleading in that it infers that there exists a depth below which water is present and above which water is absent. In fact, the transition from complete saturation of the pore space to partial saturation above the water table is gradual and difficult to pinpoint. There is a transition from a surficial zone (which may be thousands of feet in arid regions) through

2*